[illegible] - 122

ORNL-5135

SOLID STATE DIVISION

MASTER

ANNUAL PROGRESS REPORT

Period Ending December 31, 1975

OAK RIDGE NATIONAL LABORATORY

BLANK PAGE

Printed in the United States of America. Available from
National Technical Information Service
U.S. Department of Commerce
5285 Port Royal Road, Springfield, Virginia 22161
Price: Printed Copy $7.50; Microfiche $2.25

ORNL-5135
UC-25 – Materials

Contract No. W-7405-eng-26

SOLID STATE DIVISION
ANNUAL PROGRESS REPORT
For Period Ending December 31, 1975

M. K. Wilkinson, Director
F. W. Young, Jr., Associate Director

MAY 1976

OAK RIDGE NATIONAL LABORATORY
Oak Ridge, Tennessee 37830
operated by
UNION CARBIDE CORPORATION
for the
ENERGY RESEARCH AND DEVELOPMENT ADMINISTRATION

Reports previously issued in this series are as follows:

ORNL-1095	Period Ending April 30, 1951
ORNL-1128	Period Ending July 31, 1951
ORNL-1214	Period Ending October 31, 1951
ORNL-1261	Period Ending January 31, 1952
ORNL-1301	Period Ending May 10, 1952
ORNL-1359	Period Ending August 10, 1952
ORNL-1429	Period Ending November 10, 1952
ORNL-1506	Period Ending February 10, 1953
ORNL-1606	Period Ending August 30, 1953
ORNL-1677	Period Ending February 28, 1954
ORNL-1762	Period Ending August 31, 1954
ORNL-1851	Period Ending February 28, 1955
ORNL-1852	Period Ending February 28, 1955
ORNL-1944	Period Ending August 31, 1955
ORNL-1945	Period Ending August 31, 1955
ORNL-2051	Period Ending February 29, 1956
ORNL-2052	Period Ending February 29, 1956
ORNL-2188	Period Ending August 31, 1956
ORNL-2189	Period Ending August 31, 1956
ORNL-2413	Period Ending August 31, 1957
ORNL-2414	Period Ending August 31, 1957
ORNL-2614	Period Ending August 31, 1958
ORNL-2829	Period Ending August 31, 1959
ORNL-3017	Period Ending August 31, 1960
ORNL-3213	Period Ending August 31, 1961
ORNL-3364	Period Ending August 31, 1962
ORNL-3480	Period Ending May 31, 1963
ORNL-3676	Period Ending May 31, 1964
ORNL-3841	Period Ending May 31, 1965
ORNL-3935	Period Ending December 31, 1965
ORNL-4098	Period Ending December 31, 1966
ORNL-4250	Period Ending December 31, 1967
ORNL-4408	Period Ending December 31, 1968
ORNL-4526	Period Ending December 31, 1969
ORNL-4669	Period Ending December 31, 1970
ORNL-4779	Period Ending December 31, 1971
ORNL-4861	Period Ending December 31, 1972
ORNL-4952	Period Ending December 31, 1973
ORNL-5028	Period Ending December 31, 1974

Special Dedication

This issue of the Solid State Division Annual Report is dedicated to the memories of two valuable Division members who died during the past year.

J. Ray Savage was a senior laboratory technician in the research group concerned with investigations of the physical properties of crystal surfaces. His various activities included the growth of highly perfect single crystals of metals, which were essential for the experiments on surfaces and for other research investigations of the Division.

Richard E. Reed, Sr., was the leader of a research group that developed techniques for the purification, crystal growth, and characterization of high-quality research materials. Through his leadership and personal efforts, many research specimens were prepared for important solid state investigations that could not have been undertaken without them. He was also the principal investigator of an experiment that he designed for the Apollo-Soyuz space flight.

Both of these men accomplished many skillful scientific and technical tasks for members of the Solid State Division, ORNL, and ERDA. Their skills and their close associations with Division members are greatly missed.

Contents

I. THEORETICAL SOLID STATE PHYSICS

SURFACE STUDIES

LATTICE DYNAMICS

PARTICLE-SOLID INTERACTIONS

BLANK PAGE

ELECTRONIC AND MAGNETIC PROPERTIES

2. PHYSICAL PROPERTIES OF SOLIDS

SUPERCONDUCTIVITY

SURFACE PROPERTIES AND CATALYSIS

OPTICAL, ELECTRICAL, AND MAGNETIC PROPERTIES OF HIGH-TEMPERATURE MATERIALS

PHOTOVOLTAIC CONVERSION OF SOLAR ENERGY

3. RADIATION EFFECTS IN METALS

ION-SOLID INTERACTIONS

LOW-TEMPERATURE RADIATION EFFECTS

X-RAY DIFFRACTION AND ELECTRON MICROSCOPY

4. NEUTRON SCATTERING

MAGNETIC PROPERTIES

LATTICE DYNAMICS

PHASE TRANSITIONS AND CRITICAL PHENOMENA

5. RESEARCH MATERIALS

6. ISOTOPE RESEARCH MATERIALS

Introduction

The arrangement of the Annual Report has been chosen to emphasize the major areas of solid state science in which the Solid State Division conducted research during the period from January 1, 1975, through December 31, 1975. These areas are Theoretical Solid State Physics, Physical Properties of Solids, Radiation Effects in Metals, Neutron Scattering, Research Materials, and Isotope Research Materials. Each of them constitutes a main section of the Report, and additional subdivisions are included within the sections. Each section has a brief introduction that indicates the scope and goals of the research and gives some highlights of the past year. It is hoped that these introductions give a clearer picture of the manner in which the individual programs are interrelated and also show how the research activities of the Solid State Division contribute to various programs of ORNL and ERDA. The last section on Isotope Research Materials represents a new research area for the Division but not for ORNL; the Isotope Research Materials Laboratory was transferred into the Solid State Division on July 1, 1975.

In the last Annual Report, it was apparent that the formation of ERDA, with its broad mission in the development of new types of energy systems, would bring changes in the research emphasis of the Solid State Division. These changes are easily seen throughout this issue of the Annual Report. Research contributions in every section include investigations associated with nonnuclear energy technologies, and the section on Physical Properties of Solids is devoted almost exclusively to investigations of that type. This is certainly not surprising, because essentially all nonnuclear energy technologies are limited by materials problems, and the solutions of those problems must rely heavily on information obtained from scientific research. The new programs that were initiated during the past year resulted almost entirely from the reorientation of existing programs.

1. Theoretical Solid State Physics

The members of the Theory Section have continued during the past year to work on a broad range of problems directly related to the diverse experimental programs within the Division. The period covered by this Annual Report was one of change within the Laboratory and within the Division, and this is reflected in the theoretical effort for the year. Thus, although theoretical research has continued in a number of areas of long-standing interest, some redirection of previously existing efforts took place, and new areas were entered. The emphasis on nonnuclear, energy-related research has grown rapidly. As the scientific staff has explored new energy-related areas in which the facilities and capabilities of the Division can be most effectively utilized, the interaction between the theorists and experimentalists has been further strengthened. For this reason, several contributions of the theoretical section will appear in research studies reported in experimental sections of the report. As in the last few Annual Reports, for convenience of discussion, the theoretical research can be grouped into the four areas of surface studies, lattice dynamics, particle-solid interactions, and electronic and magnetic properties. The work in these different areas is often interrelated, and any one theorist may work in a number of them concurrently.

Research in the area of surface physics has continued to grow in the Division during the last year, once again emphasizing the increasing importance of surface studies to materials problems related to advanced energy systems. Studies of reflection of light atoms from solid surfaces, which are important for the plasma-stability problem in controlled thermonuclear reactor (CTR) devices such as ORMAK, have been expanded in scope and improved in methodology. Two of the most common experimental techniques for studying surfaces are low energy electron diffraction (LEED) and Auger-electron spectroscopy; the Division has a substantial program utilizing both of these methods. The theoretical interpretation of data generated by LEED and Auger experiments suffers from the lack of a well-developed theory of the various surface and near-surface effects leading to the observed results. The theorists of the Division have made significant contributions during the past year in this area. It has been rather straightforward to modify many theoretical ideas and computational techniques, previously developed for describing bulk properties, for use in surface-related work. However, it also has been necessary to develop new techniques, and this development will continue in the future. An exciting new area is the use of ion channeling and backscattering and the use of LEED and Auger spectroscopy as complementary and contrasting techniques for determining and verifying surface structural information. ORNL appears to have unique capacity to exploit this area experimentally and theoretically.

Research on lattice dynamics continues to cover a wide variety of theoretical studies and calculations on the vibrational properties of perfect crystals, random alloys, and crystals with point imperfections. One of the most interesting pieces of work reported in the last Annual Report concerned the possibility of observing self-interstitials in fcc metals directly by neutron scattering. The configuration of the self-interstitial has long been a matter of controversy, but recently considerable progress has been made in establishing it to be of the dumbbell or ⟨100⟩-split interstitial form. Direct observation by neutron scattering experiments of effects due to self-interstitials has now been made and is reported in Sect. 4 of this Annual Report. These measurements, in connection with theoretical work, open up the possibility of applying neutron scattering to a variety of problems not heretofore accessible to this powerful tool. A potentially important reformulation of the random alloy problem has been carried out by a member of the Theory Section working together with a mathematician from the Computer Sciences Division. At the very least, this reformulation helps to elucidate some of the approximations made in previous treatments of random alloys, and it may lead to improved computational approaches. Another worthwhile step forward in alloy calculations has been taken with the construction of a computer program for the calculation of the lattice dynamics of large clusters of atoms. Cluster calculations are useful in providing insight into certain aspects of alloy theory, and if the clusters can be made large enough, while the computational time is kept within reasonable bounds, the calculations may provide valuable quantitative information.

The theoretical studies of particle-solid interactions deal with problems that are either directly or indirectly related to atomic collisions in solids. Some of these topics, such as ion radiation damage in metals, are of direct relevance to technical problems in the development of both fission and fusion power reactors. Others, such as channeling, are primarily of interest either to fundamental studies of solids or to detailed studies of the atomic collisions themselves. Recently a proposal has been made by a member of the Theory Section to use ion-channeling techniques to investigate interstitial configurations in copper and other fcc metals. Such work, if it proves to be feasible, could complement and supplement studies by neutron scattering of the configurations and vibrational properties of interstitials. As in previous years, work on channeling has continued in an effort to make it an accurate and reliable method for probing lattice potentials and ion positions in many different materials. Theoretical work on the simulation of fast-neutron damage by heavy-ion bombardment has also been pursued during the past year; a description of this work will be found in Sect. 3 on Radiation Effects in Metals.

The theoretical research on the electronic and magnetic properties of materials is concentrated on studies of bulk properties of metals, insulators, and semiconductors, both with and without point imperfections. Results of electronic energy band calculations are often used directly in the interpretation of the electronic structure and optical properties of perfect crystals, but more importantly, they form an indispensable basis for the calculation of magnetic and vibrational properties of materials. In last year's Annual Report, calculations of the wave-number- and frequency-dependent magnetic susceptibilities of iron were described. These calculations yielded satisfactory agreement with the experimental results obtained by the neutron scattering group in the Division and, together with earlier calculations on nickel, showed that at low temperatures the band picture of electronic states in crystals is not incompatible with the occurrence of ferromagnetism in nickel and iron. Recent work in this area provides an excellent example of the effective interplay of theoretical and experimental research; the calculations on spin waves in nickel motivated new experiments which verified the theoretical prediction of "optical" spin waves. Theoretical work on the electronic susceptibility in high T_c superconductors was continued during the past year, but this is a formidable problem and further development of both the theory and the computational procedures is needed. Calculations of the electronic structure of simple defects in alkaline earth oxides were also continued. This work has particular significance for the experimental research on high-temperature ceramics, and it is anticipated that similar calculations can be made on semiconducting materials which are of direct significance for the program of solar energy conversion now developing in the Division.

SURFACE STUDIES

THEORETICAL ANALYSIS OF ANGULAR-DEPENDENT AUGER SPECTROSCOPY

H. L. Davis Theodore Kaplan

Theoretical studies have been initiated concerning the possible utilization of angular dependent Auger spectroscopy (ADAS) as a tool for quantitative surface-structure determination. Recent observations have shown that considerable structure exists in the angular distributions of 62-eV $M_{2,3}VV$ and 107-eV M_1VV Auger electrons emitted from (100), (110), and (111) clean copper surfaces.[1–3] As an illustration of the structure found experimentally, the lower curve in Fig. 1.1 represents data obtained at ORNL for 62-eV Auger electrons observed about a (100) copper surface.[3] The angles θ and ϕ describe the angular position of the Auger electron detector above the surface: the polar angle θ is measured relative to the surface normal, and the azimuthal angle ϕ is measured relative to the [011] surface direction. The measured intensity variations with θ are seen to be large; large variations also have been observed[1–3] in intensity vs θ plots for other azimuthal angles above the (100) copper surface and in angular intensity distributions above the Cu (110) and (111) surfaces. Such variations have given rise to the hope that ADAS will eventually evolve into a quantitative tool for surface-structure determinations. However, difficult questions remain to be answered before ADAS can be firmly established as a useful tool, and addressing these questions is the major thrust of the present program.

In order to utilize ADAS for surface analysis, it is necessary to fully understand the fundamental mechanisms responsible for the observed angular variations. The most likely mechanisms are (1) anisotropic Auger emission at the individual atomic sites and/or (2) diffraction caused by the scattering of the Auger electrons (after emission) by the atoms in the surface region. Both of these mechanisms might reasonably be assumed to be operative for Auger emission from a general crystalline surface. To test their relative importance for the specific case of copper surfaces, we have performed model calculations in which the emitted Auger electrons are assumed to have various angular momenta. That is, the amplitude at $\mathbf{r}$ due to emission at the atomic site $\mathbf{r}_n$ is taken to be of the form $h_l^{(1)}(\kappa|\mathbf{r}-\mathbf{r}_n|)Y_{lm}(\mathbf{r}-\mathbf{r}_n)$, where $h_l^{(1)}$ is a spherical Hankel function of the first kind and the Y_{lm} are complex

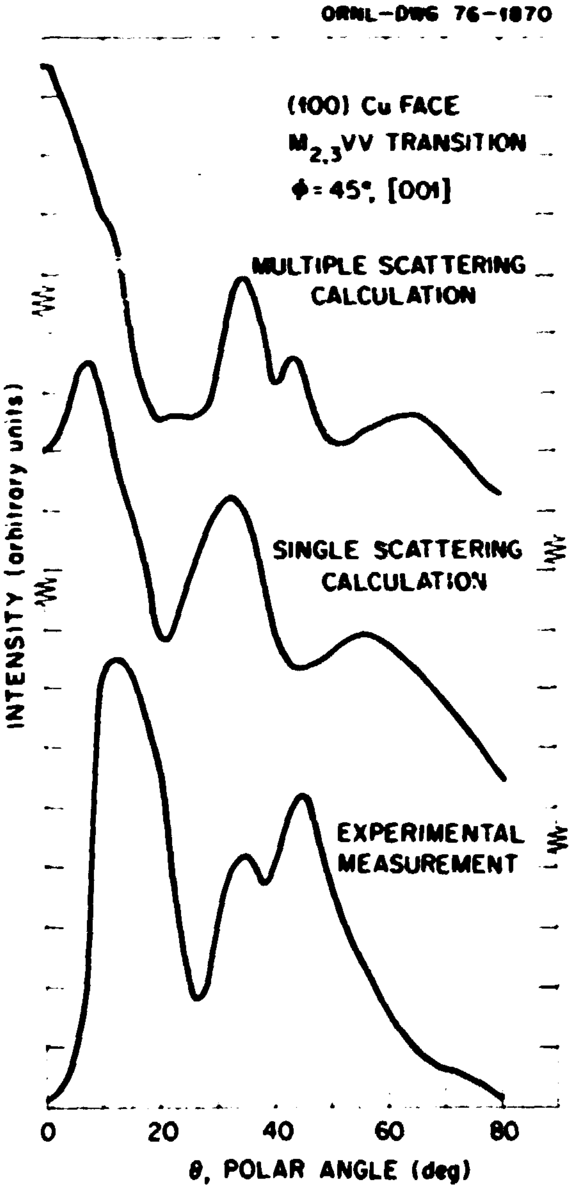

Fig. 1.1. Angular dependence of 62-eV copper Auger transition.

spherical harmonics. The complex wave number is $\kappa = (E - V_0)^{1/2}$, where E is the energy of the emitted electron outside the crystal and V_0 is a complex background potential within the crystal. In addition, V_0 has an imaginary component in order to simulate absorption of the emitted wave via inelastic scattering processes, which cause electrons to have a finite path length inside the crystal. The magnitude of this path length is such that only Auger electrons emitted in the first few atomic layers of the surface can effectively reach an external detector.

In our model, the emitted partial wave is allowed to scatter from atomic sites in the surface region, and then the total wave amplitude and the corresponding intensity are calculated at the detector position. For fixed θ and ϕ, the total detected intensity is the sum of intensities for emission originating in each of the individual atomic layers of the surface region. These individual intensities must be weighted by probability factors for the occurrence of Auger emission in the respective layers; for example, the experimental results of Fig. 1.1 were obtained[3] by stimulating the emission via bombardment with 350-eV electrons whose path length in copper is approximately 10 Å. Because of the probability weighting and the absorption of the Auger electrons after emission, only emission in the first five or six layers of the Cu (100) surface will contribute significantly to the observed total intensity. The scattering of the partial waves by the atomic sites has been accounted for by employing scattering parameters (phase shifts and V_0 values) identical to those used by others[4] in calculations which produced reasonable agreement with results from LEED experiments on copper.

Calculations based on the above model were first performed using emitted partial waves having completely isotropic or s-state emission; that is, $(l,m) = (0, 0)$. Single-scattering approximation results obtained for this case, calculated employing a formalism due to Holland,[5] are shown as the middle curve of Fig. 1.1. Quite similar results have been obtained by McDonnell, Woodruff, and Holland,[1] who also employed the single-scattering approximation but used a different formalism. Although there is not good agreement between the theoretical results and the experimental data, the calculations do reproduce some general features of the experimental results, such as the general magnitude of the variations with angle. However, if only single-scattering results were available, it would be difficult to determine whether the discrepancies between calculation and experiment would be assigned to anisotropic emission mechanisms or to multiple-scattering effects. In fact, it has been speculated[6] that the principal cause of the discrepancies between the lower two curves in Fig. 1.1 is the neglect of multiple-scattering effects in the calculations. In order to test this speculation, we proceeded with calculations in which all multiple-scattering effects were correctly included.

The results given by the top curve of Fig. 1.1 were obtained for s-state emission by employing a multiple-scattering formalism described by Pendry.[7] Although the multiple- and single-scattering results do differ significantly, major differences also remain between the multiple-scattering calculations and experiment. Thus, even though multiple-scattering effects are seen to be very important, Woodruff's speculation[6] concerning the reason for the differences between the lower two curves must be discounted. The most obvious difference between the multiple-scattering results and experiment occurs near $\theta = 0^\circ$, where the experimental intensity is almost zero. In an attempt to determine whether this large difference near $\theta = 0^\circ$ could be removed by varying the calculational parameters (phase shifts, E, and V_0) while retaining the assumption of s-state emission, a series of calculations was performed in which these parameters were allowed to vary over physically reasonable ranges. None of these calculations produced results in which the $\theta = 0^\circ$ intensity was greatly reduced from that of the top curve of Fig. 1.1. At present, then, we are forced to conclude that a principal cause of the discrepancies between the calculated and experimental results is anisotropic emission at the atomic sites. In fact, we have performed multiple-scattering calculations for emitted partial waves having $(l,m) = (1, 1)$ and $(1, \ 1)$; these produce zero intensity at $\theta = 0^\circ$. This also occurs for any partial wave with $m \neq 0$ relative to a coordinate system whose z axis is normal to the surface.

Since the 62-eV Auger emission for copper involves electron transitions between the valence band and core states, it appears highly unlikely that any model that represents the emitted electron by a single partial wave can produce results in good overall agreement with the experimental results. However, by full consideration of the details of the emission process and of the electronic band structure of copper, a model could be formulated in which the emission is represented by a linear combination of partial waves having different (l, m) values. Such a model would not only entail rather elaborate calculations, but it would also require knowledge about features of the electronic structure near the surface which are not adequately understood at present. Thus, it might be more fruitful for the possible development of ADAS as a tool for surface-structure analysis if experiments were performed using Auger transitions involving only core states.

---

1. L. McDonnell, D. P. Woodruff, and B. W. Holland, *Surf Sci* 51, 249 (1975).
2. D. M. Zehner, J. R. Noonan, and L. H. Jenkins, *Solid State Commun.* 18, 483 (1976).
3. J. R. Noonan, D. M. Zehner, and L. H. Jenkins, *J. Vac. Sci. Technol.* 13, 183 (1976).
4. D. W. Jepsen, P. M. Marcus, and F. Jona, *Phys. Rev. B* 5, 3933 (1972).
5. B. W. Holland, *J. Phys. C* 8, 2679 (1975).
6. D. P. Woodruff, *Surf. Sci.* 53, 538 (1975).
7. J. B. Pendry, *J. Phys. C* 8, 2413 (1975).

NUMERICAL TECHNIQUES FOR LOW ENERGY ELECTRON DIFFRACTION ANALYSES

H. L. Davis

Low energy electron diffraction (LEED) is now an established technique for the investigation of surface structure. Valuable information concerning the symmetry of surface structures can be obtained directly from the diffraction patterns observed in LEED experiments, and much more information becomes potentially available if beam intensities are measured as a function of electron energy. Given intensity data from a surface, however, extensive numerical calculations are required for the extraction of information such as the atomic locations and the bond distances in the surface region. These calculations necessarily must be concerned with the mechanics of how the incident electrons are multiply scattered by the atoms in the surface region to produce the reflected beams observed in the LEED experiments. In the past few years, developments in the underlying theoretical foundations[1] have resulted in several reliable techniques for performing multiple-scattering calculations, but each of these techniques requires the construction of elaborate computer codes before it can be exploited.

As part of the growing surface-studies program within the Division, computer codes that will be useful in extracting surface information from LEED intensity measurements have now been developed. The codes are based on the renormalized forward scattering method of Pendry[2] and should prove useful for treating data obtained from clean surfaces for energies in the range of about 20 to 250 eV. The codes have been extensively debugged by comparing the results obtained from them with those of several published LEED calculations.[3,4] It is anticipated that the first new application of our codes will be to the treatment of LEED intensity data from the (110) surface of copper, which is soon to be considered by the Division's experimental surface group. At the same time, several multiple-scattering subprograms of the codes have already been very useful in the theoretical analysis of angular dependent Auger spectroscopy.[5]

---

1. See, for example, J. B. Pendry, *Low Energy Electron Diffraction*, Academic Press, New York, 1974.
2. J. B. Pendry, *J. Phys. C* 4, 3095 (1971).
3. S. Y. Tong and L. L. Kesmodel, *Phys. Rev. B* 8, 3753 (1973).
4. D. W. Jepsen, P. M. Marcus, and F. Jona, *Phys. Rev. B* 5, 3933 (1972).
5. H. L. Davis and T. Kaplan, "Theoretical Analysis of Angular-Dependent Auger Spectroscopy," this report.

COMPUTER STUDIES OF THE INTERACTION OF LOW-ENERGY LIGHT IONS WITH SOLID SURFACES[1]

O. S. Oen M. T. Robinson

Through charge exchange, ions can escape from the magnetically confined plasma of a controlled thermonuclear reactor and can interact with the walls of the containment vessel. Some of these escaping neutral atoms will be reflected from the walls back into the plasma with reduced energy, and others will slow down and come to rest within the walls. This particle recycling is very important in the design of a thermonuclear reactor since it affects the particle energy balance of the system. A comprehensive program to study the interaction of light ions with solid surfaces was initiated two years ago,[2] and during the past year two papers have been written[3,4] describing some of the results. The studies utilized the binary collision cascade program MARLOWE,[5] which was modified to treat the reflection of low-energy light ions. The calculations were performed for 0.01- to 20-keV H, T, and He ions incident upon amorphous targets of Al, Cu, Nb, and Au. In the simulation the incident particles are followed, collision by collision, until they either leave the target surface again or slow down to some cutoff energy (5 eV). Each collision with a target atom consists of an elastic part described by a Thomas–Fermi potential and an inelastic part based on a semiempirical model. For each set of initial conditions, 1000 or more incident particles were followed, and statistical information was recorded for those particles coming to rest within the solid and for those reflected.

The mean penetration depth for low-energy light ions is found to be only a small fraction of their total path length. This is due to the many large random deflections, which lead to a diffusion-like motion for the projectile. For a specific projectile the mean penetration depth in any of the target materials is expressible in terms of a universal curve. This universality breaks down at the lowest projectile energies, where the nuclear stopping component is an appreciable fraction of the total stopping. The penetration depths calculated for hydrogen ions are from 50 to 100% greater than those found analytically by Schiøtt.[6] These differences are believed to be due mainly to the different treatments of the free surface, which is difficult to include properly in an analytical treatment; the present computer simulation automatically treats the presence of the surface by separating the reflected particles from those stopping within the solid. It is also found that the mean penetration depth has only a weak dependence on the angle of beam incidence, whereas it might be expected to have a cosine dependence. This rather surprising result is understandable on the basis of the diffusion-like motion of the projectiles, which quickly "forget" their original direction of motion upon entering the solid. However, the fraction of the beam that stops within the solid decreases as the incident angle increases away from the surface normal, and total reflection occurs at a critical angle which depends on energy and on the projectile target combination in a manner analogous to that for planar channeling. The calculated penetration depths are found to be rather weakly dependent on the electronic stopping. For instance, increasing the electronic stopping by 50% decreases the mean penetration depth of 4-keV ^{3}He in Nb by only 13% and produces only small changes in the overall penetration profile. The calculated penetration profiles agree fairly well with the recent experimental work of Behrisch et al.[7] for low-energy ^{3}He in Nb.

The fraction of particles and the fraction of energy reflected are found to increase with increasing atomic number of the target material and to decrease with increasing incident energy. For hydrogen incident normal to amorphous niobium, the reflected particle number fraction decreases from 0.63 to 0.14 as the incident energy increases from 0.1 to 10 keV. The peak in the energy distribution of the reflected particles shifts to a lower fraction of the incident energy as the incident energy increases. A qualitative understanding of the overall results can be obtained by viewing the reflected fraction of particles as consisting of two components: (1) particles that are directly backscattered from the surface layer of the target and (2) particles that penetrate the surface and undergo a diffusive-type motion in the solid before escaping through the surface. The calculations agree fairly well with the limited experimental data available.

---

[1] Summary of paper to be published.

[2] M. T. Robinson and O. S. Oen, *Solid State Div. Annu. Prog. Rep. Dec. 31, 1974*, ORNL-5028, p. 16.

[3] O. S. Oen and M. T. Robinson, "Computer Studies of the Penetration Depth of Low Energy Light Ions in Solids," to be published.

[4] O. S. Oen and M. T. Robinson, "Computer Studies of the Reflection of Light Ions from Solids," to be published.

[5] M. T. Robinson and I. M. Torrens, *Phys. Rev. B* 4, 5008 (1974).

[6] H. E. Schiøtt, *K. Dan. Vidensk. Selsk. Mat.-Fys. Medd.* 35, No. 9 (1965).

[7] R. Behrisch, J. Bøttiger, W. Eckstein, U. Littmark, J. Roth, and B. M. U. Scherzer, *Appl. Phys. Lett.* 27, 199 (1975).

RELAXATION OF SURFACE ATOMS

John H. Barrett

Davies et al.[1] recently reported channeling measurements showing the effect of relaxation of the topmost layer of atoms on the (111) surface of platinum. Their method was to measure the effective number of surface atoms per row contributing to backscattering. From their results, they inferred that the surface layer relaxes outward by 0.31 ± 0.05 Å.

A series of computer simulations has been completed for the same set of conditions. The results are shown in Fig. 1.2. The general nature of the calculated values is similar to that of the experimental ones, but the magnitude of the relaxation inferred is appreciably smaller, being 0.20 ± 0.03 Å. The error estimate here is partly due to scatter in the simulation values but is mostly due to scatter in the experimental values. The main difference between the relaxation value just given and the earlier one of ref. 1 is probably due to the inclusion here of the effects of thermal vibrations and the exclusion of them in the procedure used by Davies et al. A value of 0.040 Å was used for ρ, the root-mean-square displacement of an atom from its row, at the experimental temperature of 40°K. It is possible that interpretation of the experiments will also need to take into account the special nature of surface vibrations and the correlation in vibrations of neighboring atoms; these factors will be explored in future calculations.

Computer simulations can be of value in interpreting such experiments in a number of ways. At present they offer the most accurate method for determining the magnitude of the relaxation. A second

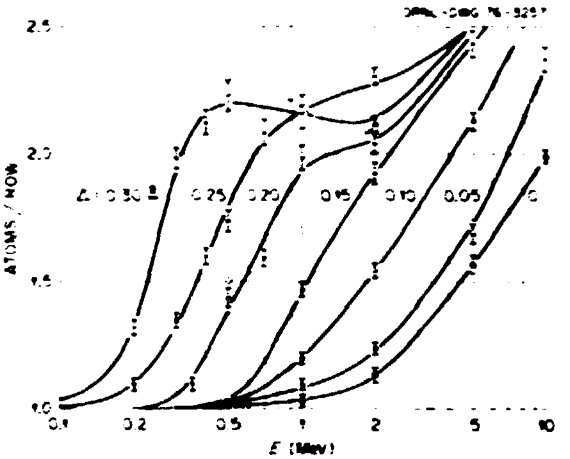

Fig. 1.2. Effective number of atoms per row contributing at 40 K to backscattering from the Pt (111) surface for helium ions incident along [011] at various energies. The crosses and curves drawn through them are computer simulation results for relaxation of the surface layer of atoms by the amount shown near each curve; the circles are experimental values of Davies et al.

useful contribution would be to establish a more accurate expression than now exists[2] for the effective number of surface atoms per row in the absence of relaxation. Such an expression will be helpful in determining just how much of the backscattering is due to relaxation of the surface layer rather than to other factors such as thermal vibrations. And, finally, computer simulations could help to validate analytical approaches to the problem; one such approach is already under way along the lines of earlier blocking calculations by Oen.[3]

---

[1] J. A. Davies, D. P. Jackson, J. B. Mitchell, P. R. Norton, and R. L. Tapping, *Phys. Lett.* **54A**, 239 (1975).

[2] J. H. Barrett, *Phys. Rev. B* **3**, 1527 (1971).

[3] O. S. Oen, *Phys. Lett.* **19**, 358 (1965); O. S. Oen, "Blocking Calculations for Surface-Structure Analysis," this report.

BLOCKING CALCULATIONS FOR SURFACE-STRUCTURE ANALYSIS

O. S. Oen

The theoretical blocking model[1] developed several years ago to interpret the first blocking experiments from bulk crystals has been found to have a new application in connection with two techniques[2,3] recently developed to measure atomic surface relaxation. The two experimental methods, although differing in principle, make use of the channeling and blocking phenomena. The two-particle, analytical blocking model includes effects of thermal vibrations which are described using a Gaussian probability distribution for the relative transverse displacement of the emitting and scattering nuclei. A computer program has been written to evaluate the integral giving the blocking pattern. The model, in addition to helping interpret experimental results, is expected to complement the detailed simulation analysis program of Barrett.[4]

---

[1] O. S. Oen, *Phys. Lett.* **19**, 358 (1965).

[2] J. A. Davies, D. P. Jackson, J. B. Mitchell, P. R. Norton, and R. L. Tapping, *Phys. Lett.* **54A**, 239 (1975).

[3] W. Turkenburg, "Proceedings of the International Conference on Atomic Collisions in Solids," special issue of *Nucl. Instrum. Methods* (in press).

[4] John H. Barrett, "Relaxation of Surface Atoms," this report.

LATTICE DYNAMICS

LATTICE VIBRATIONS IN $Rb_{1-c}K_c$ ALLOYS IN THE COHERENT POTENTIAL APPROXIMATION

Mark Mostoller   Theodore Kaplan

Coherent inelastic scattering measurements of lattice vibrations in a sequence of $Rb_{1-c}K_c$ alloys were performed at ORNL several years ago.[1] The concentrations of potassium in the crystals studied were $c = 0.06$, 0.18, and 0.29, and as expected, a local mode band was observed which grew in intensity as the concentration of the lighter mass atoms increased. For comparison with the experimental results, coherent potential approximation (CPA) calculations were carried out in which the potassium atoms were treated simply as mass defects in the rubidium lattice, and force-constant changes in the alloys were neglected.[2]

The mass-defect CPA calculations gave results in poor agreement with experiment. In particular, the calculated local mode band fell above the observed peak position, suggesting the need to incorporate force-constant changes in the theoretical treatment. Also, for scattering wave vectors near the zone boundary along the [110] direction, the observed longitudinal in-band and local mode peaks were much sharper and more distinct than predicted by the mass-defect CPA. This kind of discrepancy is not unexpected since the single-site CPA is a self-consistent mean field theory not capable of reproducing shape structure in the local mode region.[2,3]

As shown by the authors,[3,4] force-constant changes can be treated within the framework of the single-site

CPA if the force constants in the alloy are assumed to superimpose linearly. A restrictive statement of this assumption, but one which is applicable for nearest-neighbor force-constant changes in an alloy like the rubidium-potassium system, is that the A-B force constants in the alloy are the arithmetic average of the A-A and B-B force constants. For the $Rb_{1-c}K_c$ alloys, we have made the further assumption that only changes in the radial nearest-neighbor force constants are important; these are the spring constants for vibrations of a pair of first neighbors along the direction between them.

Despite the apparently drastic nature of the simplifying assumptions made concerning the force-constant changes, the CPA-F, as we will refer to our CPA treatment including force-constant changes, is computationally somewhat difficult to apply. For bcc alloys with mass differences and radial nearest-neighbor force-constant changes, the CPA-F yields six complex equations that must be solved self-consistently, and in these equations appear real-space CPA-F lattice Green's functions that can only be evaluated by numerical integration over the Brillouin zone. The numerical techniques used are discussed in refs. 2–5.

Figure 1.3 shows illustrative calculated results for $Rb_{0.82}K_{0.18}$ for three values of the local force-constant change assumed, ranging from mass defects only ($\Delta = 0$) to a negative change of roughly 20% ($\Delta = -400$ dyn/cm). The calculations were performed for a neutron scattering wave vector of $Q = (2\pi/a)\ (2.5,2.5,0)$, and the results shown include instrumental resolution. For the host or reference crystal, a virtual crystal model was used; that is, the force constants of the reference crystal were taken to be concentration-weighted arithmetic averages of the force constants in pure rubidium and potassium crystals.[6,7] As indicated in Fig. 1.3, the local mode peak shifts down in frequency as the force-constant change becomes more negative, while the in-band peak shifts relatively little.

Fig. 1.4 compares calculated mass-defect CPA and CPA-F results with the neutron scattering data for $Q = (2\pi/a)\ (2.5,2.5,0)$ in $Rb_{0.82}K_{0.18}$; for the CPA-F calculations, a local force-constant change of −300 dyn/cm was used. At this scattering wave vector for this concentration, substantially better agreement with experiment is achieved when force-constant changes are included. However, the experimental peaks remain sharper and more distinct than those calculated. Furthermore, the same force-constant change does not give agreement as good as that shown in Fig. 1.4 for other scattering wave vector directions and/or other alloy concentrations, although the CPA-F does generally do a better job than the mass-defect CPA.

A number of conclusions can be drawn from the comparison between the experimental data for $Rb_{1-c}K_c$ alloys and the calculations just described. As suggested

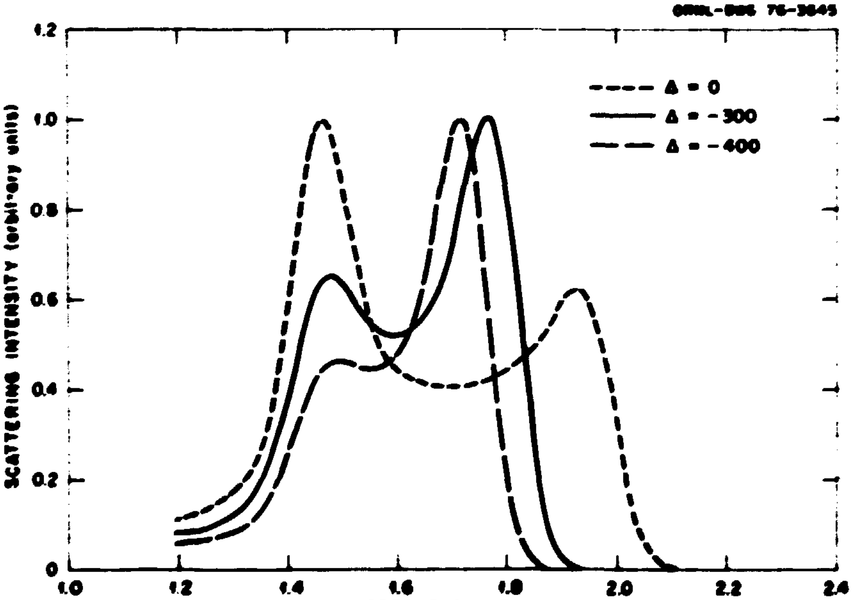

Fig. 1.3. Calculated neutron scattering cross sections for $Rb_{0.82}K_{0.18}$ in the CPA-F for three values of the local force-constant changes Δ. The scattering wave vector is $Q = (2\pi/a)(2.5,2.5,0)$, and the results shown include a Gaussian resolution function with a width of 0.10 THz (FWHM).

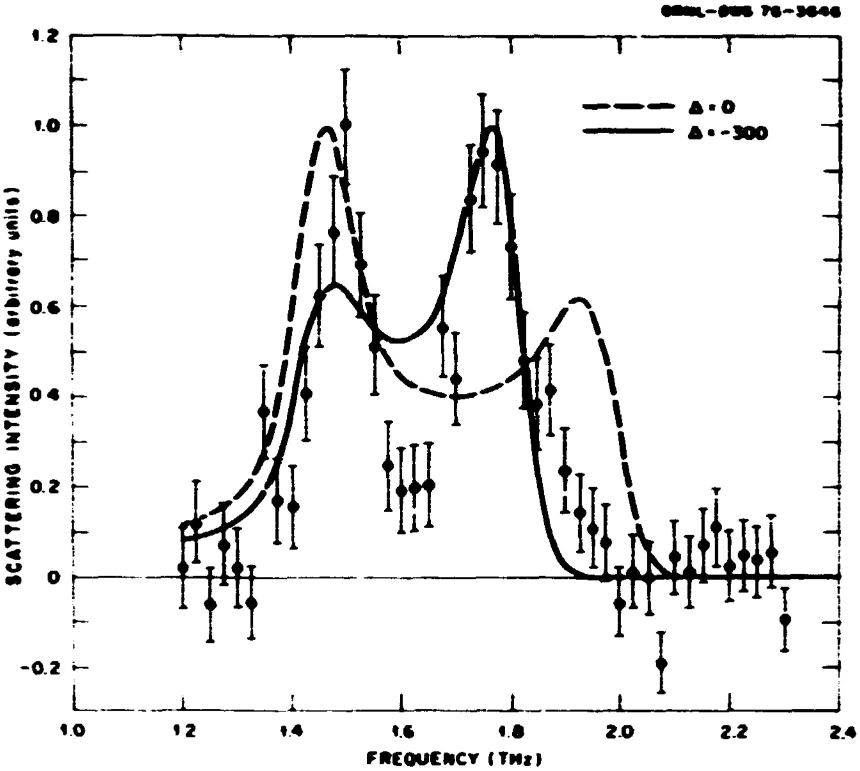

Fig. 1.4. CPA-F and mass-defect CPA results compared to the neutron scattering data for $Q = (2\pi/a)(2.5,2.5,0)$ in $Rb_{0.82}K_{0.18}$. The calculated curves include a Gaussian resolution function with a width of 0.10 THz(FWHM).

in ref. 1, the discrepancy between calculated and experimental results may reflect the single-site, mean field approximations embodied in the CPA-F, which cannot describe scattering from clusters. On the other hand, inclusion of more force-constant changes within the CPA-F might improve the agreement between theoretical and experimental results. More sophisticated theoretical approaches[8] and brute force calculations for large clusters of atoms[9] may provide the answers to these questions.

---

1. W. A. Kamitakahara and J.R.D. Copley, *Solid State Div. Annu. Prog. Rep. Dec. 31, 1973*, ORNL-4952, p. 96; W. A. Kamitakahara, *Bull. Am. Phys. Soc.* 19, 321 (1974).
2. D. W. Taylor, *Phys. Rev.* 156, 1017 (1967); T. Kaplan and M. Mostoller, *Phys. Rev. B* 9, 353 (1974).
3. T. Kaplan and M. Mostoller, *Phys. Rev. B* 9, 1783 (1974).
4. T. Kaplan and M. Mostoller, *Phys. Rev. B* 10, 3610 (1974).
5. D. W. Taylor, *Solid State Commun.* 13, 117 (1973).
6. J.R.D. Copley and B. N. Brockhouse, *Can. J. Phys.* 51, 657 (1973).
7. R. A. Cowley, A. D. B. Woods, and G. Dolling, *Phys. Rev.* 150, 487 (1966).
8. Theodore Kaplan and L. J. Gray, "Off-Diagonal Disorder in Random Substitutional Alloys," this report.
9. Mark Mostoller and Theodore Kaplan, "Lattice Dynamics of Large Clusters," this report.

OFF-DIAGONAL DISORDER IN RANDOM SUBSTITUTIONAL ALLOYS

Theodore Kaplan L. J. Gray[1]

A theory for elementary excitations in random substitutional alloys with off-diagonal as well as diagonal disorder has been developed. The theory parallels Mookerjee's[2,3] treatment of alloys with diagonal disorder only. It can be divided into two parts: (1) construction of a new (nonrandom) Hamiltonian such that configuration averages in real space are equal to inner products in what we shall refer to as the augmented space and (2) evaluation of the Green's function in the augmented space by applying a recursion method[4] to the new Hamiltonian. Transformation to the augmented space (which we shall define shortly) allows one to evaluate the configurationally averaged, real-space Green's function directly by computing the

Green's function of the transformed Hamiltonian. This method has many advantages over other theories for disordered systems. Besides including off-diagonal disorder correctly, it works well in both the short and long mean-free-path regions and it generates a translationally invariant Green's function that is always analytic. The essential difference between our treatment and Mookerjee's involves writing both the diagonal and off-diagonal elements of the Hamiltonian matrix in terms of functions of an appropriate set of independent random variables and applying the transformation to the augmented space in its most general form. In general, the matrix elements of the Hamiltonian in real space must be represented by functions that involve products of Kronecker delta functions. By treating the Kronecker delta function as the limit of a exponential function, the transformation to the augmented space can be easily handled.

The theory is quite general and can be applied equally well to phonons, excitons, magnons, etc. In order to be more specific, we investigate here the electronic properties of a binary A-B alloy with a nearest-neighbor, single-band, tight-binding Hamiltonian. The Hamiltonian **H**, is given by the relation

$$\mathbf{H}_{ij} = e_i \delta_{ij} + W_{ij} . \tag{1}$$

The diagonal element e_i equals either e_A or e_B, and the off-diagonal element W_{ij} takes on the values W_{AA}, W_{BB}, or $W_{AB} = W_{BA}$ depending on the occupation of sites i and j. Also, $W_{ij} = 0$ if $i = j$ or if i and j are not nearest neighbors. The relative concentrations of the A and B constituents are denoted by c_A and $c_B = 1 - c_A$ respectively. The theory treats the diagonal element e_i as an independent random variable with probability distribution $p(e_i)$. Then W_{ij} can be written explicitly as a function of e_i and e_j as

$$W_{ij} = W_{AA}\delta(e_i, e_A)\delta(e_j, e_A) + W_{AB}\delta(e_i, e_A)\delta(e_j, e_B)$$

$$+ W_{BA}\delta(e_i, e_B)\delta(e_j, e_A) + W_{BB}\delta(e_i, e_B)\delta(e_j, e_B) . \tag{2}$$

where $\delta(e_i, e_A)$ is the Kronecker delta function.

We want to evaluate the configurationally averaged Green's function $\overline{G_{ij}(\epsilon)}$, which is given by the relation

$$\overline{G_{ij}(\epsilon)} = \int\int \cdot \cdot \int \langle \omega_i | [\epsilon \mathbf{I} - \mathbf{H}\,[\{e_k\}]]^{-1} | \omega_j \rangle$$

$$\times\, p(e_1)p(e_2) \ldots$$

$$p(e_k) \ldots de_1 de_2 \ldots de_k \ldots . \tag{3}$$

where ω_i is the vector defined such that $\mathbf{H}_{ij} = \langle \omega_i | \mathbf{H} | \omega_j \rangle$.

To construct the augmented space as described by Mookerjee,[2] proceed as follows. First, choose a Hilbert space ϕ_k, a unit vector v_0^k in ϕ_k, and a self-adjoint operator $\mathbf{M}^k$ such that

$$p(e_k) = \frac{1}{\pi} \lim_{\epsilon \to e_k + i\delta} \mathrm{Im} \langle v_0^k | (\epsilon \mathbf{I} - \mathbf{M}^k)^{-1} | v_0^k \rangle . \tag{4}$$

Such a relation can always be found for any positive, integrable function p. If the Hamiltonian is originally defined on the Hilbert space Ω, then construct a new Hilbert space which is the direct product of the spaces of the random variables and Ω. This space is the augmented space and is defined as

$$\psi = \Omega \otimes \phi_1 \otimes \phi_2 \otimes \ldots \otimes \phi_k \ldots = \Omega \otimes \Phi , \tag{5}$$

where $\otimes$ indicates the direct product. In this space, we define the operator

$$\tilde{H} = \sum_i \mathbf{P}_i \otimes \mathbf{Q}_i + \sum_{ij} \mathbf{T}_{ij} \otimes \mathbf{R}_{ij} . \tag{6}$$

where $\mathbf{P}_i$ is the projection operator onto the site i, $\mathbf{T}_{ij}$ is the projection operator onto the pair of nearest-neighbor sites i and j.

$$\mathbf{Q}_i = \mathbf{I} \otimes \mathbf{I} \otimes \ldots \mathbf{I} \otimes \mathbf{M}^i \otimes \mathbf{I} . \tag{7}$$

$$\mathbf{R}_{ij} = W_{AA}\,(\mathbf{I} \otimes \mathbf{I} \otimes \ldots \otimes \mathbf{f}_A^i \ldots \otimes \mathbf{f}_A^j \otimes \mathbf{I} \ldots)$$

$$+ W_{AB}\,(\mathbf{I} \otimes \mathbf{I} \otimes \ldots \otimes \mathbf{f}_A^i \ldots \otimes \mathbf{f}_B^j \otimes \mathbf{I} \ldots)$$

$$+ W_{BA}\,(\mathbf{I} \otimes \mathbf{I} \otimes \ldots \otimes \mathbf{f}_B^i \ldots \otimes \mathbf{f}_A^j \otimes \mathbf{I} \ldots) ,$$

$$+ W_{BB}\,(\mathbf{I} \otimes \mathbf{I} \otimes \ldots \otimes \mathbf{f}_B^i \ldots \otimes \mathbf{f}_B^j \otimes \mathbf{I} \ldots) . \tag{8}$$

and

$$\mathbf{f}_A^i = \delta(e_A \mathbf{I}, \mathbf{M}^i) , \ \mathbf{f}_B^i = \delta(e_B \mathbf{I}, \mathbf{M}^i) . \tag{9}$$

The superscript i on $\mathbf{M}^i$ and $\mathbf{f}^i$ indicates that these operators appear in the same position in the direct-product definitions of $\mathbf{Q}_i$ and $\mathbf{R}_{ij}$ as ϕ_i appears in the definition of Φ given in Eq. (5). For a binary alloy, each ϕ_k has dimension 2 and

$$\mathbf{M} = \begin{bmatrix} a & b \\ b & c \end{bmatrix} . \tag{10}$$

where

$$a = \epsilon_A c_A + \epsilon_B c_B ,$$
$$b = (\epsilon_A - \epsilon_B)\sqrt{c_A c_B} ,$$
$$c = \epsilon_A + \epsilon_B - a ,$$
$$v_0 = \begin{bmatrix} 1 \\ 0 \end{bmatrix} .$$

We approximate the Kronecker delta as the limit as $\sigma \to 0$ of the exponential

$$\delta(\epsilon_A I, W) = f_A{}^I = \lim_{\sigma \to 0} \exp(-(\epsilon_A I - W)^2/\sigma^2) \quad (11)$$

and find that

$$f_A = \begin{bmatrix} c_A & \sqrt{c_A c_B} \\ \sqrt{c_A c_B} & c_B \end{bmatrix} , \quad f_B = \begin{bmatrix} c_B & -\sqrt{c_A c_B} \\ \sqrt{c_A c_B} & c_A \end{bmatrix} . \quad (12)$$

In the augmented space formalism we then have

$$\overline{G_{ij}(\epsilon)} = \langle \omega_i \otimes \gamma_0 | (\epsilon I - \tilde{H})^{-1} | \omega_j \otimes \gamma_0 \rangle . \quad (13)$$

where

$$\gamma_0 = v_0{}^1 \otimes v_0{}^2 \otimes \ldots v_0{}^k \otimes \ldots . \quad (14)$$

We have defined the augmented space and the relation between the averaged Green's function and the matrix elements in this new space. Everything to this point is exact. The approximation is introduced when the Green's function in the augmented space is evaluated. We choose to use the recursion method of Haydock, Heine, and Kelly[4] as did Mookerjee in his theory for diagonal disorder. This method generates a continued-fraction approximation to the Green's function. The accuracy of the approximation is determined by the number of levels of the continued fraction which are evaluated exactly. For n levels the contributions from the first $2n$ moments are included exactly, while the effects of larger moments are approximated as a background effect. This method is particularly attractive since it always generates an analytic Green's function.

As an example, we have calculated the density of states of a one-dimensional binary alloy with $\epsilon_A = 2.5$, $\epsilon_B = -2.5$, $W_{AA} = 0.5$, $W_{AB} = W_{BA} = 0.5$, $W_{BB} = 1.0$, and $c_A = c_B = 0.5$ using the augmented space theory with a recursion level of 9. The results of these calculations are shown in Fig. 1.5, where they are compared with essentially exact results obtained using the Schmidt method.[5] Note that with only 9 levels in the recursion approximation, the theory agrees reasonably well with the exact results, even for this split-band case. The theory correctly predicts some of the major peaks in the density of states and approximately matches the unequal band widths of the two bands. For a similar three-dimensional system, the exact density of states is considerably smoother, and even fewer levels in the recursion method should be needed.

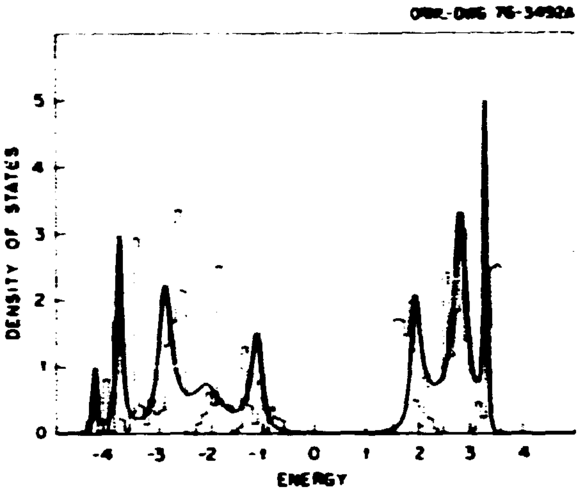

Fig. 1.5. Calculation of the density of states by the augmented space theory with a recursion level of 9 (smooth line) and exact results (histogram) for a one-dimensional electronic alloy with $\epsilon_A = -\epsilon_B = 2.5$, $W_{AA} = 0.5$, $W_{AB} = W_{BA} = 0.8$, $W_{BB} = 1.0$, and $C_B = 0.5$.

One final comment is necessary. Mookerjee[6] has also attempted to include off-diagonal disorder using the augmented space formalism. As he noted himself, he failed to include the correlations between sites correctly. He simply replaced the hopping integrals randomly and thus neglected the fact that if site i contains an A atom, then W_{ij} must equal W_{AA} or W_{AB} for all j coupled to i. Similarly if site i contains a B atom, W_{ij} must be W_{BA} or W_{BB}. The theory we have presented here properly accounts for these correlations between sites.

---

[1] Computer Sciences Division, UCC-ND.

[2] Abhijit Mookerjee, *J. Phys. C* **6**, L205 (1973).

[3] Abhijit Mookerjee, *J. Phys. C* **6**, 1340 (1973).

[4] R. Haydock, V. Heine, and M. J. Kelly, *J. Phys. C* **8**, 2591 (1975).

[5] H. Schmidt, *Phys. Rev.* **105**, 425 (1957).

[6] Abhijit Mookerjee, *J. Phys. C* **8**, 2943 (1975).

LATTICE DYNAMICS OF LARGE CLUSTERS

Mark Mostoller Theodore Kaplan

When analytical theories cannot adequately describe the vibrational properties of alloys, it is sometimes possible to use large cluster calculations to model these properties directly. However, despite the size and speed of present computers, relatively special techniques must still be sought in order to treat sufficiently large clusters that is, clusters comprising hundreds or even thousands of atoms. One technique that has been used successfully by Haydock, Heine, and Kelly[1] to treat the electronic properties of alloys is the recursion method. This is a form of a technique originally devised by Lanczos.[2] Using the recursion method, we are able in principle to calculate any desired elements of the displacement-displacement Green's function in the cluster.

At present we are investigating the speed and accuracy of the recursion method for simple cubic, fcc, and bcc crystals. A particular system of interest is the metallic alloy K_cRb_{1-c}. Calculations based upon the coherent potential approximation (CPA) do not yield results in satisfactory agreement with the neutron scattering studies of these alloys performed at ORNL, even when force constants are included within the CPA framework in the manner proposed by the authors.[3,4] It is hoped that by studying large cluster models, we may be able to gain some added insight by accounting for those variations in the force constants and those multi-site scattering correlations which the CPA does not include.

Results of one of our typical cluster calculations are shown in Fig. 1.6. The curve plotted is the density of states at the central site of a 259-atom cluster, averaged over ten randomly generated cluster configurations, for a nearest-neighbor force model of $K_{0.18}Rb_{0.82}$ (nominal concentration). The sharpness of the structure in Fig. 1.6 is in part due to the relatively small cluster size, and to the small number of configurations averaged over.

It is hoped that the recursion method will enable us to evaluate neutron scattering cross sections, but it is not known at present how well suited this method is for such calculations. Another technique which may be preferable for neutron scattering calculations is the equation-of-motion method, which has been used by Alben et al.[5] to calculate electronic spectral density functions for large clusters. This method is also under investigation.

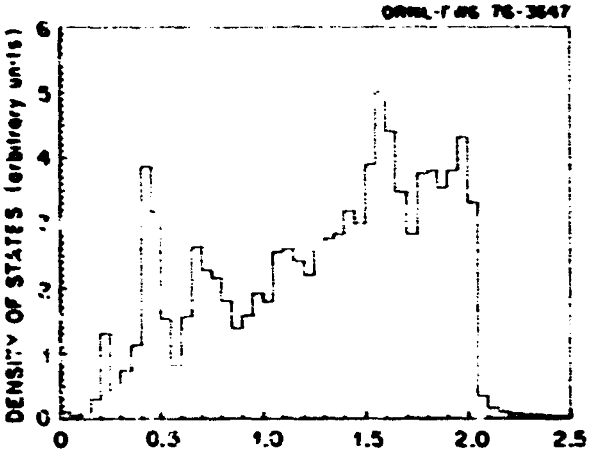

Fig. 1.6. Density of states at the central site of a 259-atom cluster of K_cRb_{1-c} averaged over ten randomly generated cluster configurations with an average concentration of c = 0.18.

---

[1] R. Haydock, V. Heine, and M. J. Kelly, *J. Phys. C* 8, 2591 (1975).

[2] J. H. Wilkinson, *The Algebraic Eigenvalue Problem*, Clarendon Press, Oxford, 1965.

[3] T. Kaplan and M. Mostoller, *Phys. Rev. B* 9, 1783 (1974).

[4] Mark Mostoller and Theodore Kaplan, "Lattice Vibrations in $Rb_{1-c}K_c$ Alloys in the Coherent Potential Approximation," this report.

[5] R. Alben, M. Blume, H. Krakauer, and L. Schwartz, *Phys. Rev. B* (in press).

NEUTRON SCATTERING FROM COMPLEX DEFECTS IN SOLIDS: SELF-INTERSTITIALS IN FCC METALS

R. F. Wood Mark Mostoller

When an atom enters a crystal as a substitutional impurity, it perturbs the phonons of the host material. If the impurity atom is lighter than the atom it replaces, or if it is much more stiffly coupled to its neighbors in the lattice, the impurity vibrations may be local modes, with frequencies above the maximum frequency of the host crystal. A heavy impurity, or one that is more loosely coupled to its neighbors, may give rise to resonant modes with frequencies within the phonon spectrum of the host. Local or resonant modes of simple substitutional impurities can be observed by inelastic neutron scattering at impurity concentrations of a few percent.

If a molecule, or molecular-like complex rather than an atom, is introduced substitutionally into a crystal, the center of mass perturbs the host phonons in the same way as a simple atomic impurity. In addition, however, a molecular impurity may have internal vibrational, rotational, or librational degrees of freedom, and these internal modes can produce effects not found for simple defects. Specifically, the internal modes of complex substitutional defects may hybridize strongly with lattice modes of the same symmetry if the impurity mode frequencies lie within the host phonon band. The theory of this hybridization can be developed in a form similar to localized perturbation theory for substitutional defects but with a resonant perturbation, that is, one which involves an energy denominator $(\omega^2 - \omega_0^2)$ which becomes large in the immediate neighborhood of the resonant frequency ω_0.[1] Through their resonant hybridization with the lattice modes, the internal modes of complex substitutional impurities may be observed by neutron scattering at impurity concentrations orders of magnitude smaller than that required for simple atomic impurities.[2-5] Several examples of complex defects in solids recently have been studied and currently are being studied in the Solid State Division. Here we will discuss the theoretical work on the ⟨100⟩-split or dumbbell interstitials in copper and aluminum; two other systems will be considered in the following two contributions to this annual report.[6,7]

At low temperatures, the stable configuration for self-interstitials in copper and aluminum appears to be the ⟨100⟩-split configuration, in which the interstitial and a host atom form a dumbbell centered at a normal lattice site and oriented along a cubic axis. The librational modes of the dumbbell are expected to be quite low in frequency[8] and to undergo resonant hybridization with the lattice modes; thus they should be observable by coherent inelastic neutron scattering.[2,3] In experiments performed last year at ORNL, unusual structure and a resonance-like frequency shift were found in the coherent scattering cross section of a neutron-irradiated copper crystal at very low temperatures.[5] However, the structure did not vary as expected with changes in the wave vector, and neither effect was completely removed by annealing at 300°K, where, it has been thought, single interstitials are no longer stable.

Several approaches are being pursued in an effort to explain some of the unexpected features of these experimental results. One approach is to include the experimental resolution function in the calculations, and preliminary results indicate that this may have a significant effect although it seems unlikely that it can explain all of the discrepancies between theory and experiment. Another approach is to use simple models to mock the effects that modified interstitials, di-interstitials, or other interstitial complexes might produce. We have further developed our computer programs to include the effects of two resonant denominators in the perturbation matrix. It was not immediately obvious how to do this, but the present state of alloy theory indicates that a suitable approximation for the situations envisaged here is to write the self-energy, Σ, as a concentration-weighted average of the two t matrices; that is,

$$\Sigma = c_1 t_1 + c_2 t_2 . \tag{1}$$

The concentrations of those defects which have resonance denominators $(\omega^2 - \omega_{0\,1}^2)$ and $(\omega^2 - \omega_{0\,2}^2)$ are c_1 and c_2, and t_1 and t_2 are the corresponding t-matrices for the individual scattering-hybridization processes. Calculations within this approach show that complicated patterns for the shift of the phonon frequencies can occur: Fig. 1.7 illustrates one such case.

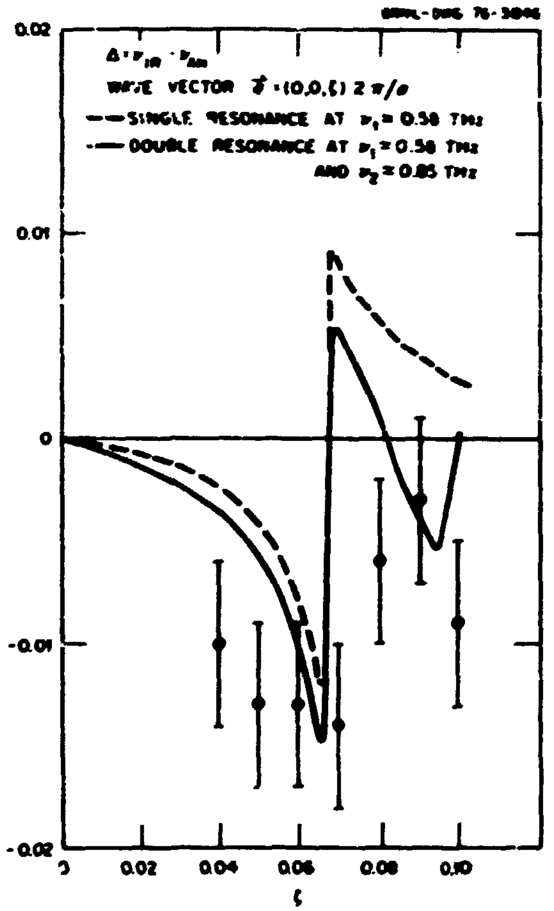

Fig. 1.7. Frequency shifts as a function of wave vector. The lines are calculated, and the points are measured shifts. The frequency is ν_{IR} when the interstitials are present, that is, after the crystal has been irradiated; ν_{AN} is the frequency after annealing out the interstitials.

Although we could continue calculations of this nature, the number of parameters involved in the model and the degree of accuracy of the experimental data make it unwise to carry out extensive new calculations until further experiments can be undertaken.

THEORY OF NEUTRON SCATTERING FROM PHONONS IN KCl:CN$^-$

R. F. Wood Mark Mostoller

Cyanide ion impurities in the alkali halides appear to behave as hindered rotators rather than as fixed librators (as the ⟨100⟩-split interstitials in copper and aluminum might be described). In the cubic crystal fields of the alkali halides, the rotational ground state is a tunnel-split multiplet involving the eight equivalent ⟨111⟩ orientations of the CN$^-$ ions, and the lowest excited states are coupled to this tunnel-split ground state by low-frequency phonons of the host crystal. In the first neutron scattering experiments carried out for the purpose of observing the resonant mixing of impurity internal modes with lattice modes, Walton, Mook, and Nicklow[1] reported striking new structure in the one-phonon coherent cross section of KCl doped with CN$^-$ ion impurities. This is shown in Fig. 1.8.

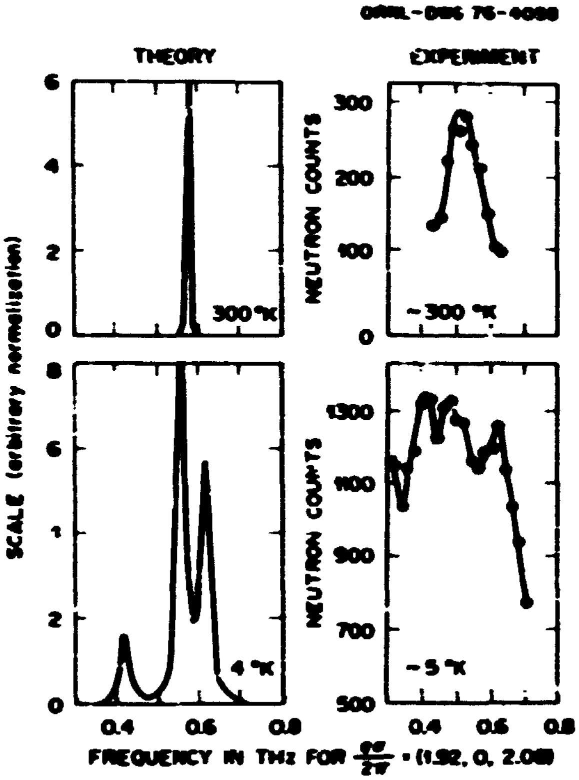

Fig. 1.8. Comparison of theory and experiment for the coherent neutron scattering cross section from KCl:CN$^-$. The theoretical evaluation was intended for illustrative purposes only, and optimum agreement with experiment was not sought. Also, the theoretical curves have not been convoluted with an instrumental resolution function.

We have performed simple model calculations, based on extensions of Klein's two-level theory for such systems,[2] which give qualitative agreement with the experimental results of Walton, Mook, and Nicklow. These calculations could easily be refined to obtain information about the coupling of the CN$^-$ ion impurities to their neighbors in the lattice if more experimental data were available. The original experiments were intended only to show that the resonance hybridization effect does occur, and additional experiments have not yet been carried out. It is not clear that such experiments should have a high priority on the Division's list of neutron scattering studies since other, similar systems may be of more immediate interest. The theory of resonance hybridization effects in KCl:CN$^-$ differs somewhat from the theory for the self-interstitial in copper and aluminum. The reasons for this are too involved to discuss here, but the most notable result is that the perturbed Green's functions become strongly dependent on the temperature. The results of Walton, Mook, and Nicklow clearly show this sensitivity to temperature in that the structure introduced by the resonance hybridization is present at 4°K but has disappeared at 300°K. Our calculations are based on a model in which resonance scattering of phonons occurs by way of virtual transitions to two excited states of the hindered rotator. The t-matrix is written in the form of Eq. (1) of the preceding contribution to this report,[3] and the Green's functions

---

1. M. Wagner, *Phys. Rev. A* 133, 750 (1964); M. V. Klein, *Phys. Rev.* 186, 839 (1969).

2. R. F. Wood and Mark Mostoller, *Phys. Rev. Lett.* 35, 45 (1975).

3. H. R. Schober, V. K. Tewary, and P. H. Dederichs, *Z. Phys.* B21, 255 (1975).

4. D. Walton, H. A. Mook, and R. M. Nicklow, *Phys. Rev. Lett.* 33, 412 (1974).

5. R. M. Nicklow, R. R. Coltman, Jr., F. W. Young, Jr., and R. F. Wood, *Phys. Rev. Lett.* 35, 1444 (1975); also, "Neutron Inelastic Scattering Measurements of Phonon Perturbations by Defects in Irradiated Copper," this report.

6. R. F. Wood and Mark Mostoller, "Theory of Neutron Scattering from Phonons in KCl:CN$^-$," this report.

7. R. F. Wood and Mark Mostoller, "Neutron Scattering from Interstitials in AgCl and AgBr at High Temperatures," this report.

8. P. H. Dederichs, C. Lehmann, and A. Scholz, *Phys. Rev. Lett.* 31, 1130 (1973).

are made temperature dependent in the manner prescribed by Klein for the case in which only one excited state is involved. The concentrations c_1 and c_2 in Eq. (1) are assumed to be the same. From the way in which they enter the theory, they should be considered as "effective concentrations" since transition probabilities are implicitly included in them. We have, in effect, assumed that both the concentration and the transition probabilities are the same for the two levels. Figure 1.8 shows the results of our calculations when ω_{01} = 1.64 THz, ω_{02} = 1.71 THz, and $c_1 = c_2$ = 0.0018. Clearly the calculations give the same behavior as that observed experimentally; however, we have made no attempt to fit the experimental results carefully, and we have not included instrumental resolution effects.

It is interesting to observe here that had the utility of neutron scattering for this type of measurement been realized earlier, the long-standing controversy over the orientation of the CN$^-$ molecule in KCl could probably have been resolved much earlier. Even at the time Walton, Mook, and Nicklow did their work, it was believed that the CN$^-$ molecule had potential minima along the ⟨110⟩ directions. Although this controversy now seems to have been resolved for KCl:CN$^-$, there are undoubtedly similar systems that could benefit from neutron scattering studies.

---

1. D. Walton, H. A. Mook, and R. M. Nicklow, *Phys. Rev. Lett.* 33, 412 (1974).
2. M. V. Klein, *Phys. Rev.* 186, 839 (1969).
3. R. F. Wood and Mark Mostoller, "Neutron Scattering from Complex Defects in Solids: Self-Interstitials in FCC Metals," this report.

NEUTRON SCATTERING FROM INTERSTITIALS IN AgCl AND AgBr AT HIGH TEMPERATURES

R. F. Wood   Mark Mostoller

Many of the silver halides exhibit anomalies in their high-temperature physical properties which seem to be associated with an abnormally large number of Frenkel defects just below the melting point.[1] In AgBr at 400°C (T_M = 422°C), for example, the concentration of Ag$^+$ ions in interstitial positions is approximately 2%. These ions are believed to move through the lattice by a so-called interstitialcy mechanism in which the interstitial ion moves on to a normal lattice site by displacing the ion previously at that site into an interstitial position. This is in contrast to a motion in which the interstitial ion migrates from one interstitial site to another without displacing lattice ions. Uncertainty about the nature of the mechanism of ionic migration is increased by the results of calculations by Hove[2] which suggest that a Ag$^+$ ion is not in its most stable configuration at any normal interstitial site of the NaCl structure but pairs with a Ag$^+$ ion at a lattice site to form a dumbbell interstitial oriented in a ⟨111⟩ direction. The same calculations suggest that the translational motion of the dumbell along the ⟨111⟩ direction (so-called "collinear interstitialcy motion") has a very low activation energy, the motion in which the dumbbell changes from one to another ⟨111⟩ orientation has a somewhat higher activation energy, and the direct interstitial migration has a very high energy. The results of these calculations were published in 1956, and high accuracy cannot be ascribed to them. Nevertheless, the calculations together with the anomalies in various physical properties are suggestive of a situation resembling that for self-interstitials in copper and aluminum.

We have been carrying out the group theoretical analysis of the ⟨111⟩ dumbbell in AgCl and AgBr. The symmetry about the dumbbell axis is D_{3d}, and the symmetry coordinates of the dumbbell and its six first-nearest-neighbor ions have been constructed in this representation. Since the symmetry coordinates normally used for O_h symmetry are written with the ⟨100⟩ directions as the principal axes of rotation, a transformation between the two sets of symmetry coordinates for the first-nearest-neighbor halide ions must be carried out. This group theoretical work is tedious and time consuming but is an essential part of the problem. It is now substantially completed, and after further checking, the computer program for calculating the Green's functions, t-matrices, etc., will be constructed and the coherent inelastic neutron scattering cross section computed. This part of the calculation should proceed rapidly since it involves only relatively minor changes in already existing computer programs.

The apparent similarities between the Ag$^+$ dumbbell interstitial in the silver halides and self-interstitials in fcc metals are intriguing. However, enough differences exist to make one wary of confidently predicting success for neutron scattering experiments on the resonant hybridization of internal and lattice modes in AgCl and AgBr. The most obvious difference is that the number of interstitials in silver halides is a sensitive function of the temperature. Near the melting point of AgBr, there are many more interstitials present than in thermal-neutron-irradiated copper at 4°K, but the temperature dependence of the phonons and the high degree of anharmonicity in the silver halides at elevated temperatures may mask the interaction of the internal and lattice modes. On the other hand, if hybridization effects can be observed in AgBr or AgCl, it may point the way to studies of superionic conductivity and high-temperature phase transitions by way of neutron scattering experiments.

---

1. See, for example, D. S. Tannhauser, L. J. Bruner, and A. W. Lawson, *Phys. Rev.* 102, 1276 (1956); Robert J. Friauf, *J. Appl. Phys. Suppl.* 33, 494 (1962); K. F. Loje and D. E. Schuele, *J. Phys. Chem. Solids* 31, 2051 (1970).
2. John E. Hove, *Phys. Rev.* 102, 915 (1956).

PARTICLE-SOLID INTERACTIONS

ENERGY LOSS ASSOCIATED WITH THE PROPAGATION OF ATOMIC COLLISION SEQUENCES ALONG LATTICE ROWS

D. K. Holmes M. T. Robinson

There is a continuing controversy over the role played by correlated collision sequences in the production of radiation damage. The present study is an attempt to establish limits to the lengths of such sequences, since some current ideas suggest extreme sequence lengths of hundreds of atoms. It is also of interest to compare the results of improved calculations with the MARLOWE cascade simulation program, for which the basic binary collision approximation is unreliable in the low energy range of interest for these collision sequences.

The calculational method used for this study is the Small Atomic Group Program (SAGP). This program accurately computes the classical trajectories of small groups of atoms in motion and can thus be set up to represent the transfer of momentum down a lattice row in the presence of close neighboring atoms. It is the energy loss to these neighboring atoms which limits the final length of collision sequences, and it is also just such losses that are poorly calculated in the binary collision approximation. The interaction potential has been taken to be the Molière or the Born–Mayer with parameters chosen to represent copper.

Table 1.1 gives some typical values for energy losses (as calculated by the SAGP) to rings of neighboring atoms for the ⟨110⟩ row in the perfect (no thermal vibrations) fcc lattice. The loss ΔE_1, to the ring alone, agrees fairly well with MARLOWE and quite well with the calculations of Andersen and Sigmund.[1] The more realistic losses ΔE_2 are larger because of the slowing down of the moving atom in the region of the ring, and they agree well with the results of Dederichs and Leibfried[2] and of Gibson et al.[3] Losses, ΔE_2, in the ⟨100⟩ and ⟨111⟩ directions have also been calculated by the SAGP, and they are much larger, as shown in Table 1.2 (to be discussed later). The E_2 losses are greatly underestimated by MARLOWE.

Table 1.1. Energy losses to rings of neighboring atoms per step of ⟨110⟩ sequences (copper, Molière potential)

E_0(eV) (primary energy)	ΔE_1(eV) (loss to the ring alone)	ΔE_2(eV) (loss to the ring with the next chain atom present)
5	0.46	0.61
10	0.28	0.68
20	0.16	0.66
50	0.07	0.53
100	0.03	0.40

For the Molière potential, the SAGP shows that the moving atom fails to break through the ring of neighbors below a certain "penetration energy" E_p. E_p is found to have the values (Molière potential) 14 eV for the ⟨110⟩ direction, 10 eV for the ⟨100⟩ direction, and 40 eV for the ⟨111⟩ direction. Below these energies, only momentum is transferred down the row; the replacement process ceases. The energy transferred may still be significant, amounting to 95% in the ⟨110⟩ case.

Another quantity of interest is the focusing energy E_F, which is defined as that energy below which the angular deviation of the motion from the lattice row decreases from step to step down the chain. In Table 1.2 these energies are given as calculated by the SAGP, both for the "bare" row $E_F^{(1)}$ of atoms and also with the rings of neighboring atoms $E_F^{(2)}$. The presence of rings steers the moving atom back toward the row, and the resultant effect is called "assisted focusing." Thus the quantity $[E_F^{(2)} - E_p]/\Delta E_2[E_F^{(2)}]$ is some measure of the minimum number of replacement collisions to be expected in a collision chain. This ratio is also given in Table 1.2.

These results of the SAGP can be used to improve the calculations of MARLOWE. In a given 400-eV radiation damage cascade in copper, the MARLOWE program will show a certain number of long replacement sequences. Using the results of the SAGP, such sequences can be corrected to more realistic, shorter lengths. Averaging over 1000 different cascades, the following results are obtained for the numbers of replacement events to be expected:

Isolated replacements	8.4
Replacements in pairs	7.0
Replacements in sequences of three or more atoms	15.0
(Number of sequences 3 atoms long or longer)	(3)
Total number of replacements	30.4

Table 1.2. Focusing energies in copper (Molière potential)

Type of row	$E_F^{(1)}$ (unassisted) (eV)	$E_F^{(2)}$ (assisted) (eV)	Energy loss to the ring at $E_F^{(2)}$ (eV)	$\frac{E_F^{(2)} - E_p}{\Delta E_2[E_F^{(2)}]}$
⟨110⟩	13	17	0.67	4.5
⟨100⟩	1	20	4.8	2.1
⟨111⟩	0.002	225	13.2	14.0[a]

[a] Actually, a value of 10 is better for the ⟨111⟩ direction because of the significant rise in ΔE_2 as the energy falls from $E_F^{(2)}$ to E_p.

Almost all the long sequences are of the ⟨110⟩ type, and only under extremely favorable conditions can a sequence be found to travel 50 atomic distances, even allowing for an initial defocusing portion and a final "momentum transfer only" portion (down to 2 eV).

A further consideration in the shortening of collision chains is the presence of thermal vibrations. The SAGP has not been adapted to include these; so the calculations have been performed using MARLOWE. Thus the influence of the neighboring rings has not been so well evaluated (for some consideration of this point, see Sanders and Fluit[4]), but the result of the displacement of chain atoms from their proper positions has been emphasized. In general, thermal vibrations tend to deflect the collision sequence off the perfect lattice direction, with consequently greater energy losses, while the focusing tendency at lower energies may partially compensate for this effect. (These points have been discussed with analytical calculations and computer simulation by Nelson, Thompson, and Montgomery,[5] by Pugacheva,[6] and by Agranovich and Kirsanov.[7]) The MARLOWE program allows the introduction of thermal vibrations, and the procedure is to perform many calculations of the collision chain length at a given temperature and to average over the results. The distribution of lengths turns out to be broad and skewed.

The result for the reduction in average sequence length with increasing amplitude of thermal vibration is shown in Fig. 1.9. In the figure, the average sequence length is plotted against the reciprocal of the root-mean-square (rms) of the amplitude of the thermal vibration, expressed in units of the lattice parameter. (To make the comparison more evident, zero-point vibrations in copper would correspond to an rms amplitude of $\frac{1}{100}$ of a lattice distance.) The sequences averaged for the results of Fig. 1.9 are ⟨110⟩ sequences in copper started at 25 eV and terminated at 10 eV. For this case the MARLOWE program gives a length of

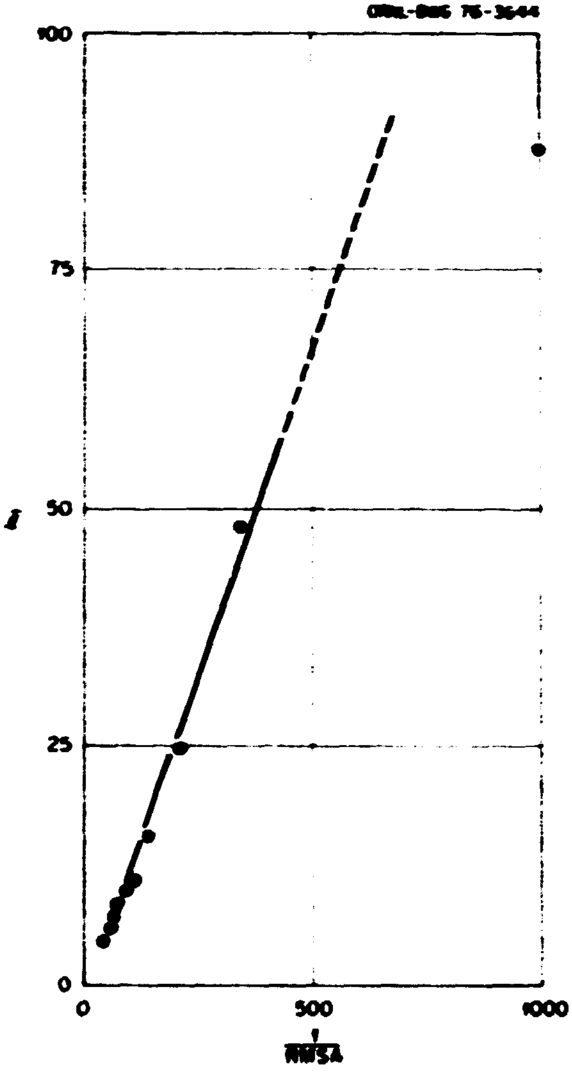

Fig. 1.9. The variation of the average sequence length $\bar{l}$ (measured in number of atoms) with 1/rmsA, the reciprocal of the root-mean-square amplitude of thermal vibrations (in units of the lattice parameter).

104 atoms in the perfect, static lattice. The results given show that even zero-point vibrations will reduce this value to ten chain distances.

It may be seen on this plot that at high amplitudes of thermal vibrations there is some tendency for the average length to vary linearly. The particular form of the plot was chosen as a result of a suggestion by Thompson and Buck[8] that sequence lengths might decrease as the reciprocal of the square root of the absolute temperature increases.

In conclusion, it must be pointed out that the effects of thermal vibrations, along with large energy losses to rings of neighbors, severely limit the expected lengths of all correlated collision sequences. The present calculations would seem to indicate that (at least in copper) sequences longer than 5–10 atomic distances are improbable.

---

1. H. H. Andersen and P. Sigmund, *K. Dan. Vidensk. Selsk., Mat.-Fys. Medd.* **34**, No. 15 (1966).
2. P. H. Dederichs and G. Leibfried, *Z. Phys.* **170**, 320 (1962).
3. J. B. Gibson, A. N. Goland, M. Milgram, and G. H. Vineyard, *Phys. Rev.* **120**, 1229 (1960).
4. J. B. Sanders and J. M. Fluit, *Physica* **30**, 129 (1964).
5. R. S. Nelson, M. W. Thompson, and H. Montgomery, *Philos. Mag.* **7**, 1385 (1962).
6. T. S. Pugacheva, *Sov. Phys. Solid State* **9**(1), 75 (1967).
7. V. M. Agranovich and V. V. Kirsanov, *Sov. Phys. Solid State* **12**(9), 2147 (1971).
8. D. O. Thompson and O. Buck, *Phys. Status Solidi* **37**, 53 (1970).

EFFECT OF CORRELATIONS IN THERMAL VIBRATIONS ON COMPUTER SIMULATION OF ION–SOLID INTERACTIONS

John H. Barrett   D. P. Jackson[1]

In computer simulation of ion–solid interactions, it is often important to include the effects of thermal vibrations. The only method that has been utilized in the past is one in which each atom in the solid is treated as if it vibrated independently of each of its neighbors. Although this approximation is much better than assuming a rigid lattice, there is some question about what effect correlations in the vibrations may have. Jackson, Powell, and Dolling[2] have calculated a set of correlations from a seventh-neighbor Born–von Kármán tensor model which was fitted to experimental phonon dispersion relations for molybdenum.[3] A method has been devised to use such a set of correlations together with a random number generator and appropriate matrix operators to produce as extensive a set of properly correlated lattice vibrations as needed for computer simulation purposes. A very large number of such sequences has been generated and their correlations checked in order to verify that the correct degree of correlation is being produced by this method. By fitting a suitable analytical expression to the results obtained from the Born–von Kármán model, it appears possible to extend the range of correlations with accuracy, if desired. Consideration has been given to minimizing computational time by expressing the required matrix operations in the most efficient form and by utilizing look-up methods in computer-stored tables.

Minimum yield and surface yield in channeling are quantities that have been shown to be strongly dependent on thermal vibrations. So the first test of the effects of correlations will be to utilize the results of Jackson, Powell, and Dolling[2] in calculating these two quantities for molybdenum both with and without correlations.

---

[1] Chalk River Nuclear Laboratories, Atomic Energy of Canada Limited, Chalk River, Ontario, Canada.

[2] D. P. Jackson, B. M. Powell, and G. Dolling, *Phys. Lett.* **51A**, 87 (1975).

[3] B. M. Powell, P. Martel, and A.D.B. Woods, *Phys. Rev.* **171**, 727 (1968).

INVESTIGATION OF INTERSTITIAL CONFIGURATIONS BY ION CHANNELING

John H. Barrett

Channeling has been used for many years to locate positions of impurity atoms in solids. More recently, this technique has been used to study interstitials trapped at impurities.[1] Use of axial channeling is more convenient in such studies because acceptance angles are large and minimum yields are small. However, use of planar channeling has frequently been found to be more powerful in deciding between different possible configurations. Because of the power of planar channeling demonstrated in several studies, an exploration was made of ways in which the sensitivity of planar channeling measurements could be increased sufficiently so that self-interstitials at attainable concentrations might be observable. A handicap is that the usual measurements of planar minimum yield give a value of about 0.2, whereas the axial value may be as low as 0.01. The use of double alignment results in each case in values that are approximately the squares of those just given. A further reduction in the planar case can be made by taking advantage of the depth dependence, which, for ions that are incident parallel to the plane of the channel, consists of a large peak at the surface, followed by a series of damped oscillations as depth increases. If good depth resolution is used to select the depth at which the first minimum occurs for parallel incidence, one can have a single-alignment yield of 0.04 or less and a double-alignment yield of 0.001 or less. Flux peaking may be expected to enhance the yield from the interstitial atoms so that concentrations of approximately 10^{-4} and perhaps even somewhat less might be observable. Such concentrations of self-interstitials, though large, are probably attainable.

In pursuing these possibilities further, a hybrid approach has been taken, based on the assumption that relaxations in and around a defect are about the same for similar metals when expressed as fractions of a lattice constant. The fractional relaxations calculated by Doyama and Cotterill[2] for copper have been applied to gold, for which some related calculations were being done for other reasons. Positions in the (111) channel of the atom(s) that make up an interstitial and for some of the neighboring atoms with large relaxations are shown in Fig. 1.10 for three of the configurations considered by Doyama and Cotterill. An existing computer program for simulating channeled ion trajectories was used to calculate the probability for ion backscattering from the atoms in and near the interstitial as well as from the undisturbed lattice; results are shown in Fig. 1.11. It may be noted that the yields are in accordance with the estimates made above. Results were also obtained for the (002) and (022) channels but are not shown because the contrasts between yield patterns for different configurations were less marked than those for the (111) channel. For all three planes the crowdion tended to have the most uniform distribution of displaced atoms across the channel, which led to a rather featureless increase in yield at all angles. The other two configurations, particularly the body centered one, feature more distinctive groupings of displaced atoms resulting in more distinctive variations of yield with angle. Proximity of the peaks in Fig. 1.11 to a zero angle can be correlated with the proximity of the atoms producing them to the center of the channel in Fig. 1.10.

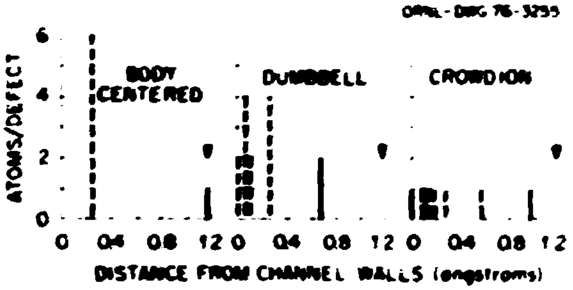

Fig. 1.10. Number of displaced atoms at various locations in the (111) channel for different interstitial configurations in gold. Solid lines identify the central atom(s) of each configuration, and broken lines indicate other displaced atoms. Arrows mark the channel center on each plot.

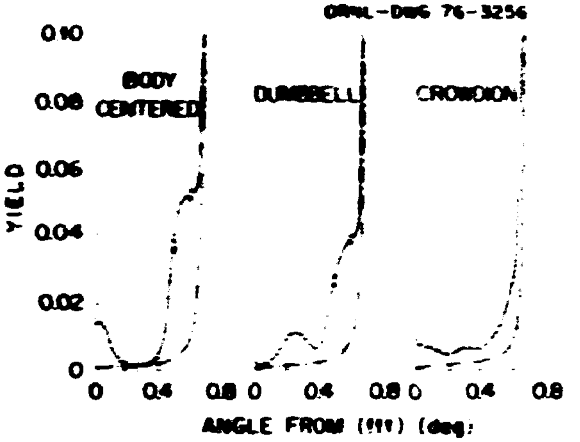

Fig. 1.11. Angular variation of double-alignment backscattering yield for 1-MeV helium in gold. Points and solid lines represent interaction with defects and the distorted lattice with the various interstitial configurations present in a concentration of 10^{-2}; broken lines indicate the perfect lattice. The yield is normalized to unity for a random direction and is taken at the depth of the first minimum in the yield at 0°.

The three sections of Fig. 1.11 appear to be distinctively different. Also, it appears that some estimate of magnitudes of displacements would be possible. However, 10^{-2} is such a high defect concentration that one would worry about the coalescence of a sizable fraction of the defects into clusters. From Fig. 1.11 it would appear possible to observe interstitial concentrations as low as $(2-5) \times 10^{-3}$ but no lower. Another problem with the technique described above is that a depth resolution of 10–20 Å would be required; such resolution is attainable, but far from routine.

Since use of planar channeling encounters problems associated with high defect levels and achievement of adequate depth resolution, it is desirable to explore what can be done using axial channeling. Preliminary considerations suggest that backscattering using axial double alignment will definitely allow observation of interstitials down to concentrations of 10^{-4} with a depth resolution of 100–200 Å and with the possibility of achieving even greater sensitivity.

Calculations have also been done to see whether computer simulation can yield a more accurate analysis than the analytical theory of channeling does for the experiments on interstitials trapped at impurity atoms.[1]

First results indicate that simulation will allow considerably more precise determination of the displacement of an impurity as a consequence of its having trapped an interstitial.

---

1. M. L. Swanson, F. Maury, and A. F. Quenneville, *Phys. Rev. Lett.* 31, 1057 (1973). M. L. Swanson and F. Maury, *Can. J. Phys.* 53, 1117 (1975).

2. M. Doyama and R.M.J. Cotterill, p. 79 in *Lattice Defects and Their Interactions*, ed. by R. R. Hasiguti, Gordon and Breach, New York, 1967.

ENERGY DISTRIBUTIONS AND RANGES OF PRIMARY RECOILS RESULTING FROM HIGH-ENERGY *d*–Be NEUTRONS IN NIOBIUM AND GOLD[1]

J. B. Roberto M. T. Robinson C. Y. Fu[2]

The use of high-energy neutrons from the deuteron-breakup reaction presents an attractive possibility for simulating the 15-MeV component of a fusion reactor neutron spectrum. The deuteron-breakup scheme offers definite advantages in flux and experimental volume over other proposed sources but it is characterized by an energy spectrum that is very broadly peaked near 15 MeV compared with the monoenergetic distribution characteristic of *d*–*t* fusion. We have investigated the effect of this broad energy spectrum on the resulting primary recoil energy distributions in niobium and gold and have correlated the results with experimental measurements of the ranges of primary recoils resulting from high-energy (*n*,2*n*) reactions using the Oak Ridge *d*–Be neutron source.

The primary recoil spectra were computed using techniques described in the following article of this report.[3] The results of the calculations for monoenergetic 15-MeV neutrons and *d*–Be neutrons (broadly peaked near 15 MeV) are shown for niobium in Fig. 1.12. Although the neutron spectra are very different for the two cases, the resulting recoil energy distributions are quite similar, each dominated by elastic scattering at lower recoil energies, with a broad shoulder due to nonelastic interactions at higher energies. It is interesting to note that the *d*–Be neutrons produce a recoil spectrum that is softer than a 15-MeV spectrum over much of the range of high-energy recoils, even though there are significant numbers of *d*–Be neutrons above 15 MeV. These higher energy neutrons, however, tend to produce relatively fewer high-energy recoils since the nonelastic scatterings are spread over a wider range of possible recoil energies. The overall results are similar for gold and indicate that spectral differences between pure 15-MeV neutrons and deuteron-breakup neutrons peaked at the same energy are not strongly reflected in the corresponding primary recoil distributions.

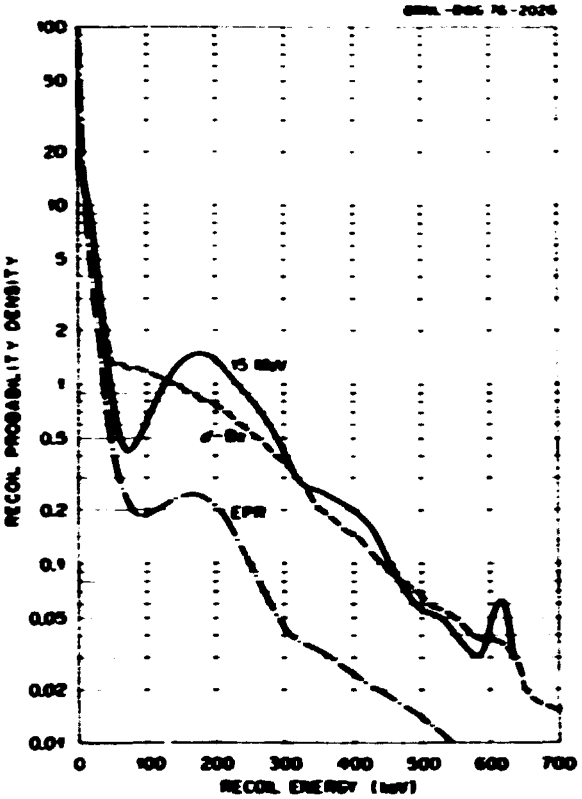

Fig. 1.12. Calculated primary recoil spectra for 15-MeV and *d*–Be neutrons in niobium. The curve labeled EPR is a recent estimate of the recoil spectrum for a niobium first wall in a *d*–*t* fusion reactor.

A good indication of the reliability of these recoil calculations can be obtained by comparing experimental ranges of primary recoils resulting from *d*–Be neutrons with theoretical ranges based on the calculated recoil energies. We have made this comparison for radioactive recoils resulting from (*n*,2*n*) reactions in niobium and gold. In the experimental measurements, the number of radioactive recoils collected on graphite catcher foils was compared with the remaining activity in the target. The emitted fraction of (*n*,2*n*) activity from the forward surface of the target foil is a direct measure of the projected range of the recoils. These experimental ranges are compared with predicted ranges based on Winterbon's[4] treatment of the Lindhard theory in Table 1.3. The (*n*,2*n*) reaction accounts for the majority of the high-energy recoils in niobium and gold, and the close agreement between

Table 1.3. Projected ranges of primary recoils with average energy $\bar{T}$ resulting from (n,2n) reactions in niobium and gold irradiated with high-energy d–Be neutrons

Material	$\bar{T}_{(n,2n)}$ (keV)	Projected range (Å)	
		Theory	Experiment
Nb	215	428	386
Au	92	96	112

theory and experiment suggests that our theoretical calculations of recoil energies are reasonable. We can conclude that neutron damage effects associated with recoil spectra should be similar for pure 15-MeV and deuteron-breakup neutrons of the same mean energy.

THE ENERGY DEPENDENCE OF NEUTRON DAMAGE IN COPPER AND NIOBIUM[1]

J. B. Roberto   M. T. Robinson

Primary recoil spectra and specific damage energies have been computed for neutron interactions in copper and niobium for neutron energies up to 32 MeV. The calculations are based on theoretical neutron cross sections[2] and are useful in the description of both sputtering and bulk radiation effects. Previous treatments of high-energy neutron damage have been limited to neutron energies less than 20 MeV, the upper limit of existing nuclear data files such as ENDF/B. The extension of the damage calculations to higher energies is necessary to understand radiation effects from proposed deuteron-breakup or spallation neutron sources that include neutrons with energies up to 50 MeV and more.

The present calculations divide the possible nuclear reactions into four groups: elastic scattering and nonelastic interactions with a neutron, a proton, or an alpha particle as the first particle emitted. Subsequent particle emissions in nonelastic events are ignored. This approach simplifies both the nuclear physics and the damage calculations and allows a convenient means for comparing relative contributions from the principal reaction types. For elastic scattering, the primary recoil probability densities were computed as sums of Legendre polynomials with energy dependent coefficients derived from the theoretical calculations.[2] Above a few million electron volts, the elastically scattered neutrons are strongly peaked in the forward direction, discounting the relative elastic contribution to the damage energy by lowering the average recoil energy.

For nonelastic interactions, the theoretical nuclear data[2] were in the form of energy spectra for light-particle (*n*, *p*, or α) emissions. These distributions were transformed into heavy-particle recoil spectra by using the kinematic scattering equations to express the primary recoil energy as a function of the light-particle recoil energy and directions. It was assumed that the energy and angular distributions of the light particles were independent. Primary recoil probability densities for (*n,n′*) and (*n,nx*) events in niobium are shown in Fig. 1.13 for various neutron energies. In the figure, *T* is the recoil energy with T_{max} its maximum possible value. These distributions are based on the assumption that the light particles are emitted isotropically in the barycentric system. The nonelastic recoils are peaked at $T_{max}/4$, which corresponds to the maximum kinematically allowed inelasticity and therefore to low light-particle energies. This result supports the approximation of neglecting the contribution of subsequent particle emissions to the recoil energy.

Damage energies were derived from the recoil spectra using the Lindhard theory of electronic stopping. The

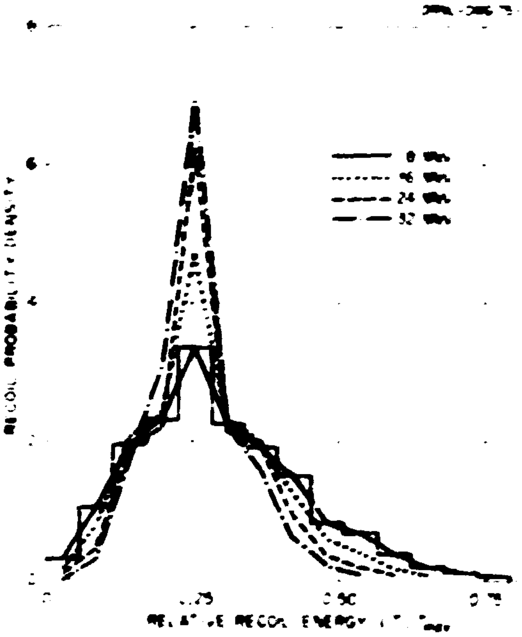

Fig. 1.13. Inelastic recoil distributions for niobium at several neutron energies.

---

1. Summary of paper to be published.
2. Neutron Physics Division, ORNL.
3. J. B. Roberto and M. T. Robinson, "The Energy Dependence of Neutron Damage in Copper and Niobium," this report.
4. K. Winterbon, *Ion Implantation Range and Energy Deposition Distributions*, vol. II, Plenum Press, New York, 1975.

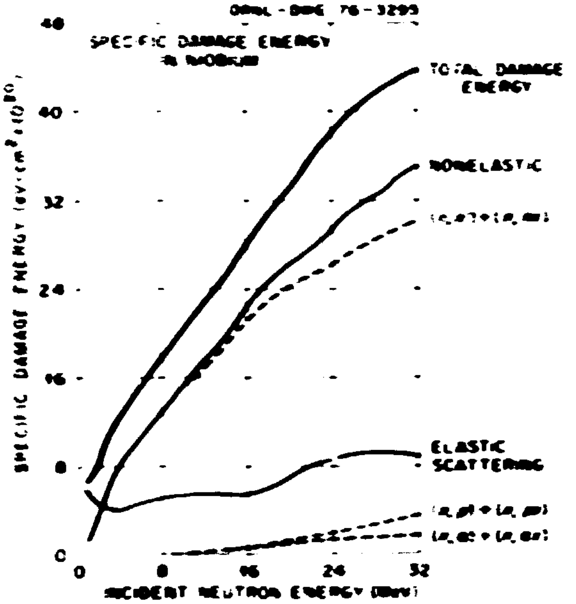

Fig. 1.14. Specific damage energy vs neutron energy for niobium.

resulting damage energies for the various nuclear interactions were multiplied by the corresponding interaction cross sections to obtain a specific damage energy per neutron. Specific damage energies for niobium up to neutron energies of 32 MeV are shown in Fig. 1.14. The increased importance of nonelastic processes at higher neutron energies is apparent from the figure, and the relative contributions of (n,p) and (n,α) interactions can also be seen. The dip in damage energy near 18 MeV reflects a reduction in the theoretical total nonelastic cross section in that energy range. Overall, the damage energy increases somewhat smoothly with neutron energy in both niobium and copper from 0 to 32 MeV. At 15 MeV, the specific damage energies from these calculations agree well with values derived from ENDF/B data.

[illegible] J. Nucl. Mater.

[illegible] J. Nucl. Mater. (in press).

ELECTRONIC AND MAGNETIC PROPERTIES

DIELECTRIC SCREENING AND THE LATTICE DYNAMICS OF TRANSITION METALS

J. F. Cooke

In a number of high-T_c superconductors, including niobium, the observed phonon spectra contain anomalies not found in the spectra of materials with low transition temperatures. One approach toward explaining these anomalies and their apparent connection with high superconducting transition temperatures would be to carry out "first principles" calculations of the phonon spectra. Such calculations require knowledge of the inverse of the dielectric screening matrix $\epsilon(\mathbf{q}+\mathbf{G}, \mathbf{q}+\mathbf{G}')$ at the wave vector $\mathbf{q}$, where $\mathbf{G}$ and $\mathbf{G}'$ are reciprocal lattice vectors.

In previously reported work on niobium, we investigated the possibility that the phonon anomalies could be simply related to the diagonal part ($\mathbf{G} = \mathbf{G}'$) of ϵ, and we found, contrary to earlier speculations in the literature, that this was not the case.[1] As a result of such calculations, it is clear that the full screening matrix must be evaluated and inverted in order to determine the effects of screening in producing the anomalies.

Since ϵ is a matrix of infinite order, it is advantageous to perform the inversion analytically, if possible, and then to use numerical techniques in evaluating the matrix elements of ϵ^{-1}. Several methods for doing this have been proposed.[2] We have independently derived an analytic expression for ϵ^{-1} based on approximations that we feel are appropriate for transition metals. The results obtained for ϵ^{-1} are similar in form to those obtained previously,[2] and general comments concerning the connection between the "first principles" theory and phenomenological approaches are therefore not altered. Calculations based on our result involve Brillouin zone integrals and reciprocal lattice sums which can be performed accurately with existing computer programs, but the amount of computer time required is prohibitive. At present, we are attempting to simplify the expression for ϵ^{-1} to the point where realistic calculations can be performed in a reasonable time.

In addition to this work, we have also carried out further calculations for the diagonal part of the electronic susceptibility matrix $\chi(\mathbf{q})$, which is linearly related to $\epsilon(\mathbf{q})$. These calculations were performed along the [111] direction for niobium in order to determine if a peak in $\chi(\mathbf{q})$ occurred at $\mathbf{q} = (2\pi/a)(\frac{2}{3}, \frac{2}{3}, \frac{2}{3})$. This would be of considerable interest since this is the characteristic wave vector of the so-called ω phase, which occurs when niobium is alloyed with zirconium.

The calculations were performed in exactly the same way as those reported previously for the [100] direction.[1] The results for the two directions are shown in Fig. 1.15. As can be seen, the [100] and [111] results are quite similar, and there are no peaks in the $\chi(\mathbf{q})$ curve for $\mathbf{q} \neq 0$ along the [111] direction. It is possible,

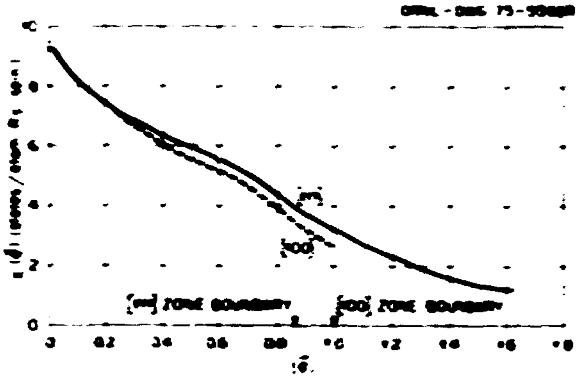

Fig. 1.15. Diagonal susceptibility χ(q) maximum for q along the [111] and [100] directions. The wave vector q is measured in units of 2π/a.

however, that a full calculation of $\chi^{-1}(\mathbf{q}+\mathbf{G}, \mathbf{q}+\mathbf{G}')$ might yield structure at $\mathbf{q}_0$ which could be correlated with the lattice transition to the ω-phase.

SPIN WAVES IN NICKEL REVISITED

J. F. Cooke

In a recent paper, Cooke and Davis[1] presented results for the transverse dynamic susceptibility χ(q, ω) of nickel, calculated within the framework of an itinerant electron formalism at low temperatures. This calculation included the band and wave-vector dependence of the relevant screened coulomb matrix elements in a self-consistent way. The calculations successfully predicted the isotropic spin-wave dispersion curve observed in nickel, as well as the disappearance of the spin waves along the [111] direction in the reciprocal lattice. In contrast to experiment, however, well-defined spin-wave peaks were obtained out to the Brillouin zone boundary along the [100] direction, and a second peak above the spin-wave peak was found over a restricted range of wave vectors. These calculations were based on a modified Gilat-Raubenheimer (GR) integration scheme. In order to investigate their accuracy further and to study in greater detail the second peak found in χ(q, ω), additional calculations have been carried out using an integration scheme based on the tetrahedron method.[2] This method is expected to give somewhat

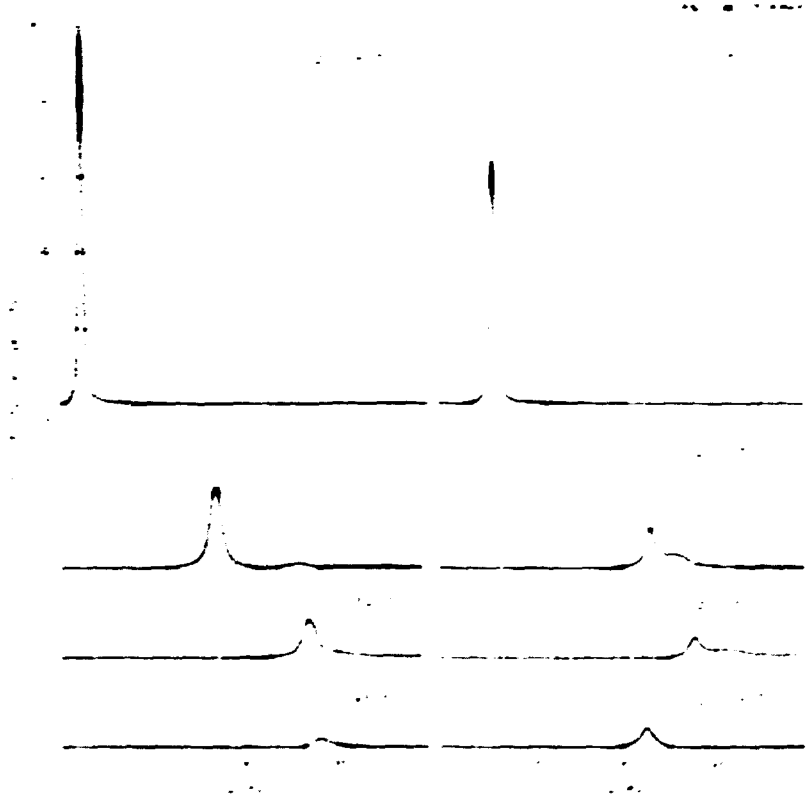

Fig. 1.16. Calculated spin wave scattering cross section [∝ Im χ(q, ω)] for nickel plotted as a function of energy for various values of q along the [100] direction. The wave vector q is measured in units of 2π/a, where a is the lattice constant.

---

[1] J. F. Cooke, H. L. Davis, and Mark Mostoller, *Phys. Rev. B* 9, 2485 (1974).

[2] See, for example, S. K. Sinha and R. N. Harmon, *Phys. Rev. Lett.* 35, 1515 (1975), and references therein.

better accuracy for that portion of the integration very near the Fermi surface.

Results for $\chi(q, \omega)$ obtained by integrating over 1024 tetrahedra in the irreducible Brillouin zone are shown in Fig. 1.16 for various values of $|q|$ along the [100] direction. A plot of the spin-wave dispersion curves obtained from the positions of these peaks is shown in Fig. 1.17. These results are essentially identical to those obtained from the GR scheme, and thus the apparent discrepancy between theory and experiment cannot be attributed to numerical errors in the calculation.

The results in Figs. 1.16 and 1.17 show quite clearly that there are two spin-wave branches. These appear to interact, and an appreciable scattering intensity occurs for the upper branch only in the region where the two branches interact strongly. The peak height of the lower branch is found to be about an order of magnitude smaller for $|q| > 0.4$ (in units of $2\pi/a$ with a the lattice constant) than for $|q| \sim 0.1$, in agreement with the earlier calculations. This relatively small scattering intensity, combined with the relatively high spin-wave energies (>100 meV), could account for the fact that the upper branch and the larger wave-vector part of the lower branch were not observed in the original experiment.

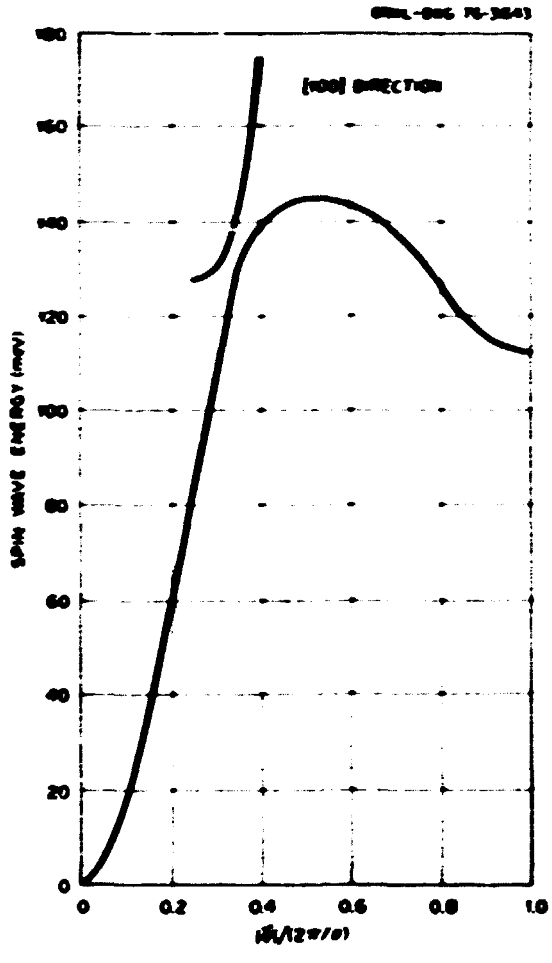

Fig. 1.17. Calculated spin-wave dispersion curve along the [100] direction for nickel.

A more recent neutron-scattering experiment[3] has shown that this is indeed the case. In this experiment, the upper spin-wave branch was observed and found to be in excellent agreement with the results shown in Fig. 1.17. In addition, the lower spin-wave branch was followed out to the zone boundary, and the dispersion curve was found to be somewhat flatter than that shown in Fig. 1.17. The latter does not represent any fundamental difficulty with the theory, since as Cooke and Davis[1] pointed out, the behavior of the lower spin-wave branch, after it bends over, is quite sensitive to slight changes in the band structure, while the low $|q|$ part of the curve is not. In particular, it was noted that in one specific calculation the dispersion curve was extremely flat after bending over, which appears to be more in line with the recent experimental results. The experimental observation of the upper spin-wave branch and of the complete lower branch along the [100] direction, therefore, not only removes the apparent discrepancy between theory and experiment, but also provides us with a very sensitive test of the ferromagnetic band structure of nickel.

---

[1] J. F. Cooke and H. L. Davis, *AIP Conf. Proc.* 10, 1218 (1972).

[2] G. Lehmann and M. Taut, *Phys. Status Solidi B* 54, 469 (1972); J. Rath and A. J. Freeman, *Phys. Rev. B* 11, 2109 (1975).

[3] H. A. Mook, D. Tocchetti, and F. Mezei, "Magnetic Excitations in Nickel," this report.

THEORETICAL CALCULATION OF THE EXCHANGE INTEGRAL FOR EUROPIUM

J. F. Cooke H. L. Davis

In the rare earth series, the s–f exchange interaction between the localized $4f$ electrons and the conduction electrons is thought to be basic to any proper description of the magnetic properties of these materials. As shown by Ruderman, Kittel, Kasuya, and Yosida (RKKY), this direct s–f exchange coupling leads to a long-range, indirect interaction between the localized $4f$ moments which, in turn, is thought to be responsible for the wide variety of magnetic ordering and related phenomena which have been observed in the rare earth metals.

In its simplest form, the RKKY interaction is equivalent to an isotropic Heisenberg model with an exchange integral $J(q)$ related to the s–f exchange matrix element and to the conduction electron band structure. Since $J(q)$ can also be determined experimentally by analyzing spin-wave dispersion curves, it represents a quantity of fundamental importance in establishing the validity of the s–f exchange model for the rare earth metals. Because $J(q)$ plays this unique role and because numerical techniques have recently been improved to the point where realistic ab initio calculations are possible, we decided to undertake calculations of $J(q)$ for europium.

We chose to perform calculations on europium primarily because it has zero orbital moment and only one atom per unit cell (bcc structure). For this case, the general expression for $J(q)$ simplifies considerably to give

$$J(q) = \sum_{n,n',k} |I_{n,n'}(k, k+q)|^2 \frac{f_{nk} - f_{n'k+q}}{\epsilon(nk) - \epsilon(n'k+q)} , \quad (1)$$

where $I_{n,n'}(k, k+q)$ is the s–f exchange matrix element, $\epsilon(nk)$ is the energy of an electron in band n with wave vector k, and f_{nk} is the Fermi occupation number. Unfortunately, $J(q)$ has not yet been measured for europium metal, but we do know something fundamental about its form: Since europium orders in a spiral-spin configuration, $J(q)$ should have its maximum value at a q corresponding to the spiral wave vector.

For the numerical evaluation of the expression given as Eq. (1), the tetrahedron method[7] was used to carry out the Brillouin zone integration, and the Korringa–Kohn–Rostocker (KKR) method was used to generate the electronic energies and band wave functions. The 4f wave functions were obtained from atomic Hartree–Fock calculations. About 1500 tetrahedra were used in the irreducible zone, and all calculations were performed for q along the [100] direction.

In order to demonstrate the role played by the s–f matrix element in determining $J(q)$, we also evaluated the expression given in Eq. (1) with constant matrix elements, that is, with $I_{n,n'}(k, k+q) = 1$. The results of this calculation are shown in Fig. 1.18, and the results for $J(q)$ when the matrix elements are included properly are shown in Fig. 1.19. It is clear that the constant matrix element approximation is completely inadequate. In fact, on the basis of the constant matrix element calculations, we would predict that europium was ferromagnetic, since the maximum value of $J(q)$ occurs at $q = 0$. On the other hand, the results in Fig. 1.19 show that $J(q)$ has its maximum value at $q \simeq 0.375$ (in units of $2\pi/a$ with a the lattice constant) when matrix elements are included, which corresponds to a spiral spin configuration with a turn angle of about 67°. This is somewhat higher than the experimental value of 50°. We found, however, that lowering the Fermi energy by about 5% reduced the turn angle to the experimental value. It thus appears that modest changes in the band structure can substantially improve the agreement between theory and experiment.

The results we have obtained demonstrate that an ab initio calculation of the exchange integral for europium,

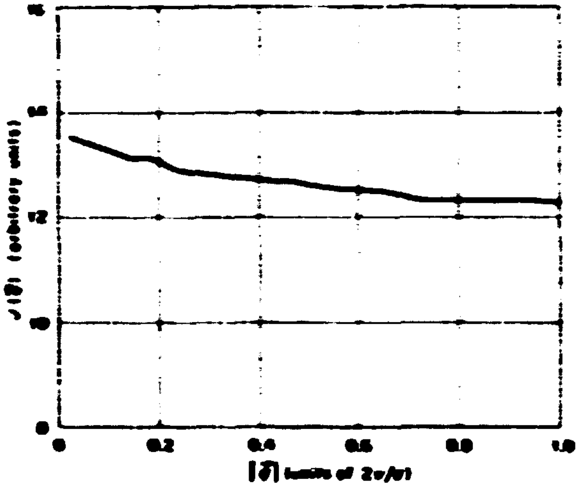

Fig. 1.18. Exchange integral $J(q)$ as a function of q along the [100] direction calculated using the constant s–f matrix element approximation.

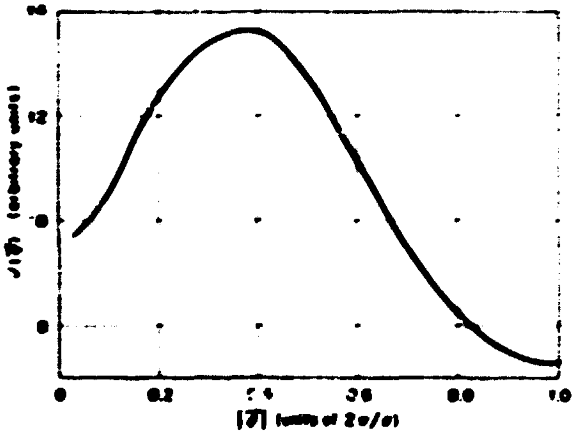

Fig. 1.19. Exchange integral $J(q)$ as a function of q along the [100] direction calculated with the s–f matrix element properly included.

when properly carried out, yields reasonably good agreement with the available experimental information and thus supports the view that the RKKY theory provides a correct description of magnetic ordering in the rare earth metals.

---

1. G. Lehmann and M. Laut, *Phys. Status Solidi B* **54**, 469 (1972); J. Rath and A. J. Freeman, *Phys. Rev. B* **11**, 2109 (1975).

ELECTRONIC STRUCTURE OF THE *F* CENTER IN SrO

T. M. Wilson[1] R. F. Wood

The energy levels and wave functions of the *F* center (two electrons in an O^{2-} vacancy) in SrO have been calculated as a function of the A_{1g} displacements of the nearest-neighbor ions of the oxygen vacancy. The calculations were made using methods previously developed and applied to a similar study of the *F* center in CaO and MgO.[2] Little is known experimentally about this center, and no prior theoretical studies have been reported. The absorption band for the *F* center has been identified and peaks at about 2.5 eV;[3] no luminescence bands have been reported.

The results of our calculations for the lowest lying states of the *F* center are shown in Fig. 1.20; they are qualitatively similar to those for the *F* center in CaO. The $^1A_{1g} \to {}^1T_{1u}$ absorption occurs at 2.46 eV for a 3% outward relaxation of the first-nearest-neighbor (*fnn*) Sr^{2+} ions. For small distortions, the $^3A_{1g}$ and $^3T_{1u}$ states were found to be considerably more localized than they were in either MgO or CaO. The charge densities out to second nearest neighbors, shown in Table 1.4, clearly demonstrate the sensitivity of the electronic wave functions for these states to the positions of the *fnn* ions. The rapid variation in the localization of the electronic wave function in the region $\delta = 0\%$ to $\delta = 6\%$ accounts for the nonparabolic shape of the energy curves for these states.

Table 1.4. Integrated charge within the second-nearest-neighbor shell of ions in SrO as a function of the A_{1g} outward distortion of the first-nearest-neighbor ions. The outward distortion δ of the ions is measured as a percentage of the perfect lattice anion–cation distance

δ (%)	$^1A_{1g}$	$^3A_{1g}$	$^1T_{1u}$	$^3T_{1u}$
0	1.90	1.81	1.82	1.90
2	1.87	1.65	1.59	1.87
4	1.82	1.21	1.18	1.81
6	1.78	1.11	1.02	1.69
8	1.73	1.03	1.01	1.57
10	1.64	1.00	1.00	1.12

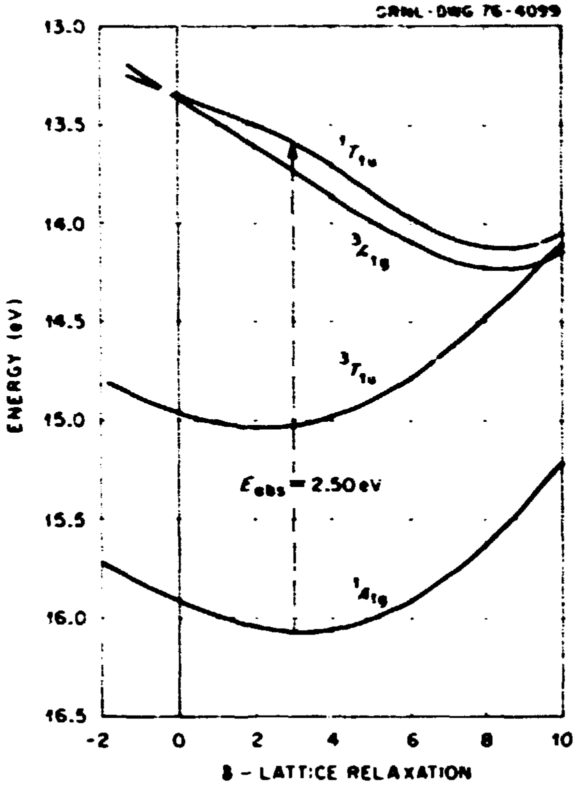

Fig. 1.20. *F*-center energy levels in SrO as a function of lattice relaxation, δ. The abscissa gives δ, expressed as a percentage of the anion–cation distance in the perfect crystal.

The calculated curves predict a $^3T_{1u} \to {}^1A_{1g}$ emission band at about 1.0 eV and a $^1T_{1u} \to {}^1A_{1g}$ band at about 1.3 eV that should be weak at low temperatures and should become more intense at higher temperatures. The calculations also suggest the possibility of observing the excited state absorption for the $^3T_{1u} \to {}^3A_{1g}$ transition at about 1.4 eV. Furthermore, since both the $^3T_{1u}$ and $^3A_{1g}$ wave functions are compact in the region of the absorption ($\delta \sim 2$ to 3%), the oscillator strength for this transition should be large.

Calculations of the Jahn–Teller coupling parameters of the $^3T_{1u}$ electronic state to the E_g and T_{2g} vibrational modes is in progress and will be used later to calculate the absorption and emission band shapes.

---

[1] Present address: Oklahoma State University, Stillwater, Okla.

2. R. F. Wood and T. M. Wilson, *Solid State Commun.* **16**, 545 (1975).

3. B. P. Johnson and E. B. Hensley, *Phys. Rev.* **180**, 931 (1969).

2. Physical Properties of Solids

During the past year the research programs concerned with the physical properties of solids have undergone a change in emphasis which reflects the expanded goals of both ERDA and the Laboratory in areas related to nonnuclear energy. So in many ways the research results reported here are of a transitional nature. It would have been unreasonable to discontinue abruptly ongoing programs which were of primary concern to the AEC, but a part of the research in such areas is being de-emphasized and attention is being directed to broader based studies in other than nuclear energy areas. Most of the work reported in this section of the Annual Report represents cooperative efforts between various groups within the Solid State Division as well as with scientists in other ORNL Divisions and in other laboratories. Such interactions and cooperation continue to be one of the vital strengths of the Division.

Fluxoid-lattice properties and structure have been investigated by means of small-angle neutron scattering. Such measurements have shown unambiguously the existence of a mixed intermediate state in niobium which permits a quantitative study of the attractive fluxoid interaction. These investigations have also demonstrated the capability of this technique to obtain other valuable information concerning fluxoid arrays at the microscopic level. Other work has provided insight into the limitations of the critical-state model for describing flux pinning in superconductors.

The surface properties program has increased research efforts related to catalytic phenomena and has continued measurements of high-energy neutron sputtering yields, which are of interest in controlled fusion device technology and which have been a subject of great controversy. The latter measurements have led to the conclusion that erosion rates of candidate first-wall materials due to neutron sputtering processes are not of technological significance. The research concerning catalysis has emphasized the development of new methods for determining lattice site locations of adsorbates on metal surfaces. Low-energy electron diffraction data can define the symmetry of adsorbates but not the lattice site or layer spacing. The angular dependence of Auger electron emission and a combination of Rutherford ion-backscattering and ion-channeling-spectroscopy techniques can be used to augment diffraction data in establishing adsorbate lattice sites. These studies have been strengthened by strong interactions with the theory and ion bombardment groups in the Division.

Examination of the optical, electrical, and magnetic properties of high-temperature materials is one of the major research programs within the Division. Some new aspects of the program initiated recently are beginning to produce some very interesting results. A new method, utilizing EPR spectrometry, has been developed to measure diffusion rates of impurities in ceramic materials; the method is quite useful for impurities having no radioactive isotopes or short-lived ones. Studies of the effects of high temperatures and high electric fields upon impurities contained in MgO have produced some rather unusual results.

Such conditions were found to reduce iron, chromium, and vanadium from the trivalent to divalent state, while manganese was unchanged. Subsequent reheating without the applied electric field led to reoxidation of the reduced species. Data analysis shows that neither reduction nor oxidation is a single simple process, nor is the redox process simply reversible. In related areas, examination of various defect centers in the alkaline earth oxides continues to be of interest, and a comprehensive study of F^+ centers in these materials has been completed. The identities of several defects were clarified, and some discrepancies concerning structure of the centers have been resolved. Initial data from lithium-doped MgO suggest that the net production of stable, intrinsic defects produced by knock-on processes is suppressed, and a reversible coloration effect that can be correlated with a known defect has been observed. Resonance Raman scattering studies of crystalline $NaClO_3$ has shown that an unstable form of O_2^- is produced in the crystals by gamma rays at room temperature. The observed thermal instability and photolytic decomposition of this O_2^- form lead to the suggestion that this species is involved in many solid state photochemical reactions. The implications for photocatalyzed solid state reactions, oxygen binding and transport in biological systems, and applications in fuel cell technology are being examined.

Photovoltaic conversion of sunlight directly into electricity is a major element of the ERDA program in solar energy. The Division initiated a small research effort in photovoltaic conversion early in the 1975 calendar year, and this effort quickly developed into one of the most important nonnuclear, energy-related programs of the Division. The program has been based on our past experience in the growth and characterization of ultrapure germanium and on our capabilities and facilities (primarily reactors) for the study of neutron-transmutation-doped silicon. At present, the work is concerned primarily with transmutation doping, annealing, and electrical property measurements of both single-crystal and polycrystalline samples of silicon, but research on other materials is also planned. In order to utilize effectively the results of this research, it is desirable to have the capability for fabricating and testing the solar cells within ORNL. Therefore, as part of the overall effort, facilities have been set up for carrying out these more applied aspects of solar cell development. In fact, tests have been made recently on solar cells fabricated entirely within the Division from our transmutation-doped silicon. From the experience gained thus far, it has become apparent that although the elementary principles of photoconversion are understood, basic research is badly needed on many important electronic and ionic processes that affect the conversion efficiency in a variety of photoconverters.

SUPERCONDUCTIVITY

SMALL-ANGLE NEUTRON DIFFRACTION STUDIES OF SUPERCONDUCTING NIOBIUM

D. K. Christen   S. Spooner[2]
F. Tasset[1]   H. A. Mook

An understanding of fluxoid behavior in Type II superconductors is important in the development of these materials for technological application. For a Type II superconductor in the mixed state, the interaction of fluxoids with one another, and in particular with pinning sites, determines the bulk magnetic properties of the material. On a fundamental level, small-angle neutron scattering is a powerful tool for the investigation of fluxoid lattice properties and fluxoid structure.

A high-resolution silicon double-crystal diffractometer has been used to measure precisely the fluxoid lattice parameter in a large single crystal of pure niobium. Two perfect crystals of silicon in a focusing geometry are used in this arrangement, which has been previously described.[3] The distinctive feature of this comparatively simple technique is its high resolution capability with the use of the ORR-HN4 thermal beam (i.e., without the need of a cold source, filter, velocity selector, or Soller slits). The sample was a 14.4-mm-diam spark-machined sphere that was chemically polished and annealed. It was mounted with the ⟨111⟩ axis in a vertical position, parallel to the applied field of a split-coil superconducting magnet. The sphere was situated in the horizontal neutron beam between the silicon monochromator and analyzer crystals. The silicon-analyzer rotation table facilitated measurement of the fluxoid Bragg scattering angle to an angular resolution of ±1 arc sec, with an overall accuracy of about 1%.

It is known that fluxoid lattice symmetry is correlated with that of the Fermi surface,[4] and for the ⟨111⟩ crystal orientation, the two-dimensional fluxoid lattice was observed to be hexagonal, as expected. With this information and with the knowledge that one fluxoid filament possesses a single quantum of magnetic flux $\phi_0 = 2.07 \times 10^{-7}$ G-cm², one may calculate from the observed scattering angle 2θ the magnetic flux density B averaged over a unit cell of the fluxoid lattice. This is given for the measured (10) reflection by the relation,

$$B = \sqrt{3}\,\phi_0\,(2\theta)^2/2\lambda^2 . \qquad (1)$$

where the neutron wavelength λ for the present setup is 2.398 Å.

In Fig. 2.1 the results of a systematic investigation of fluxoid neutron diffraction angles and the corresponding average flux densities calculated from Eq. (1) are given. These measurements were conducted at the fixed temperature $T = 5.06$°K as a function of the applied magnetic field H_a and of the field history. Each applied field was established either by increasing the field from zero (fluxoid entrance into specimen) or by decreasing the field from above the upper critical field H_{c2} (fluxoid exit from the specimen). It is evident that field-history effects on the fluxoid lattice parameter are minimal. This result is striking because it is a well-established fact that a pure, well-annealed bulk sample will exhibit some magnetic hysteresis, a phenomenon that is presumably due to surface effects, since previous work *has shown that this hysteresis largely can be* eliminated by the formation of a thin thermal oxide surface layer.[5]

Another noteworthy feature of Fig. 2.1 is the knee that occurs at the applied field 1054 Oe, below which the fluxoid lattice parameter is essentially constant. This is a phenomenon that occurs in low-κ Type II superconductors, such as niobium, and is the consequence of an attractive fluxoid interaction which defines an equilibrium flux density B_0 at an internal field equal to the lower critical field H_{c1}. The demagnetizing effect of spherical geometry serves to broaden this transition such that the interpretation is that of an "intermediate mixed state" for applied fields $(\frac{2}{3})H_{c1} < H_a < (\frac{2}{3})H_{c1} + (\frac{1}{3})B_0$, whereby the sample possesses domains of a constant-parameter fluxoid lattice. At the applied field $H_a = (\frac{2}{3})H_{c1} + (\frac{1}{3})B_0$, this constant-parameter lattice completely fills the sample, and for all applied fields above this value (mixed state) the parameter is smaller.

Although the fluxoid lattice parameter is a nearly reversible function of an applied field, the neutron measurements did reveal magnetic hysteresis in the sample. This was manifested by field-history-dependent rocking-curve integrated intensities, with the decreasing-field-history reflections yielding the larger intensities and narrower rocking-curve widths. In all cases the fluxoid diffraction width was limited by the instrument resolution (a FWHM of about 30 sec). These results indicate that the fluxoid lattice is always well defined, but the mosaic spread and general lattice perfection suffer when the lattice is formed by fluxoids having entered the sample.

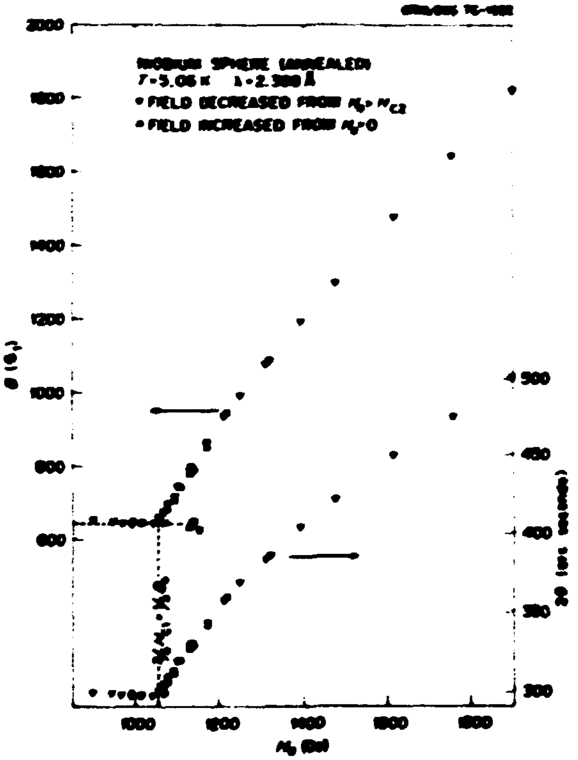

Fig. 2.1. The scattering angle 2θ for the (10) fluxoid reflection and the calculated flux density B vs the applied field H_a at the fixed temperature $T = 5.06$°K.

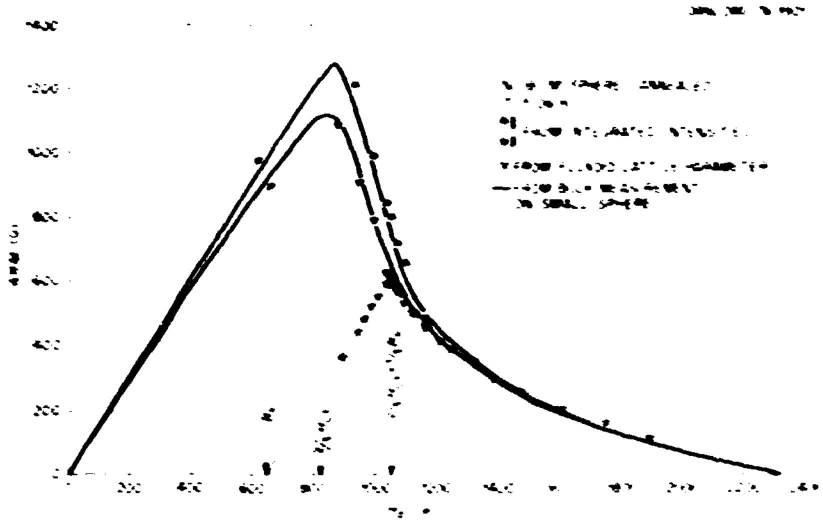

Fig. 2.2. The magnetization $-4\pi M$ vs the applied field H_a, derived from diffracted neutron intensities and measured fluxoid lattice parameters. Included are the results of magnetometer measurements on a smaller niobium sphere.

To assess these hysteretic effects quantitatively and to facilitate direct comparison of the neutron data with bulk measurements, the following procedure was employed. At a given applied field in the mixed state, the average flux density, calculated from Eq. (1), was assumed to represent the real macroscopic average magnetic induction in the sample for the decreased-field-history case. This assumption is justified by previous experiments on pure niobium which indicate that when surface hysteretic effects are removed by the oxide treatment, the reversible bulk properties closely coincide with those of the initial decreased-field-history case.[5] The average bulk induction for the field-increased case was then computed by normalizing the calculated flux density by the ratio of the fluxoid rocking-curve integrated intensities for field-increased and field-decreased history. For the intermediate mixed-state-field regime, all inductions were derived from the observed B_0, normalized by the ratio of integrated intensities for both field histories with respect to the field-decreased integrated intensity at $H_a = (2/3)H_{c1} + (1/3)B_0$. Finally, all average inductions and applied fields were used to calculate effective neutron data magnetizations $-4\pi M$.

Because of the large sample size, magnetization measurements have been performed to date only on a smaller sphere (3.3 mm in diameter), which was spark-machined from the same niobium stock and given identical polishing and annealing treatments. For preliminary comparison, therefore, we present in Fig. 2.2 both the derived neutron results and the magnetometer data. General agreement is good, and the bulk magnetic hysteresis seems to be described adequately on the microscopic level by the diffracted intensity results. By inspection of Figs. 2.1 and 2.2, it is apparent that the neutron experiments yield the critical parameters H_{c1} and B_0 to a precision that cannot be attained from macroscopic measurements on the sample in its present annealed state. These quantities are of fundamental interest and traditionally have been difficult to determine owing to the effect of weak residual hysteresis near H_{c1}. Experiments presently are under way to determine precisely B_0 and H_{c1} as a function of temperature and to investigate the effects of crystal anisotropy on these parameters.

---

[1] Guest scientist from Institut Max von Laue–Paul Langevin, Grenoble, France.

[2] Consultant from Georgia Institute of Technology, Atlanta, Ga.

[3] H. A. Mook, *J. Appl. Phys.* **45**, 43 (1974).

[4] K. Takanaka, *Prog. Theor. Phys.* **46**, 357 and 1301 (1971).

[5] S. T. Sekula and R. H. Kernohan, *Phys. Rev. B* **5**, 904 (1972).

ALTERNATING CURRENT LOSSES IN TYPE II SUPERCONDUCTORS

H. R. Kerchner   S. T. Sekula

We have undertaken a study of ac losses in the mixed state of Type II superconductors when flux-line motion is limited both by viscous damping and by the interaction between flux lines and defects in the superconducting material. Motivation for this study was an apparent inconsistency (i.e., the frequency dependence of the flux-flow resistivity) in our previous study of the ac permeability of defect-free Type II superconductors.[1] A second motivation was the continuing general interest in limitations of the critical-state model for describing flux motion in superconductors.

We will discuss two types of measurements: the imaginary part of the ac permeability, which is a direct measure of the total loss, and the voltage waveform, which is proportional to the time rate of change of flux in the sample. For both types of measurements, a cylindrical or prolate spheroidal sample was placed in a large axial dc magnetic field and a small parallel ac field. Measurements were made at various dc fields, ac amplitudes, and frequencies. We studied samples of several niobium-based alloys with differing critical current densities. Our measurements consistently indicated the existence of some excess loss which could not be accounted for either by the critical-state model or by the usual model of viscous loss which we employed in our previous study.[1]

Clem has modified the critical-state model to include viscous damping to the lowest order in the frequency.[2] Although the result for the ac permeability is complicated in general, one can derive simple analytic expressions for the zero-frequency and infinite-amplitude limits of the imaginary part of the permeability μ''. Our measurements indicated that the zero-frequency limit did not have the expected amplitude dependence, and the infinite-amplitude limit did not have the expected frequency dependence. Furthermore, extrapolating the measurements of μ'' to both zero frequency and infinite amplitude gave a nonzero result, which is in contradiction to the theory.

Measurements of the voltage waveform revealed a phase shift of the zero crossing. Physically, this means *that flux continues to enter the sample after the applied* field reaches its peak and begins to decrease. Such an effect cannot arise in a critical-state model but is to be expected in the presence of viscous drag. However, the magnitude of the observed phase shift was much larger than expected. Similar anomalously large phase shifts have been observed previously and reported in the literature.[3] The effect has been believed to be associated with the sample surfaces. However, we found it difficult to reconcile the amplitude and frequency dependence of the phase shift with any reasonable picture of surface behavior.

We believe that the correct interpretation of our experimental results must take into account the nonlinear relation between current density and electric field. It has long been known from dc flux-flow measurements[4] that in a nonideal superconductor the electric field E rises nonlinearly with increasing current density J when J is small and approaches the relation $E = \rho_f(J - J_c)$ only when $J \gg J_c$. The flux-flow resistivity ρ_f is analogous to, but smaller than, the normal-state resistivity. When $J \approx J_c$, there is some "excess" electric field which was neglected by Clem. Low-frequency ac measurements such as ours probe this region where $J \approx J_c$.

It is possible to obtain the function $E(J)$ from measurements of the phase shift of the zero crossing. One must measure the phase shift φ as a function of amplitude and/or frequency. As long as $\varphi \ll 1$, Maxwell's equations can be solved approximately to obtain $E(J)$. In Fig. 2.3, we show an example of the results that can be obtained. The dependence of E on J which we observed is similar to that observed in dc flux-flow experiments.[4]

The origin of the excess electric field is not well understood. Uniform motion of flux lines should produce an electric field that is proportional to the current density. However, the presence of material defects that pin flux lines complicates flux-line motion. Variations in the size and nature of pinning defects, the irregular motion of flux lines in the vicinity of defects, and thermally activated creep of flux lines past defects may all contribute to the excess electric field. It is hoped that additional experiments on flux-line motion may shed some light on this problem.

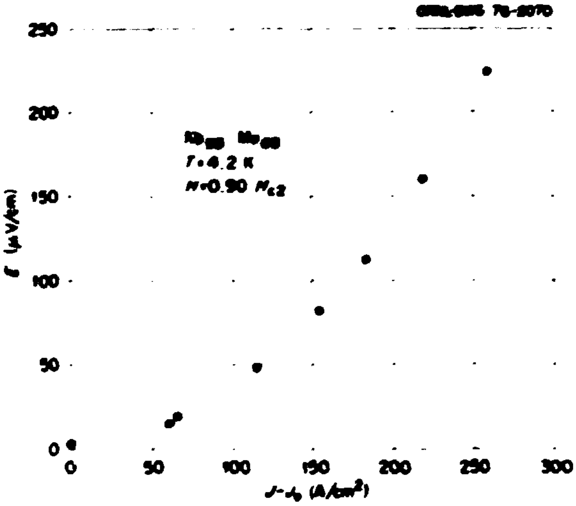

Fig. 2.3. The experimental relation between the electric field E and the current density J for a heat-treated $Nb_{0.6}Mo_{0.4}$ sample. The current density was determined only to within an arbitrary constant J_0.

---

1. J. R. Clem, H. R. Kerchner, and S. T. Sekula, *Solid State Div. Annu. Prog. Rep. Dec. 31, 1974*, ORNL-5028, p. 45.
2. John R. Clem, private communication.
3. R. W. Rollins, Heinz Kupfer, and Wolfgang Gey, *J. Appl. Phys.* 45, 5392 (1974).
4. Y. B. Kim, C. F. Hempstead, and A. R. Strnad, *Phys. Rev.* A 139, 1163 (1965).

FAST-NEUTRON DAMAGE STUDIES IN SUPERCONDUCTING VANADIUM-GALLIUM COMPOUNDS

D. U. Gubser[1]   H. R. Kerchner
D. K. Christen   S. T. Sekula

A collaborative program is in progress to study the influence of fast-neutron irradiation in well-characterized V-Ga samples in order to clarify further the role of radiation-produced defects in the superconducting behavior of technologically important compounds with the A-15 crystal structure.

Several bulk samples of the nominal composition V_3Ga were cast containing 23.3 at. % Ga, 25.6 at. % Ga, and 27.5 at. % Ga. Specimens of these samples were heat-treated at 1400°C for 4 hr while others received an additional heat treatment at 1150°C for 7 hr to increase the degree of atomic order. Prior to irradiation, measurements were made of the superconducting transition temperature, the isothermal dc magnetization behavior at 4.2°K, and the ac permeability.[2] These samples have been irradiated at an estimated maximum temperature of 60°C in the CP-15 fast-neutron facility at the Bulk Shielding Reactor for various fast-neutron fluences ranging up to 6×10^{18} neutrons/cm^2 ($E > 1$ MeV).

Earlier studies[2] have shown that the transition temperature T_c in all the samples decreased by about 2% following an irradiation to a fluence of 1×10^{18} neutrons/cm^2 ($E > 1$ MeV). In addition, the magnetization measurements and ac permeability data at 4.2°K indicated an increase in flux pinning in these samples, and there was a simultaneous decrease of magnetic stability as evidenced by an increase in the occurrence of random-like flux jumps that resulted from radiation-produced defects.

More recent irradiations to a fluence of 3×10^{18} neutrons/cm^2 ($E > 1$ MeV) indicate a reduction in T_c of about 5% in all the samples. Lattice parameter studies using x-ray techniques revealed that the lattice parameter of all the V-Ga samples had increased following irradiation. The increase is similar to that reported by Sweedler and Cox[3] for neutron-irradiated Nb_3Al. For this neutron fluence, any expected changes in the order parameter would be small, and no changes could be detected with x-ray measurements. Although T_c of these samples was significantly reduced by neutron irradiation, it is interesting to note that the magnetization curves showed no further increase in hysteresis due to flux pinning, but the samples demonstrated an increase in the number of flux jumps. The ac permeability measurements up to fields of 30 kOe also showed the increased occurrence of flux jumps, but the large critical current densities of the samples in this field region were too large for quantitative assessment. (The upper limit of combined apparatus-sample sensitivity is estimated to be about 2×10^4 A/cm^2.)

With further irradiation to a fluence of 6×10^{18} neutrons/cm^2 ($E > 1$ MeV), it was found that T_c was reduced in all the samples by about 20%. The ac permeability measurements showed that the critical current densities in fields up to 30 kOe remained above the upper limit of apparatus sensitivity and the samples exhibited a large amount of flux jumping. Magnetization studies and x-ray measurements are currently in progress.

---

1. U.S. Naval Research Laboratory, Washington, D.C.
2. D. U. Gubser and S. T. Sekula, *Solid State Div. Annu. Prog. Rep. Dec. 31, 1974*, ORNL-5028, p. 44.
3. A. R. Sweedler and D. E. Cox, *Phys. Rev. B* 12, 147 (1975).

A SURVEY OF RADIATION DAMAGE EFFECTS IN SUPERCONDUCTING MAGNET COMPONENTS AND SYSTEMS[1]

J. F. Guess[2]   R. R. Coltman, Jr.
R. W. Boom[3]   S. T. Sekula

A compilation and study of published work on the low-temperature irradiation of components of superconducting magnets has been completed in order to establish potential radiation damage problems in the use of superconducting magnets in CTR systems.

For fast-neutron fluences up to about 5×10^{18} neutrons/cm^2 ($E > 0.1$ MeV), it appears that the problems of degradation of important superconducting parameters [$J_c(H)$, the critical current density, and T_c, the transition temperature] by radiation damage for NbTi alloys and Nb_3Sn are minimal. Above this fluence, $J_c(H)$ for NbTi material can be decreased substantially. It is also expected that significant degradation of $J_c(H)$ and T_c can occur for Nb_3Sn for fast-neutron fluences above 5×10^{18} neutrons/cm^2 ($E > 0.1$ MeV) as based on correlative comparison with published non-radiation studies and available fast-neutron irradiation data.

The radiation-induced increases in resistivity of copper and aluminum (both used as the normal stabilizing metal matrix in the fabrication of multifilamentary composite superconducting wire) can be quite large, amounting to about 100 nΩ-cm for copper and 300 nΩ-cm for aluminum, for low-temperature fluences of about 2×10^{17} neutrons/cm^2. Thus radiation damage in these materials can be expected to have considerable effect on the stability characteristics of the composite wire and cable for use in magnet systems. This has been borne out to some extent by studies of radiation effects in composite wire material. Annealing at 300°K can remove approximately 85% of the damage-induced resistivity in copper and about 100% for aluminum.

A number of polymer materials have been demonstrated to be possibly useful for doses of approximately 8×10^8 rads ($\approx 3.2 \times 10^{17}$ neutrons/cm^2, $E > 0.1$ MeV). However, nothing is known of the effect of low-temperature irradiation on the dielectric breakdown strength of these materials or the effect of subsequent annealing of radiation defects on low-temperature performance.

Studies of the mechanical properties of structural stainless steels irradiated at low temperatures indicate that no deleterious changes in these properties are expected for fluences of about 1×10^{17} neutrons/cm^2 ($E > 0.1$ MeV).

---

1. Summary of report ORNL TM-5187, December 1975.

2. ORAU faculty research participant from Nashville Trevecca College, Nashville, Tenn.

3. University of Wisconsin, Madison, Wis.

CONSTRUCTION OF SQUID PREAMPLIFIER

H. R. Kerchner C. C. Watson[1]

We have constructed an ultrastable, ultra-low-noise preamplifier based on a superconducting quantum interference device (SQUID). The SQUID is mounted in a variable-temperature cryostat; so the preamplifier may be used in measurements of low-level signals encountered in basic research on the properties of Type II superconductors. We built this preamplifier (see Fig. 2.4) because of our interest in measuring the derivative of the magnetization M of superconducting samples with respect to the applied field H. One can obtain a direct measurement of dM/dH by ramping the field at a constant rate and measuring the voltage across two identical coils wound in series opposition with the sample in one of them. The voltages to be measured are of the order of 10 μV. Other amplifiers available to us

ORNL-DWG 76-2069

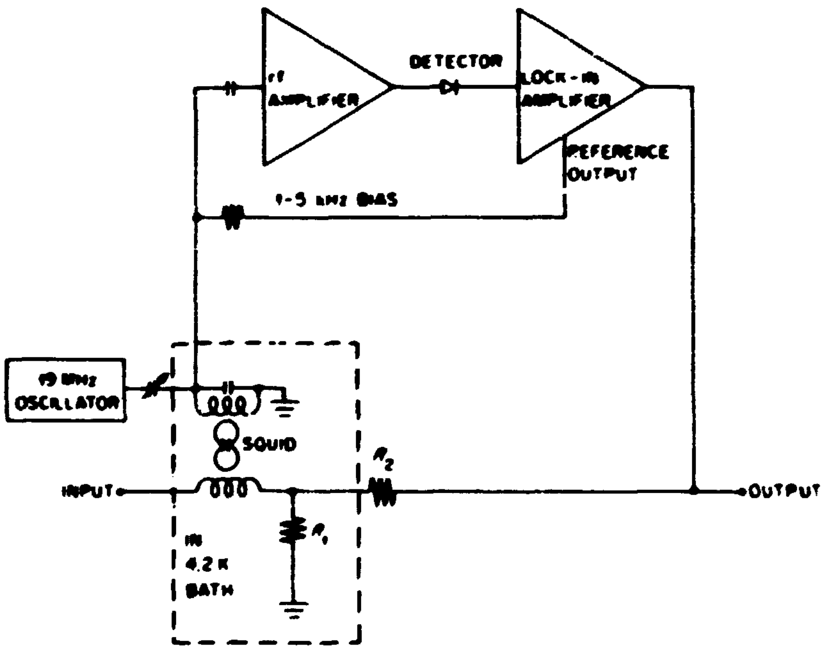

Fig. 2.4. Block diagram of the SQUID preamplifier.

were too noisy, insufficiently stable, or had an unacceptably long response time.

Accurate measurements of dM/dH are of interest for a variety of reasons.

1. dM/dH is needed in the interpretation of ac loss measurements.
2. dM/dH is discontinuous at phase transitions at the fields $H_{c1}(1-n)$ and H_{c2} and in low-κ materials $H_{c1}(1-n)+B_0 n$, where H_{c1} is the lower critical field, H_{c2} is the upper critical field, B_0 is the equilibrium flux density in the intermediate mixed state, and n is the demagnetizing factor. The temperature dependence of the fields at which these transitions occur can be compared with microscopic theories of the mixed state.
3. dM/dH, evaluated at H_{c2}, can also be directly compared with microscopic theory.

Of particular interest at present is the temperature dependence of B_0. Values of B_0 measured by this method will be compared with values obtained by neutron diffraction.[2] In addition, we will use this technique to extend measurements of B_0 to higher temperatures than can be reached in a neutron-diffraction experiment. We hope that higher-temperature measurements will clarify an apparent contradiction between previous experimental results and the theory of the mixed state at temperatures near the superconducting critical temperature.[3]

The design of the SQUID cryostat permits relatively easy conversion to an ultrasensitive flux-measuring device. Thus one can easily convert the equipment to measure the magnetization of samples over wide ranges of magnetic susceptibility.

The general design of the amplifier is simple and is similar to previously published designs.[4] A portion of the lock-in amplifier output is compared to the input voltage. The SQUID, which is sensitive to magnetic flux, acts as a null detector for current flowing in the input. The gain of the preamplifier is $1 + R_2/R_1 = 10^4$. We modified the previous designs to meet our special needs for a high effective input impedance and a high-frequency roll-off that properly matches the frequency response of the pickup coils. The entire input circuit is at liquid-helium temperature so that thermal electromotive forces, which would degrade stability, are minimized.

Preliminary measurements of dM/dH for a niobium sphere have been made at a number of temperatures. Three phase transitions show up clearly over most of the temperature range. As expected, accurate measurements become increasingly more difficult as one approaches the critical temperature. Our preliminary results for the temperature dependence of B_0 agree with previous experimental results.[3]

---

[1] Summer research participant from Yale University, New Haven, Conn.

[2] D. K. Christen, F. Tasset, S. Spooner, and H. A. Mook, "Small-Angle Neutron Diffraction Studies of Superconducting Niobium," this report.

[3] J. J. Wollan, K. W. Blazey, John R. Clem, and D. K. Finnemore, *Phys. Rev. B* 10, 1874 (1974).

[4] A. Davidson, R. S. Newbower, and M. R. Beasley, *Rev. Sci. Instrum.* 45, 838 (1974).

SURFACE PROPERTIES AND CATALYSIS

LINE-SHAPE ANALYSIS OF THE Cu $M_{2,3}VV$ AUGER SPECTRUM

F. B. Tubbs III[1]　Mark Mostoller
L. H. Jenkins　D. M. Zehner
J. R. Noonan

The angular intensity distribution of the Cu $M_{2,3}VV$ Auger emission spectrum has been measured using phase-sensitive detection. At low modulation voltages (<2 V peak-to-peak), the contributions from the M_2VV and the M_3VV transitions can be partially resolved. The structure in the line shape arising from the two transitions varies as a function of emission angle. To understand this variation with angle, the Auger spectrum needs to be separated out, or deconvolved, from other effects included in the measured line shape, such as instrumental resolution, electron energy losses, and true secondary electron contributions.

A simple first approach toward analysis of the observed $M_{2,3}VV$ Auger line shapes has been made based on the measurements of Yin et al.[2] on the photo-excited L_3VV Auger spectrum in copper. This occurs at an energy of about 920 eV, while the $M_{2,3}VV$ transition falls at roughly 60 eV. However, if valence band effects were the same in the two transitions and if Koster-Kronig processes were unimportant in the $M_{2,3}VV$ spectrum, then the latter could be reconstructed from the L_3VV spectrum by addition in a 2:1 ratio at the proper energy separation (around 2 eV) of the M_2 and M_3 levels. Not unexpectedly, this simple approach yielded results that did not agree well with the data for the $M_{2,3}VV$ spectrum, even when such things as the M_2:M_3 contribution ratio, the M_2-M_3 energy separation, and the (assumed Gaussian) measurement function were treated as adjustable.

The problem of deconvolving the "true" spectrum from the observed data is particularly difficult for many electron spectroscopic results because not only instrumental broadening but also intrinsic electronic processes occurring in the sample "distort" the signals observed. Several techniques for treating these problems in line-shape analysis and thus for improving the understanding of the underlying material properties involved have been proposed.[3] Use of such techniques appears to be required for the full interpretation of the angular intensity distribution of the Cu $M_{2,3}VV$ Auger spectrum.

---

[1] Great Lakes College Association science semester student from Earlham College, Richmond, Ind.

[2] L. Yin, I. Adler, T. Tsang, M. H. Chen, and B. Crasemann, *Phys. Lett.* 46A, 113 (1973).

[3] For example, H. H. Madden and J. E. Houston (to be published).

ANGULAR EFFECTS IN AUGER ELECTRON EMISSION FROM Cu (110)[1]

D. M. Zehner J. R. Noonan L. H. Jenkins

Recently, the ejection of Auger electrons from single crystalline solids into the vacuum continuum has been found to occur anisotropically.[2-4] We have investigated the angular intensity distribution of the Cu $M_{2,3}VV$ (62 eV) Auger electron emission from a clean Cu (110) surface. The copper crystal, grown in our laboratory, was cut, lapped, and polished, using chemical methods developed here,[5] to produce a surface oriented to within 0.5° of the (110). The sample was cleaned in vacuum using an ion-sputtering and annealing procedure such that no Auger signals, other than those from copper, could be detected during the data acquisition period.

The Auger electron intensity variations as a function of emission angle, primary electron beam energy, and angle of incidence have been studied. Data were collected using a 4-grid LEED Auger system, which also contained a moveable Faraday cup (energy resolution, ≈0.5%; aperture acceptance angle, 4.3°). The sample was aligned by establishing correct angular positions for diffracted primary electron beams. Using this technique, the sample could be repositioned with respect to the primary electron beam direction to within ±1°. The data were obtained with the Faraday cup using standard phase-sensitive detection techniques and were recorded in the second derivative mode, $N''(\epsilon)$. It was assumed that, to the first order, changes in the peak-to-peak height of the $N''(\epsilon)$ signal as a function of the detector's position were a reasonable approximation of the changes in intensity of the emitted Auger electron current. Data were analyzed as a function of θ, the emergent polar angle, defined with the respect to the surface normal; ϕ, the azimuthal angle, defined in a counterclockwise direction from the [011]; γ, the incident beam polar angle, defined about a rotation axis in the [001] direction; and the primary beam energy.

The angular variations as a function of θ for the Cu $M_{2,3}VV$ Auger transition along three principal azimuthal directions are shown in Fig. 2.5. From the results of repeated measurements, the accuracy of the intensity values is judged to be ±5%. The angular distributions show large intensity variations and are dominated by a maximum at the surface normal ($\theta = 0°$). The full width at half maximum (FWHM) of the narrowest peaks appears to be limited by the spatial resolution of the detector. However, other peaks appear to be quite broad. Comparison with model calculations shows that the distribution details cannot be fully explained by a model that considers multiple scattering of an electron and assumes only isotropic emission at the atom.[4]

Variation of the incident beam energy, E_p, at constant current and normal incidence produced changes in the measured absolute intensities but did not alter the shape of the angular distribution. The intensity variations of the distributions closely followed the changes of the integrated intensity of the Auger transition as measured with the 4-grid LEED optics; that is, each portion of the curve showed the same electron-impact ionization yield dependence as the integrated signal. The distribution was strongest for an E_p between 600 and 700 eV.

In general, the incident beam direction did not alter the shape of the angular Auger electron distribution. However, changing γ while keeping the incident and emission azimuths constant affected the absolute intensity of the distribution. For example, Fig. 2.6 illustrates the effects of rotating the sample about the [001] axis on selected portions of the curve along the [$\bar{1}$10]. Since the Auger emission process is not coupled with the core vacancy creation, these variations reflect a modulation of the number of core vacancies created as the primary beam angle of incidence is varied. The initial decrease in intensity as the beam is moved from normal incidence is possibly related to changes in the elastic reflection coefficient and to different multiple-scattering events undergone by the primary beam. The subsequent increases in intensity with larger angles of incidence γ are apparently due to the fact that, as the incident beam angle approaches the surface plane, the primary beam electrons penetrate less deeply into the solid, and at the same time a larger surface area is exposed to the beam. Consequently, more energy is deposited in the surface region, creating more vacancies near the surface. At angles beyond γ ≈ 50°, the cup aperture no longer sampled the total surface area excited by the incident beam. Therefore, a correction is made for data obtained beyond γ = 50°, as seen for γ = 55° in Fig. 2.6.

In summary, we have presented data of the angular variations in intensity of Auger electrons emitted from a copper single crystal having a (110) surface orientation. The angular distributions exhibit significant and complex structure. Comparison with theoretical models that include multiple scattering suggests that the emission is not isotropic at the copper-atom site. In addition, shapes of the distributions are found to be relatively insensitive to effects of both primary beam energy and angle of incidence. However, the absolute intensity of emission is affected by changes in either parameter.

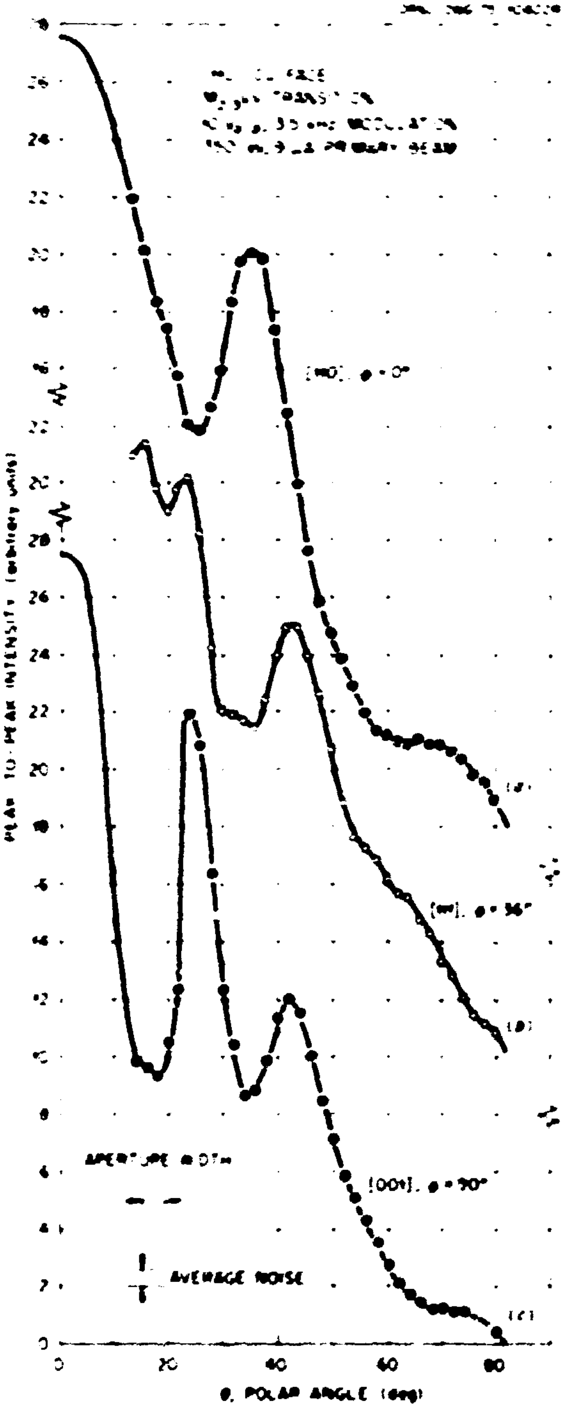

Fig. 2.5. Experimental angular dependence of the $M_{2,3}VV$ (62 eV) Auger transition from Cu (110) for (a) φ = 0°, [$\bar{1}$10], (b) φ = 36°, [$\bar{1}$11], and (c) φ = 90°, [001], as a function of θ. Incident beam is normal to the surface. Intensity values for curves (a) and (b) have been shifted up, but incremental scales are identical for all curves.

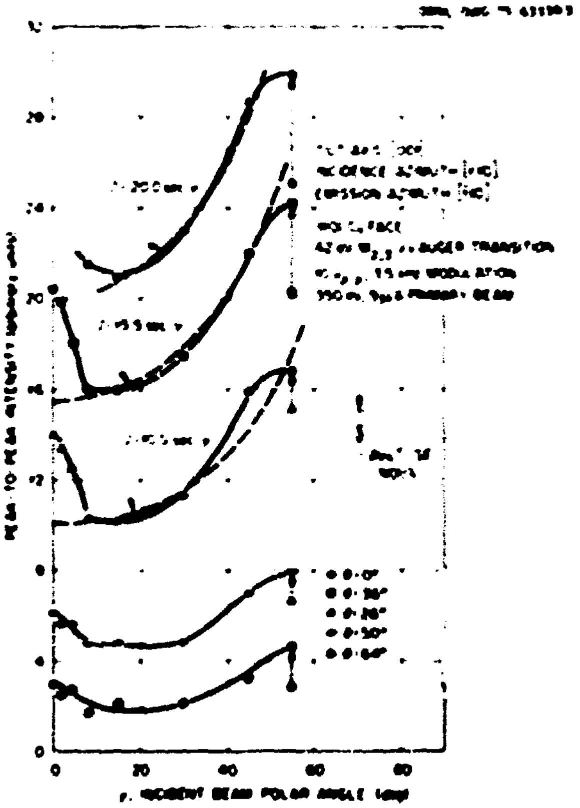

Fig. 2.6. Experimental angular dependence for several values of θ of the $M_{2,3}VV$ (62 eV) Auger transition from Cu (110) for φ = 0°, [$\bar{1}$10], as a function of γ.

1. Summary of paper: *Solid State Commun.* 18, 485 (1976).
2. L. McDonnell, D. P. Woodruff, and B. W. Holland, *Surf. Sci.* 51, 249 (1975).
3. T. Matsudaira, M. Watanabe, and M. Onchi, *Jpn. J. Appl. Phys. Suppl.* 2(2), 181 (1974).
4. T. Rusch and W. P. Ellis, *Appl. Phys. Lett.* 26, 44 (1975).
5. L. H. Jenkins, *J. Electrochem. Soc.* 117, 630 (1970).
6. H. L. Davis and Theodore Kaplan, "Theoretical Analysis of Angular-Dependent Auger Spectroscopy," this report.
7. P. W. Palmberg, *Appl. Phys. Lett.* 13, 183 (1968).

ANGULAR-RESOLVED AUGER EMISSION SPECTRA FROM A CLEAN Cu (100) SURFACE[1]

J. R. Noonan D. M. Zehner L. H. Jenkins

Considerable effort has been expended to make Auger electron spectroscopy (AES) a quantitative technique.[2] The studies usually involve several simplifying assumptions: for example, the electron is emitted isotropically and is only attenuated as it propagates. However, recent investigations have shown that Auger electron emission from a single-crystal solid occurs anisotropically.[3,4] A study of the angular intensity distribution of Auger electron emission has been extended to include the Cu $M_{2,3}VV$ (62 eV) emission from a clean Cu (100) surface. The purpose of the study was to examine further the emission anisotropy to provide insight into possible mechanisms, such as multiple scattering and valence band effects, responsible for anisotropy in the Auger emission process.

The crystal was prepared in a fashion similar to the Cu (110) crystal described earlier.[3] The crystal was oriented to within 0.5° of the (100) face and was aligned such that the (100) face was normal to the primary electron beam to within ±1°. The data were collected with a moveable Faraday cup employed as a retarding field analyzer using conventional phase-sensitive detection techniques and measured as a function of the angular parameters described earlier.[3]

Fixed azimuthal distributions, ϕ, show significant structure as a function of polar angle, θ, as shown in Fig. 2.7. Importantly the structure is entirely different from that obtained from the Cu (110) surface for the same Auger transitions.[3] Even in the same direction, such as along the [011], the distributions are unique to the different surfaces, indicating that emission from several layers indeed is involved. Furthermore, in contrast to the (110) surface, the emission produces a deep minimum in intensity at the surface normal. These experimental observations have been compared with calculations of diffraction effects that included multiple scattering.[5] The comparison shows that the deep minimum at $\theta = 0$° cannot be explained by a model that includes the assumption of an isotropic emitting source at the atom. Secondly, the details of calculated emission profiles do not compare well with the experimentally determined curves. From these results, one concludes that any theoretical model that reproduces the experimental curves must include an anisotropic electron source. The data can be compared with another experimental study of the angular distribution of Auger electron emission from a Cu (100) surface.[4]

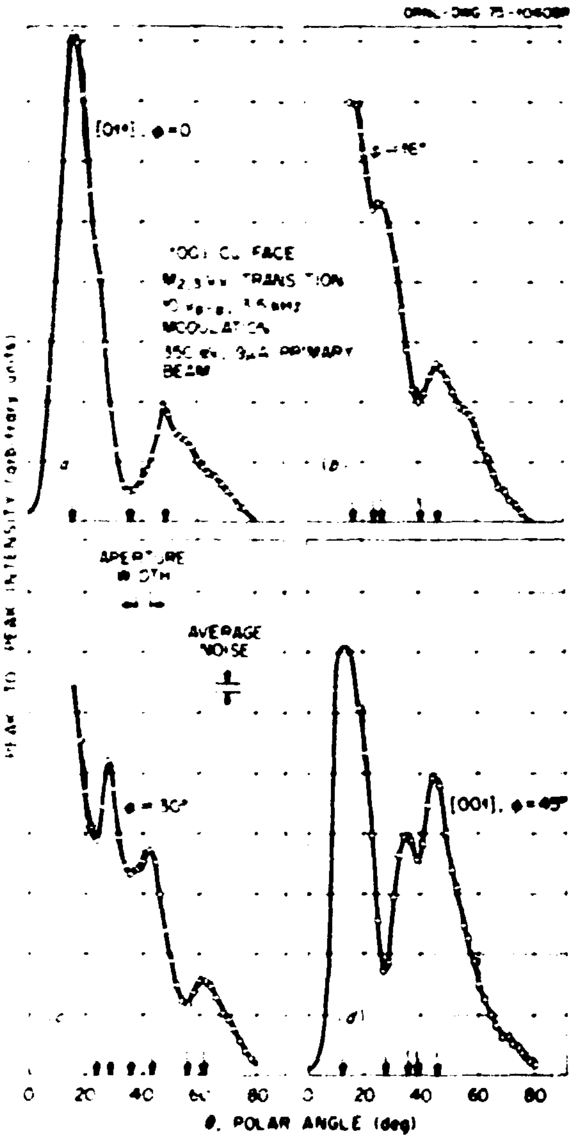

Fig. 2.7. Experimental angular dependence of the $M_{2,3}VV$ (62 eV) Auger transition from copper (100) for (*a*) ϕ = 0°, [011], (*b*) ϕ = 16°, (*c*) ϕ = 30°, and (*d*) ϕ = 45°, [001], as a function of θ. Incident beam is normal to the surface.

The spectrum reported here appears to be somewhat better resolved, presumably due to the smaller acceptance angle of our detector. Furthermore, while the data of McDonnell, Woodruff, and Holland[4] show intensity variations in azimuths related by symmetry, this study finds that data for peak positions from symmetrically equivalent azimuths agree to within ±1°, and the intensities are the same to within ±5%.

The measured intensity variation at $\theta = 12°$ in the [001] azimuth has been determined as a function of the incident polar angle of the primary beam, γ, for several different primary beam energies, E_p, as illustrated in Fig. 2.8. A similarly shaped family of curves was observed for other values of θ. As in the previous study, the intensity distribution generally remained unchanged as a function of γ, although small fluctuations in the distribution were observed. However, the absolute intensity of the distribution changed as a function of both primary beam energy and angle of incidence. Interestingly, the intensity vs γ curve for a given θ and ϕ appears to be different for the Cu (100), (110), and (111) surfaces.[3,4] Previously, changes in intensity as a function of the primary beam angle of incidence had been attributed to changes with angle of the elastic reflection coefficient and to angle-sensitive effects in electron multiple-scattering processes. The changes in intensity as a function of the primary beam energy would also be consistent with this model. Eventually, the overall intensity distribution increased with increasing γ, which agrees with the earlier hypothesis that at larger primary beam incident angles, the energy deposited in the surface region is greater than at normal incidence, causing the intensity increase. Finally, although the intensity distribution from the (100) surface followed the same overall trends with changing values of γ, small variations within the distribution occurred. Since Auger electron emission should be decoupled from the core vacancy creation process, the observation may be related to the number of vacancies created. For example, the intensity measured at any position is a fraction of the sum of all emission events occurring in several atomic planes near the surface, weighted by an escape probability for each layer. Therefore, a change in the planar distribution of vacancies created with a given incident beam could result in a change of the fraction measured. The absolute and relative changes of the angular distribution of the emitted Auger electron as a function of either primary beam energy or angle of incidence suggest that care must be exercised when combining measurements obtained with different values of E_p or angles of incidence.

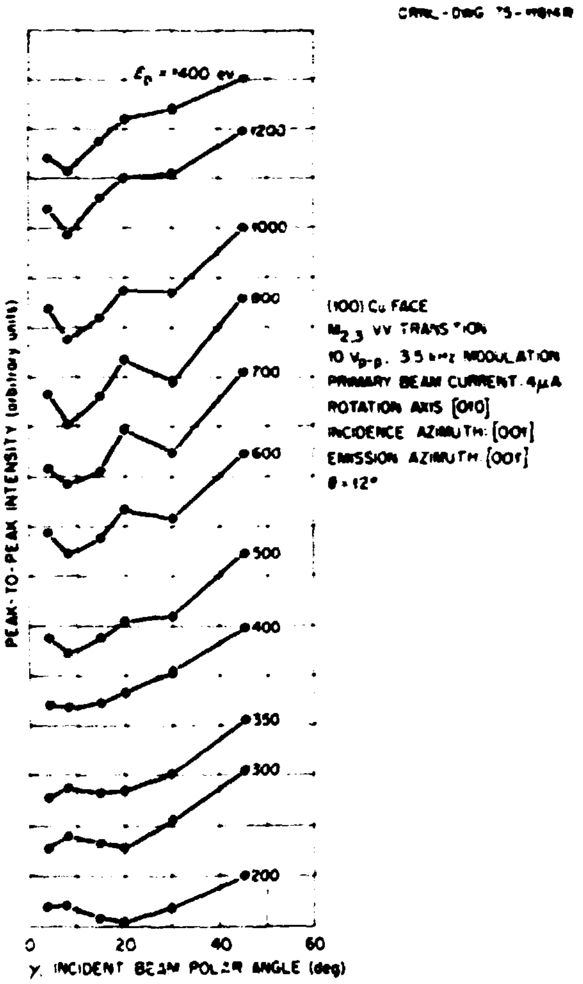

Fig. 2.8. *Experimental angular dependence for several values of primary energy E_p of the $M_{2,3}VV$ (62 eV) Auger transition from Cu (100) for $\phi = 45°$, [001], as a function of γ.*

In summary, the angular intensity distributions of Cu $M_{2,3}VV$ electrons emitted from a Cu *(100) surface* show much structure. Although the intensity variations measured are comparable in magnitude to those observed from a (110) copper surface, the emitted Auger electron distribution is unique to each surface. Comparison of the experimental observations with predictions of a theoretical model that assumes isotropic emission at the atom site provides little agreement, and it is apparent that anisotropic emission at the atomic site must be involved. Absolute and relative changes in intensity distributions are affected by variations of either the primary beam energy or angle of incidence. Also it is clear that the simple assumptions that have been made in attempting to make Auger electron spectroscopy a quantitative technique are incorrect, and more complex effects, such as anisotropic emission, must be included.

---

1. Summary of paper: *J. Vac. Sci. and Technol.* 13, 183 (1976).

2. See, for example, C. C. Chang, *Surf. Sci.* 48, 9 (1975); P. Staib and J. Kirschner, *Appl. Phys.* 3, 421 (1974); M. P. Seah, *Surf. Sci.* 32, 703 (1972).

3. D. M. Zehner, J. R. Noonan, and L. H. Jenkins, "Angular Effects in Auger Electron Emission from Cu (110)," this report.

4. L. McDonnell, D. P. Woodruff, and B. W. Holland, *Surf. Sci.* 51, 249 (1975).

5. H. L. Davis and Theodore Kaplan, "Theoretical Analysis of Angular-Dependent Auger Spectroscopy," this report.

ADSORPTION ON THE Cu (100) SURFACE: ANGULAR RESOLVED AES AND LEED STUDIES

J. R. Noonan D. M. Zehner L. H. Jenkins

Determination of the angular dependence of Auger electron emission from adsorbate-covered single-crystal surfaces has recently been suggested as a useful means for locating adsorption sites.[1] This possibility is being investigated in a study of oxygen or sulfur adsorption on a Cu (100) surface, using low-energy electron diffraction (LEED) and measurements of the angular intensity distribution of emitted Cu $M_{2,3}VV$ (62 eV) Auger electrons. A $(\sqrt{2} \times 2\sqrt{2})$-R45° LEED pattern was observed after exposures of a clean Cu (100) surface to $O_2 \gtrsim 500$ L. Subsequent to exposure to sulfur (10 – 10^3 L H_2S), a more complex diffraction pattern, a (2 × 2) with streaking followed by splitting of the $(h, k + \frac{1}{2})$ order spots, was observed with increasing coverage. In each case, either greater exposure or annealing only sharpened the observed diffraction patterns. The principal effect of the adsorbates was to attenuate the emitted Auger signal and produce a small redistribution in the angular emission intensity, as illustrated in Fig. 2.9. The data are presently being analyzed to determine if these types of measurements can be used successfully to identify adsorbate positions. Angular distributions of the adsorbate-emitted Auger electrons are also being studied as another possible method of establishing site geometry.

---

1. D. P. Woodruff, *Surf. Sci.* 53, 538 (1975).

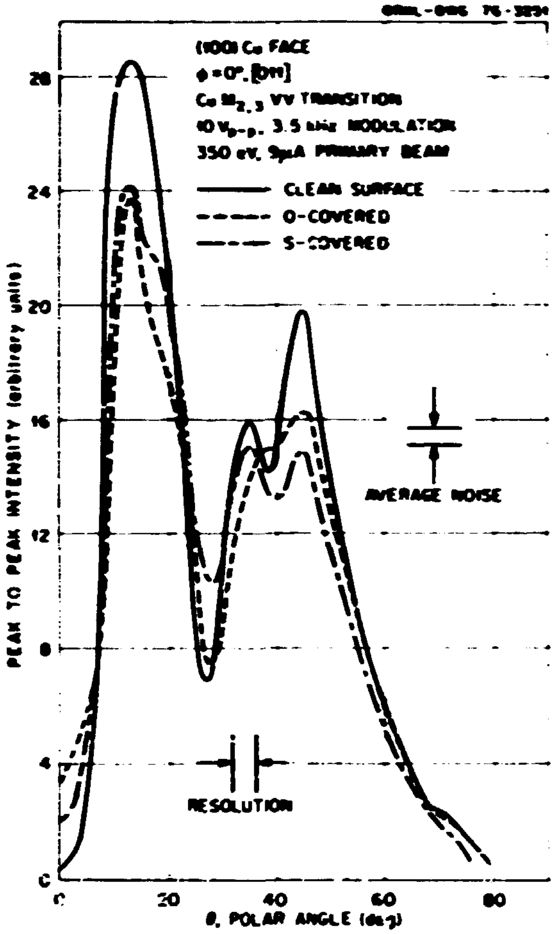

Fig. 2.9. Effect of sulfur and oxygen adsorbates on the experimental angular distribution of the Cu $M_{2,3}VV$ (62 eV) Auger transition from a Cu (100) surface along the [011], ϕ = 0°.

INVESTIGATIONS OF REORDERED SURFACES

D. M. Zehner J. F. Wendelken

For some time it has been known that clean surfaces of some single-crystalline metals, particularly those known to possess catalytic properties, undergo structural conversions such that the ordering of surface atoms is different from that of the substrate bulk. Gold surfaces also are known to exhibit such properties, and since they can be maintained clean for long periods of time under reasonable ultrahigh vacuum conditions, the physical surface properties of gold are being investi-

PHOTO 1248-76

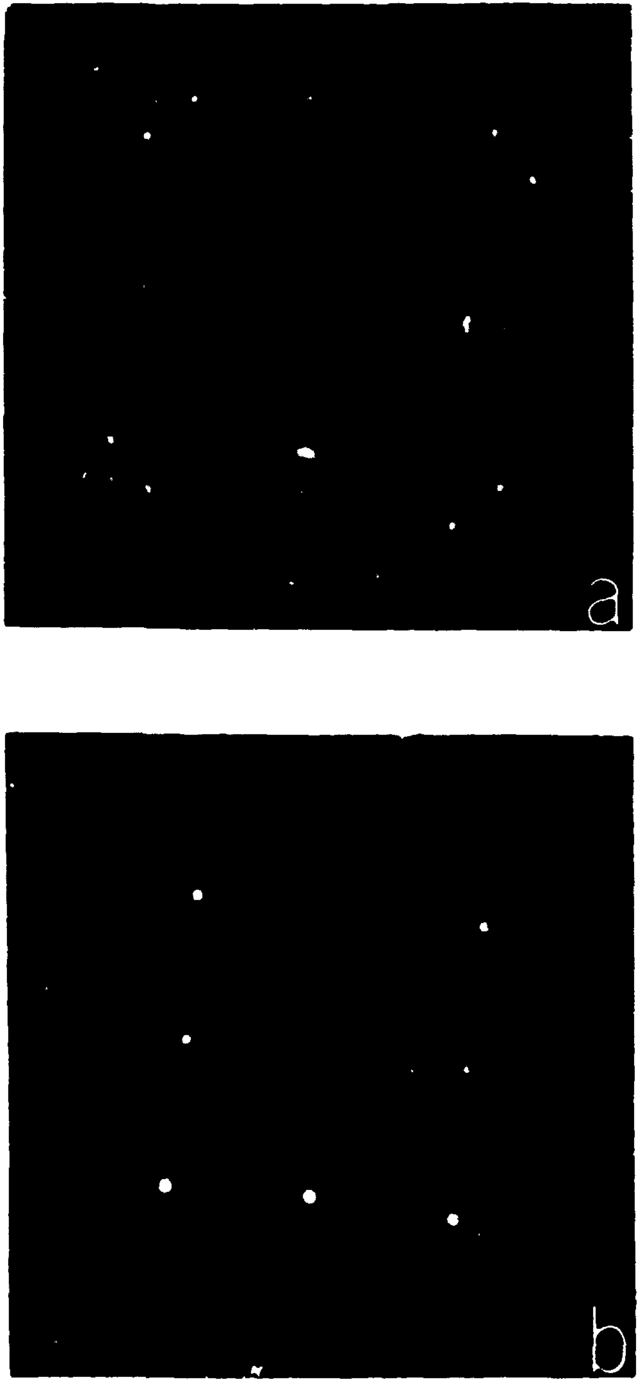

Fig. 2.10. LEED patterns from (001) gold surfaces: (*a*) clean reordered (5 × 20) structure and (*b*) normal (1 × 1) structure produced by O_2^+ ion bombardment. Primary beam energies (*a*) 64 eV and (*b*) 107 eV

gated using combined LEED, AES, and PICS techniques.

Although previous investigations[1] have shown that the normal gold (1 X 1) surface structure on the (001) surface can be obtained by long-term exposure to atmospheric environment, a more controlled method for producing this atomic arrangement is desirable. Recent observations with a (001) platinum surface[2] suggested that interaction of oxygen with the clean gold surface might produce the desired result. The conversion of the reordered gold (5 X 20) surface structure to the normal (1 X 1), as shown in Fig. 2.10, could be effected by bombarding the reordered surface with a 1-μA beam of O_2^+ ions at 200 eV for 1 hr in an oxygen pressure of 7×10^{-6} torr. Examination of this normal surface with Auger electron spectroscopy revealed no detectable contaminants. Exposure of the clean surface to molecular oxygen at pressures up to 10^{-5} torr with sample temperatures ranging from 22 to 700°C resulted in no detectable adsorption or surface rearrangement.

A clean (110) surface of gold was found to possess a (1 X 2) surface structure instead of the normal (1 X 1), an observation in agreement with previous work.[3] However, the (1 X 1) structure could be generated by heating the sample above 500°C. Upon cooling, the surface was observed to revert back to the (1 X 2) structure. Studies of the effects of oxygen ion interaction with this surface are currently under way, and PICS measurements will be initiated when the studies have been completed.

---

[1] D. M. Zehner, B. R. Appleton, T. S. Noggle, J. W. Miller, J. H. Barrett, L. H. Jenkins, and O. E. Schow III, *J. Vac. Sci. Technol.* **12**, 454 (1975).

[2] H. P. Bonzel, C. R. Helms, and S. Kelemen, *Phys. Rev. Lett.* **35**, 1237 (1975).

[3] D. G. Fedak and N. A. Gjostein, *Acta Metall.* **15**, 827 (1967).

SOFT X-RAY APPEARANCE POTENTIAL SPECTROMETRY

D. Kammer[1] D. M. Zehner J. F. Wendelken

A soft x-ray appearance potential spectrometer, similar in design and construction to that of Musket and Taatjes,[2] has been assembled and its performance evaluated and compared with the Auger electron spectroscopy (AES) technique. Some of the materials examined include gold, chromium, rhenium, and stainless steel. A major drawback of this technique is its inability to detect sulfur on these materials although it can be readily detected with AES. Another problem with the particular design concerned sample heating which resulted from the high electron bombardment current (1–10 mA) required with this simple arrangement. Surface conditions were frequently modified as a result of excessive heating.

An extensive effort, including ion bombardment and high-temperature heating in both a vacuum and an oxygen environment, was made to obtain a clean Cr (100) surface. Although the sample contained less than 10 ppm carbon, it was impossible to reduce the carbon concentration in the surface region below the detection limits of both techniques. On the cleanest possible surface the intensity ratio of the carbon L_3 to L_2 transitions was found to be almost 3:2 and not 1:1, as reported by Park and Houston.[3] It is believed that the reason for this difference is connected with the stainless steel photocathode used by Park and Houston.

---

[1] Oak Ridge Associated Universities faculty research participant from Albion College, Albion, Mich.

[2] R. G. Musket and S. W. Taatjes, *J. Vac. Sci. Technol.* **9**, 1041 (1972).

[3] R. L. Park and J. E. Houston, *Phys. Rev. B* **6**, 1073 (1972).

NEUTRON-SPUTTERING YIELDS FROM COBALT, NIOBIUM, AND GOLD[1]

L. H. Jenkins J. F. Wendelken
G. J. Smith[2] M. J. Saltmarsh[3]

High-energy neutron-sputtering yields have been determined for cobalt, niobium, and gold using a neutron source based upon the $^{9}\mathrm{Be}(d,n)$ reaction which employed 40-MeV deuterons from the ORIC to obtain neutron fluences $\approx 10^{16}$ neutrons/cm^2.

Using the experimental arrangement previously described,[4] two experiments have been conducted. In the first, graphite catcher foils were used because of their high purity and lack of activation products. In the second, polished silicon wafers were used as catcher foils in order to facilitate SEM examinations for "chunks" of material ejected from niobium targets supplied by groups at Argonne National Laboratory (ANL) and Battelle Pacific Northwest Laboratories (PNL).

From data collected in the first experiment the neutron-sputtering yields of cobalt, niobium, and gold were determined to be in the range of 10^{-5} to 10^{-4} particle per incident neutron. Careful examination of the collector foils from the second experiment showed no evidence for "chunk" emission from any of the foils supplied by either ANL or PNL.

---

[1] Summary of paper to be published.

[2] Present address: Brookhaven National Laboratory, Upton, Long Island, New York.

[3] Physics Division, ORNL.

[4] L. H. Jenkins, T. S. Noggle, R. E. Reed, M. J. Saltmarsh, and G. J. Smith, *Appl. Phys. Lett.* **26**, 426 (1975).

OPTICAL, ELECTRICAL, AND MAGNETIC PROPERTIES OF HIGH-TEMPERATURE MATERIALS

AN APPLICATION OF ELECTRON PARAMAGNETIC RESONANCE SPECTROSCOPY TO THE MEASUREMENT OF DIFFUSION RATES: Mn^{2+} IN MgO

Andre Chatelain[1] R. A. Weeks

The electrical resistivity of an insulating crystal is determined by the concentration of vacancies, interstitials (i.e., the stoichiometry of the crystal), and impurities. In many cases, charge is transported through a crystal by these defects. Thus, it is necessary to know the diffusion rates of mobile charged defects in order to determine their contributions to charge transport.

The most abundant impurities usually present in insulating refractory oxides are elements from the first transition series. When present in insulating crystals at low concentrations, these elements are usually present in valence states which have net magnetic moments. Consequently, electron paramagnetic resonance (EPR) spectra can usually be detected,[2] and the integrated intensity of any species' spectrum which is proportional to the number of ions in the crystal can be used as a measure of concentration of that impurity. For the case of diffusion of Mn^{2+} from the vapor phase into an MgO single crystal, the time rate of change of intensity of the Mn^{2+} EPR spectrum can be used to measure diffusion rates.

The solution of the diffusion rate equation for a plane sheet sample geometry (used in the experiments described here) has been given;[3] for small times and for the case in which $\sqrt{Dt}/l_x << 1$, then

$$\frac{N(t) \quad N_0}{S(C_1 \quad C_0)} = 4\sqrt{Dt/\pi}\,. \tag{1}$$

where $N(t)$ is the number of Mn^{2+} ions in an MgO sample at time t, N_0 is the number present in the sample at $t = 0$, C_0 is the concentration at $t = 0$, C_1 is the concentration of diffusion species at the surface of the sample, S is the surface area of the sample, l_x is one-half of the sample thickness, and D is the rate of diffusion.

The EPR spectrum of an ion in a crystal is determined in part by magnetic dipole-dipole and exchange interactions between the ions.[4] Assuming that the ions are randomly distributed in a crystal, these interactions alter the spectrum when ion concentrations are greater than 0.1 at. %. For example, for ion concentrations of 0.05% or less, the spectrum of Mn^{2+} in MgO consists of 30 lines, but for ion concentrations of 0.2% or more there is only one broad line.[5] In a first-order approximation to the case of Mn^{2+} diffusing into a planar crystal of MgO, the spectrum that will be observed will consist of two parts, one due to the interior of the crystal, in which the concentration is less than 0.1%, and one due to a region extending from the crystal surface to that region in the crystal at which the local Mn^{2+} concentration is about 0.1%. Of course, the transition from one spectral component to the other is a smooth function of the concentration but does occur between 0.05 and 0.20%. Figure 2.11 illustrates the geometry for this two-region approximation. The dashed line labeled $\epsilon(t)$ identifies the plane at which the local concentration changes from <0.1% to >0.1%. This definition of the transition is a mathematical constraint.

It is assumed that the concentration of a diffusing species C_1 at $-l_x$ and $+l_x$ is greater than C_0; that is, $C_1 >> C_0$. Hence the high-concentration spectrum is due to the diffusing species in the regions l_x to $\epsilon(t)$ and $\epsilon(t)$ to $+l_x$ and the low-concentration spectrum to the species in the region $l_x + \epsilon(t)$ to $l_x \quad \epsilon(t)$. The total number of diffusing ions is given by $N(t) = N_B(t) + N_N(t)$, where the subscripts B and N refer to the high- and low- concentration regions respectively. For small times (i.e., $2\sqrt{Dt}/l_x << 1$), then $N_B(t) >> N_N(t)$ and Eq. (1) is appropriate, for which $N(t) \approx N_B(t)$. The contribution from the low-concentration region can be shown to be

$$\frac{N_N(t) \quad 2C_0S_x[l_x \quad \epsilon(t)]}{S_x(C_1 \quad C_0)}$$

$$= 4\sqrt{Dt/\pi}\,\Bigg|\exp\left\{\quad[\epsilon(t)/2\sqrt{Dt}]^2\right\}$$

$$\frac{\epsilon(t)}{2}\sqrt{\pi/Dt}\;\mathrm{erfc}\;\epsilon(t)/2\sqrt{Dt} \tag{2}$$

$$\exp\left(\quad\left\{[2l_x \quad \epsilon(t)]/2\sqrt{Dt}\right\}^2\right)$$

$$+\left\{[2l_x \quad \epsilon(t)]/2\sqrt{Dt}\right\}\sqrt{\pi}\;\mathrm{erfc}\;[2l_x \quad \epsilon(t)]/2\sqrt{Dt}\,\Bigg|$$

In all cases considered here, $2\sqrt{Dt}/l_x \ll 1$ and $l_x \gg \epsilon$, and hence

$$\frac{N_x(t) - N_0}{S_x(C_1 - C_0)} = 4\sqrt{Dt/\pi}\left[\exp(-p^2) - p\sqrt{\pi}\,\mathrm{erfc}\,p\right], \quad (3)$$

where $p = \epsilon(t)/2\sqrt{Dt}$, a dimensionless quantity. Also, the concentration at the boundary ϵ can be calculated from the relation

$$C(\epsilon) = C_1\ \mathrm{erfc}\,p = \text{constant},$$

since C_1 and p are constants. If the derivation is valid, then it would be expected that $C(\epsilon) \approx 0.1\%$.

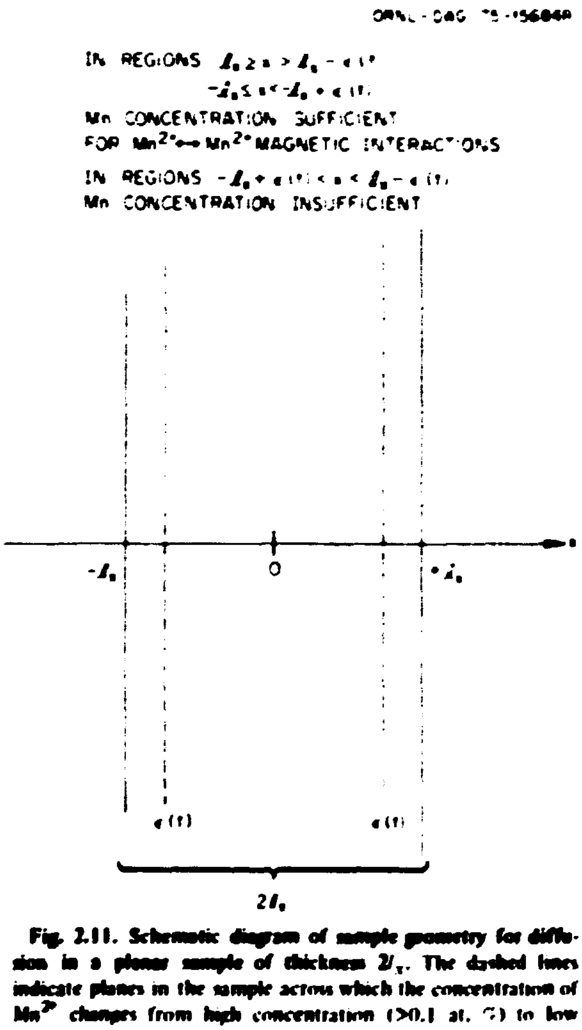

Fig. 2.11. Schematic diagram of sample geometry for diffusion in a planar sample of thickness $2l_x$. The dashed lines indicate planes in the sample across which the concentration of Mn^{2+} changes from high concentration (>0.1 at. %) to low concentration (<0.1 at. %).

The diffusion of Mn^{2+} into MgO single crystals was accomplished by sealing single-crystal platelets in evacuated quartz tubes containing manganese metal particles and heating in an electric furnace for increasing times at a particular temperature. Since the EPR measurement was nondestructive, the same sample was used for all the measurements at one temperature. The diffusion into the samples occurred by deposition of manganese vapor onto the surface of the samples. As a first approximation, it was assumed that the surface was covered with a monolayer of manganese atoms. With this assumption, the value of C_1 was equal to the density of manganese metal; that is, $C_1 = 8.1 \times 10^{22}$ cm^{-3}.

Single crystals from two sources, Norton Company and Abraham-Chen,[4] both grown by the arc-fusion method, were used. Impurities in these crystals were measured by flame spectroscopy; in the Norton crystal the sum of the impurities was <400 ppm, and in the Abraham-Chen crystal it was <120 ppm. Both specimens contained Mn^{2+}, but the concentrations differed greatly. The values of C_0 measured by EPR spectroscopy for the samples used in these experiments are given in Table 2.1. The absolute error in these measurements is ±30%, while the relative error is ±7%. Sample dimensions were approximately 0.1 × 0.3 × 1.0 cm. In evaluating D, corrections to S_x were incorporated to account for the four edge surfaces.

Diffusion anneals on samples of both crystals were made at four temperatures and four times up to 7 × 10[illegible] sec. The data are given in Table 2.1, and in Fig. 2.12 the diffusion rates are plotted vs $1/T$. In Table 2.1, the value given for D at each temperature is an average of the values for each sample. The values given for p and $C(\epsilon)$ could be determined only from data on the Abraham-Chen samples.

Within the error of the measurement, p is a constant with a value of 2.32 ± 0.04, and $C(\epsilon)$ also has a constant value to within ±12%. The value of $C(\epsilon)$ is in agreement with measurements on the concentration dependence of the spectrum of Mn^{2+} which show the transition from a low-concentration spectrum to a high-concentration spectrum occurring at about 0.2 wt %.[5]

In Fig. 2.12, the slope of the curve (a least-squares fit of the function $\ln D = \ln D_0 - E/kT$, where E is an activation energy, k is the Boltzmann constant, and T is temperature) gives a value $E = 2.10 \pm 0.25$ eV. The diffusion constant is $D_0 = 4.6 \times 10^{-6} \pm 30\%$ cm^2/sec. Measurements at two temperatures on manganese-metal-plated samples gave values of D which are also plotted in Fig. 2.12. For these samples, E has the same value, but D_0 is approximately three times as large as

Table 2.1. Data on diffusion rates of Mn^{2+} in MgO single crystals

T (°K)	C_0 (Norton) (spins/cm^3)	C_0 (A C) (spins/cm^3)	D (cm^2/sec)	p	$C(\epsilon)$ (wt %)
1223	4.65×10^{18}	5.67×10^{16}	1×10^{-14}	2.34	0.15
1313	4.37×10^{18}	5.50×10^{16}	4.2×10^{-14}	2.28	0.18
1403	4.63×10^{18}	5.30×10^{16}	1.4×10^{-13}	2.29	0.17
1511	4.38×10^{18}	5.78×10^{16}	4.3×10^{-13}	2.35	0.14
				2.32[a] ±0.04[b]	0.16[a] ±0.02[b]

[a] rms value.
[b] rms deviation.

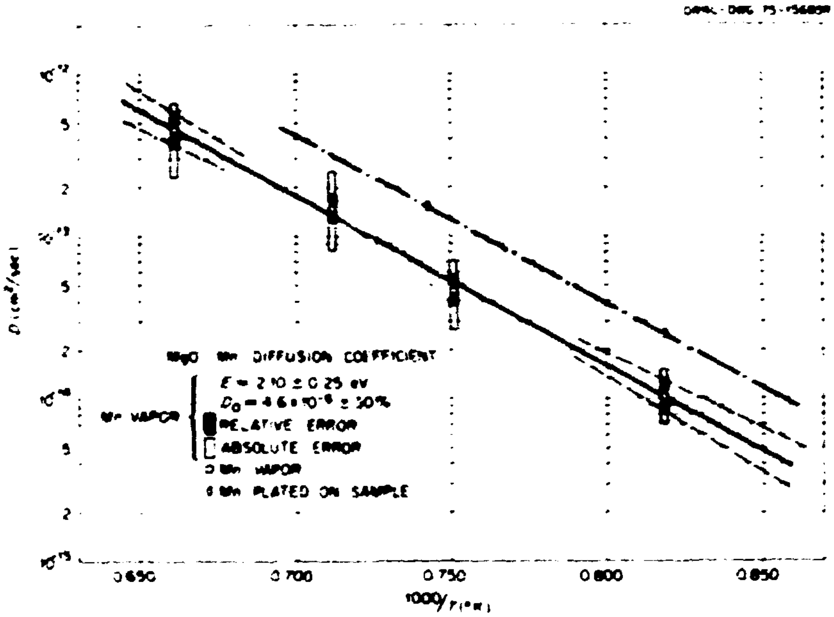

Fig. 2.12. Diffusion rate of Mn^{2+} in an MgO single crystal as a function of $1/T$ (°K).

the values for the vapor-diffusion experiments. We suggest that this higher value of D_0 indicates that the value assumed for C_t in the vapor diffusion experiment is too large and that the surface of the MgO crystals was not covered by a complete monolayer of Mn^{2+}.

The values for E and D_0 calculated from these experiments are larger than those reported by Tagai et al.[7] using electron-microprobe techniques for measuring concentration profiles. They give values $E = 1.2$ eV and $D_0 = 4.1 \times 10^{-7}$ cm^2/sec. For some divalent ions of the first transition series (Co^{2+}, Fe^{2+}, and Ni^{2+}), Weunch and Vasilos[8] found $1.8 \leq E \leq 2.1$ eV and $1.8 \times 10^{-5} \leq D_0 \leq 5.78 \times 10^{-5}$ cm^2/sec; the measurements reported here are in reasonable accord.

---

[1] Summer research participant from Ecole Polytechnique, Lausanne, Switzerland.

2. J. W. Orton, chap. 11 in *Electron Paramagnetic Resonance*, Iliffe Books, Ltd., 1968.

3. J. Crank, chap. IV in *The Mathematics of Diffusion*, Oxford University Press, 1956.

4. G. E. Pake and T. L. Estle, chap. 6 in *The Physical Principles of Electron Paramagnetic Resonance*, 2d ed., W. A. Benjamin, Inc., 1973.

5. J. A. Boatner, p. 83 in "A Magnetic Resonance Study of *S*-State Ions in Cubic Crystalline Fields," thesis, Vanderbilt University, June 1966.

6. M. M. Abraham, C. T. Butler, and Y. Chen, *J. Chem. Phys.* 55, 3752 (1971).

7. H. Tagai, S. Iwai, T. Iseki, and M. Saho, *Radex Rundsch.* 4, 577 (1965).

8. B. J. Wuensch and T. Vasilos, p. 99 in *Mass Transport in Oxides*, ed. by J. B. Wachtman and A. D. Franklin, National Bureau of Standards Special Publication 296.

OXIDATION OF ELECTRIC-FIELD-REDUCED MgO SINGLE CRYSTALS

J. C. Pigg R. A. Weeks
K. F. Kelton[1]

Application of electric fields (500 to 2000 V/cm) through platinum electrodes to MgO single crystals containing impurities from the first transition series of elements reduces the valence state of these impurities.[2] For example, Fe^{3+} is reduced to at least Fe^{2+}. Direct evidence of the presence of iron in the 2+ state has not been obtained, and its presence is inferred on the basis of the experiments described below.[2] These reduced valence states are oxidized if the reduced samples are heated in air in the absence of an electric field.

The effect of isochronal anneals on the intensity of the charge-transfer band of Fe^{3+} at 2850 Å and the absorption at 2400 Å is shown in Fig. 2.13. After treatment in an electric field, no band is resolved at 2850 Å, and a small band remains at 2125 Å, where previously the sample had been opaque. At temperatures in excess of 1300°K, bands are resolved at 2800 Å and 2125 Å, which increase with additional annealing. Using the absorption coefficient of an untreated crystal cut from the same ingot adjacent to the crystal treated by the electric field as α_0, it is evident that for temperatures above 1640°K the concentration of Fe^{3+} exceeds that present initially. Since the slope of the curve drawn through the data points is approximately constant between 1450 and 1675°K, the highest temperature reached in these anneals, it is evident that anneals at higher temperatures will further increase the concentration of Fe^{3+}.

Data for the recovery of the 2850-Å absorption band for two temperatures are plotted in the usual way in Fig. 2.14. The same value for α_0 was used as that in Fig. 2.13. There is considerable uncertainty in the values at 2850 Å for values of $f(\Delta\alpha)$ below 0.4 due to the presence of the strong band at about 2125 Å, which appears to recover in the same manner as the 2850 Å band.

It is clear from the data displayed in Figs. 2.13 and 2.14 that the growth of the absorption bands is not a simple process. Activation energies taken from the isothermal curves[3] increase linearly from 1.5 eV at $f(\Delta\alpha) = 0.4$ to 3.9 eV at $f(\Delta\alpha) = 0.9$. This is similar to

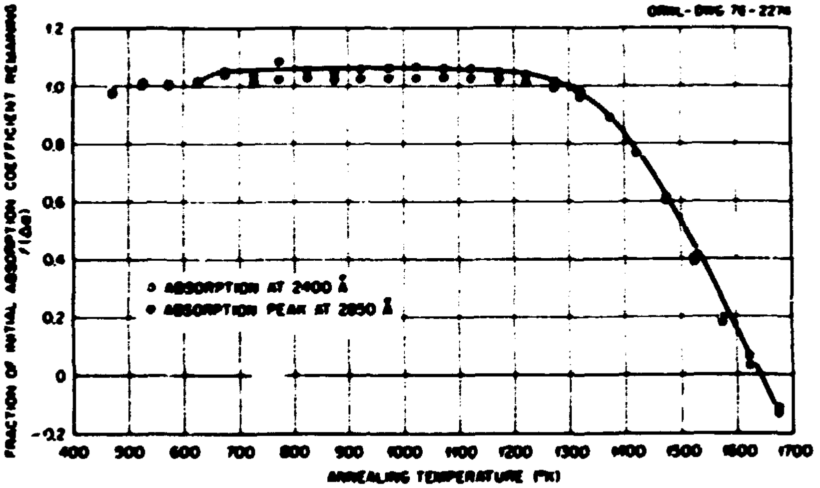

Fig. 2.13. Fractional changes in the absorption coefficient at 2400 and 2850 Å of a section of treated MgO crystal as a function of isochronal anneals of 1-hr pulses from 470 to 1670°K. The treatment of the crystal was $E = 1000$ V/cm, $900 < T < 1200$°C in air for 100 hr.

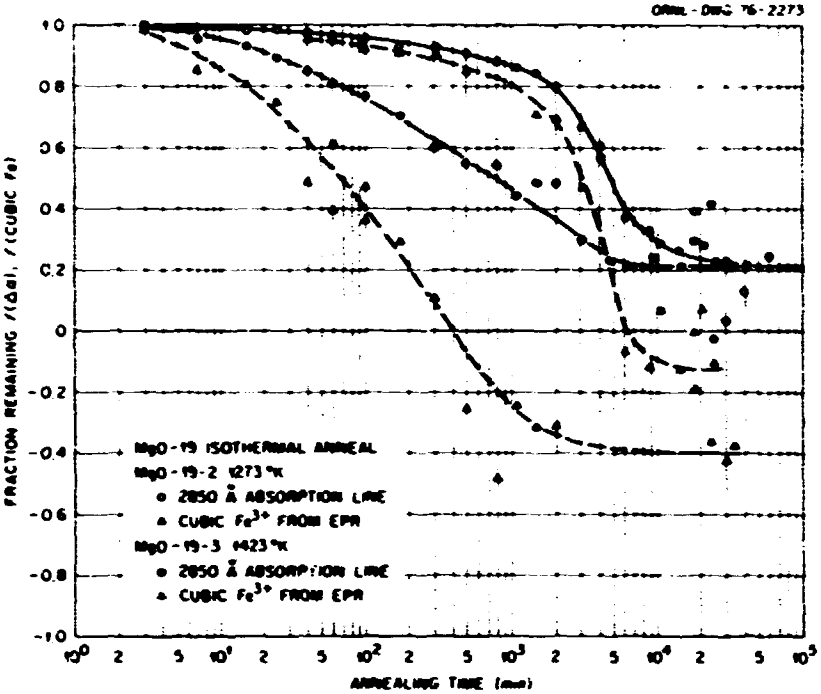

Fig. 2.14. Fractional changes in the optical absorption coefficient at 2850 A and the Fe^{3+} concentration measured by EPR of section of treated MgO crystal as a function of isothermal anneals at two temperatures. The treatment of the crystal was E = 1000 V/cm, $900 < T < 1200$°C in air, for 100 hr.

the range of activation energies measured previously for electrical conductivity.[4-9]

From measurements of the intensity of the EPR spectra of Fe^{3+} in sites of cubic symmetry, the concentration of Fe^{3+} in these sites was deduced. Data for the fractional charge of these sites are also shown in Fig. 2.14. It is evident from the EPR measurements that the saturation value of the Fe^{3+} concentration after anneal exceeds the initial concentration as measured in the untreated sample. The Fe^{3+} state generated in this manner does not bleach when exposed to room light, as does the irradiation-induced Fe^{3+} state in the treated sample.[2]

Heating an untreated sample in air at these temperatures increased the Fe^{3+} concentration by <10%, while after the electric field treatment and subsequent anneals in air in the same temperature range increases of > 30% were observed. This effect indicates that the movement of the charge carriers through the crystal had increased the concentration of entities which, after oxidation, can compensate the excess charge on Fe^{3+}. Although the concentration of Fe^{3+} is greater than it is in the untreated crystal, it is still less than the total concentration of iron as measured by either flame spectroscopy or x-ray fluorescence analysis. Hence some fraction of the iron still has a valence less than +3.

REDUCTION OF Fe^{3+} IN MgO SINGLE CRYSTALS BY APPLICATION OF ELECTRIC FIELDS

R. A. Weeks L. D. Hulett[1]
J. C. Pigg K. F. Kelton[2]

Magnesium oxide crystals, grown by the arc-fusion technique (Norton Company), have been subjected to electric fields (500 to 2000 V/cm) at temperatures in the range 900 to 1200°C, in air, for periods up to 150 hr. Optical and electron paramagnetic resonance (EPR) measurements have been made before treatment and as

---

1. ORAU undergraduate research trainee from Arkansas Polytechnic University, Russellville, Ark.

2. R. A. Weeks, J. C. Pigg, L. D. Hulett, and K. F. Kelton, "Reduction of Fe^{3+} in MgO Single Crystals by Application of Electric Fields," this report.

3. A. C. Damask and G. J. Dienes, p. 146 in *Point Defects in Metals*, Gordon and Breach, New York and London, 1963.

4. S. P. Mitoff, *J. Chem. Phys.* 31, 1261 (1959).

5. H. Schmalzried, *J. Chem. Phys.* 33, 940 (1960).

6. S. P. Mitoff, *J. Chem. Phys.* 33, 941 (1960).

7. S. P. Mitoff, *J. Chem. Phys.* 36, 1383 (1962).

8. S. P. Mitoff, *J. Chem. Phys.* 41, 3561 (1964).

9. R. A. Weeks and J. C. Pigg, *Solid State Div. Annu. Prog. Rep. Dec. 31, 1974*, ORNL-5028, p. 73.

a function of position in the sample with respect to the positive and negative electrodes after treatment. Principal impurities present in these crystals, in ppm, were Fe (125), Mn (10), Ni (10), Cr (15), V (<5), Ca (65), Al (10), Si (10), and Zr (10). On the basis of a comparison of the amount of iron measured by x-ray fluorescence spectroscopy with the amount of Fe^{3+} deduced from EPR and optical measurements, approximately 20% of the iron present in the untreated crystal was in the +3 valence state, a major fraction of which was located in regular octahedral crystal sites, but some of the Fe^{3+} was in noncubic sites. Before treatment, the EPR spectra of the crystals contained components due to the presence of Mn^{2+}, Cr^{3+}, and V^{2+} (ref. 3).

After lengthy application of an electric field at high temperature, the crystals were cut into slabs whose faces were perpendicular to the direction of the electric field. These slabs typically were 0.1 cm in thickness, and between eight and ten slabs were obtained from each sample. The curves in Fig. 2.15 are the absorption coefficients vs light energy before treatment, after treatment, and after irradiation in a ^{137}Cs source. The two bands with peaks at 4.3 and 5.8 eV are charge-transfer bands[4] of Fe^{3+}. The decrease in the Fe^{3+} concentration following treatment, indicated by the decrease in the charge-transfer bands, was corroborated by EPR measurements. The Fe^{3+} concentration was reduced to <0.05 times the initial concentration. As can be seen in Fig. 2.15 and corroborated by EPR measurements, the concentration of Fe^{3+} after gamma-ray irradiation was about half the initial concentration. Increasing the radiation dose above 10^5 *R* did not increase the Fe^{3+} concentration. This enhancement could be either bleached with ambient room light or annealed at room temperature over a period of about 24 hr.

In samples heated to the same temperatures under the same conditions, but without the electric field, the concentration of Fe^{3+} increased by ≤10%. Irradiation of these samples with gamma rays to the same dose as the treated samples did not alter the Fe^{3+} concentration to within the accuracy of the measurement.

The concentration of iron measured with an x-ray fluorescence spectrometer was the same before and after treatment to within the accuracy of the measurement (±10% relative).

On the basis of these experiments, we tentatively conclude as follows: (1) The crystal is reduced by heating in an electric field, the reduction being indicated by the decrease in Fe^{3+} concentrations. (2) Approximately 50% of the initial Fe^{3+} can be regenerated by gamma-ray irradiation. The regenerated Fe^{3+} is unstable. The enhancement of Fe^{3+} concentration after irradiation is attributed to an excitation of an electron from Fe^{2+} ions and the trapping of the electrons in shallow traps. (3) The Fe^{3+} which is observed by EPR spectroscopy after treatment and after gamma-ray irradiation occupies crystal sites similar to those occupied before treatment. Hence, the

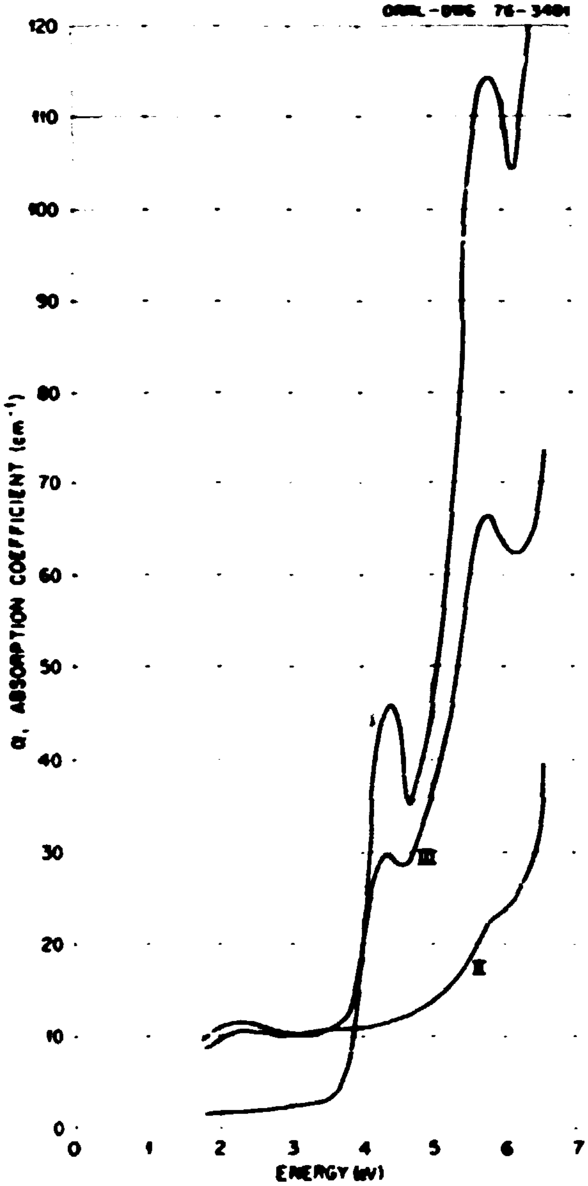

Fig. 2.15. Optical absorption of MgO single crystals: I, as received; II, heated for about 100 hr at 900 ≤ *T* ≤ 1200°C, in electric fields of about 1000 V/cm and in air; III, irradiated with 10^6 R of ^{137}Cs gamma rays.

alterations in the crystal produced by the electric field do not appear to affect the site symmetry of an impurity such as iron.

---

1. Chemistry Division, ORNL.

2. ORAU undergraduate research trainee from Arkansas Polytechnic University, Russellville, Ark.

3. J. W. Orton, chap. 11 in *Electron Paramagnetic Resonance*, Iliffe Books Ltd., 1968.

4. R. W. Soshea, A. J. Dekker, and J. P. Sturtz, *J. Phys. Chem. Solids* 5, 23 (1958).

PRODUCTION OF POINT DEFECTS IN 14.8-MeV NEUTRON-IRRADIATED MgO[1]

Y. Chen M. T. Robinson
M. M. Abraham J. B. Mitchell[2]
R. A. Van Konynenburg[2]

Magnesium oxide is an ideal host to study the characteristics of the radiation damage resulting from fusion neutrons compared with those resulting from fission neutrons, because many of the fundamental point defects in MgO have been identified using optical and magnetic resonance spectroscopy. Quantitative measurements of the various types of defects are therefore readily accessible. In this study, high-purity MgO crystals grown at ORNL were irradiated in the LLL 14.8-MeV rotating-target neutron source (RTNS) to doses varying from 1.8×10^{16} to 5.7×10^{17} neutrons/cm^2. The optical absorption spectra of these crystals resembled those irradiated in fission reactors and exhibited bands principally at 4.95, 3.5, 2.2, and 1.3 eV, as shown in Fig. 2.16. The band with the largest absorption coefficient, that at 4.95 eV, is due to anion vacancies. The bands at 3.5 and 1.3 eV, attended by zero-phonon lines at 3.430 and 1.187 eV respectively, have been attributed to different optical transitions of anion divacancies. Our investigations indicate that the net production rates of the point defects resulting from irradiations with 14.8-MeV neutrons are about twice those resulting from fission neutrons in the Oak Ridge Research Reactor (ORR), as shown in Fig. 2.17. This ratio is in reasonable accord with theoretical estimates based on damage energy calculations.

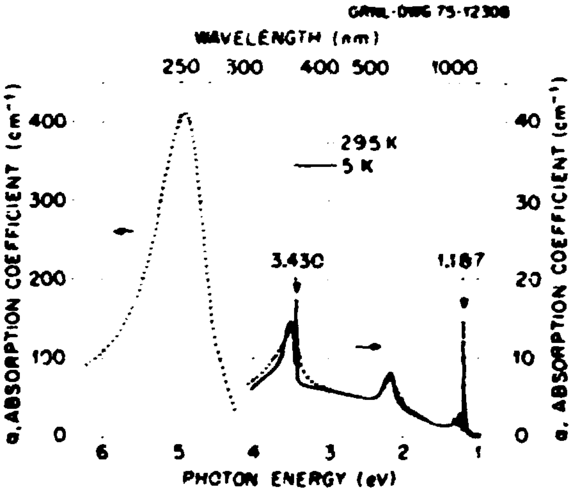

Fig. 2.16. Optical spectra of an MgO crystal irradiated with 14.8-MeV neutrons to a fluence of 5.8×10^{17} neutrons/cm^2.

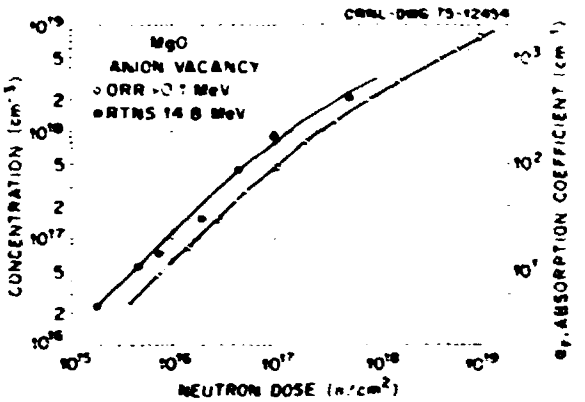

Fig. 2.17. Concentration of anion vacancies and absorption coefficient of the 4.95-eV band for MgO resulting from neutron irradiations in the RTNS and ORR.

---

1. Summary of paper: *Radiation Effects and Tritium Technology for Fusion Reactors*, ed. by F. W. Wiffen and J. S. Watson, ERDA report CONF-750989, Oak Ridge, Tenn., in press.

2. Lawrence Livermore Laboratory, Livermore, Calif.

OPTICALLY DETECTED PARAMAGNETIC RESONANCE OF DEFECTS IN BaO[1]

F. A. Modine Y. Chen

There has been long-standing interest in BaO because its electronic properties have found useful application in oxide-coated cathodes. These properties have always been attributed to defects that donate electrons, but only recently has progress been made toward identifying these defects.[2] Although several defects in BaO have been revealed by their optical spectra and to a lesser extent by their paramagnetic resonance spectra, their identities have been much debated. Most of the controversy has concerned the identity of the defects giving optical absorption bands at 2.0 and 2.6 eV.[3,4]

Each band has been variously assigned to the one-electron F^+ and the two-electron F center.

An optically detected paramagnetic resonance study was undertaken to establish conclusively the identities of the defects which produce the optical bands. The study utilized a microwave-optical double-resonance technique that detects the changes in the magnetically induced circular dichroism (MCD) of an optical band resulting from the ground-state spin-temperature variations caused by resonant microwave absorption. Figure 2.18 shows an optically detected resonance spectrum measured for the largest dichroism peak of the 2-eV optical band. The F^+-center EPR spectrum[5] is clearly revealed. The large central line derives from the 30% of the centers that have no neighboring magnetic isotopes. Hyperfine lines are also seen. The lines indicated on the figure derive from the 40% of the centers having only one near-neighbor magnetic isotope (I = 3/2), either 6.6%-abundant ^{135}Ba or 11.3%-abundant ^{137}Ba. Many weaker, unresolved lines can be attributed to centers with two or more magnetic isotopes. However, the spectrum also exhibits prominent lines not attributable to F^+ centers, notably one near 8.63 kG and a pair flanking the central line. These lines are associated with other defects. They appear because the optical bands of these defects underlie the F^+ band and because of cross-relaxation processes.

The bands that underlie the F^+ band were revealed by measuring thermally annealed crystals. A short anneal at 150°C removed about 95% of the F^+ centers, and the spectra of defects having greater thermal stability than the F^+ center were better resolved. Optical spectra showed weak overlapping absorption bands at 1.5, 1.7, 2.0, and 2.6 eV. The optically detected paramagnetic resonance spectra measured at the dichroism peaks of these bands are shown in Fig. 2.19. Hyperfine structure is unresolved in these weaker spectra, but three stronger lines are clearly detected. The center line has g = 1.935 ± 0.002 and is a remnant of the F^+-center spectrum. The lines flanking the F^+ line were revealed as due to ⟨100⟩ axial defects by standard microwave absorption measurements. Actually, the axial lines belong to two axial sets. The low-field line is a double perpendicular with $g_\perp$ = 1.940 ± 0.002. The higher field line is composed of the parallel line of this set with $g_\parallel$ = 1.930 ± 0.002 and the superimposed double perpendicular of another set with $g_\perp$ = 1.930 ± 0.002. The parallel line of this other set has $g_\parallel$ = 1.886 ± 0.002 and is at a higher field than measured in the optical spectra.

The differences in the optically detected spectra reveal the origins of the optical bands. The 640-nm dichroism peak of the 2-eV band shows the strongest response to the center line, reaffirming its assignment to the F^+ center. A relatively stronger response to the axial lines is found for the MCD peak at 720 and 440 nm, implying that the 1.7- and 2.6-eV bands are associated with the axial defects. The peak at 800 nm correlates with none of the strong lines but displays a broad decrease at about 8.88 kG which probably correlates with an EPR line that is too broad to appear in a microwave absorption-derivative spectrum.

This study eliminates further doubt regarding the identity of the F and F^+ bands in BaO. The 2.0-eV band is due to the F^+ center. The 2.6-eV band is due to an axial defect and is, therefore, neither the F nor the F^+ band, although it may be due to an axial variant of

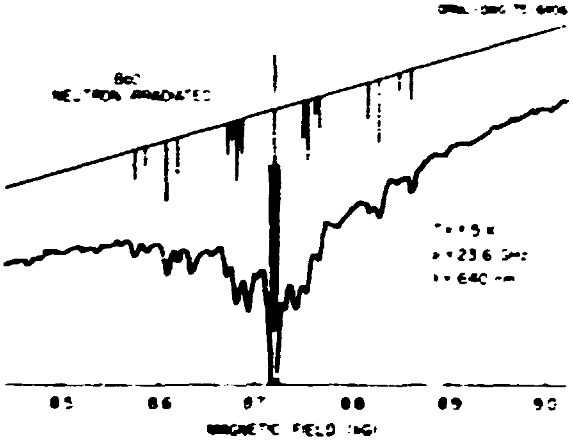

Fig. 2.18. An optically detected paramagnetic resonance spectrum showing the F^+ central line and hyperfine structure.

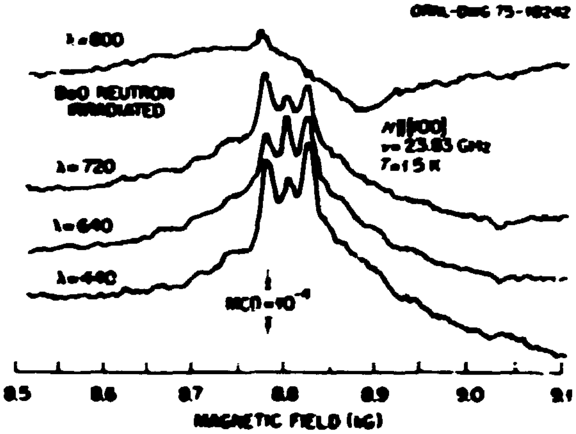

Fig. 2.19. Optically detected paramagnetic resonance spectra measured after a thermal anneal to decrease the F^+-center concentration.

the F^+ center. Moreover, other investigators[2] have recently made a well-based assignment of the F band at 2.3 eV, and all questions regarding these bands are, therefore, resolved.

---

[1] Summary of paper to be published.

[2] B. H. Rose and E. B. Hensley, *Phys. Rev. Lett.* 29, 861 (1972).

[3] T. J. Turner, *Solid State Commun.* 7, 635 (1969) and references therein.

[4] P. D. Townsend and J. C. Kelly, *Colour Centres and Imperfections in Insulators and Semiconductors*, Crane Russak and Co., New York, 1973.

[5] K. E. Mann, L. V. Holroyd, and D. L. Cowan, *Phys. Status Solidi* 33, 391 (1969).

MAGNETO-OPTICAL STUDY OF F^+ CENTERS IN MgO and BaO[1]

F. A. Modine R. W. Major[2]
Y. Chen

Magneto-optical spectra of neutron-irradiated MgO and BaO have been studied in order to complete a spectroscopic investigation of the properties of F^+ centers in alkaline-earth oxide crystals. Optical absorption and magnetic circular dichroism (MCD) measurements were made in order to verify the optical band assignments and to determine the spin-orbit interaction between the excited electron and the lattice ion cores. The results are pertinent to the understanding of defects in oxide materials.

Spectra of the F^+ center were more difficult to resolve in MgO and BaO than in the CaO and SrO crystals investigated earlier.[3] Other spectra overlap the F^+ band in both cases. For MgO the problem was solved by using very high purity crystals that were especially low in impurity Fe^{3+}, which contributed most of the difficulty. In BaO, overlapping spectra are contributed by other irradiation-produced defects, and a complete resolution of the F^+-center spectra was not possible.

Spectra were analyzed by the method of moments.[4] In the BaO case, the strong overlapping spectra necessitated an approximate analysis, and only the lower energy portion of the spectrum was analyzed. The spin-orbit splittings in the unrelaxed optically excited states were found to be 18 ± 3 cm^{-1} for MgO and 380 ± 190 cm^{-1} for BaO. Both results are in surprising agreement with values previously obtained from less accurate Faraday rotation (FR) measurements.[5,6] Although there is no basis for disagreement between MCD and FR results, agreement could not be foreseen. Prior to this investigation only disparate MCD and FR results for the spin-orbit splittings in CaO and SrO had been obtained.[3] For MgO, higher moments of the spectra could be analyzed, and they imply an optical bandwidth predominantly contributed by noncubic lattice modes.

---

[1] Summary of paper to be published.

[2] On leave from University of Richmond, Richmond, Va.

[3] F. A. Modine, R. W. Major, Y. Chen, and J. M. Wilson, *Solid State Div. Annu. Prog. Rep. Dec. 31, 1974*, ORNL-5028, p. 78.

[4] C. H. Henry, S. E. Schnatterly, and C. P. Slichter, *Phys. Rev.* 137, A583 (1965).

[5] J. C. Kemp, J. C. Cheng, E. H. Izen, and F. A. Modine, *Phys. Rev.* 179, 818 (1969).

[6] R. G. Bessent, B. C. Cavenett, and I. C. Hunter, *J. Phys. Chem. Solids* 29, 1523 (1968).

EFFECT OF PLASTIC DEFORMATION ON HOLE-DEFECT FORMATION IN MgO[1]

Y. Chen L. C. Templeton
M. M. Abraham E. Sonder

Previous investigators have shown that plastic deformation causes the intensity of the 2.3-eV trapped-hole-center band in MgO to increase. They interpreted this increase in terms of formation of new vacancies. Our present study indicates that the deformation-induced

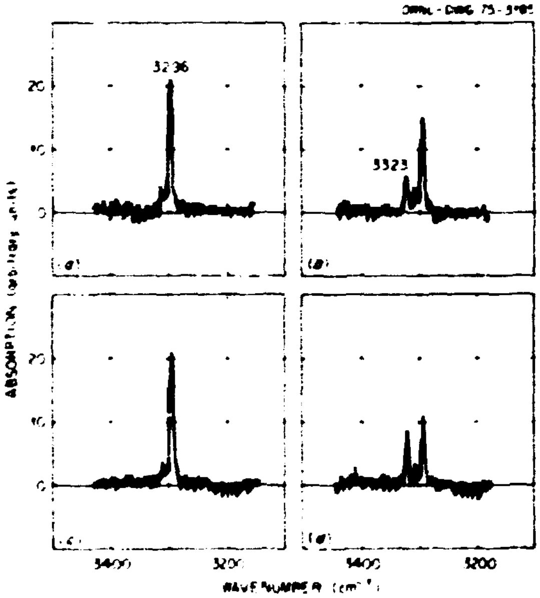

Fig. 2.20. Infrared adsorption of a hydrogen-containing MgO crystal after (*a*) quenching, (*b*) gamma irradiation, (*c*) deformation to 2.6%, and (*d*) gamma irradiation.

increase occurs only in hydrogen-containing crystals. EPR and ENDOR results have shown that for such crystals, the increase is almost exclusively due to the increase of V_{Al} (linear configuration Al^{3+} O^- [Mg vacancy] O^{2-}) and V_{OH} (configuration O^- [Mg vacancy] H^+O^{2-}) centers. For the case of V_{OH} centers, we have further been able to show by observing the infrared OH stretching vibration at 3323 cm^{-1} (V_{OH} sites) and 3296 cm^{-1} (V_{OH} sites), shown in Fig. 2.20, that the number of V_{OH} centers increases at the expense of the V_{OH} centers and that no new hydrogen-associated vacancies are formed by deformation. *The increase in the optical band is, therefore, due to impurity-associated vacancies present before deformation.* For hydrogen-free crystals, deformation does not increase the V_F and V_{Al} concentrations, and furthermore no V^- or V^0 centers could be detected. Hence we conclude that in hydrogen-containing crystals, deformation stimulates the conversion of existing vacancies to their trapped-hole counterparts, the V_{Al}, V_{OH}, and V_F centers.

---

1. Summary of paper to be published.

LUMINESCENCE IN DEFORMED MgO, CaO, and SrO[1]

Y. Chen T. J. Turner[2]
M. M. Abraham C. M. Nelson[3]

Plastic deformation in the alkaline-earth oxides produces optical absorption bands, the most pronounced of which occurs at 5.7 eV in MgO, 4.6 and about 5.8 eV in CaO, and 4.1 and about 5.0 eV in SrO. Excitation in these energy regions generates luminescence bands, with peaks at 2.9 (violet), 2.6 (blue), and 2.3 (green) eV in MgO, CaO, and SrO respectively. The dependence of the emission spectra on temperature and on anisotropy give clear indications that multibands are involved. The visible emission provides a convenient means of observing slip systems without artificial decoration techniques. Correlation between emission intensity pattern and dislocation etch-pit density has been demonstrated in MgO. The luminescence effect permits an instantaneous and clear observation of gross imperfections as they are being formed in a solid, either on the surface or in the bulk, so that the dynamical processes of dislocation interactions can be studied. By monitoring the emission intensity as a function of stress and strain, such as shown in Fig. 2.21, it was found that the defects responsible for the emission are formed at the onset of plastic deformation. No observable emission was detected prior to compression, and emission did not take place during the initial phase of compression. Luminescence began to take place when the stress-strain curve deviated from linearity, as indicated by the vertical dotted line near the 1% compression mark. That the luminescence intensity was not enhanced in the linear portion, which has previously been attributed to the elastic region, is evidence that the luminescence is due to intrinsic defects induced by plastic flow. As cracks developed, evidenced by the spontaneous decrease of the shear stress with presumably more defects being formed, the emission intensity increased correspondingly.

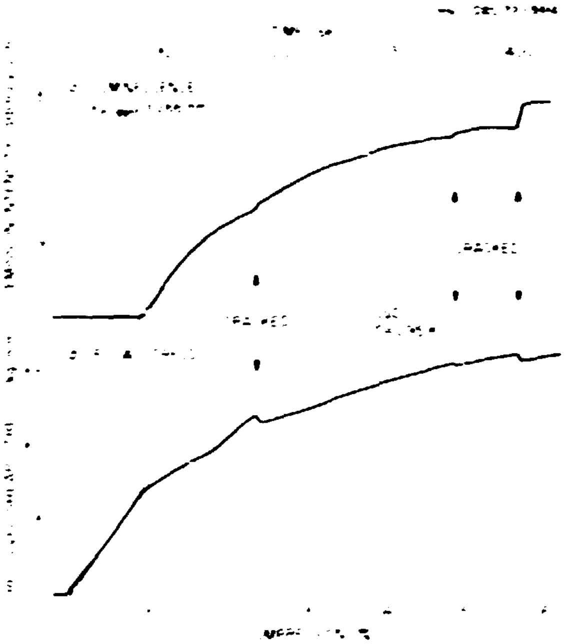

Fig. 2.21. Intensity of luminescence (upper curve) and shear stress (lower curve) as a function of compression with a CaO crystal under ultraviolet excitation. Upper abscissa represents scanning time for both curves.

---

1. Summary of paper: *Philos. Mag.* 32, 99 (1975).
2. Wake Forest University, Winston-Salem, N.C.
3. Emory and Henry College, Emory, Va.

THE USE OF SELF-TRAPPED HOLE-CENTER EPR SPECTRA FOR DETERMINING CRYSTAL PARAMETERS CONNECTED WITH THE CUBIC-TETRAGONAL PHASE TRANSITION IN RbCaF₃

E. Sonder[1] L. F. Haliburton[2]

It is now well known[3-5] that $RbCaF_3$, which has a cubic perovskite structure at temperatures above 200°K.

undergoes a phase change and becomes increasingly tetragonal as the temperature is lowered below 193°K. Upon cooling through the critical temperature, single crystals develop domains whose unique axes are usually aligned along two of the original ⟨100⟩ axes. It has been shown that the tetragonal symmetry of a domain results from the twisting of CaF_6 octahedra about the tetragonal axis.[3]

Irradiation of $RbCaF_3$ at low temperature (for example, 15 min at 78°K in a 10^6-R hr^{-1} ^{137}Cs gamma source) produces an EPR spectrum that can be identified as being due to a self-trapped hole ($[F_2^-]$ molecular ion). The following discussion concerns a portion of the EPR spectrum, in particular that portion which in a cubic crystal (e.g., $KMgF_3$) (ref. 6) corresponds to a single line that appears at the high-field end of the spectrum of a sample with a cubic axis parallel to the magnetic field. That line is single because all self-trapped holes have their axes aligned 45° to the magnetic field. Rotating such a sample around an axis perpendicular to the magnetic field increases the angle between the center axis and magnetic field direction of some of the self-trapped holes and decreases it for others. This procedure produces splitting of that line which increases with rotation.

In our case ($RbCaF_3$), for which tetragonal domains exist, the high-field EPR line will be very similar to that for a cubic crystal *for those domains whose tetragonal axes* (which are also the axes of CaF_6 octahedra rotation) *are parallel to the magnetic field*. For those

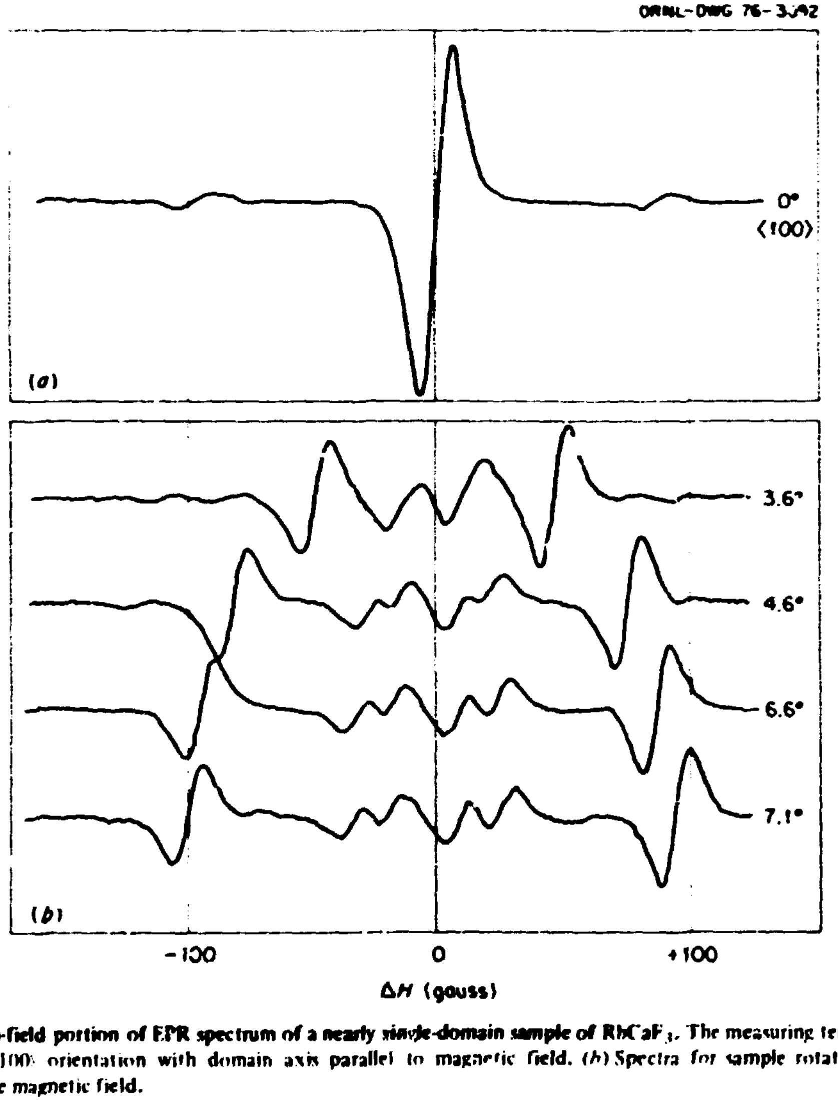

Fig. 2.22. High-field portion of EPR spectrum of a nearly single-domain sample of $RbCaF_3$. The measuring temperature is 95°K. (*a*) Spectrum for ⟨100⟩ orientation with domain axis parallel to magnetic field. (*b*) Spectra for sample rotated around an axis perpendicular to the magnetic field.

domains, however, for which the tetragonal axes are perpendicular to the magnetic field, the CaF_6 octahedra are rotated so that some of the self-trapped hole axes are off the 45° angle. This produces a line splitting, the amount of which depends upon the angle of rotation of the octahedra.

Fig. 2.22*a* depicts the high-field portion of the EPR spectrum for a sample with a majority of domains having their axes parallel to the magnetic field. This orientation produces the large line in the center of the portion of the spectrum shown. The two satellites are due to domains with perpendicular axes. Figure 2.22*b*, drawn on the same field scale, shows the splitting of the large line due to rotation of the whole crystal about an axis perpendicular to the magnetic field. The splitting becomes the same as that of the satellites in the [100] orientation (Fig. 2.22*a*) when the crystal is turned about $6^1/_2$° off the [100] axis. This correspondence in splitting shows that the satellites correspond to domains rotated around the unique crystal axis by about $6^1/_2$° at the temperature of measurement, 95°K. Detailed computer calculations now in progress confirm this reasoning and will permit accurate determination of EPR Hamiltonian parameters and bending angles, as well as rotation angles, by using not only the extreme lines shown here but the entire EPR spectrum.

---

1. The author carried out this research while on leave at Oklahoma State University, Stillwater, Okla.
2. Oklahoma State University, Stillwater, Okla.
3. F. A. Modine, E. Sonder, W. P. Unruh, C. B. Finch, and R. D. Westbrook, *Phys. Rev. B* 10, 1623 (1974).
4. C. Ridou, M. Rousseau, J. Y. Gesland, J. Novet, and A. Zarembowitch, *Ferroelectrics*, to be published.
5. J. B. Bates, R. W. Major, and F. A. Modine, *Solid State Commun.* 17, 1347 (1975).
6. T. P. P. Hall, *J. Appl. Phys.* 17, 1011 (1966).

RADIATION-INDUCED OPTICAL ABSORPTION IN $NaMgF_3$

J. R. Seretlo[1] E. Sonder

The compound $NaMgF_3$ is one of a number of orthorhombic perovskite fluorides.[2] Comparison of its radiolysis behavior with that of cubic $KMgF_3$ permits an assessment to be made of the effect of crystal symmetry on point-defect production in similar materials.

Large-grained polycrystalline, multidomain samples of $NaMgF_3$ were irradiated in the electron Van de Graaff accelerator. Sample temperature and radiation dose were varied, and growth curves were obtained for the radiation-induced absorption bands. From the spectra and growth-curve shapes, it was possible to identify tentatively a number of radiation-produced defects. These are summarized in Table 2.2. The identifications were based upon analogy with the radiation behavior of alkali halides and $KMgF_3$, as well as upon comparison of the growth rates of the different bands observed for $NaMgF_3$. For example, the F_2 center was identified by the fact that its absorption band intensity varied as the square of that of the F band as the bands grew.

The results indicate that differences in structure have little influence on the defect production behavior of these perovskite compounds.

Table 2.2. Optical absorption band in $NaMgF_3$

Band peak position (nm)	Half width at 80°K (eV)	Temperature range in which band can be observed (°K)	Tentative identification
290	0.7	10->300	*F* center
350		10-130	Self-trapped hole
230		80->300	Interstitial clusters
405		>200	F_2 center
500		>200	*F* aggregate centers
700			

---

[1] Fulbright-Hays Scholar from the University of Fort Hare, South Africa.

[2] M. H. Lewis and M.W.A. Bright, *Am. Mineral.* 56, 1[illegible] (1971).

TEMPERATURE DEPENDENCE OF FRENKEL-PAIR PRODUCTION FROM *F*-AGGREGATE-CENTER DESTRUCTION[1]

E. Sonder

Measurements of the radiation destruction of *F*-aggregate centers between 70 and 250°K have yielded values for the primary Frenkel-pair production efficiencies in NaCl, RbCl, KBr, and KI as a function of temperature. The so far unexplained increase in production efficiency with temperature originally demonstrated for KCl has also been observed in these materials and has been found to be only a slight function of the species of cation but a strong function of anion species making up the alkali halides. The apparent agreement between the activation energy obtained for KBr in these measurements and pulsed radiolysis measurements is discussed, and a problem concerning previously proposed explanations is indicated. In addition, the very strong temperature dependence previously observed in KI and attributed to the disappearance of luminescence has been observed and correlated with the thermal quenching of the 3.31-eV component of the fundamental luminescence.

---

[1] Abstract of paper: *Phys. Rev. B* 12, 1516 (1975).

REACTION PRODUCTS AND STORED ENERGY RELEASED FROM IRRADIATED SODIUM CHLORIDE BY DISSOLUTION AND BY HEATING[1]

G. H. Jenks[2] C. D. Bopp[2]
E. Sonder J. R. Walton[3]
S. Lindenbaum[4]

As a part of a study of energy stored in irradiated NaCl, we found that heats evolved upon aqueous dissolution of irradiated samples were consistently about 50% lower than the stored energy released during heating of the samples. It seemed likely that these differences could be explained in terms of the reactions that take place during dissolution; therefore we conducted a combination of measurements to help identify such reactions. Parameters determined included heat release upon thermal bleaching and upon dissolution of irradiated samples, identity and quantity of gases evolved during aqueous dissolution, and concentrations of hypochlorite ion in solutions of irradiated salt. Analyses of our experimental data and other information indicated that during dissolution a reaction occurs between irradiation-activated NaCl molecules and H_2O, in which the principal solution products are OCl^-, HOCl, and H_2 in addition to Na^+ and Cl^-. The results indicated that the energy per radiation-activated molecule of NaCl is approximately equal to the heat of formation of NaCl from the elements. The results of this work confirm that heat of solution as well as drop calorimetry can be used to measure stored energy in irradiated NaCl and, probably, other solids. However, it is essential that the species formed by dissolution of the displaced atoms be known in order to interpret the solution calorimeter data correctly.

---

[1] Summary of paper: *J. Phys. Chem.* 79, 871 (1975).

[2] Chemical Technology Division, ORNL.

[3] Analytical Chemistry Division, ORNL.

[4] University of Kansas, Lawrence, Kan.

THERMAL CONDUCTIVITY OF IRRADIATED, ADDITIVELY COLORED, AND DEFORMED MgO[1]

Judith B. Hartmann[2] Harold Weinstock[2]
Y. Chen

Low-temperature thermal conductivity measurements have been made in neutron-irradiated, electron-irradiated, additively colored, and deformed MgO. Resonant scattering of phonons is observed in all these crystals at $T \approx 15$ to 20°K. Correlations with optical absorption measurements indicate that this resonance is associated with anion vacancies. In addition, a resonance at $T \approx 1$°K in neutron-irradiated crystals is attributed to defect aggregates, which are virtually absent in electron-irradiated and additively colored samples.

Thermal conductivity measurements on high-purity MgO deformed to about 2% along a [100] direction show a decrease after the deformation over a broad temperature range, with maximum decrease occurring at $T \approx 15$ to 20°K. Optical measurements indicate the presence of a broad deformation-induced absorption band at 5.7 eV, which is probably caused by higher order point defects. An MgO crystal deformed 2% normally contains about 2×10^{16} F^+ centers per cubic centimeter. In addition, dislocation dipoles and other defects are also produced during deformation. Hence, at this time, it is not certain whether it is the anion vacancies, other defects, or dislocation dipoles that are responsible for the decrease in thermal conductivity. However, following annealing at about 1000°K, the thermal conductivity over part of the temperature range approached values obtained for the undeformed sample.

At this temperature, most of the point defects, including anion vacancies, were annealed out, and some of the dislocation dipoles were converted into dislocation loops.

---

1. Summary of paper: p. 190 in *Phonon Scattering in Solids*, Plenum Publishing Co., New York, 1976.

2. Illinois Institute of Technology, Chicago, Ill.

DEUTERATION OF CRYSTALLINE CaO

M. M. Abraham   Y. Chen
W. P. Unruh[1]

Single crystals of CaO doped with deuterium have been grown by the submerged arc fusion method, and V_{OD} centers were produced by gamma irradiation at 77°K. Although the observed EPR line widths are extremely narrow, electron-nuclear double-resonance (ENDOR) measurements at 4.2°K were required to obtain the quadrupole interaction constant and the signs of the hyperfine parameters. EPR and ENDOR measurements yield the following spin-Hamiltonian parameters: $g_\parallel = 2.0020(2)$, $g_\perp = 2.0730(2)$, $A_\parallel = +0.423(1)$ MHz, $A_\perp = 0.212(1)$ MHz, and $P = +0.188(1)$ MHz. Relative signs were obtained experimentally, and the assignment of the absolute signs follows from the assumption of a positive dipolar interaction of the hole with the reported positive deuterium nuclear moment. The magnetic hyperfine interaction is essentially all dipolar and implies a slight outward (100) relaxation of the axial oxygens. The measured electric field gradient at the deuteron is compared in Fig. 2.23 with the corresponding case in MgO and with other substitutional-impurity trapped-hole centers in the cubic oxides.

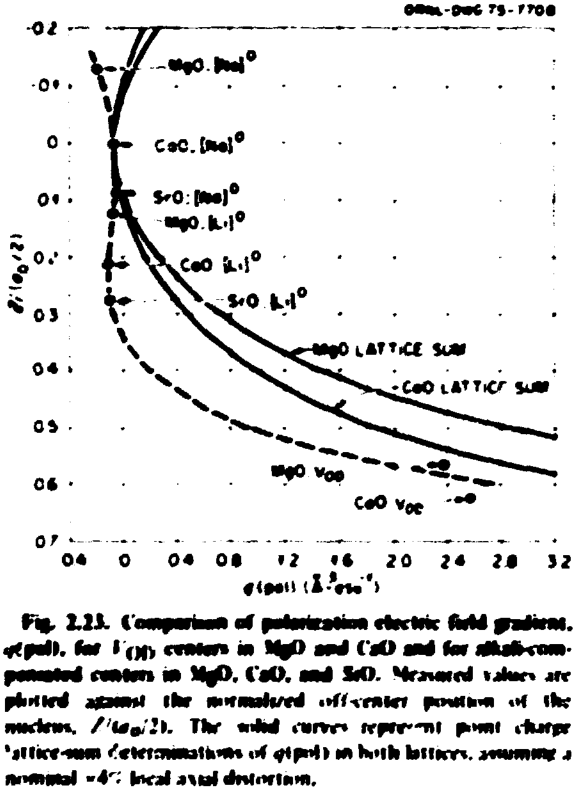

Fig. 2.23. Comparison of polarization electric field gradient, q(pol), for V_{OH} centers in MgO and CaO and for alkali-compensated centers in MgO, CaO, and SrO. Measured values are plotted against the normalized off-center position of the nucleus, $l/(a_0/2)$. The solid curves represent point charge lattice-sum determinations of q(pol) in both lattices, assuming a nominal +4% local axial distortion.

---

[1] Present address: University of Kansas, Lawrence, Kan.

FIRST-ORDER IMPURITY-INDUCED RAMAN SCATTERING FROM Ni^{2+} IONS IN LiCl[1]

J. B. Bates   G. E. Shankle[2]

First-order Raman scattering is normally forbidden by symmetry in alkali-halide crystals. However, introduction of a substitutional impurity ion into the cubic lattice destroys the translational symmetry at the substitutional site, and Raman scattering from vibrational motion of the impurity and its nearest neighbors can be observed. In simple terms, the Raman spectra can be viewed as arising from the normal modes of an MX_6 octahedral species, where M is a substitutional cation impurity and X is a halide anion. The measured frequencies and observed band shapes depend on the M–X force constants and on the static and dynamic interaction of MX_6 with the surrounding lattice. The case of Ni^{2+} ions in LiCl presents an additional complication to this situation because there must exist an equal number of Li^+ vacancies to compensate for the excess charge of Ni^{2+}. Thus in addition to induced scattering about the Ni^{2+} centers, induced scattering could also occur about the Li^+ vacancies.

Raman measurements were made at 12 K on LiCl crystals containing 0.2 and 0.4 wt of nickel. These weight percentages correspond to 4×10^{19} and 8×10^{19} Ni^{2+} ions cm^{-3} respectively. Polarized Raman spectra from (100) and (110) crystals were obtained. The scattering observed from a (100) crystal is shown in Fig. 2.24. For an octahedral MX_6 species, the irreducible representations for the fundamental vibrational modes are given by $\Gamma(O_h) = A_{1g} + E_g + T_{2g} + 2T_{1u} + T_{2u}$. The A_{1g}, E_g, and T_{2g} modes are Raman active, and the T_{1u} and T_{2u} modes are infrared active. For a (100) crystal, the A_{1g} and E_g modes appear in $z(xx)y$ polarization while the T_{2g} mode appears in $z(yx)y$.

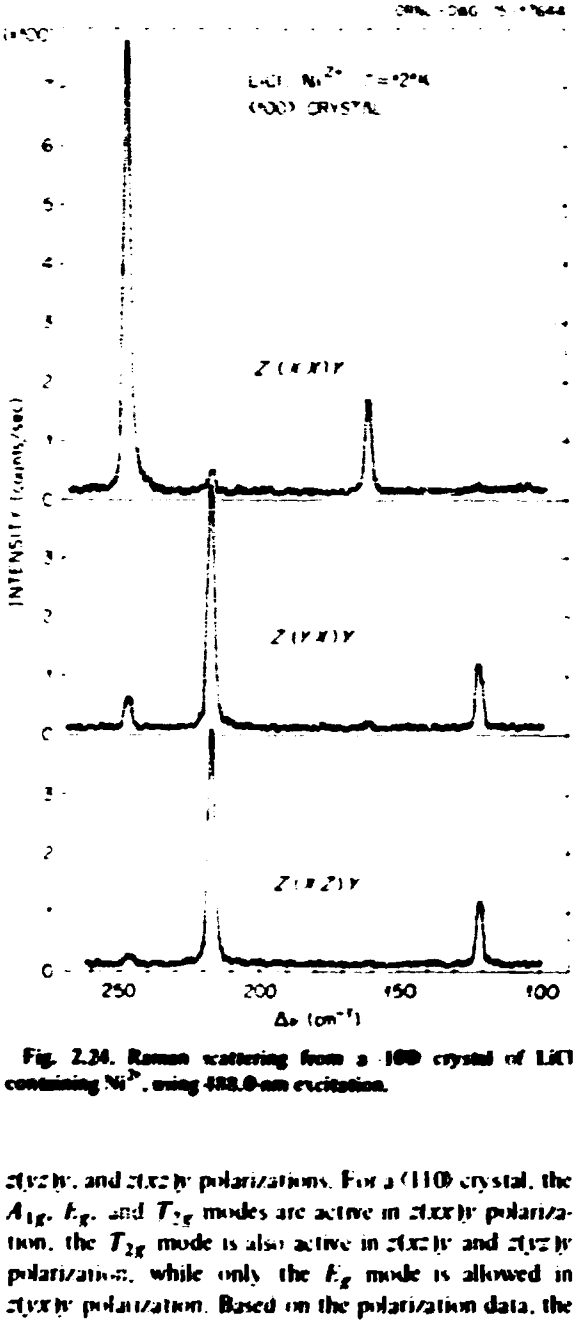

Fig. 2.24. Raman scattering from a (100) crystal of LiCl containing Ni^{2+}, using 488.0-nm excitation.

z(yz)y, and z(xz)y polarizations. For a (110) crystal, the A_{1g}, E_g, and T_{2g} modes are active in z(xx)y polarization, the T_{2g} mode is also active in z(xz)y and z(yz)y polarizations, while only the E_g mode is allowed in z(yx)y polarization. Based on the polarization data, the bands at 247, 216, 161, and 122 cm^{-1} (Fig. 2.24) are assigned to A_{1g}, T_{2g}, E_g, and T_{2g} modes respectively. Since an MX_6 octahedral structure has only one T_{2g} mode, one of the two T_{2g} bands observed is probably due to the charge-compensating cation vacancy.

RESONANCE RAMAN AND INFRARED SPECTRA OF ClO$_3$ RADICALS IN ELECTRON-IRRADIATED NaClO$_3$ [1]

J. B. Bates H. D. Stidham[2]

The ClO$_3$ radical has been identified by ESR measurements[3] as a product formed by x-ray irradiation of NaClO$_3$ at 77°K or at lower temperatures. It was found in this work that ClO$_3$ is formed at two nonequivalent sites and that the radicals formed at one site were rapidly decomposed at 77°K when the irradiated sample was exposed to light with wavelengths longer than 5500 Å. We have observed the Raman and infrared spectra of ClO$_3$ radicals produced in crystalline NaClO$_3$ by irradiation with 1.5-MeV electrons at 77°K. To the best of our knowledge this is the first observation of any of the vibrational bands of this species.

Irradiations of NaClO$_3$ samples were made at 77°K using a 1.5-MeV beam of electrons from a Van de Graaff accelerator. The beam current was 20 to 40 μA, and the irradiations were made for 30 to 120 sec, depending on the sample and the experiment to be performed. Single crystals of NaClO$_3$ were used in the Raman and electronic absorption measurements. For the infrared studies, a film of NaClO$_3$ was formed on an NaCl window by slowly cooling a melted sample of powdered material (mp = 284°C) between the salt window and a glass slide. The slide was removed after the film had cooled to room temperature.

The Raman measurements were made using the 6328-Å line of a He–Ne laser and the 5145-Å line of an argon-ion laser as exciting lines in different runs. The laser power was maintained at 50 mW or less to prevent bleaching, and $x(x_z z)y$ scattering geometry was employed in all measurements. The results of the Raman measurements are shown in Fig. 2.25. With 6328-Å excitation, the band assigned to ν_1 of ClO$_3$ radicals at site *a* appears at 812 cm^{-1}, and with 5145-Å excitation the band assigned to ν_1 of ClO$_3$ radicals at site *b* appears at 819 cm^{-1}. The decay rates of the "red" (6328 Å) sensitive radicals and the "green" (5145 Å) sensitive radicals were determined by measuring the respective band intensities relative to the intensity of the ν_1 band of ClO$_3^-$ at 936 cm^{-1} as a function of time. The decay curve of the 819 cm^{-1} band had the form $I = I_0 e^{-\alpha t}$, where α = 0.024 min and the half-life of the decay was 29 min. The decay curve of the 812-cm^{-1} band was linear over a 2-hr interval with a small negative slope (0.11 min^{-1}).

Infrared spectra of irradiated films of NaClO$_3$ on NaCl were measured with a Fourier transform spectrometer. By plotting the ratio of irradiated sample

---

[1] Summary of paper to be published.

[2] Oak Ridge Associated Universities faculty research participant from San Angelo State University, San Angelo, Tex.

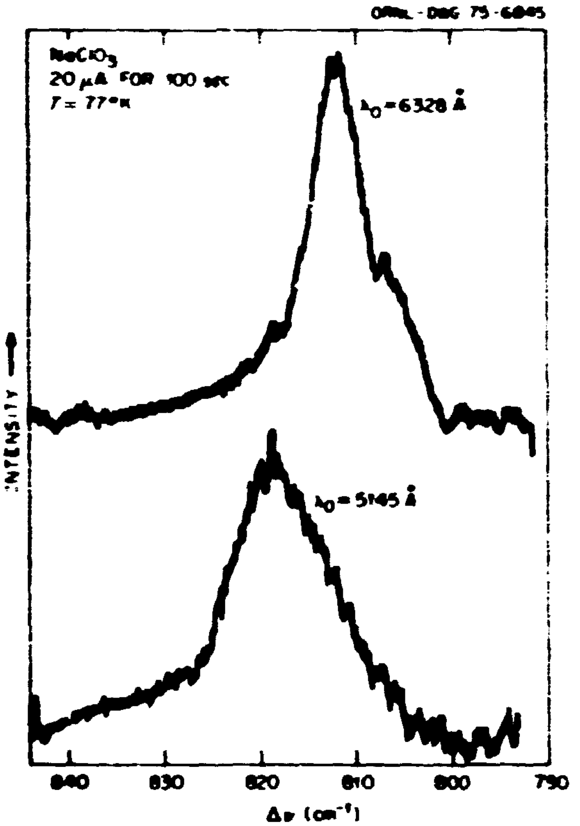

Fig. 2.25. Raman spectra in the ν_3 region of NaClO$_3$ irradiated at 77 K with 1.5-MeV electrons for 100 sec using a beam current of 20 μA. For 6328-Å excitation, slits = 4.5 cm^{-1}, and for 5145-Å excitation, slits = 5 cm^{-1}. Sensitivity = 100 counts/sec full scale.

spectrum to unirradiated sample spectrum, two bands were found at 850 and 857 cm^{-1}, which were assigned to the ν_3 modes of ClO$_3$ radicals at sites *a* and *b* respectively. The disappearance of these bands upon bleaching the sample with 4880-Å light at room temperature supports this assignment. Taken together, the results of the Raman and infrared spectra of ClO$_3$ radicals in NaClO$_3$, including identification of ν_1 and ν_3 of ^{37}ClO$_3$, support the hypothesis of a pyramidal (C_{3v}) structure for this species.

---

1. Summary of paper *Chem Phys Lett* 37, 25 (1976).

2. On leave from the University of Massachusetts, Amherst, Mass.

3. O. Vinther, *J Chem Phys* 57, 183 (1972).

RESONANCE RAMAN SCATTERING FROM METASTABLE O_2 MOLECULES IN GAMMA-IRRADIATED NaClO$_3$ [1]

J. B. Bates H. D. Stidham[2]

It has been known for some time that O_2 is produced in alkali-metal chlorates by the action of ionizing radiation.[3] In all cases, the O_2 was detected as a gas liberated from dissolved or crushed material. Apparently no direct observation of O_2 in an irradiated chlorate has been made. In a recent study[4] of O_3^- ions in irradiated KClO$_3$ and NaClO$_3$, a band was reported at 1547 cm^{-1} in the Raman spectrum of irradiated NaClO$_3$. Subsequent investigations were initiated to determine the origin of this band (observed at 1544 cm^{-1} in more careful measurements), its polarization properties, and its behavior in terms of intensity variation with different excitation lines.

In order to confirm that the 1544-cm^{-1} band is due to an oxygen species, the Raman spectrum of an irradiated powdered sample of NaClO$_3$ containing 46 at. % ^{18}O was measured. The observed bands reported in Table 2.3 agree within experimental error with the calculated values assuming ^{18}O substitution of O_2 to produce ^{16}O ^{18}O and ^{18}O ^{18}O molecules. A search for a resonance Raman effect with the 1544-cm^{-1} band was made by measuring the intensity of this band as a function of exciting line wavelength. The measurements were made with the eight lines of an argon laser and several frequencies from a tunable cw dye laser using rhodamine 6G. The results obtained in the 1520–1580-cm^{-1} region are presented in Fig. 2.26 for several of the exciting lines used. As shown in this figure, the intensity of the 1544-cm^{-1} band decreases from a maximum for 457.9-nm excitation to a minimum for 625.6-nm excitation. These results show that a resonance Raman effect occurs with this band. Using the $\nu_1(a_1)$ band of ClO$_3^-$ as an internal intensity standard, an excitation profile of intensity vs exciting wavelength

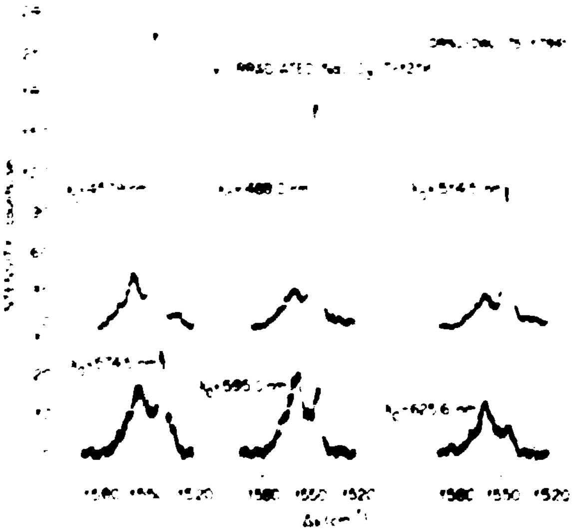

Fig. 2.26. Raman spectra in the 1580- to 1520-cm^{-1} region of γ-irradiated NaClO$_3$ measured at 12 K. The wavelength of the exciting line is given by the value of λ_0.

Table 2.3. Isotopic frequencies and overtones of the 1544-cm^{-1} band in gamma-irradiated NaClO$_3$

A. ^{18}O isotopes of O$_2$ in polycrystalline NaClO$_3$ (46 at % ^{18}O)

Species	Frequency (cm^{-1})	
	Observed	Calculated
^{16}O ^{16}O	1544	
^{16}O ^{18}O	1501	1501
^{18}O ^{18}O	1457	1456

B. Observed and calculated fundamental and overtone frequencies of O$_2$ in single crystal NaClO$_3$

Mode	Frequency (cm^{-1})	
	Observed	Calculated[a]
ν	1544	
2ν	3058	3056
3ν	4536	
4ν	5990	5984

$\omega_0 = 1560\ \text{cm}^{-1}$, $\omega_0 x_0 = 16.0\ \text{cm}^{-1}$

[a] Calculated values from the term value equation, $G(n) = \omega_0 n - \omega_0 x_0 n^2$, where ω_0 and $\omega_0 x_0$ were determined from $G(1) = \nu$ and $G(3) = 3\nu$

was constructed. An excitation profile closely follows the optical absorption band for the particular electronic transition that is coupled to the vibrational state (or states) through which resonance Raman scattering occurs. For the 1544-cm^{-1} band, the excitation profile appears to approach a maximum value just above 457.9 nm, which indicates the presence of an optical band associated with the O$_2$ species in this region. The spectra in Fig. 2.26 also show another band at 1557 cm^{-1}. This band does not exhibit a resonance Raman effect and is assigned to ordinary O$_2$ trapped in the NaClO$_3$ lattice.

Raman spectra of irradiated NaClO$_3$ were measured daily over a period of up to six days after irradiation and after sixteen days of storage at room temperature in the dark. The 1544-cm^{-1} band intensity decreased as a first-order decay process described by $I = I_0 e^{-\alpha t}$, where $\alpha = 0.50$ days^{-1} and the half-life $t_{1/2} = 1.4$ days. After sixteen days, the 1544-cm^{-1} band was not observed with 457.9-nm excitation whereas the intensity of the 1557-cm^{-1} band remained unchanged, within experimental error. The 1544-cm^{-1} band was also found to decay when exposed to 150 mW of 457.9-nm laser radiation at temperatures above 130°K. These results show that the O$_2$ species associated with the 1544-cm^{-1} band are (1) unstable in the dark at room temperature and (2) can be photolytically destroyed by irradiation with 457.9-nm light at temperatures above 130°K.

Since the intensity of the 1544-cm^{-1} band is derived from a resonance interaction with an electronic transition near the visible region, the intensity of the overtones of this band may also be expected to be

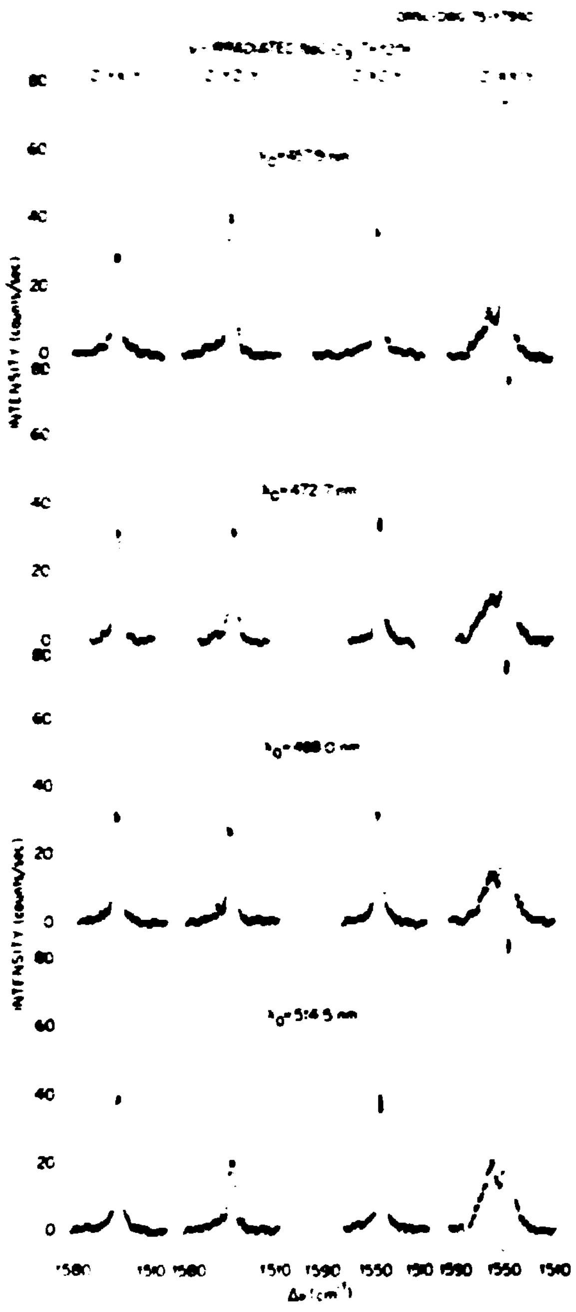

Fig. 2.27. Polarization measurements of the 1544- and 1557-cm^{-1} Raman bands in gamma-irradiated NaClO$_3$. The exciting line wavelength is given by λ_0.

enhanced. The overtones observed are reported in Table 2.3. The good agreement between the observed and calculated values of 2ν and 4ν using the simple diatomic term value equation, $G(n) = \omega_0 n - \omega_0 \chi_0 n^2$, lends additional support to the assignment of the 1544-cm^{-1} band to diatomic oxygen. Also, the large value of $\omega_0 \chi_0$ (Table 2.3) is characteristic of a diatomic species.

Polarized Raman spectra of irradiated ⟨100⟩ crystals of $NaClO_3$ were also measured with different exciting lines, and the results are illustrated in Fig. 2.27. Several important points can be noted from these spectra. First, the 1557-cm^{-1} band is polarized, with a linear depolarization ratio, $\rho_l = I(xy)/I(xx)$, of less than 0.1. This means that the ordinary O_2 molecules are either (1) randomly oriented or (2) oriented along the equivalent ⟨111⟩ axes of the crystal. Second, the 1544-cm^{-1} band appears to be depolarized with $\rho_l^{ave} = 0.44$ (average of the ratios for the three off-diagonal polarizations) for $\lambda_0 = 457.9$ nm. Because the 1544-cm^{-1} band is due to the totally symmetric O–O stretching vibration, this result means that the metastable O_2 molecules have preferred orientations along the equivalent ⟨110⟩ or ⟨111⟩ directions in the crystal. However, the observed dispersion in the $z(yz)y$ component (Fig. 2.27) complicates this situation so that a unique orientation cannot be specified.

The results of the measurements described above show that an unusual form of O_2 is initially formed in $NaClO_3$ upon gamma irradiation at room temperature. This species is unusual because a resonance Raman effect was observed with the O–O stretching mode, which means that the vibration is coupled to an allowed electronic transition located near the visible region. However, the lowest-lying allowed transition of O_2 ($^3\Sigma_g^- \rightarrow {}^3\Sigma_u^+$) occurs in the ultraviolet region ($\nu >$ 50,000 cm^{-1}). A model to account for the resonance effect and the instability of the O_2 species has not been developed. Possibly the metastable oxygen is a complex of O_2 weakly bonded to an unstable radical such as ClO_2. If this is the case, then resonance could occur through vibronic coupling of the O–O stretching motion with an electronic transition localized primarily on ClO_2. An $[O_2 \cdot ClO_2]$ "exchange" complex has been proposed to explain the ESR spectra of x-ray irradiated $KClO_4$.[5]

---

[1] Summary of two papers: *Chem. Phys. Lett.* 37, 20 (1976) and *J. Chem. Phys.* (in press).

[2] On leave from the University of Massachusetts, Amherst, Mass.

[3] See, for example, C. F. Burchill, P. F. Patrick, and K. J. McCallum, *J. Phys. Chem.* 71, 4560 (1967) and references contained therein.

[4] J. B. Bates and J. C. Pigg, *J. Chem. Phys.* 62, 4227 (1975).

[5] J. R. Byberg and J. Linderberg, *Chem. Phys. Lett.* 33, 612 (1975).

VIBRATIONAL SPECTRA OF SYNTHETIC SINGLE-CRYSTAL TEPHROITE Mn_2SiO_4 [1]

H. D. Stidham[2] J. B. Bates C. B. Finch[3]

The dynamical properties of silicates of the olivine structure have not been well characterized, possibly because of the difficulty of preparing single-crystal samples of a suitable size and optical quality for spectroscopic studies. Because the olivine structure readily substitutes a variety of metal ions without essential modification of the silicate framework, naturally occurring olivines are mixed crystals. Single crystals of Mn_2SiO_4 were grown from the melt at 1315 ± 5°C and at 1 atm total pressure by the Czochralski (pulling) method. To assure the divalent form of manganese, an oxygen partial pressure of 10^{-10} torr was applied over the melt in the form of an argon–4% hydrogen gas current through the growth system.

The olivines belong to the orthorhombic space group, D_{2h}^{16}. The unit cell contains four SiO_4^{4-} ions located on C_s sites and eight Mn^{2+} ions located on C_s and C_i sites. The irreducible representations of the 81 $\underset{\sim}{k} = \underset{\sim}{0}$ optical modes were derived from correlation diagrams and are given by $\Gamma^{op} = 11A_g + 11B_{1g} + 7B_{2g} + 7B_{3g} + 10A_u + 9B_{1u} + 13B_{2u} + 13B_{3u}$. The A_g, B_{1g}, B_{2g}, and B_{3g} modes are Raman active, while the B_{1u}, B_{2u}, and B_{3u} modes are infrared active. An example of the polarized Raman spectra observed using 488.0-nm excitation is shown in Fig. 2.28. The observed Raman bands were assigned to the A_g, B_{1g}, B_{2g}, and B_{3g} components derived from the ν_1, ν_2, ν_3, and ν_4 modes of SiO_4^{4-} and to the gerade components of the external modes derived from rigid-body libration and translation of the SiO_4^{4-} ions and translation of the Mn^{2+} ions. The infrared absorption spectrum of powdered tephroite suspended in Nujol at 77°K (Fig. 2.29) provided most of the frequencies of the transverse components of the infrared-active vibrations. The transverse electric reflectance spectra, also shown in Fig. 2.29, provided polarization data for assignment of the observed bands as well as data concerning relative band intensities and band widths, which are a measure of the longitudinal optical–transverse optical mode splitting. The transverse magnetic reflectance spectra obtained at high angles of incidence from principal faces contained evidence of coupling of some out-of-face polarized longitudinal optical modes with the electric vector of the incident light.

A comparison of the correlation field split components of the ν_1, ν_2, ν_3, and ν_4 modes of SiO_4^{4-} in Mn_2SiO_4 with those in Mg_2SiO_4 showed that the internal mode approximation remains valid for components of ν_1 and ν_3 that occur above 700 cm^{-1}. However, the comparison showed that for the infrared-active vibrations of tephroite and especially of forsterite, the external vibrations of the metal ions on C_s sites mix somewhat with the ν_4 vibrations. By contrast, the motions of the metal ions located on C_i sites do not contribute to the Raman-active modes due to symmetry. Also, the Raman-active components are apparently not significantly mixed with the metal ions on C_s sites. For the infrared-active modes, however, both metal ion sublattices move against the ν_2 and ν_4 bending motion of SiO_4^{4-}, and the resulting vibrations are mixed modes. The extent of mixing depends on the relative proximity of the internal and external mode

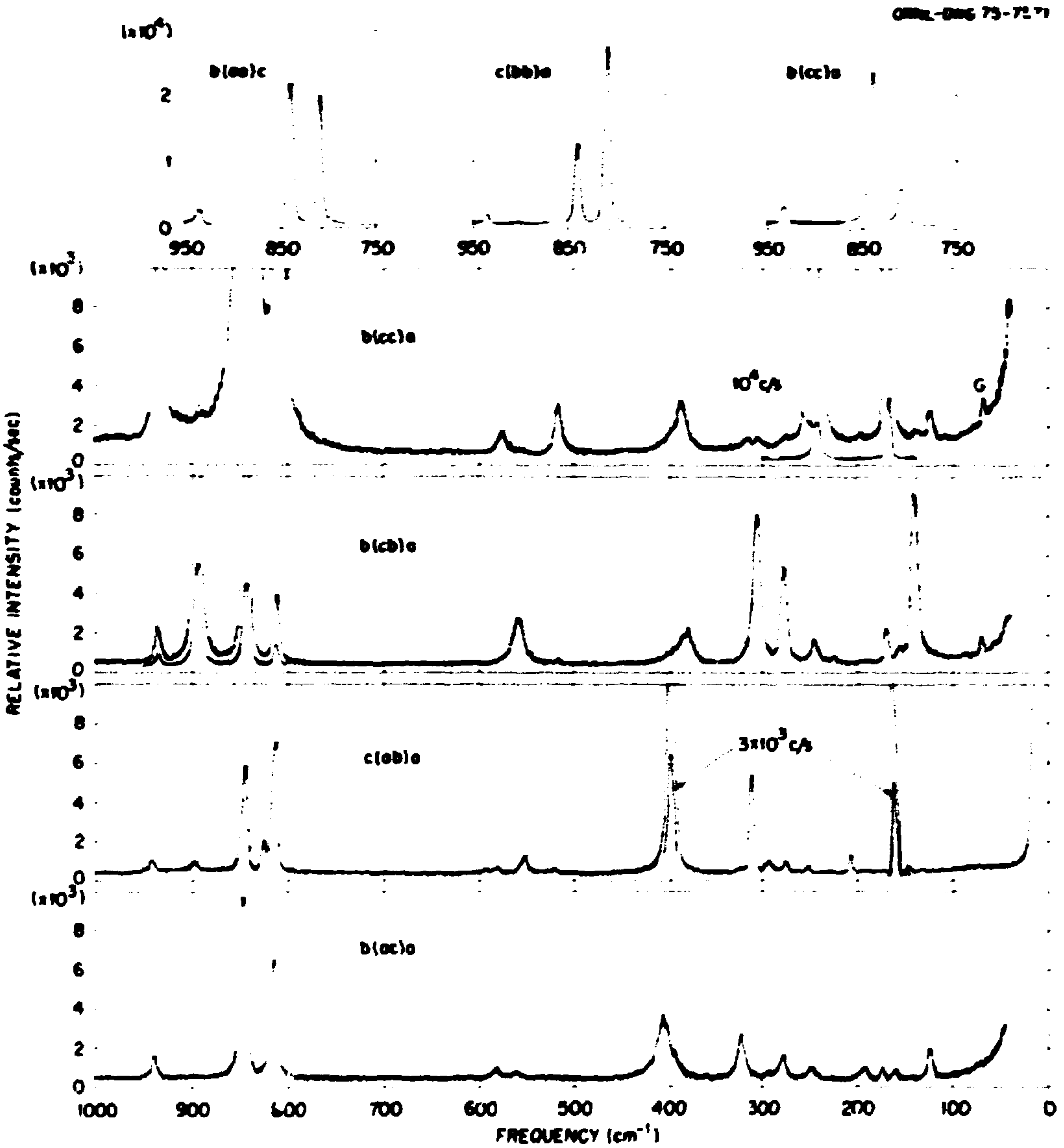

Fig. 2.28. Polarized Raman spectra of tephroite at 14° K. G is a grating ghost.

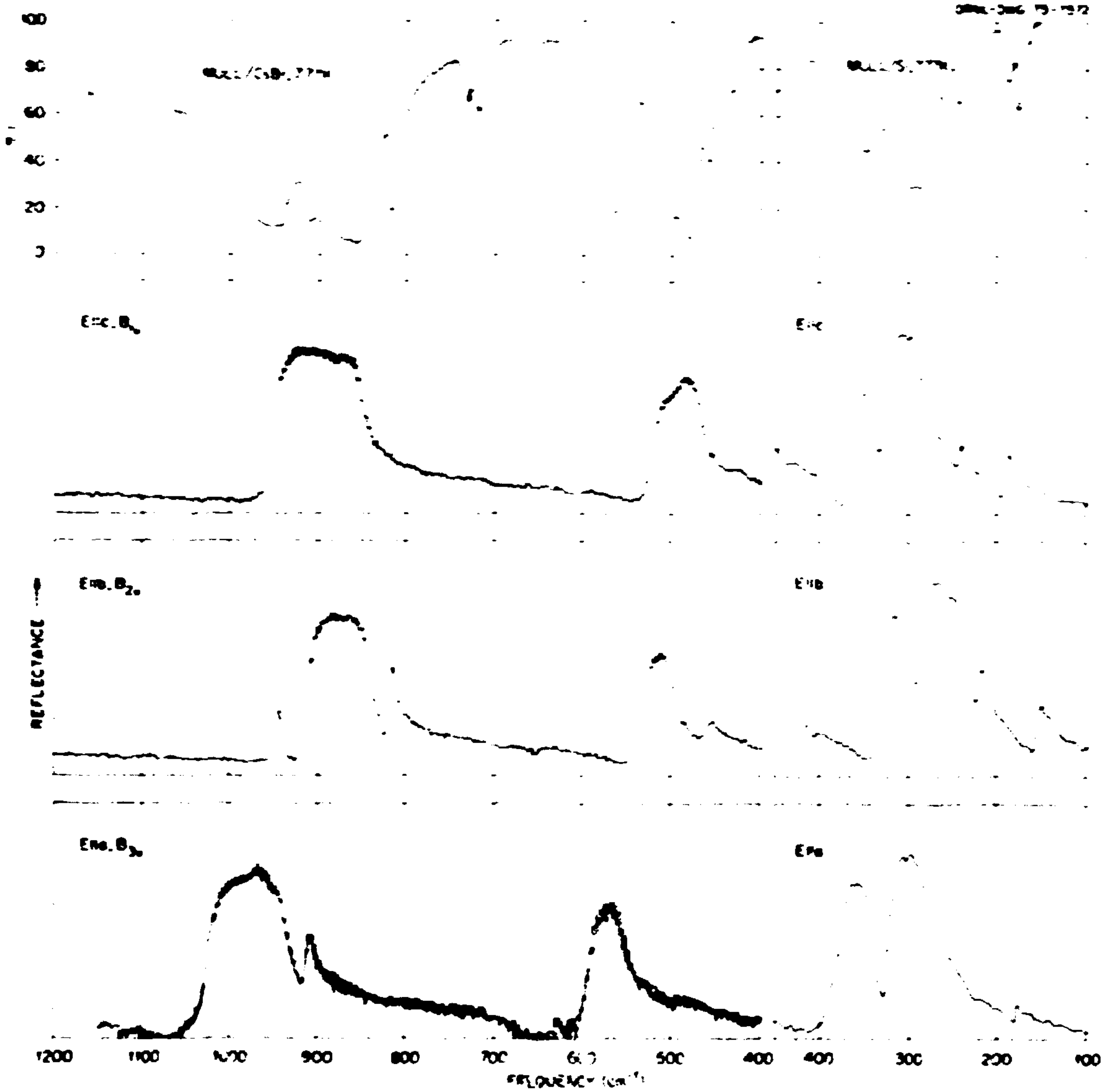

Fig. 2.29. Absorption and transverse electric reflectance infrared spectra of tephroite. Top: Absorption spectrum of hydrocarbon suspension of tephroite powder at 77 K spread on CsI or Si plates. In descending order: Room-temperature reflectance spectra in *c*, *b*, and *a* polarizations respectively.

frequencies and in the case of Mn_2SiO_4, all of the infrared-active components of ν_2 were assigned as mixed modes.

THE ELECTRONIC AND VIBRATIONAL SPECTRA OF *trans*-$[NiCl_4(H_2O)_2]^{2-}$ ANIONS IN CRYSTALLINE $Rb_2NiCl_4 \cdot 2H_2O$ AND THE EFFECTIVE SYMMETRY OF MIXED-LIGAND NICKEL(II) COMPLEXES[1]

G. E. Shankle[2] J. B. Bates

The electronic spectra of compounds containing geometrically distorted $NiF_6{}^{4-}$ or $NiCl_6{}^{4-}$ octahedra closely resemble the spectra of their cubic counterparts.

---

[1] Summary of paper: *J. Phys. Chem.* (in press).

[2] On leave from the University of Massachusetts, Amherst, Mass.

[3] Metals and Ceramics Division, ORNL.

These results suggest that the orbitally degenerate wave functions of octahedrally coordinated Ni^{2+} are to a large extent insensitive to small variations in the geometry of their local environment for those cases in which the ligands are the same. The question arises whether or not significant orbital splittings of Ni^{2+} can be produced by a mixed-ligand environment similar to those present in the hydrated cobalt(II) chlorides. For example, the ligand-field spectrum of $CoCl_2 \cdot 6H_2O$ was successfully analyzed[3] in terms of a sizable tetragonal perturbation created by the presence of two different ligands in *trans*-$[CoCl_2(H_2O)_4]$ octahedra. The compound $Rb_2NiCl_4 \cdot 2H_2O$ contains unlinked *trans*-$[NiCl_4(H_2O)_2]^{2-}$ anions in which both small geometric distortions and a mixed-ligand environment about the Ni^{2+} ion are present. The ligand-field spectrum of this compound was measured in order to investigate the extent to which each noncubic perturbation produces spectral modification. Because most octahedral Ni^{2+} ligand-field transitions are vibronically induced, the vibrational spectrum of $Rb_2NiCl_4 \cdot 2H_2O$ was also measured in order to aid in the assignment of vibronic fine structure and to establish whether or not the vibrational and electronic eigenstates are determined by potential fields of the same effective symmetry.

The double salt $Rb_2NiCl_4 \cdot 2H_2O$ crystallizes in the space group $P\bar{1}$ with one formula unit in the unit cell. The Ni^{2+} occupies a C_i site, and all O–Ni–O axes are parallel.[4] Although the $[NiCl_4(H_2O)_2]^{2-}$ anion has rigorous C_i symmetry, the symmetry may be assumed to be as high as D_{4h} if small differences in geometry are ignored. A perspective drawing of the anion (minus hydrogen atoms) as viewed along a direction perpendicular to the [001] plane is shown in Fig. 2.30.

The internal and external modes of the $[NiCl_4(H_2O)_2]^{2-}$ anion were observed from Raman and infrared spectra of $Rb_2NiCl_4 \cdot 2H_2O$. The internal and external modes of the H_2O ligands occur in a region between 3400 and 450 cm^{-1}. The internal and external modes of the $NiCl_4O_2$ group (Fig. 2.30) occur in the region from 360 to 55 cm^{-1}. Although the internal modes of this group were assigned from a vibrational calculation assuming a diamond-based structure having D_{2h} symmetry, the anion geometry cannot be said to be higher than C_i on the basis of the observed spectra. By contrast, based on the observed band contours of the ligand-field spectra of Ni^{2+}, the electronic crystal field is essentially cubic. These results show that the vibrational Hamiltonian of the $[NiCl_4(H_2O)_2]^{2-}$ anion is far more sensitive to small departures from idealized geometries than are its electronic and vibronic Hamiltonians. Water molecules and chlorine ions are customarily assigned significantly different positions in the spectrochemical series. Yet in $Rb_2NiCl_4 \cdot 2H_2O$, the water-chlorine mixed-ligand environment produces electronic state splittings which are small compared to the widths of the broad electronic band contours and which can only be detected by resolving zero-phonon spin-orbit fine structure and associated vibronic side bands.

Fig. 2.30. Structure and orientation of the $[NiCl_4(H_2O)_2]^{2-}$ anion in $Rb_2NiCl_4 \cdot 2H_2O$, viewed along a direction normal to the [001] plane. Ni–O, 2.077 Å; Ni–Cl(2), 2.431 Å; Ni–Cl(3), 2.438 Å; O–Ni–Cl(2), 89.5°; O–Ni–Cl(3), 89.1°; Cl(2)–Ni–Cl(3), 90.1° (data from ref. 4).

---

[1] Summary of paper: *J. Chem. Phys.* 64, 2539 (1976).

[2] Oak Ridge Associated Universities faculty research participant from San Angelo State University, San Angelo, Tex.

[3] J. Ferguson and T. E. Wood, *Inorg. Chem.* 14, 184 (1975).

[4] G. D. Sproul, Ph.D. Dissertation, University of Ill., 1971.

PHOTOVOLTAIC CONVERSION OF SOLAR ENERGY

NEUTRON TRANSMUTATION DOPING OF SILICON

J. W. Cleland R. T. Young
R. D. Westbrook R. F. Wood

It has long been recognized that thermal-neutron irradiation can be used to introduce certain impurity atoms in semiconducting materials as a consequence of the transmutation process.[1] For example, normal isotopic silicon contains 3.05% of ^{30}Si, which transmutes to ^{31}P after thermal-neutron absorption with a half-life of 2.6 hr. The range of the neutrons in silicon is 2 m; so it is possible to obtain a very uniform distribution of

^{31}P, a standard *n*-type dopant in silicon. In contrast to this, there is no known method of crystal growth that provides a uniform distribution of any chemical impurity dopant in silicon. Recent work has shown that the use of neutron-transmutation-doped (NTD) silicon significantly improves the performance of avalanche detectors and high-power rectifiers and thyristors,[2] and a similar improvement may be attainable in the efficiency of silicon solar cells.

The most serious problem that we anticipated in studies of NTD silicon was the removal of radiation damage that is introduced by (*n*,γ) recoils following thermal-neutron absorption and by all other damage mechanisms activated as a consequence of the reactor irradiation. The effect of the radiation damage is to reduce the minority carrier lifetime (MCL) and the carrier mobility, which are important parameters in device operation. Studies of the carrier concentration, mobility, and MCL before and after irradiation, and as a function of annealing, have been carried out on samples of NTD silicon from a number of different reactor locales. The results of these studies are presented in the other reports in this subsection.

In this contribution, we merely wish to point out that, in addition to our own in-house research activities, we have carried out numerous irradiations in the Bulk Shielding Reactor in response to the request of external groups. Selected ingots or slices have been irradiated and distributed for cooperative experiments to other ERDA laboratories, to universities, and to industrial organizations. Most of these experiments are still in progress and we cannot report on them at this time. Also, some results may have to be considered as proprietary information. However, all the results to date indicate that the use of NTD silicon will be of considerable importance in many device applications. This conclusion is based on the performance of devices that have actually been fabricated from our NTD silicon and tested by other university and industrial laboratories. The preparation, irradiation, postirradiation characterization, and shipment of neutron-irradiated silicon samples is considered as a service to other organizations and represents an integral part of the overall program.

REACTOR IRRADIATION FACILITIES FOR NEUTRON TRANSMUTATION DOPING OF SILICON

J. W. Cleland

The starting point in selecting the proper reactor facility for producing neutron-transmutation-doped (NTD) silicon depends to a great extent on the impurity concentration of the starting material, the desired NTD concentration, and the required axial and radial dopant uniformity after irradiation. Normal isotopic silicon contains $\approx 4.99 \times 10^{22}$ atoms cm^{-3}. The total thermal-neutron-absorption cross section is $\approx 0.09 \times 10^{-24}$ cm^2 (barns); so the total rate of thermal-neutron absorption is $\approx 4.5 \times 10^{-3}$ cm^{-1} × φ, where φ is the thermal-neutron flux (neutrons cm^{-2} sec^{-1}). Absorption is followed by an immediate release of gamma rays in the (*n*,γ) process. The kinetic energy of recoil may produce an interstitial silicon atom and lattice site vacancy (I-V), and the recoiling silicon atom may produce additional I-V-type defects. The ^{28}Si and ^{29}Si isotopes transmute to ^{29}Si and ^{30}Si, and the ^{30}Si isotope (3.05% abundant) has a thermal-neutron-absorption cross section of $\approx 0.12 \times 10^{-24}$ cm^2 (barns). It also recoils by the (*n*,γ) process and later transmutes to ^{31}P (2.6-hr half-life) by emitting a 1.48-MeV β particle. These data indicate that the actual rate of introduction of ^{31}P by the NTD process is ≈ 1.86–2.06×10^{-4} φ cm^{-1}, where the larger value makes allowance for absorption by ^{30}Si of some epithermal neutrons.

Extended irradiation to introduce $\approx 10^{16}$ ^{31}P cm^{-3} will result in a second activation of some of the ^{31}P to produce ^{32}P, which later transmutes to ^{32}S (14.8-day half-life) by emitting a 1.71-MeV β. However, the curie content of a silicon ingot with 10^{16} ^{31}P cm^{-3} introduced by the NTD process is only 10 μCi cm^{-3} due to the ^{32}S; the silicon can be handled with gloves during device fabrication under adequate ventilation.

The (*n*,γ) recoil and fast-neutron-induced lattice damage may take the form of interstitial-vacancy pairs, defect clusters, and disordered regions which act as carrier traps to decrease the carrier concentration and mobility of *n*- or *p*-type silicon; this lattice damage must be removed by annealing. Because every (*n*,γ) event or fast-neutron impact produces lattice defects, the defect concentration is much greater than the transmutation-induced ^{31}P donor concentration, even if the irradiation locale has a large thermal- to epithermal-neutron ratio. A considerable number of

---

1. J. W. Cleland, K. Lark-Horovitz, and J. C. Pigg, *Phys. Rev.* 78, 814 (1950).

2. M. Schnoller, p. 313 in *IEEE Transactions on Electron Devices*, vol. ED-21, 5 (1974).

Table 2.4. Thermal-neutron flux in different reactor locales

Reactor locale	Experimental locale	Moderator	Thermal flux (neutrons cm^{-2} sec^{-1})	Thermal to epithermal ratio	Maximum ingot size, diam times length (in.)
Bulk Shielding Reactor (BSR, ORNL)	In core C715	H_2O	1.3×10^{13}	3:10	3 × 12
	SW, SB holes	D_2O	5.5×10^{12}	200	2 × 12
	Center hole	D_2O	1.9×10^{12}	850	2.7 × 12
	N, S holes	D_2O	1.5×10^{12}	1700	1.2 × 6
National Bureau of Standards Reactor (NBSR)	G-2 hole in core	D_2O	1.0×10^{14}	55	1.2 × 10
	V-3 hole reflector	Graphite	3.2×10^{13}	150	[a]
Oak Ridge Research Reactor (ORR)	Hydraulic tube	H_2O	5.7×10^{14}	3:10	0.5 × 3
	In core	H_2O	3.5×10^{14}	3:10	3 × 36
High Flux Isotope Reactor (HFIR, ORNL)	Engineering facility EF-2	Outside beryllium reflector	2.5×10^{14}	1000	3 × 36[b]

[a] V-3 has no experimental thimble at present, but V-3 and G-2 can accommodate 3-in. ID thimbles.

[b] Experimental facility being constructed. Flux value and ratio are estimates.

irradiation experiments have been carried out in different reactor locales. The thermal-neutron flux, thermal- to epithermal-neutron ratio, and maximum sample size that can be accommodated in the reactors are indicated in Table 2.4. The actual flux, flux ratio, and size depend, in turn, on the reactor power level, fuel loading configuration, and available experimental facility. The data in Table 2.4 are comparative data for actual irradiation conditions applicable to experiments already performed or in progress. The various irradiation facilities have been used to introduce up to 2×10^{15} ^{31}P cm^{-3} in a thermal- to fast-neutron ratio of 200, up to 3×10^{16} ^{31}P cm^{-3} in a ratio of 55, and more than 10^{17} ^{31}P cm^{-3} in a ratio of 3:10.

ANNEALING OF RADIATION DAMAGE IN NEUTRON-TRANSMUTATION-DOPED SINGLE-CRYSTAL SILICON

R. D. Westbrook   R. F. Wood

It has already been mentioned that we must generally consider two types of lattice damage in neutron-transmutation-doped (NTD) silicon, that is, that due to (n,γ) recoils arising from the capture of a thermal neutron and that due to epithermal and fast neutrons. The damage produced by thermal neutrons is thought to consist of approximately two interstitial-vacancy pairs per captured neutron on the average. Fast neutrons, on the other hand, are believed to produce clusters of defects which may contain as many as 1000 defects.[1] It is generally believed that fast-neutron damage is more difficult to anneal out completely than is thermal-neutron damage, but completely reliable and comprehensive studies in this area have not yet been conducted. The nature, annealing characteristics, and influence on electrical properties of lattice damage in NTD silicon are obviously of crucial importance in choosing reactor locales for irradiation purposes.

We have undertaken a detailed study of time and temperature schedules for the annealing of lattice damage in NTD silicon to the extent that both carrier mobility and lifetime are recovered. Neutron radiation damage apparently introduces large concentrations of traps with energies that cluster near the center of the energy gap between the valence and conduction bands. Thus, after irradiation but before annealing, the transmutation-induced carriers are electrically inactive, and the material tends to exhibit approximately intrinsic behavior. Tanenbaum and Mills[2] found that the defects begin to anneal upon heating for 1 hr at 400°C, as indicated by slight decreases in resistivity. They found that rapid annealing occurs at 600°C and that annealing was generally completed after 16 hr at 625°C. They heated some of their samples at temperatures as high as 1200°C for 12 hr and found no additional annealing. Tanenbaum and Mills apparently thought they were dealing primarily with thermal-neutron-induced damage, but it is by no means clear that there was not also extensive fast-neutron damage present in their samples. Gunnersen and Ellis,[3] in an investigation into the use of NTD silicon for nuclear particle spectrometers, were under the impression that they were dealing with fast-neutron damage. They found that, after neutron irradiation, they had to anneal *n*-type silicon (already doped) for 10 hr at 700°C in order to recover the minority carrier lifetime (MCL). They state in their report that the MCL is more sensitive than resistivity to damage by fast neutrons by approximately a factor of 1000, but it is not clear how they arrived at this number. Although the Tanenbaum Mills and Gunnersen Ellis studies are not directly comparable, the annealing times and temperatures are quite similar and may suggest that both studies were dealing with essentially the same type of neutron damage. The studies clearly indicate the uncertainty that persists concerning the nature of neutron-induced damage in silicon.

Some representative data from our studies are shown in Table 2.5; they were taken on different samples irradiated for different times and in different reactor

Table 2.5. Annealing data for various samples of NTD silicon

Annealing conditions		Net ^{31}P concentration $[(N_D - N_A) \times 10^{14}\ cm^{-3}]$	ρ (Ω-cm)	μ (cm²/V·sec)[a]	τ (μsec)[a,b]
Temperature (°C)	Time (hr)				
Irradiation conditions: locale, BSR-CP15;[c] irradiation time, 120 hr; n_{th}/n_f, 10/1					
600	2	(*p*-type)	~10^5	≈200	
600	20	4.0	11	1400	T
600	70	5.2	7.4	1650	T
700	70	7.6	5.0	1640	T
750	70	7.6	4.8	1770	25
800	70	8.5	4.4	1650	20
850	70	7.9	4.6	1710	25
1000	70	7.6	4.7	1730	20
Irradiation conditions: locale, BSR-SW (D_2O); irradiation time, 289 hr; n_{th}/n_f, 200/1					
600	20	4.9	8.3	1560	T
600	90	4.6	7.8	1720	30(T)[d]
700	70	4.9	7.5	1610	20
750	70	4.7	7.8	1680	20
800	70	5.0	7.4	1680	15
850	70	5.3	7.7	1550	20
Irradiation conditions: locale, ORR-HYD; irradiation time, 25 days; n_{th}/n_f, 8/1					
600	2		~10^5	NS	NS
600	20		10^5	NS	NS
650	46	800	0.12	≈800[e]	NS
700	70	800	0.10	300	NS
800	70	800	0.11	800	NS
1000	70	800	0.10	800	NS
1200	16	800	0.10	800	NS
Irradiation conditions: locale, BSR-CL; irradiation time, 90 hr; n_{th}/n_f, 800/1					
600	20	0.64	61	1600	T
700	20	0.66	59	1600	40
800	20	0.65	53	1600	60

[a] The letters NS indicate that no signal was obtained for the particular measurements noted.

[b] The letter T indicates that excessive trapping prevented MCL measurements, a condition that always occurred at lower annealing temperatures.

[c] BSR-CP15, etc., refer to irradiation positions in the Bulk Shielding Reactor, and ORR-HYD refers to the hydraulic tube of the Oak Ridge Research Reactor.

[d] Small trapping effects observed.

[e] Approximate value obtained from literature.

locales at the reactor ambient temperature. The subtitles indicate the reactor locale, irradiation time, and ratio of thermal- to fast-neutron flux. The first two columns show the annealing schedule. The third column gives the measured net ^{31}P concentration after each anneal. Since both electrons and holes (donors and acceptors) can be present in different numbers at different temperatures of annealing, the net ^{31}P concentration is the difference between the number of donors, N_D, and the number of acceptors N_A. The fourth column gives the measured electrical resistivity ρ, and the fifth column gives the derived majority (electron) carrier mobility μ. The last column lists the room-temperature MCL τ, as determined by the photoconductive decay (PCD) technique. Two control groups of silicon crystals, conventionally doped with P, were subjected to approximately the same annealing schedules. Samples in the first group were initially about 200 Ω-cm *n*-type ($N_D - N_A \approx 10^{13}$ cm^{-3}) with MCL values ≥100 μsec. Their final resistivities were 250–300 Ω-cm *n*-type. Their MCL began to degrade as a consequence of annealing at ≈700°C to a final value of 35–50 μsec after annealing at 800°C. The other samples were initially 4 Ω-cm *n*-type ($N_D - N_A \approx 2 \times 10^{15}$ cm^{-3}) with MCL values of 50 μsec; the corresponding values after annealing were about 4 Ω-cm *n*-type and 20–30 μsec. Lifetime degradation as a consequence of heat treatment in conventionally doped silicon is well known and generally attributed to the presence of oxygen. Note, however, that little or no effect on the resistivity of conventionally doped samples was observed.

The results in Table 2.5 are quite consistent with those from the studies of refs. 2 and 3 insofar as they can be compared, that is, primarily with respect to the resistivity. Each of our samples showed almost complete recovery of the resistivity at annealing times and temperatures roughly comparable to those found in ref. 2, and no further recovery occurred up to 1200°C. Since the resistivity after recovery was roughly consistent with the donor concentration expected from the irradiations, it seems safe to conclude that almost complete annealing of those defects (probably electron traps) which affect resistivity has occurred in the annealing range 600°C/20 hr–700°C/70 hr. The electron mobility μ appears to be recovered in about the same annealing range as the resistivity and for the first two samples reached values comparable to the 4-Ω-cm control sample. The available data for the mobility in the BSR-CL sample is also roughly what one would expect from conventionally doped material. The mobility data for the ORR-HYD sample has been estimated from the resistivity measurements.

The minority carrier (holes, in this study) lifetime τ, as determined by the PCD technique, appears to be recovered at slightly higher annealing temperatures and times than are ρ and μ; however, the data are inconclusive on this point. It is known that the MCL is very sensitive to certain types of lattice damage, and we anticipated that its recovery would require more annealing (temperature and/or time) in the heavily damaged samples than in the lightly damaged ones. To date, there is little evidence to support this idea, and, in fact, the conventionally doped 4-Ω-cm control sample carried through the annealing process showed the same MCL as a comparable annealed NTD sample. No PCD signals for τ were observable in the ORR-HYD sample because of the high ^{31}P concentration which put detection beyond the range of our equipment with the light source available. This range is $\tau \approx 5$ μsec and greater, if the light source is intense enough to excite a sufficient number of carriers at a particular doping level. Measurements[4] of the MCL in solar cells with *n*-type substrate suggest that the value of μ at approximately 8×10^{18} doping concentration should be in the range of 1–10 μsec. Similar measurements[5] on *p*-type, as-grown material suggest an MCL of about 10 μsec. Neither of these measurements is directly comparable to our measurements on the ORR sample for several reasons; however, they do suggest that even with an appropriate light source we would have difficulty determining τ for that sample. Thus our failure to obtain a signal in no way implies that we have an exceptionally low MCL at high doping levels in the NTD silicon.

These studies are not yet complete, and it is perhaps premature to draw any definite conclusions from them. However, they do suggest that there is no great difference in the annealing characteristics between samples irradiated in the various thermal- to fast-neutron fluxes we have been able to obtain thus far and at the doping levels we have been using. Gunnersen and Ellis state that if the thermal-to-fast ratio is of the order of 1000, the fast-neutron damage will completely dominate; but they give no proof or reference for this statement. It does appear, however, that we should take a closer look at lightly doped samples, irradiated at thermal-to-fast ratios of 1700 to 1; and this work is now under way.

---

1. See, for example, V. A. J. van Lint and R. E. Leadon, "Lattice Defects in Semiconductors 1974," p. 227 in *Conference Series No. 23*, Institute of Physics, London and Bristol.

2. M. Tanenbaum and A. D. Mills, *J. Electrochem. Soc.* **108**, 171 (1961).

3. E. M. Gunnersen and R. Ellis, AERE 0-24/66, United Kingdom Atomic Energy Authority, 1966.

4. P. A. Iles and S. I. Soclof, p. 19 in *Proceedings Eleventh Photovoltaic Specialists Conference*, IEEE, Inc., New York, 1975.

5. H. Fischer and W. Pschunder, p. 25 in *Proceedings Eleventh Photovoltaic Specialists Conference*, IEEE, Inc., New York, 1975.

NEUTRON TRANSMUTATION DOPING OF POLYCRYSTALLINE SILICON FOR SOLAR CELLS

J. W. Cleland R. F. Wood
R. D. Westbrook R. T. Young

Neutron-transmutation-doped (NTD) single-crystal silicon has been proven to be substantially superior to conventionally doped silicon in the very important area of avalanche detectors and high-power devices such as rectifiers and thyristors. In each case higher operating voltages are possible because of the extremely uniform phosphorus dopant concentration obtained by the NTD process. It is possible that NTD silicon also offers advantages in solar cell applications, although for different reasons. Solar cells for terrestrial use require a much higher doping level, and being large-area devices, they require a uniform macroscopic as well as microscopic doping concentration, which NTD provides. Another intrinsic characteristic of NTD is that it does not introduce other impurities, such as may occur in standard doping techniques. Very small (trace) amounts of certain heavy metal impurities, for example, silver, gold, and copper, are known to degrade the minority carrier lifetime (MCL) in semiconducting materials, and maintaining a maximum MCL in heavily doped solar cell silicon is of vital importance to realizing a high photovoltaic conversion efficiency.

Because of the large cost differential between single-crystal silicon wafers and chemically vapor-deposited (CVD) polycrystalline silicon films (polysil), the latter are more attractive for large-area terrestrial solar cell applications. Typical grain sizes in polysil range up to a few tens of microns in films as deposited on metal or graphite, two substrates in common use. The electrical properties of CVD polysil have been investigated, but attempts to incorporate a dopant during the CVD process have not been very successful to date.[1,2] It is believed that the dopant migrates to the grain boundaries during the film deposition process. Some dopant atoms may be required in the grain boundaries to neutralize the broken bonds that otherwise would cause space-charge layer widening in the grains, but it has not been possible to obtain a uniform and controlled dopant concentration at the desired dopant concentration by CVD polysil film techniques to date.[1,2] In CVD polysil, the material remains essentially intrinsic until a certain fraction of the grain boundary bonds are neutralized, and the presence of too many dopant atoms in the grain boundaries may lead to enhanced electrical conduction, thereby decreasing the shunt resistance across a polysil solar cell and reducing the photovoltaic conversion efficiency.

Introduction of phosphorus into polysil ingots, wafers, or films by NTD offers the obvious advantage of a uniform initial dopant distribution regardless of grain size. Very preliminary experiments have been carried out, using samples as prepared from commercially available (Texas Instruments Co.) high-purity (undoped) CVD 1-in.-diam polysil rods intended for float zone crystal growth and 3-in.-diam polysil sections intended as charge material for Czochralski growth. Figure 2.31 is a photograph of a slice from a CVD polysil section which shows the varying grain size and grain orientation.

Samples were prepared in which the grains were parallel or perpendicular to the surface, and the van der Pauw technique was used to determine the donor concentration and mobility after reactor irradiation and annealing for 16-20 hr at 800°C to remove the radiation damage. Figure 2.32 is a graph of the measured donor concentration vs the predicted donor concentration for typical samples. The solid line indicates the results that would be anticipated for single-crystal silicon samples. These data show that NTD can be used to dope this type of polysil at any desired donor concentration $\geq 2 \times 10^{15}$ cm^{-3} and that impurity migration to grain boundaries cannot be measured as a consequence of annealing up to 800°C. The carrier mobility is much less in polysil than in single-crystal silicon because of the small grain size, but the mobility increases from ≈ 4 to 40 cm^2 V^{-1} sec^{-1} in these samples when the dopant concentration increases from $\approx 10^{15}$ to 10^{16} cm^{-3}. The MCL was ≈ 40-60 μsec at these doping concentrations, which is a comparable value to that observed for single-crystal silicon.

These studies are just under way and will be continued on polysil films as prepared by different techniques such that the grain size and orientation can be controlled and maximized. The fact that the anticipated donor concentration was observed after annealing at 800°C is of special interest in that a *p-n* junction must be formed to fabricate a solar cell, and preferential migration of impurities along grain boundaries has been predicted for conventional high-temperature diffusion

Fig. 2.31. Photograph of a slice from a chemically vapor-deposited polycrystalline boule of silicon.

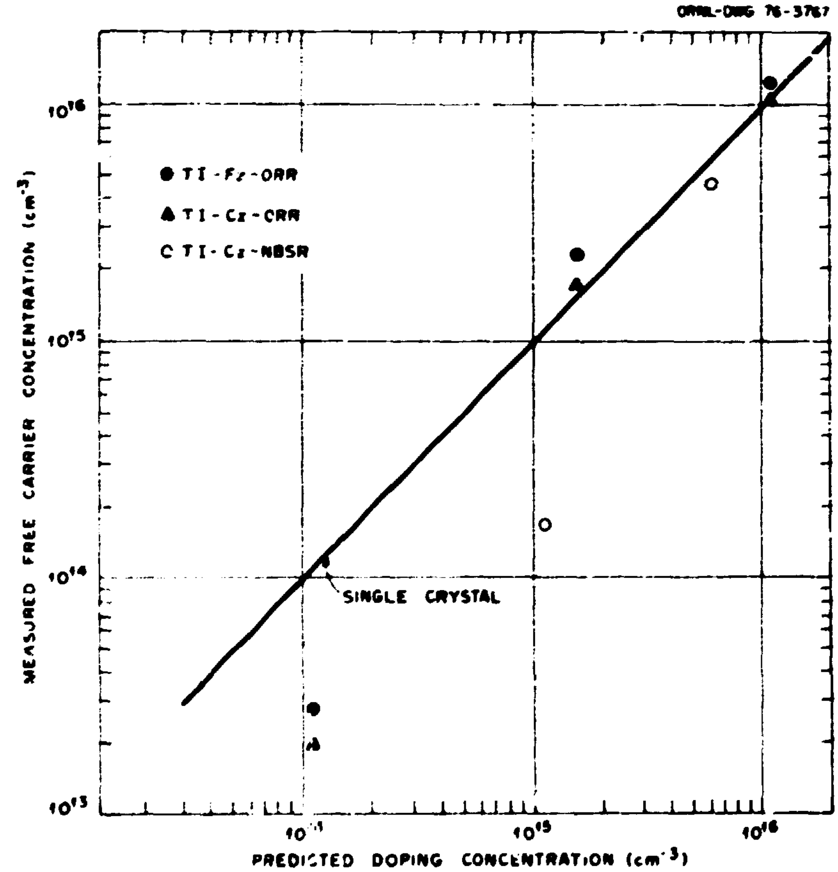

Fig. 2.32. Graph of the measured donor concentration vs the predicted donor concentration for various samples of NTD polycrystalline silicon. The solid line indicates anticipated results for single-crystal silicon.

experiments. It is anticipated that one can form a *p-n* junction in NTD polysil film by ion implantation and that low temperature (800°C) annealing will remove any ion implant damage, without introducing any grain boundary impurity migration. Preliminary experiments to fabricate *p-n* junctions in NTD polysil by ion implantation are also under way.

---

1. A. L. Fripp, *J. Appl Phys* 46, 1240 (1975).

2. M. E. Cowher and T. D. Sedgwick, *J. Electrochem. Soc* 119, 1565 (1972).

SOLAR CELL STRUCTURE STUDIES

D. W. Ramey B. F. Early C. A. Culpepper

In support of efforts to improve the efficiency of photovoltaic solar cells, studies are in progress to ascertain effective nondestructive methods of applying electrical conductor elements to surfaces of silicon devices. Contact resistance and capacitance must be minimized to effect efficient charge collection; such contacts must survive possible hostile environmental conditions and therefore must be made with essentially inert materials with high conductivity. Studies of nondestructive surface etching cleaning methods include chemical etching (H_2O_2 HF) and ion etching (plasma sputtering). Formation of conductor surface segments in precise geometric arrangements is being studied by a variety of techniques: sputter deposition, vacuum vapor deposition, and drawing (using epoxy-matrix metal "paints"). In the case of sputter or vapor deposition, maximum adherence of conductor layers is attained using multilayer metal deposits, for example titanium and silver. Sequential combinations of metal films are necessary to bond conductor metals to the silicon surface; physical characteristics of the bond zone are being studied metallographically using a scanning electron microscope. Definition of conductor geometry involves use of precision-fabricated metal masks designed to prevent shadowing during metal deposition; eventually photoresist technology may be used to perform this masking function.

MATHEMATICAL MODELING OF SOLAR CELL PERFORMANCE

J. E. Breitling[1] R. F. Wood

The results of mathematical modeling of solar cell performance can often be useful guides in solar cell design, development, and modifications. As part of the Solid State Division's growing effort in photovoltaics, such mathematical modeling studies have been initiated. A computer program has been written which enables the operating characteristics of a solar cell with a *p-n* junction to be calculated under a variety of circumstances.

The efficiency, η, of a solar cell is defined very simply as the power output of the cell divided by the total solar power falling on the cell; that is, $\eta = P_{out}/P_{in}$. The total incoming power can be calculated from the integral

$$P_{in} = \int_0^\infty P_{in}(\lambda)\, d\lambda \qquad (1)$$

where $P_{in}(\lambda)$ is the power at wavelength λ. There are several different versions of the function $P_{in}(\lambda)$ depending on where the solar spectrum is measured. For example, in outer space the air mass zero (AM0) distribution would be used, but for terrestrial applications a standard reference form for $P_{in}(\lambda)$ (to be known as AM2) has not yet been completely defined. In any case, the function $P_{in}(\lambda)$ is essential input to the computer program, and the integral in Eq. (1) can be evaluated numerically for different distributions $P_{in}(\lambda)$.

The determination of P_{out} is much more difficult since it must reflect the influence of all the material and operating characteristics of the cell. The maximum output power is the product of a current density j_{max} and a voltage V_{max} and is given by $P_{out} = j_{max} \cdot V_{max}$. This can be written in terms of the light-generated current j_l and the electron energy gap E_g of the semiconductor by the following procedure. Let

$$P_{out} = j_l \cdot E_g \cdot F_v \cdot F_f \, . \qquad (2)$$

where

$$F_v \equiv V_{oc}/E_g \qquad F_f \equiv j_{max} \cdot V_{max}/j_l \cdot V_{oc} \, . \qquad (3)$$

The factor V_{oc} is the open-circuit voltage obtainable from the cell; F_v and F_f are called the "voltage factor" and the "fill factor" respectively. The values F_v and F_f are largely determined by the materials characteristics of the cell. The light-generated current can be determined from the equation

$$j_l = q \int_0^\infty N_{ph}(\lambda)\gamma(\lambda)\, d\lambda \, , \qquad (4)$$

in which $N_{ph}(\lambda)$ is the photon flux, $\gamma(\lambda)$ is the overall collection efficiency at the wavelength λ, and q is the electronic charge. Note that $\gamma(\lambda)$ can be a complicated function of the reflection and absorption coefficients at λ and of the efficiency of collection of the light-generated electrons and holes. This collection efficiency is generally different in the various parts of the cell and at the very least should be separated into terms corresponding to collection in the base region, in the extended *p-n* junction (depletion region) itself, and in the top or diffused region. Once $\gamma(\lambda)$ is known, the integral for i_l can be evaluated numerically.

The maximum voltage is determined from the two equations

$$V_{oc} = \frac{kT}{q} \ln (i_l A_l / i_0 A_d + 1) \qquad (5)$$

and

$$V_{max} = V_{oc} - \frac{kT}{q} \ln (q V_{max} / kT + 1) . \qquad (6)$$

Here, A_d is the effective area of the *p-n* junction, and A_l is the surface area effective in absorbing the light, that is, it does not include the area of the metallic finger and edge contacts. In Eq. (5), i_0 is the so-called reverse saturation current and is a directly measurable quantity although theoretical expressions also exist for it. Once V_{oc} is known or assumed, Eq. (6) can be solved iteratively at any given temperature.

Although only the most basic equations have been written down, it should be apparent that the modeling of solar cell performance can become quite complicated. The actual mathematics involved is usually simple, and the construction of appropriate computer programs is straightforward, but determining the correct (or best) assumptions to make about the physical processes involved is a more difficult question. The present studies will be continued to make them as complete and flexible as needed for the photovoltaic program of the Division.

---

[1] Oak Ridge Associated Universities undergraduate research trainee from Bethany Nazarene College, Bethany, Okla.

3. Radiation Effects in Metals

The research programs on radiation effects in metals are primarily concerned with the basic interactions of energetic particles in solids and with the fundamental processes associated with radiation damage in metals. Although much of the work provides basic information of direct interest to fission and fusion reactor materials programs, many of the techniques developed and employed for the study of ion-solid interactions and radiation damage have general utility in the study of defects in solids. The use of ion scattering to obtain detailed information on the variations in the depth composition of a high T superconducting NbGe film illustrates how the capabilities developed for the study of basic ion-solid interactions can be employed to study materials of interest for nonnuclear energy applications.

During the past few years, it has been demonstrated that the velocity dependence of the electronic stopping of heavy ions does not follow the theoretical predictions and that this can lead to significant errors in the calculated damage distributions as a function of penetration depth. Studies of this aspect of ion-solid interactions have been continued both by energy loss measurements and by electron microscope observations of damage distributions. A new experiment was initiated during the past year to study damage production rates as a function of penetration depth. Experimental data of this type have not been available for comparison with the theory employed to calculate damage rates. The first experimental results have indicated that the thin film technique employed in this experiment should provide reliable information for testing the part of the theory that deals with the displacement of atoms.

The neutron scattering experiment on the split interstitial in copper required development of a method for transferring specimens from the Low Temperature Irradiation Facility (LTIF) without warm-up from liquid helium temperature. The extended irradiation time (24 days) required for this experiment is close to the maximum time that can be considered practical for the LTIF, and the need for higher doses has led to plans for modifying the D_2O tank between the reactor core and the LTIF cryostat to provide a higher intensity neutron flux at the cryostat. When this modification is completed, the facility will be used for various types of irradiations in addition to those for further neutron scattering studies; the higher attainable doses and low-temperature-transfer capability will provide opportunities for experiments that heretofore could not be undertaken.

Last year it was noted that the x-ray and electron microscope programs, which in the past had concentrated on the study of defect clusters in reactor-irradiated copper, had been extended to other types of irradiations and other metals. This change in emphasis is further reflected in this Annual Report, in which it is notable that no x-ray and electron microscopy investigations are reported on reactor-irradiated copper. This is a natural development of these programs, in which the theory and techniques developed in the study of damage clusters in copper can now be applied to obtain quantitative information on defect clusters in other materials.

ION–SOLID INTERACTIONS

ENERGETIC HEAVY-ION CHANNELING AS AN EXPERIMENTAL TECHNIQUE FOR SIMULATING RADIATIVE ELECTRON CAPTURE BY PLASMA AND IMPURITY IONS IN A CTR-TYPE PLASMA[1]

B. R. Appleton T. S. Noggle
R. H. Ritchie[2] S. Datz[4]
J. A. Biggerstaff[3] C. D. Moak[3]
H. Verbeek[5]

The initial investigations of the radiative electron capture (REC) phenomenon of highly stripped oxygen ions channeled through thin single crystals[6] were pursued because the special conditions imposed on channeled ions (frozen charge states, reduced backgrounds, and primarily conduction-electron interactions) made this a particularly promising technique for determining the velocity distributions of the (conduction) electrons in the solid. This heavy-ion channeling technique may also prove to be a new simulation method for studying a variety of interactions experienced by highly stripped impurity ions in a controlled thermonuclear reactor (CTR) plasma. Because of the important role played by impurities in a plasma both as a stabilizing influence and as a contributing factor to several detrimental energy loss effects,[7] it is essential to understand the details of these processes for use in present-day modeling calculations required to predict the behavior of future CTR's. Direct experimental measurements are extremely difficult since sufficiently energetic and dense plasmas are not available and existing CTR's are not amenable to such measurements. The basis of the proposed experimental technique arises from the unique constraints imposed on the interactions of energetic heavy ions in single crystals as a result of the channeling phenomenon. It can be shown that 40-MeV O^{8+} ions channeled along low-index axial or planar directions in a metal single crystal are confined to large-impact-parameter collisions with the lattice atoms and so interact primarily with the conduction electrons of the solid.[6] Viewed from the rest frame of the oxygen ion, this situation is the experimental analog of a fully stripped oxygen ion (impurity) at rest, bombarded by a 1.4-keV electron gas having a density comparable with the conduction-electron density in a solid, and thus simulates the environment experienced by an impurity ion in a plasma.

Measurements were made of the photon distributions resulting from highly stripped 17- to 40-MeV oxygen ions channeled along various axial directions in thin silver and silicon single crystals.

Radiation was identified as arising from (1) inverse bremsstrahlung which results from the Coulomb field of the incident ion acting on the conduction electrons, (2) knock-on-electron or secondary-electron bremsstrahlung which results when a struck electron recoils and collides with other lattice atoms, (3) ion deexcitation, in those cases where the incoming ion has its own electrons which can be excited, and (4) radiative electron capture (REC), where a conduction electron is captured directly into the ground state of the fully stripped ion and emits a photon of well-defined energy.

Detailed investigations of the REC phenomenon support the following conclusions: (1) The energy of the REC peaks coincides with that expected for capture of a conduction electron directly into the ground state of an O^{8+} ion. (2) The measured widths of the REC peaks are in good agreement with widths calculated specifically for the channeling situation. The calculations incorporate standard radiation theory and a statistical model of the electron states in the single crystal. The space-varying electron density is averaged over impact parameters appropriate for channeled ions. (3) The measured REC cross sections show a marked deviation from the calculations, which emphasizes how poorly REC is understood for highly stripped heavy ions.

The experimental technique outlined here is suitable for studying the phenomena of REC, direct ion-electron bremsstrahlung, and ion energy loss, excitation, ionization, and charge exchange in a dense electron gas and is equally applicable to impurity and plasma ions alike. However, much work remains to establish the extent to which such results are directly applicable to a CTR-type plasma.

---

[1] Summary of paper to be published.

[2] Health Physics Division, ORNL.

[3] Physics Division, ORNL.

[4] Chemistry Division, ORNL.

[5] Guest scientist from Max-Planck-Institut für Plasmaphysik, Garching, West Germany.

[6] B. R. Appleton, T. S. Noggle, C. D. Moak, J. A. Biggerstaff, S. Datz, H. F. Krause, and M. O. Brown, p. 499 in *Atomic Collisions in Solids*, vol. II, ed. by S. Datz, B. R. Appleton, and C. D. Moak, Plenum Press, New York, 1975.

[7] R. Behrisch and B. B. Kadomtsev, *Plasma Physics and Controlled Nuclear Fusion Research*, vol. II, IAEA-CN 33/S (1974).

ANALYSIS OF HIGH-T_c Nb–Ge FILMS BY ION SCATTERING TECHNIQUES[1,2]

B. R. Appleton J. W. Miller[3] J. R. Gavaler[4]

The discovery that sputtered thin films of Nb–Ge can exhibit superconducting behavior at onset temperatures as high as about 22 to 23°K has stimulated considerable activity to determine the origin of these effects[5-11] because of the potential saving in refrigeration costs that would result to the various energy schemes that employ superconductors. Some investigations of Nb–Ge films have suggested that formation of the stoichiometric A-15 phase Nb_3Ge is an important factor, while others indicate that this may not be the most important dependence.[8] It has been proposed that sputtered Nb–Ge films have high or low T_c depending on the presence or absence of unidentified microscopic defects.[8,9] The role played by impurities in these sputtered films has also been considered.[10,11] Crucial to all these considerations is the need for quantitative analysis of the elemental composition of the films being investigated.

We have recently investigated the composition of high-T_c (>22°K) Nb–Ge films, sputter-deposited on sapphire substrates, by the combined techniques of Rutherford elastic scattering, ion scattering resonance techniques, and ion-induced x rays. Both niobium and germanium compositions vs depth were determined in a nondestructive manner by deconvoluting a series of Rutherford backscattering spectra obtained using 2.0- to 3.2-MeV helium ions at several incidence and scattering angles, and the results are shown in Fig. 3.1. Confirmation of these results was provided by analyzing the yields of niobium and germanium characteristic x rays as a function of the angle of beam incidence. Of particular interest in the present study was the depth profile of oxygen contained in the Nb–Ge film, which was measured using a sharp ion scattering resonance, $^{16}O(\alpha,\alpha)^{16}O$, to provide enhanced sensitivity. By systematically changing the energy of the incident ^4He beam, the resonance was "stepped" through the film thickness, and the results were deconvoluted to obtain the oxygen profile shown in Fig. 3.2.

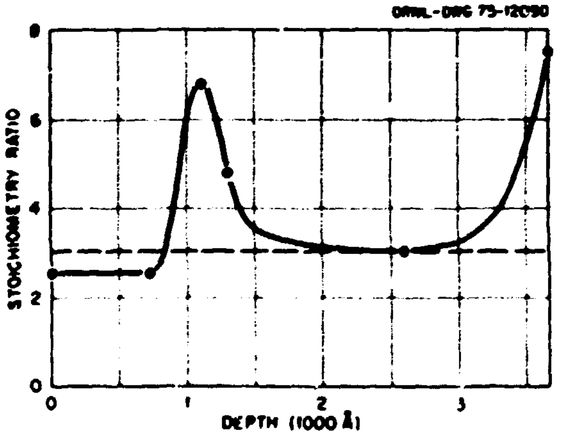

Fig. 3.1. Nb:Ge ratios as a function of depth determined from deconvolution of 3.2-MeV Rutherford scattering analysis of an Nb–Ge film sputter-deposited on an Al_2O_3 substrate.

Comparison shows an exact correspondence between the two Nb:Ge peaks in Fig. 3.1 with the two oxygen peaks in Fig. 3.2 located near the substrate interface and within the body of the film. The location of the peak within the film can be directly related to the time when the sputtering was interrupted. The increased oxygen content indicated in Fig. 3.2 near the outside surface of the film apparently resulted from adsorption of oxygen into the surface after sputtering was completed and thus could not exert an influence on the Nb:Ge composition. However, the presence of oxygen during the sputtering process, as evidenced by the other peaks, appears to have had a dramatic effect on the Nb:Ge ratio. It seems likely that nonuniform Nb–Ge concentration in the film is, at least partially, due to a chemical effect caused by the changing oxygen concentration. We theorize that the niobium atoms react preferentially with oxygen, causing the germanium sticking coefficient to be relatively low when the sputtering is initiated. As the oxygen content becomes lower with increasing thickness, progressively more germanium combines with niobium until finally an equilibrium condition is achieved.

The question now arises whether this oxygen is having an effect on critical temperature, either positive or negative. The answer depends largely on whether the oxygen is actually incorporated into the Nb_3Ge A-15 structure, as has been hypothesized in the case of chemically vapor-deposited Nb–Ge films,[11] or whether it is present only as some niobium oxide second phase. Analysis of the film by x-ray diffraction suggests that there is a niobium–oxygen compound in the film. However, these data do not eliminate the possibility that some oxygen is also entering into the Nb–Ge crystal structure. If this actually does occur, it could explain why the normally unstable stoichiometric Nb_3Ge phase can be prepared by thin-film techniques. One can hypothesize that oxygen, incorporated into the film during the deposition process, stabilizes the A-15 structure, thus allowing the growth of the normally unstable stoichiometric Nb–Ge compound. Another experimental fact which is not presently understood is the observation of high critical temperature in films in which the Nb:Ge ratios are far removed from ideal 3:1 stoichiometry.[8] In this case, if one assumed that a significant amount of oxygen combines with niobium and germanium to form the pseudobinary alloy $Nb_3(Ge_xO_{1-x})$, the Nb:Ge ratio could indeed be far

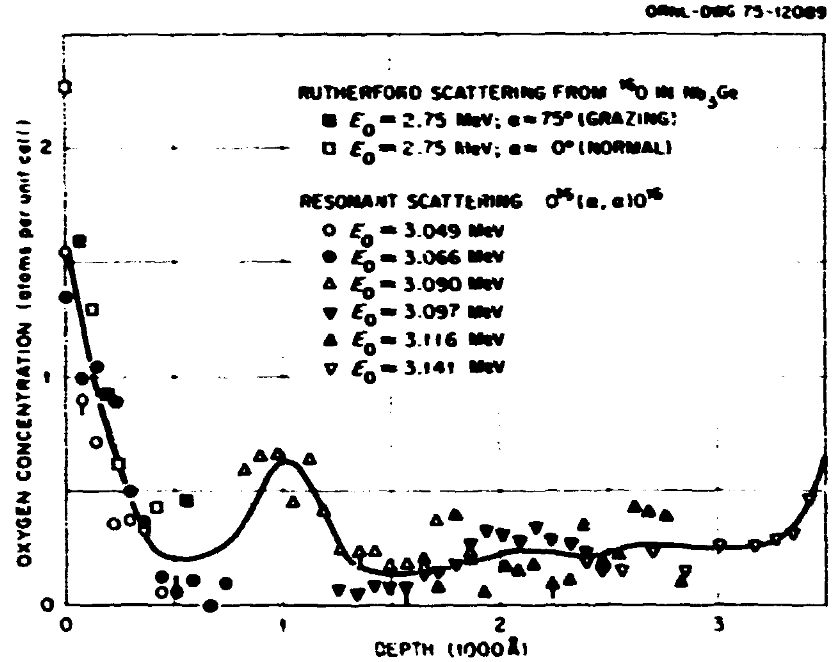

Fig. 3.2. Oxygen distribution as a function of depth obtained using an enhanced elastic scattering resonance $^{16}O(\alpha,\alpha)^{16}O$ at 3.045 MeV for the same film as in Fig. 3.1.

off 3:1 stoichiometry, while the Nb:(Ge + O) ratio could have the proper stoichiometric value. A more detailed analysis of the backscattering measurement may supply information on this problem.

MEASUREMENTS OF THE VELOCITY DEPENDENCE OF ELECTRONIC STOPPING POWER AT VERY LOW VELOCITIES

B. R. Appleton O. E. Schow III
T. S. Noggle H. Verbeek[1]

Studies of many of the materials problems associated with fission and fusion reactors are inexorably tied to the phenomena of ion energy loss in solids, particularly in the low-velocity region. Most radiation damage in fission reactor materials is caused by recoiling knock-on atoms. First-wall materials used for confinement of plasmas in CTR devices are subjected to massive bombardment by low-energy ions, which leads to sputtering, gas bubble formation, blistering, etc. Understanding each of these separate phenomena requires an accurate knowledge of the energy loss, range, or damage energy of the bombarding ions and/or recoiling atoms.

The low-velocity region of ion stopping is particularly relevant since that is the pertinent region for both recoiling atoms and primary ions from CTR plasmas. An accurate understanding in this velocity range is complicated because the ions lose energy by two competing mechanisms, which can be rather naturally separated for discussion purposes into (1) ionizing

---

[1] Summary of paper to be published.

[2] Research supported in part by AFOSR Contract No. F 44620-74-0042.

[3] Present address: Scientific Associates Inc., McLean, Va. 22101.

[4] Westinghouse Research and Development Center, Pittsburgh, Pa. 15235.

[5] J. F. Gavaler, *Appl. Phys. Lett.* 23, 480 (1973).

[6] L. R. Testardi, J. H. Wernick, and W. A. Royer, *Solid State Commun.* 15, 1 (1974).

[7] J. R. Gavaler, M. A. Janocko, and C. K. Jones, *J. Appl. Phys.* 45, 7 (1974).

[8] L. R. Testardi, R. L. Meek, J. M. Poate, W. A. Royer, A. R. Storm, and J. H. Wernick, *Phys. Rev. B* 11, 4304 (1975).

[9] J. M. Poate, L. R. Testardi, A. R. Storm, and W. M. Augustyniak, *Phys. Rev. Lett.* 35, 1290 (1975).

[10] A. T. Santhanam and J. R. Gavaler, *J. Appl. Phys.* 46, 3633 (1975).

[11] E. R. Newkirk, F. A. Valencia, and T. C. Wallace, proceedings of the 5th International Conference on Chemical Vapor Deposition, London, England, 1975, to be published.

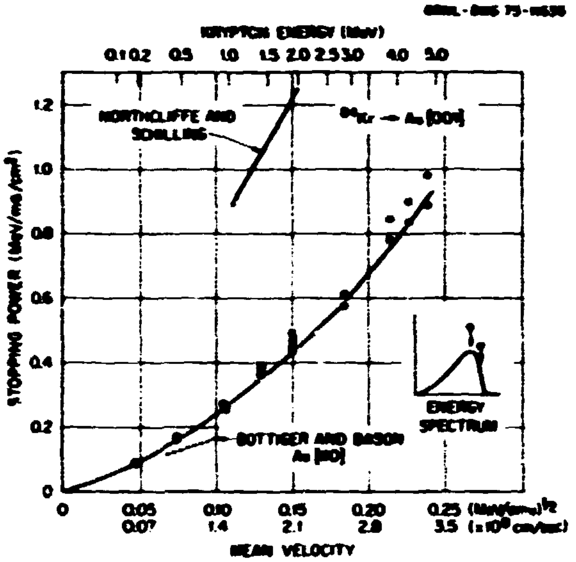

Fig. 3.3. Measured stopping power of well-channeled ^{84}Kr ions transmitted parallel to the [001] axis of a thin gold single crystal.

collisions, which contribute to the slowing of ions in the solid, and (2) nuclear collisions, in which the ions displace atoms of the solid, causing radiation damage, sputtering, etc. The most widely used theories to explain stopping powers by ionizing collisions (so-called electronic stopping region) are due to Lindhard, Scharff, and Schiøtt[2] and Firsov,[3] both predict that the stopping power S_e obeys the relationship $S_e = KE^{1/2}$, where E is the ion energy.

Previous measurements[4] of the stopping power of iodine ions transmitted through thin single crystals of silver showed that the electronic stopping power was *not* proportional to $E^{1/2}$. These measurements, however, only extended to velocities in the region $(E/A)^{1/2} \geq 0.1$, where E and A refer to the energy (in MeV) and atomic mass number of the iodine ions. Recently these measurements were extended to even lower velocities using krypton ions from the Solid State Division's 2.5 MV Van de Graaff accelerator channeled through gold single crystals. The results are shown in Fig. 3.3, and even at the lowest measured velocities the electronic stopping is *not* velocity-proportional. The technique of channeling ensures that the ions lose energy by ionizing interactions only[4] and allows one to measure the functional dependence of the electronic stopping component without interference from nuclear stopping, which is normally dominant in this situation.

2. J. Lindhard, M. Scharff, and H. E. Schiøtt, *K. Dan. Vidensk. Selsk., Mat.-Fys. Medd.* 33, No. 14 (1963).

3. O. B. Firsov, *Zh. Eksp. Teor. Fiz.* 36, 1517 (1959) [*Sov. Phys.-JETP* 9, 1076 (1959)].

4. C. D. Moak, B. R. Appleton, J. A. Biggerstaff, M. D. Brown, S. Datz, T. S. Noggle, and H. Verbeek, *Proc. of VI International Conf. on Atomic Collisions in Solids, Nucl. Instrum. Methods* (in press).

DAMAGE PRODUCTION RATES OF 5-MeV ALUMINUM IONS IN ALUMINUM

T. S. Noggle J. M. Williams
B. R. Appleton J. A. Biggerstaff[1]

There is very little direct experimental information on damage production rates of heavy ions in solids. In particular, there are virtually no measurements of damage production rates as a function of penetration depth, which can be used to test the theoretical calculations of the atomic displacements along the paths of ions. This lack of experimental measurements of damage production rates is due to the very short ranges of heavy ions in solids, which preclude the use of bulk specimens of the type employed in studies of fast-neutron and electron damage in metals. This report gives information on the first irradiation of aluminum with 5-MeV aluminum ions in an experiment that is designed to measure damage production rates as a function of the penetration depth of the ions. In this experiment, a thin film specimen is irradiated at 4°K, and the observed resistance changes give a measure of the displacement damage introduced by the ion irradiation. By interposing absorber foils in the beam, the path lengths of the ions in the solid can be varied, and the specimen acts as a damage sensor for the increment of path length from X to $X + \Delta X$, where X is the absorber foil thickness and ΔX the specimen thickness.

Figure 3.4 shows the type of specimen developed for this experiment. The aluminum substrate plate provides the support for the evaporated thin film specimen, which is electrically isolated from the plate by the anodized oxide layer. Electrical connections are made with spring contacts in the specimen holder, which is attached to the cryotip of a Heli-Tran[2] sample cooling system. This arrangement is shown in Fig. 3.5, which is a photograph taken during assembly. The open frame projecting below the assembly is one of three slides on which absorber foils can be mounted and which can be translated during the experiment so that absorber foils can be centered in front of the specimen. Figure 3.6 shows one of these slides with a 0.5-μm evaporated aluminum film mounted over the bottom window and a 1-μm film mounted over the top window. Five films of

---

[1] Guest scientist from Max-Planck-Institut für Plasmaphysik, Garching, Germany.

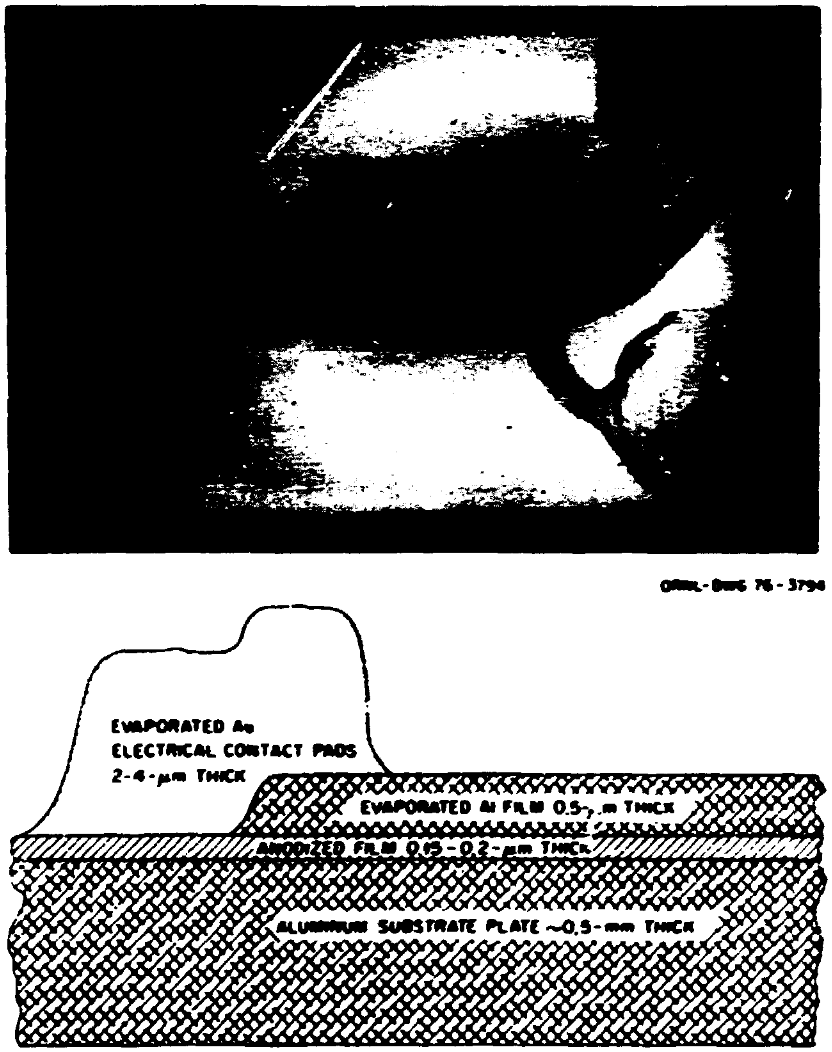
PHOTO 1255 76

ORNL-DWG 76-3794

Fig. 3.4. Thin film aluminum resistance specimen. Top: Evaporated aluminum thin film specimen with 2.0 mm width, 0.5 μm thickness, and 5.0 mm between voltages probes. The four circular regions are gold contact pads deposited by evaporation. Bottom: Schematic diagram showing details of the thin film specimen. The aluminum plate provides a support for the thin film, which can be put into good thermal contact with the specimen holder. The anodized layer provides electrical isolation between the specimen and the substrate plate.

different thicknesses were mounted so that by inserting films singly or in series, the absorber path length could be varied by 0.5-μm increments up to a maximum of 3.5 μm. The specimen holder and absorber foils are surrounded by a thermal shield, which can be seen in Fig. 3.5 as the structure clamped to the cryotip tube. This thermal shield supports a scattering aperture, which is fastened to the inclined end of the tube that extends out from the shield. During the ion irradiations, a 50-cm-long collimator provides a beam with dimensions larger than this aperture, and the aperture defines the beam that impinges on the specimen. Scattering from the part of the beam that is stopped by the aperture is detected by the solid-state detector. The assembly of Fig. 3.5 and the beam collimator were mounted in an irradiation chamber, which was constructed using ultrahigh vacuum fittings and techniques wherever practicable. This was done to ensure a clean environment and a good vacuum in order to minimize cryopumping by the specimen and absorber films.

The ion irradiations were made with 5-MeV ^{27}Al ions from the ORNL tandem Van de Graaff. Because of equipment problems that occurred during the first run, damage rate measurements were made only for the

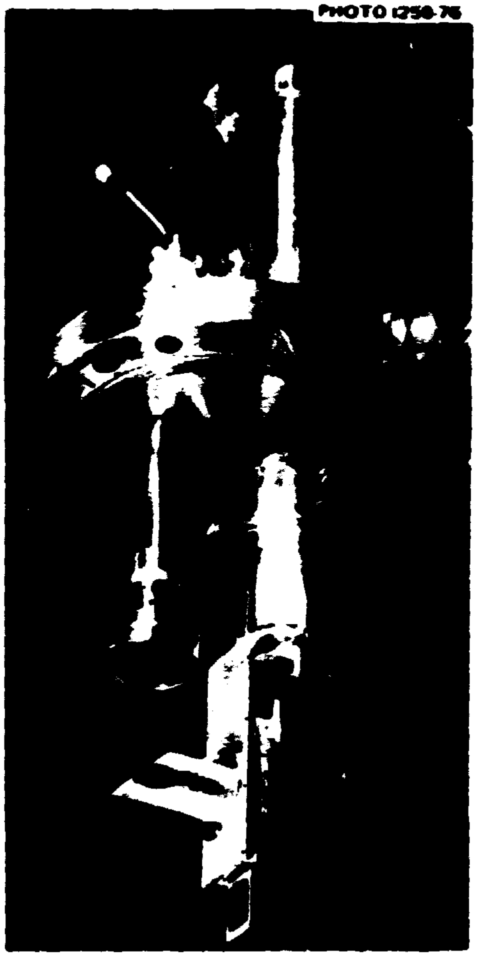

Fig. 3.5. Low-temperature ion-irradiation specimen holder. The specimen holder is fastened to the end of the cryotip tube. The two projections from the side of the holder are electrical leads used in the resistance measurements. The thermal shield, which is incomplete in this photograph, completely surrounds the specimen holder and supports the scattering aperture, which is mounted on the inclined end of the tube that extends out from the shield. The structures between the detector mounting tube and the cryotip tube are the slide mechanisms for translating the frames on which absorber foils are mounted.

open beam and with the 2-μm absorber foil. Short irradiations for each condition were alternated to obtain two sets of data, from which two damage rate curves ($d\Delta R/d\phi$ vs ΔR) were obtained. The intermeshing of the measurements allows interpolation, so that the apparent damage rates ($d\Delta R/d\phi$) for the two conditions can be compared at the same damage concentration. The ratio of the apparent damage rates, $(d\Delta R/d\phi)_{2\mu}/(d\Delta R/d\phi)_0$, was 5.40 ± 0.65. This ratio can be compared with a similar ratio obtained from theoretical damage cross sections calculated by Oen, if it is assumed that the electrical resistance changes are directly proportional to the damage energy. The ratio of the cross sections averaged over the intervals from 2 to 2.5 μm and from 0 to 0.5 μm gives a value of 3.17 for calculations using the LSS value[3] of $k = 0.14$ for the electronic stopping parameter and a value of 4.84 for calculations using a value of $k = 0.17$, which was derived from the stopping power tables of Northcliffe and Schilling.[4] The experimental ratio is clearly most consistent with the calculations using the value for $k = 0.17$; this result follows the general observation of the past few years that significant differences are frequently found between the theoretical values of k based on the LSS theory and those determined by experiment.

Although the basic concept of this ion-irradiation experiment is quite simple, there are many details which give rise to complications. Foremost among these is the size effect in the electrical resistance of thin films, which causes each thin film specimen to be almost a unique material in its electrical resistance variation with the introduction of defects. It is believed that the present method of obtaining relative damage rates minimizes this difficulty and that the result of this first

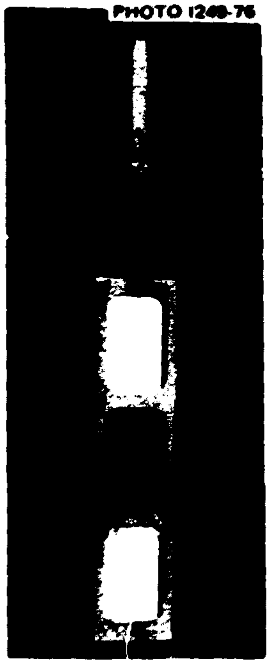

Fig. 3.6. Absorber foil frame. The example shown has a 0.5-μm film mounted over the bottom window and a 1.0-μm film over the top window. The frames are made of 0.4-mm-thick aluminum sheet, and the windows are 1.0 by 1.5 cm in size. The dark band on each side is due to hard anodizing to minimize friction between the frame and guide grooves in the specimen holder.

irradiation experiment indicates that this technique will generate the desired detailed information on the damage rates of heavy ions in solids.

---

1. Physics Division, ORNL.
2. Manufactured by Air Products and Chemicals, Inc., Allentown, Pa.
3. J. Lindhard, M. Scharff, and H. E. Schiøtt, *K. Dan. Vidensk. Selsk., Mat.-Fys. Medd.* 33, No. 14 (1963).
4. L. C. Northcliffe and R. F. Schilling, *Nucl. Data* A7, 233 (1970).

ION DAMAGE IN NICKEL

J. Narayan   O. S. Oen

High-purity nickel single crystals were irradiated with 4-MeV nickel ions at room temperature to a fluence of 2.5×10^{13} ions/cm^2 using the ORNL 5-MV Van de Graaff Accelerator. To study the depth distribution of damage, these crystals were electroplated with nickel and sectioned normal to the interface. Sectioning was done with a spark cutting machine, and the small amount of surface damage introduced by the spark machine was removed by subsequent electropolishing. The samples were thinned at the interface for electron microscope observations. The density of point defects contained in the observed dislocation loop structure was determined as a function of depth. This is shown in Fig. 3.7, where the data are plotted as a histogram. The smooth curves give the calculated damage energy deposited by the incident ions using the EDEP-1 computer code,[1] which is based on the atomic collision theory of Lindhard, Scharff, and Schiøtt (LSS).[2] It is of interest to note that the observed damage peak is 15% deeper than that calculated using the theoretical value of the electronic stopping power parameter, k_{LSS} = 0.162. To get good agreement with the observed damage peak, k has to be reduced to a value of 0.126. The reason for these lower stopping powers has been discussed earlier for the case of copper and nickel ions incident on a copper target.[3] However, it is of particular interest that the difference between the observed and calculated damage peaks is less for nickel ions incident on a nickel target than that for nickel ions incident on a copper target. This suggests that nickel ions are subject to oscillations in the stopping power as a function of the target atomic number. This result is similar to that observed for helium[4] and nitrogen[5] ions, for which a sharp minimum in the electronic stopping has been reported at $Z = 29$.

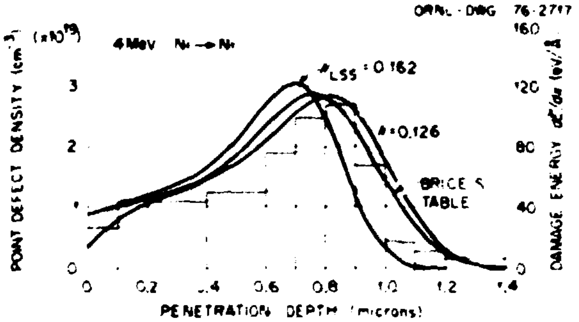

Fig. 3.7. Experimental histogram of point-defect density and calculated damage energy as a function of penetration depth. The smooth curves are for two values of the electronic stopping parameter, k_{LSS} = 0.162 and k = 0.126, and for Brice's tabulated values of the damage energy.

The calculated damage energy from the tables of Brice[6] is also included in the figure. Brice used a three-parameter formula for the electronic stopping, which is claimed to reproduce the semiempirical tables of Northcliffe and Schilling.[7] The agreement between Brice's calculations and the present experimental data is within 5%. Thus, the tables of Brice predict the depth distribution of damage for nickel ions in nickel more accurately than the EDEP-1 code with the LSS electronic stopping parameter value.

---

1. I. Manning and G. P. Mueller, *Computer Phys. Commun.* 7, 85 (1974).
2. J. Lindhard, M. Scharff, and H. E. Schiøtt, *K. Dan. Vidensk. Selsk., Mat.-Fys. Medd.* 33, No. 14 (1963).
3. J. Narayan, O. S. Oen, and T. S. Noggle, *Fundamental Aspects of Radiation Damage in Metals*, ed. by M. T. Robinson and F. W. Young, Jr., ERDA report CONF-751006, Oak Ridge, Tenn. (in press).
4. J. F. Ziegler and W. K. Chu, *At. Data Nucl. Data Tables* 13, 463 (1974).
5. D. G. Simons, D. J. Land, J. G. Brennan, and M. D. Brown, *Proceedings of the International Conference on Ion Beam Surface Analysis*, Plenum Press, New York (in press).
6. D. K. Brice, *Ion Implantation Range and Energy Deposition Distributions*, vol. 1, Plenum Press, New York, 1975.
7. L. C. Northcliffe and R. F. Schilling, *Nucl. Data* A7, 233 (1970).

SELF-ION DAMAGE IN COPPER

J. Narayan   O. S. Oen   T. S. Noggle

Copper single crystals were irradiated at room temperature with 5-, 16-, 27-, and 38-MeV copper ions to a fluence of approximately 5×10^{12} ions/cm^2 using the ORNL tandem Van de Graaff accelerator. The retained damage in the form of dislocation loops was studied as a function of depth by a transmission electron microscope technique. The experimental point-defect density vs depth curves were compared with the damage energy deposited by the incident ions. The deposited damage energy was calculated with the widely used EDEP-1 code,[1] which is primarily based on the atomic collision theory of Lindhard, Scharff, and Schiøtt (LSS).[2] Figure 3.8 shows the experimental histogram of point-defect density as a function of depth for 5-MeV and 27-MeV irradiations. The smooth curves in the figure give the calculated damage energy as a function of depth for two values of the electronic stopping power parameter *k*. The vertical scaling of the calculated curves is arbitrarily chosen to give a good overall fit with the data. The observed point defects are about 4 to 6% of the defects predicted by the damage energy calculations.

To obtain good agreement with the experimental data, it is necessary to use smaller values of the electronic stopping parameter *k* than that predicted by

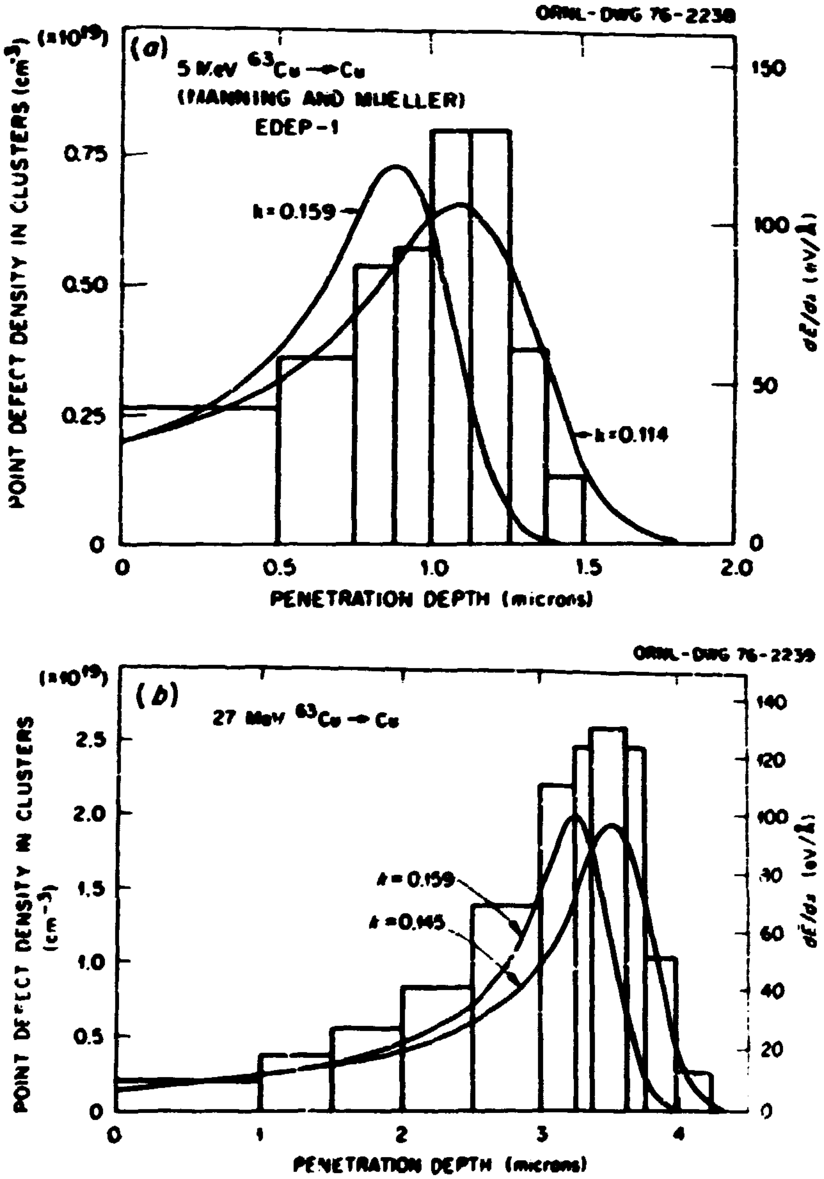

Fig. 3.8. Self-ion damage in copper. Experimental histograms of point-defect density and calculated damage energy as a function of depth. (*a*) 5-MeV copper ions on copper, for k_{LSS} = 0.159 and *k* = 0.114; (*b*) 27-MeV copper ions on copper for k_{LSS} = 0.159 and *k* = 0.145.

the LSS theory, k = 0.167. The reduction is a few percent for 38-MeV, 10% for 27-MeV, 16% for 16-MeV, and 28% for 5-MeV irradiations. The result that k depends on the ion irradiation energy indicates that the electronic stopping does not depend linearly on the ion velocity. The relative changes in k as a function of energy are qualitatively similar to our previous nickel ions in copper irradiation results. As discussed in that paper, the relatively low electronic stopping in copper is related to the oscillations in the electronic stopping when plotted as a function of target atomic number, Z_2. Copper lies at a local minimum in such a curve. These osciallations are related to the charge density oscillations and have been discussed briefly in a recent review paper by Sigmund.[3] In addition to the Z_2 oscillations, there are also oscillations in the electronic stopping when plotted as a function of the projectile atomic number, Z_1. Since copper projectile ions lie near a local minimum in the Z_1 oscillations, this effect will also contribute to a decrease of the electronic stopping; however, it appears that the Z_2 effect is the more important in the projectile-target combinations that have been investigated to date.

---

1. I. Manning and G. P. Mueller, *Comput. Phys. Commun.* 7, 857 (1974).

2. J. Lindhard, M. Scharff, and H. E. Schiøtt, *K. Dan. Vidensk. Selsk., Mat.-Fys. Medd.* 33, No. 14 (1963).

3. P. Sigmund, p. 3 in *Radiation Damage Processes in Materials*, ed. by C.H.S. Duprey, Noordhoff, Leyden, 1975.

LOW-TEMPERATURE RADIATION EFFECTS

PROGRESS ON AN INTERLABORATORY PROGRAM TO STUDY LOW-TEMPERATURE DAMAGE RATES IN DILUTE VANADIUM, NIOBIUM, AND MOLYBDENUM ALLOYS

J. M. Williams   J. K. Redman
C. E. Klabunde   R. R. Coltman, Jr.

A cooperative program designed to make use of the special capabilities of a number of laboratories seeks to measure the resistivity damage rates near 4°K for electron, proton, fission-neutron, and 14-MeV-neutron irradiations of dilute alloys of zirconium in vanadium, niobium, and molybdenum. The ORNL commitment to this program consists of sample preparation, which has been completed by the Research Materials Section, and the fission-neutron irradiations, which are being undertaken by the Low-Temperature Irradiation Group. Specifications for the sample materials and conditions of measurement, a list of the participants, and a description of earlier progress in the program have been presented previously.[1,2]

During the past year, construction and testing of all portions of the fission-neutron experiment assembly were completed, and the first irradiation was made on a V–300-ppm-Zr ribbon at 4.6°K for 258 hr. A photograph of the component parts of the assembly is shown in Fig. 3.9. The function and a description of each are as follows:

Upper — an Nb–Ti superconducting magnet (1.9 cm bore, 2.5 cm long; H_{max} = 12.7 kOe at 4.2°K) to suppress specimen superconductivity.

Middle — a high-purity copper heat exchanger containing a ^{235}U ring (1.110 cm in diameter, 3.18 mm wide, and 0.127 mm thick) bonded with tin to a central internal groove. The innermost surface of the ^{235}U ring is backed with a matching 0.025-mm gadolinium foil to partly shield the nearby sample from thermal neutrons. A thin (0.127-mm) stainless steel liner serves as a fission-product containment and as a heat barrier between the neutron converter and the sample. During the present irradiation, the converter generated 6.7 W and produced a pure fission-neutron flux at the specimen of 6.0×10^{11} neutrons cm^{-2} sec^{-1} (30% of external thermal-neutron flux). The thermal-neutron contribution to the damage in the specimen is less than 3% of the total.

Lower — an anodized aluminum holder centers ribbon-shaped specimens (1.034 cm in diameter, 0.81 mm wide, and 0.025 mm thick) adjacent to the converter inside the exchanger. Channels and milled flats provide convection cooling while accurate sample positioning is maintained.

Since each component is independent, a variety of arrangements can be irradiated in the sample chamber of the LTIF, including the magnet with an encapsulated collection of specimens. Rapid change of ribbon specimens on the pictured holder is also easily accomplished.

The temperature of the sample during irradiation, which was verified using the temperature dependence of the sample resistance measured before irradiation, was lower than expected. This is attributed to the high fission-heat-removal rate afforded by the convection-cooling-channel design of the sample holder and the apparently good bond between the ^{235}U ribbon con-

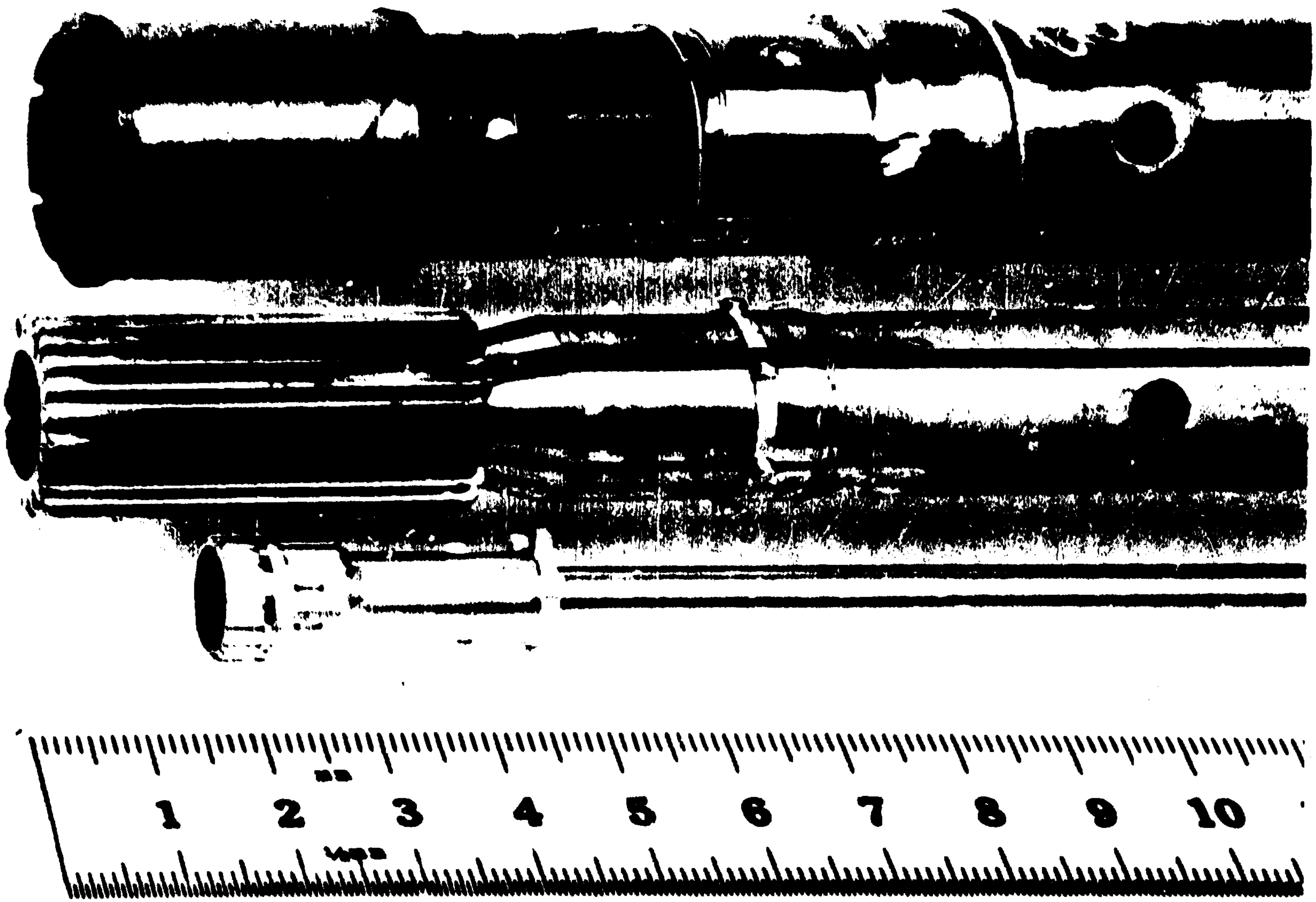

Fig. 3.9. Photograph of the components of an experiment assembly for measuring fission-neutron damage rates at liquid-helium temperatures.

verter and the high-purity copper heat exchanger. During early design considerations, the possibility was recognized that the high heat flux from the converter ring might envelop the nearby (0.038 cm) specimen in a doughnut-shaped helium-vapor bubble. This would produce an unacceptable rise in sample temperature which could only be corrected by reducing reactor power. Containment of fission-product activity in the converter assembly was found to be satisfactory according to postirradiation surveys of the sample-holder surface and of a charcoal trap serving the sample chamber of the Low Temperature Irradiation Facility (LTIF).

Figure 3.10 shows the fission-neutron damage rate of the sample as a function of the damage resistivity. Although some small fluctuations developed in the measurements beyond $\Delta\rho \approx 100$ nΩ-cm, the data-point averaging indicated in the figure gives results which show a transient reduction in the damage rate before a typical linear decrease takes over at about 100 nΩ-cm. In contrast, Jung and Lucki[3] found no transient when they studied 1.2-, 1.9-, and 2.8-MeV electron damage production on the same material as part of the interlaboratory program. Since the same material was used in both cases, the difference cannot be explained by the electrical size effect; however, a deviation in Matthiessen's rule cannot be ruled out. Since the transient effect is not large, however (13% as given by the zero-dose damage-rate values indicated in Fig. 3.10), it cannot have a strong influence on future comparisons of these and other types of damage which will be made using detailed collision cross-section information as part of the intended program. The present results can also be compared with those obtained by Brown et al.[4] on less pure vanadium (resistance ratio ≈ 15) irradiated at 18°K with a slightly energy-degraded fission-neutron spectrum. Their initial damage rate (linear extrapolation) was 38% greater than the present value. This difference may be related to the difference in impurity content. The possibility[5] that defect migration may be occurring at the irradiation temperature could also be very significant in explaining this difference.

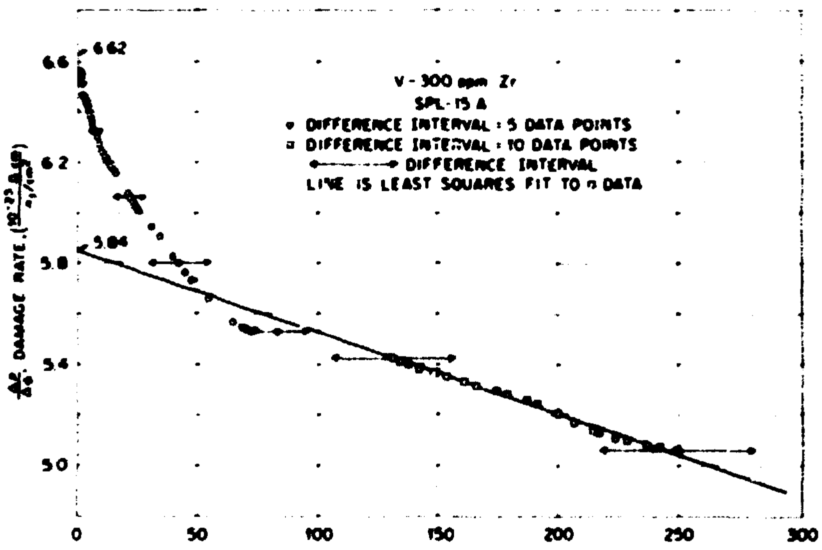

Fig. 3.10. The fission-neutron damage rate of V–300 ppm Zr at 4.6 K vs damage resistivity. The initial resistivity, ρ_0, was 151 nΩ-cm ($R_{305}/R_{4.5}$ = 141), and the total damage increment was 281 nΩ-cm (1.86 ρ_0) produced by a neutron fluence of 5.2×10^{17} neutrons/cm^2. All measurements were made with a magnetic field of 3.6 kOe.

---

[1] R. F. Reed, C. E. Klabunde, J. K. Redman, and R. R. Coltman, Jr., *Solid State Div. Annu. Prog. Rep. Dec. 31, 1973*, ORNL-4952, p. 29.

[2] J. M. Williams, C. E. Klabunde, J. K. Redman, and R. R. Coltman, Jr., *Solid State Div. Annu. Prog. Rep. Dec. 31, 1974*, ORNL-5028, p. 42.

[3] P. Jung and G. Lucki, *Radiat. Eff.* (to be published).

[4] B. S. Brown, T. H. Blewitt, T. L. Scott, and A. C. Klank, *J. Nucl. Mater.* 52, 215 (1974).

[5] C. E. Klabunde, R. R. Coltman, Jr., and J. M. Williams, *Fundamental Aspects of Radiation Damage in Metals*, ed. by M. T. Robinson and F. W. Young, Jr., ERDA report CONF-751006, Oak Ridge, Tenn. (in press).

INDIRECT EVIDENCE FOR VACANCY CLUSTERING DURING STAGE III ANNEALING IN COPPER[1]

H. Schroeder[2] P. Wienhold[2] C. E. Klabunde
K. Sonnenberg[3] R. R. Coltman, Jr. J. M. Williams

High-purity copper foil specimens were doped with relatively high defect concentrations (200 to 1000 ppm) by electron irradiation at low temperatures. Following the doping irradiation, the specimens were isochronally annealed between 100 and 500°K; however, after each annealing step some specimens were given either of two test-dose irradiations which were small compared with the original doping doses:

1. irradiation at 80°K to measure the damage production rate.
2. irradiation at 4°K followed by annealing at 65°K to measure the damage, $\Delta\rho_I$, remaining after stage I recovery.

Both the damage rate at 80°K and $\Delta\rho_I$ are essentially determined by the branching ratio of two reaction possibilities for the freely migrating interstitials produced by the test doses:

1. trapping by interstitial clusters formed during the previous doping dose.
2. annihilation at doping-dose vacancies.

Reactions between test interstitials and impurities or self-interaction of test interstitials can be neglected, since the doping defect concentration was much higher than the test defect concentration.

As a function of the isochronal annealing temperature of the doping defects, both the damage rate at 80°K and $\Delta\rho_I$ show a drastic increase in the temperature range of the stage III recovery. This increase can be easily understood if the competition for test-dose interstitials by doping-dose vacancies is reduced as a result of their clustering during stage III recovery.

---

[1] Summary of paper: *Fundamental Aspects of Radiation Damage in Metals*, ed. by M. T. Robinson and F. W. Young, Jr., ERDA report CONF-751006, Oak Ridge, Tenn. (in press).

[2] Institut für Festkörperforschung, KFA Jülich, Germany.

[3] Guest scientist from Institut für Festkörperforschung, KFA Jülich, Germany.

CRYOGENIC IRRADIATION AND TRANSFER OF LARGE COPPER SAMPLE

J. M. Williams R. R. Coltman, Jr.
C. E. Klabunde J. K. Redman

The neutron-scattering experiment[1] designed to study the phonon perturbations produced by the dumbbell interstitial presented special problems in preparation of the sample for the study. The resolution requirements of the experiment dictated that the product of sample volume by interstitial concentration be as high as possible. It was therefore decided in this initial approach to use a large sample (0.6 × 1.8 × 3.8 cm, weight 37 g) and to achieve a uniformly dispersed configuration of Frenkel pairs by use of neutron irradiation. The irradiation was done in the Low Temperature Irradiation Facility (LTIF) of the Bulk Shielding Reactor. This facility is a liquid-helium-cooled chamber situated in a thermalized neutron flux of 2.5 × 10^{12} neutrons cm^{-2} sec^{-1}. Damage in the form of a few Frenkel pairs per neutron capture event is produced by the (n,γ) recoils.

The difficult part of the task was to transfer the sample from the LTIF without warming above liquid-helium temperature, which would have allowed the interstitials to anneal out. This was accomplished by use of a specially constructed miniature aluminum dewar which served as both the irradiation "capsule" and the transfer dewar. This small dewar (about 15 cm long), with a single vacuum annulus, would hold liquid helium for about 1.5 min while exposed to air at room temperature. The sample was irradiated for 24 days, and then the cold transfer was successfully completed.

---

[1] R. M. Nicklow, R. R. Coltman, Jr., F. W. Young, Jr., and R. F. Wood, "Neutron Inelastic Scattering Measurements of Phonon Perturbations by Defects in Irradiated Copper," this report.

A CRYOPUMPED VACUUM SYSTEM FOR ANNEALING SMALL SPECIMENS BY JOULE HEATING

R. R. Coltman, Jr. J. K. Redman

It is anticipated that the fission-neutron damage rates near 4°K will be measured for a large number of elements, using the ^{235}U converter system described elsewhere in this report.[1] It is known that some of the high-melting-point (>1000°C) elements to be studied in this program can be further purified by the purging of impurities that is afforded through annealing near the melting point. This is most easily accomplished for small samples (wires and ribbons) by Joule heating. Some of these, however, are refractory metals which react readily with gases at high temperature and therefore require a better vacuum during annealing[2] than can be reached with typical diffusion-pumped cold-trapped systems. To meet this need and at the same time provide for the relatively rapid treatment of samples, an economical cryopumped vacuum system was constructed as shown schematically in Fig. 3.11.

The principal design feature is a close-slide-fit piston which divides the upper cylindrical chamber into two compartments. The compartments are connected by a U-tube, however, which is immersed in a conventional commercial liquid-helium storage vessel to provide the cryopumping action. After a specimen has been mounted in the left, or sample, compartment, the device is evacuated using a conventional vacuum system and then sealed off, and the U is immersed in liquid helium. Typical vapor sources such as O-rings and valve seats which limit conventional systems are found only in the right compartment, and their emissions can reach the specimen compartment only through the narrow piston clearance (0.025 mm) or through the U-tube, where they are frozen out en route.

Although the vacuum achieved in the sample compartment has not yet been measured, early use of the device indicates substantial improvement over a conventional system. After cryopumping for 18 hr, an as-received tantalum foil (0.025 mm) with an initial resistance ratio of about 40 was annealed near the melting point and the resistance ratio increased to 540. It is well known that this element is very sensitive to gas pickup during high-temperature annealing. Much further use is anticipated for this simply operated device, which consumes an insignificant amount of liquid helium.

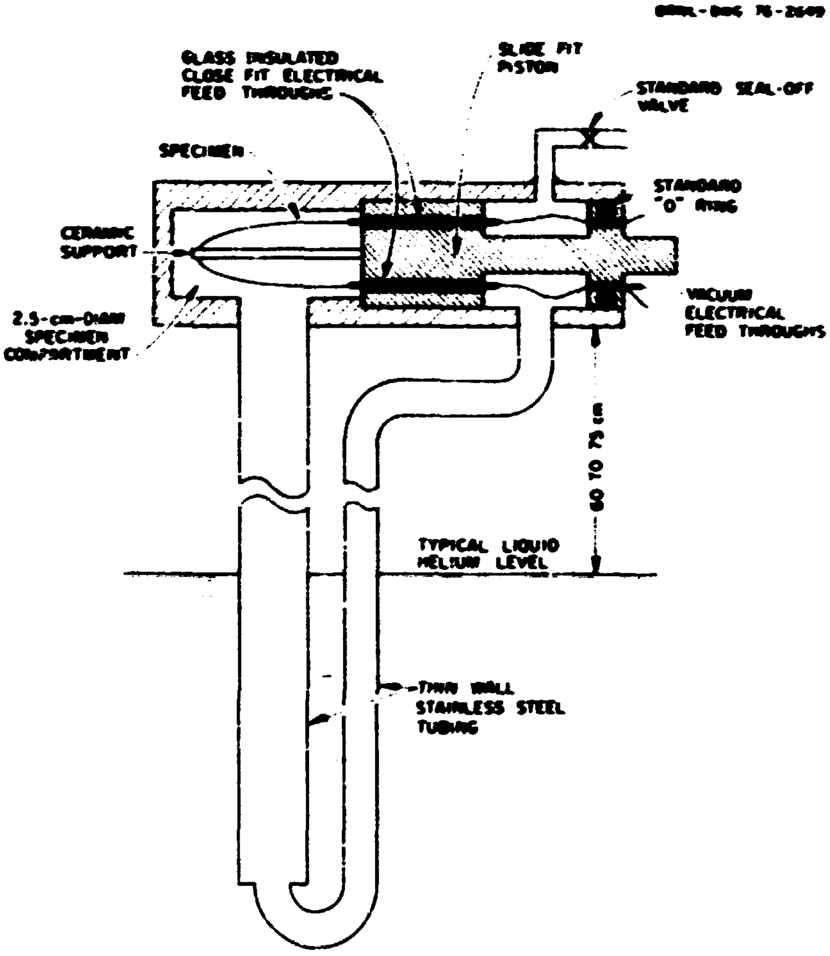

Fig. 3.11. Schematic representation of a cryopumped device for annealing small specimens by Joule heating. A small water flow through a jacket surrounding the upper cylinder (not shown in the figure) serves to maintain the cylinder at room temperature during specimen heating.

---

1. R. R. Coltman, Jr., C. E. Klabunde, J. K. Redman, and J. M. Williams, "Progress on an Interlaboratory Program to Study Low-Temperature Damage Rates in Dilute Vanadium, Niobium, and Molybdenum Alloys," this report.

2. Eckehard Fromm and Hermann Jehn, *Metall. Trans.* 3, 1685 (1972).

DEGRADATION OF STABILITY OF A SUPERCONDUCTING MAGNET BY RADIATION DAMAGE

C. E. Klabunde H. R. Kerchner
S. T. Sekula J. M. Williams

Stability in a superconducting magnet refers to its ability to resist quenching induced by "fluctuations" (such as current changes) at currents appreciably below the critical current, I_c. Serious instability is evidenced by quenching far short of I_c when the current is being increased too rapidly. To enhance their stability, commercial Nb Ti wires utilize multifilamentary construction with a matrix of a good normal conductor, copper, between the alloy filaments. Under neutron irradiation, this stabilizing copper undergoes radiation damage, which increases its resistivity and may therefore decrease its stabilizing effectiveness.

A small solenoid (described earlier[1]) wound with commercial Nb Ti wire was studied under the effects of low-temperature thermal-neutron irradiation in the liquid-helium cryostat at the Bulk Shielding Reactor. Measurements were made both on the magnet's normal resistance (at 10°K, just above the critical temperature) and on its stability at 3.8°K, before and after irradiation and again after a room-temperature anneal. Stability was quantified as the maximum power supply compliance voltage, V_m, which could produce a stable, nonquenched start-up of the magnet from zero to a fixed test current, $I_T < I_c$, set by the power supply current limiter.

The thermal-neutron dose in this study was 1.7×10^{18} neutrons/cm^2, which in bulk pure copper should produce[2] a resistivity rise of 4.2×10^{-9} Ω-cm (corresponding to about 16 displaced atoms per million), of which about 20% should remain after annealing at room temperature. We observed a radiation-induced rise of 23% in the 10°K resistance of the solenoid (which converts to a resistivity increment twice as large as the prediction), and 16% of this remained after anneal. As measured at 3.8°K, the corresponding changes in other properties were as follows: (*a*) the critical current decreased by 1.4% and was unchanged by anneal; (*b*) stability, as measured by the maximum voltage for stable start-up (under the rather stringent criterion of a *fixed* test current 3.6% below the initial I_c), was reduced to 84% of its preirradiation value and returned to 90% upon anneal. Under a less stringent criterion of a *variable* test current set at 3.6% below the *prevailing* I_c, the stability showed only barely measurable changes: 3% loss and complete recovery.

In view of the rather high initial room-temperature resistivity calculated for the copper and its very low resistivity ratio ($R_{293°K}/R_{10°K} = 48$), both of which suggest influences of impurities, cold work, and electrical size effect, it is to be expected, as observed, that the radiation-induced resistivity changes would be greater than predicted for pure bulk copper. The observed changes in stability definitely show a real and permanent decrease induced by radiation damage.

---

1. C. E. Klabunde, S. T. Sekula, and J. M. Williams, *Solid State Div. Annu. Prog. Rep. Dec. 31, 1974*, ORNL-5028, p. 47.
2. R. R. Coltman, Jr., C. E. Klabunde, and J. K. Redman, *Phys. Rev.* 156, 715 (1967).

X-RAY DIFFRACTION AND ELECTRON MICROSCOPY

NUMERICAL CALCULATIONS OF DIFFUSE SCATTERING FROM DISLOCATION LOOPS IN METALS

Bennett C. Larson[1] H. Trinkaus[2]

The application of x-ray scattering to the study[3] of radiation damage in metals depends on an accurate knowledge of the diffuse scattering cross sections for dislocation loops. The high-intensity Huang scattering that lies closest to Bragg reflections can be dealt with largely on an analytical basis with only a minimum of numerical calculations required. However, the cross sections for the large-angle Stokes-Wilson region must be accurately known also in order to carry out loop size distributions and concentration analyses. The scattering in these tails arises mainly from the highly distorted regions close to the dislocation loop where the lattice distortions can only be specified in a numerical form, and therefore the scattering contributions from these regions must be calculated numerically.

Numerical displacement field data[4] appropriate for an edge dislocation loop in an isotropic medium have been used to calculate diffuse scattering cross sections in the Stokes-Wilson region for various loop orientations and reciprocal lattice vectors. The scattering patterns were found to be quite complicated in this region, as could be expected from the anisotropy of the distortions around the loops. However, an understanding of the important characteristics of the scattering was achieved by relating the observed structure to that expected under the conditions of localized Bragg reflections from the highly strained regions near the loop. Analytical models for the strain were used in these comparisons, and the results proved to be particularly useful in interpreting the details of specific calculations. As an example, the scattering pattern around the 222 reflection for a 50-Å loop on a (111) plane is plotted in the form of isointensity curves in Fig. 3.12. The dotted lines correspond to the position where the scattering amplitudes change sign and therefore denote lines of zero intensity. The scattering patterns closest to the reciprocal lattice point are similar to Huang scattering contours and indeed can be understood as the continuation of the Huang scattering profiles into the Stokes-Wilson region. The most significant feature of the scattering pattern is the presence of the single satellite peak that appears at a distance of $qR \approx 3$ above the reciprocal lattice point; q is a distance in reciprocal space, and R is the loop radius. In contrast to the large number of oscillations (or satellite peaks) typical for the scattering from spherical precipitates, the presence of only a single peak here is a result of the nearly constant strain throughout the highly deformed region close to the dislocation loop. That is, the position of this peak relative to the Bragg peak corresponds to that expected for local Bragg reflection from the region near the loop, remembering that the local lattice parameter will be altered as a result of the strain generated by the loop.

The importance of these observations in connection with the analysis of diffuse scattering measurements can be demonstrated with the help of Fig. 3.13. In this plot, the intensities (multiplied by q^2 for ease of plotting) for directions parallel and antiparallel to the 222 reciprocal lattice vector are shown. In this case, loops on all equivalent {111} planes are considered, as required for actual defect systems in cubic-symmetry crystals, and therefore the oscillations as observed in Fig. 3.12 are smeared out, and no zero points occur. However, a pronounced shoulder does appear at $qR \approx 3$ in the upper curve, which is a result of the satellite peak observed at the same position in Fig. 3.12. This is in contrast to a smooth intensity falloff with the slope of the solid line which would be predicted by the analytical approximations that are normally used. Shoulders such as this have recently been observed[5] in

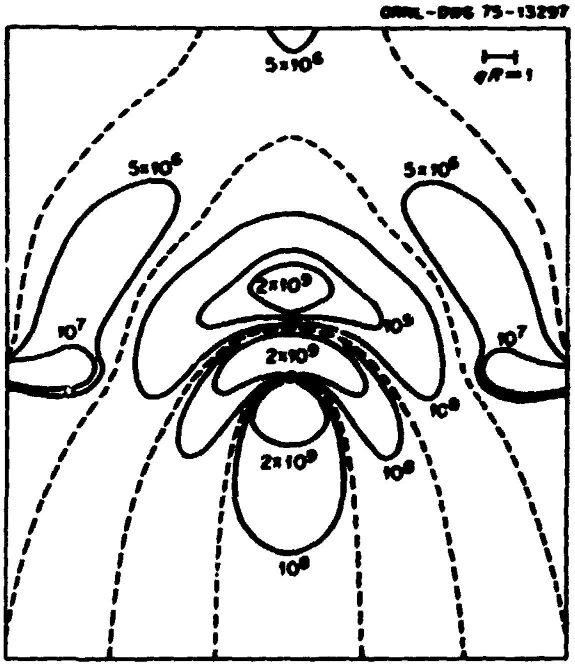

Fig. 3.12. Diffuse scattering contours near the 222 reciprocal lattice point (filled circle) for a 50-Å-radius loop on a (111) plane. The [222] direction is vertical in this figure.

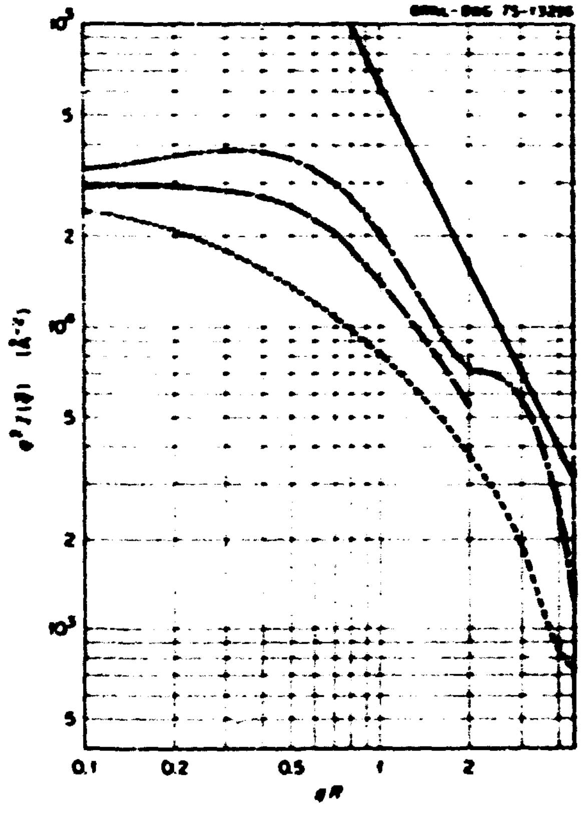

Fig. 3.13. Diffuse scattering from loops for q parallel (upper) and q antiparallel (lower) to the 222 reciprocal lattice vector plotted as a function of qR. The middle curve is the symmetric part of the intensity.

experimental diffuse scattering measurements on electron-irradiated copper and until now have precluded a detailed analysis of the data and tend to emphasize the need for detailed calculations.

Further calculations have been carried out for other dislocation loop and scattering geometries, and analytical strain models have been employed to predict the characteristics of the scattering patterns for the various configurations.

---

[1] The author carried out this research while on foreign assignment at Institut für Festkörperforschung, KFA Jülich, Germany.

[2] Institut für Festkörperforschung, KFA Jülich, Germany.

[3] Bennett C. Larson, *J. Appl. Crystallogr.* 8, 150 (1975).

[4] S. M. Ohr, *J. Appl. Phys.* 43, 1361 (1972).

[5] P. Ehrhart, *Fundamental Aspects of Radiation Damage in Metals*, ed. by M. T. Robinson and F. W. Young, Jr., ERDA report CONF-751006 (in press).

X-RAY STUDIES OF IRRADIATION-INDUCED DISLOCATION LOOPS IN METALS[1]

Bennett C. Larson

Theoretical and experimental progress has resulted in the increased use of x rays for the study of defects and defect clusters in crystals. In this paper an outline of the theoretical framework associated with Huang, Stokes-Wilson, and integral diffuse scattering from dislocation loops is presented, and an account of recent experiments on radiation-induced loops is given. These studies include low-temperature, ambient-temperature, and elevated-temperature irradiations of metals with electrons, neutrons, and accelerated ions and pertain to the study of the thermal annealing characteristics as well as the as-produced damage structure. The information obtained by x rays as to the type, size, and concentrations of dislocation loops is contrasted with existing electron microscopy, electrical resistivity, and lattice parameter data in order to establish correlations and identify areas of disagreement.

---

[1] Abstract of paper: *Fundamental Aspects of Radiation Damage in Metals*, ed. by M. T. Robinson and F. W. Young, Jr., ERDA report CONF-751006, Oak Ridge, Tenn. (in press).

X-RAY STUDY OF INTERSTITIAL TRAPPING IN LOW-TEMPERATURE ELECTRON-IRRADIATED Al(0.2 at. %)Ge

Bennett C. Larson[1] H.-G. Haubold[2]

X-ray diffuse scattering has been applied to the study of impurity trapping of interstitials in Al(0.2 at. %)Ge following irradiation with 2 × 10^{18} 3-MeV electrons per square centimeter at 4°K. A high-intensity (100 kW) rotating-anode x-ray generator and a multidetector system developed for the study of self-interstitials in metals[3] was used to measure the low-level diffuse scattering between the Bragg reflections. High-precision measurements of this scattering were carried out after irradiation and after postirradiation anneals to 40, 55, 105, 155, and 195°K, from which the net diffuse scattering could be deduced through comparisons with the scattering present both before irradiation and after annealing to 393°K. Simultaneous measurement of the electrical resistivity changes in a companion specimen provided an additional monitor on the defect system and supplied a direct link to previous studies[4] of interstitial trapping. All of the expected stage II annealing characteristics were observable in the resistivity specimen, and making use of a nearest-neighbor force model to interpret the diffuse scattering, initial results after annealing to 40°K indicated that the interstitials were trapped either as (100) Al-Al dumbbells adjacent to substitutional germanium or as (100) Al Ge dumbbells. The higher temperature anneals indicated that the interstitials remained trapped to 105°K with indications of detrapping and clustering at 155°K and above. Further measurements are currently in progress in order to more precisely specify the defect configurations.

---

[1] The author carried out this research while on foreign assignment at Institut für Festkörperforschung, KFA Jülich, Germany.

[2] Institut für Festkörperforschung, KFA Jülich, Germany.

[3] H.-G. Haubold, *J. Appl. Crystallogr.* 8, 175 (1975).

[4] P. B. Peters and P. E. Shearin, *Phys. Rev.* 174, 691 (1968).

NICKEL-ION DAMAGE IN COPPER AND NIOBIUM[1]

J. B. Roberto J. Narayan

We have used x-ray diffuse scattering to investigate nickel-ion damage in copper and niobium and have correlated the results with transmission electron microscopy measurements in copper. The emphasis of the work has been to develop quantitative techniques for studying ion damage in solids, particularly x-ray diffuse scattering. Three general areas were explored. First, the retained damage from ambient-temperature nickel-ion irradiations in copper and niobium was characterized and compared with comparable-damage-energy fast-neutron irradiations. Second, nickel-ion damage in copper was compared at 4 and 60 MeV to check for a dependence of the damage on incident ion energy. Finally, the applicability of x-ray diffuse scattering techniques to the study of ion-damaged crystals was demonstrated.

In the experiment, single crystals of copper and niobium were irradiated at room temperature with nickel ions to a fluence of 1.2×10^{13} cm^{-2} at 60 MeV, and copper was also irradiated to 5×10^{12} cm^{-2} at 4 MeV. The resulting loop-type defect clusters in the copper samples were characterized using x-ray diffuse scattering and transmission electron microscopy. The TEM measurements were performed using a sectioning technique[2] which allowed viewing the damage in depth profile, while the x-ray measurements were based on a generalization of the integral diffuse scattering technique[3] to take into account the inhomogeneous nature of the depth distribution of ion damage. The defect clusters in niobium were studied using the x-ray method, since the TEM sectioning technique is not applicable to niobium.

Loop size distributions for ion-irradiated copper and niobium as determined by x-ray diffuse scattering are compared in Fig. 3.14. The damage energies are about the same for the two cases, and although the size distributions are somewhat similar, it is obvious that approximately four times fewer defects in loops have survived the ambient-temperature irradiations in niobium than in copper. This reduced defect survivability in niobium has also been observed in TEM measurements in fast-neutron irradiations. In copper, loop size distributions determined by the x-ray and TEM methods were in good absolute agreement and were qualitatively similar to distributions produced using fast neutrons. The nature of the damage in copper was not strongly dependent on ion energy at 4 and 60 MeV. Finally, the results have demonstrated the usefulness of x-ray diffuse scattering for studies of accelerator-damaged crystals.

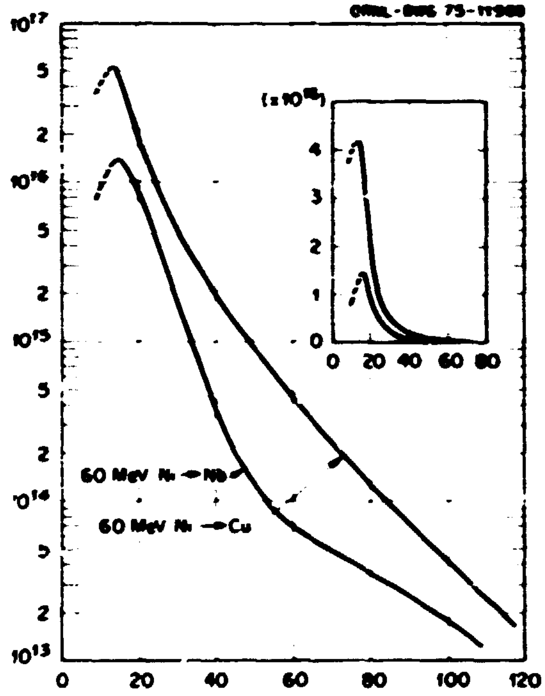

Fig. 3.14. Loop size distributions for copper and niobium irradiated with the same fluence of 60-MeV nickel ions. The distributions were determined by x-ray diffuse scattering and are also plotted linearly in the inset.

---

1. Summary of paper: *Fundamental Aspects of Radiation Damage in Metals*, ed. by M. T. Robinson and F. W. Young, Jr., ERDA report CONF-751006, Oak Ridge, Tenn. (in press).

2. O. S. Oen, J. Narayan, and T. S. Noggle, p. 639 in *Applications of Ion Beams to Metals*, ed. by S. T. Picraux, E. P. EerNisse, and F. L. Vook, Plenum Press, New York, 1974.

3. B. C. Larson, *J. Appl. Crystallogr.* 8, 150 (1975).

15-MeV NEUTRON DAMAGE IN COPPER AND NIOBIUM[1]

J. B. Roberto J. Narayan M. J. Saltmarsh[2]

Recent experimental studies and theoretical calculations have suggested that high-energy neutrons ($E \approx 15$ MeV) are substantially more effective in producing displacement damage than fission neutrons. In this work, we have attempted to quantify some of the differences between high-energy- and fission-neutron damage in copper and niobium and to correlate the experimental results with theoretical calculations. The experiments have involved irradiations near room temperature followed by characterization of the retained damage in the resulting loop-type defect clusters. The work also represents the first utilization of high-energy neutrons from the deuteron-breakup or "stripping" reaction to perform radiation damage experiments and provides direct evidence of the usefulness of such neutron sources.

The high-energy neutrons were generated at the Oak Ridge Isochronous Cyclotron by stopping a 40-MeV deuteron beam in a thick beryllium target. The associated deuteron-breakup (*d,n*) reaction results in a neutron spectrum which is broadly distributed in energy about a maximum at 15 MeV with some neutrons above 30 MeV. This broad energy distribution presents somewhat of an interpretative problem for radiation damage experiments. In particular, the effects of the high-energy tail of the spectrum must be considered. We have approached this problem by computing[3] the displacement damage energy in copper and niobium as a function of incident neutron energy. The damage energy is that part of the primary recoil energy which is ultimately available for producing atomic displacements and is therefore useful for comparing displacement damage at various neutron energies.

The copper and niobium samples were high-purity single-crystal platelets that were essentially perfect from the standpoint of Borrmann topography. High-energy *d*-Be neutron irradiations were carried out in an open-ended aluminum capsule with the samples mounted one behind the other along the beam axis. Nickel and cobalt dosimetry foils were placed before and after the sample capsule, and the neutron fluence decreased 13% from the first to the last sample. The irradiations were carried out at room temperature on a continuous basis over a period of 30 hr with a total-spectrum dose of 2.0×10^{17} neutrons/cm^2 to the center of the first sample. The fission reactor irradiations were performed at the Solid State Division's Bulk Shielding Reactor, with total fluences of 1.0×10^{18} and 5.0×10^{17} neutrons/cm^2 ($E > 0.1$ MeV), respectively, for the copper and niobium samples.

Transmission electron microscopy measurements were carried out on both the copper and niobium crystals to determine the size distributions of the defect clusters which resulted from the irradiations. The defects in the copper crystals were also characterized using x-ray integral diffuse scattering.[4] The results of these measurements in *d*-Be and fission-neutron-irradiated copper are summarized in Figs. 3.15 and 3.16. In Fig. 3.15, bright-field micrographs are shown for fission-neutron and ≈15-MeV damage. Loop size distributions in copper as determined by TEM and x-ray measurements are compared in Fig. 3.16. General similarities between the retained damage from high-energy- and fission-neutron irradiations in copper are apparent from Figs. 3.15 and 3.16, and the results for niobium were comparable.

In order to compare the *d*-Be and fission-neutron damage on an absolute basis, the size distribution curves for copper and niobium were integrated to determine retained point-defect densities. When adjusted for differences in fluence, these point-defect densities give a relative indication of the damage effectiveness of the high-energy and fission neutrons. Ratios of the damage effectiveness of *d*-Be neutrons in terms of fission neutrons as determined both from the experimentally observed point-defect densities and from the theoretical damage energies are compared in Table 3.1. The agreement between theory and experiment is quite remarkable and indicates that the damage effectiveness of a *d*-Be neutron with a mean energy of 15 MeV is about three times that of a fission neutron in copper and niobium. Overall, the results suggest similarities between high-energy- and fission-neutron damage when compared using the damage energy concept and demon-

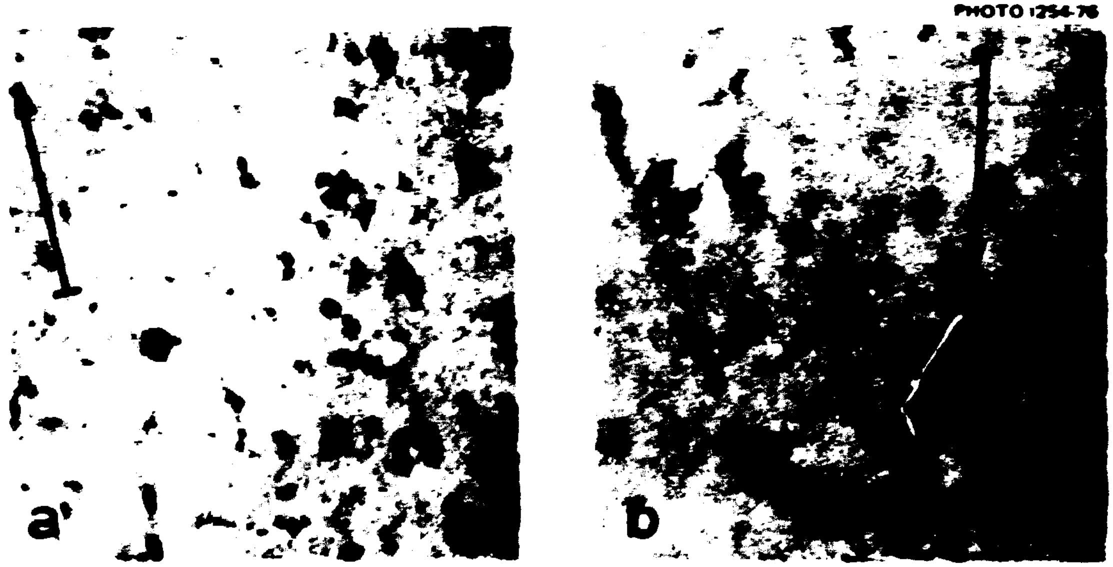

Fig. 3.15. TEM micrographs of copper irradiated with (*a*) fission neutrons and (*b*) ≈15-MeV neutrons. The arrow indicates the diffraction vector [$\bar{2}20$] and corresponds to 0.2 μm.

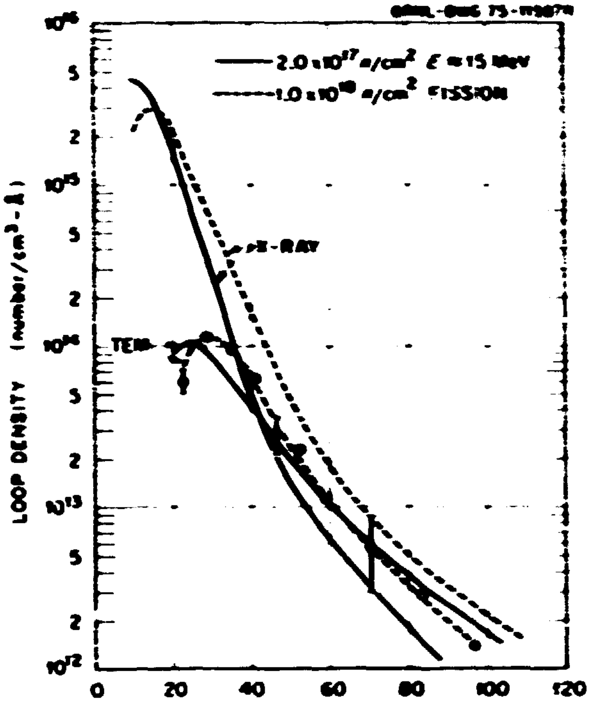

Fig. 3.16. Loop size distributions in copper for fission and ≈15-MeV-neutron irradiations as determined by TEM and x-ray techniques. The x-ray data for fission neutrons are from ref. 4.

Table 3.1. Damage effectiveness of *d*-Be neutrons ($E \approx 15$ MeV) as compared with fission reactor neutrons in copper and niobium

Material	Experimental retained damage, ratio *d*-Be/fission	Theoretical damage energy, ratio *d*-Be/fission
Cu	3.3 (x-ray) 4.0 (TEM)	3.4
Nb	2.5 (TEM)	3.1

strate the usefulness of deuteron-breakup neutron sources for performing high-energy neutron damage experiments.

THE CHARACTERISTICS OF 15-MeV- AND FISSION-NEUTRON DAMAGE IN NIOBIUM[1]

J. Narayan   S. M. Ohr

The nature of defect clusters produced by 15-MeV and fission neutrons at 30°C has been studied by transmission electron microscopy in high-purity single crystals of niobium. The high-energy neutrons were generated at the Oak Ridge Isochronous Cyclotron facility by stopping a 40-MeV deuteron beam in a thick beryllium target.[2] The low-energy neutron irradiations were performed at the Oak Ridge Bulk Shielding Reactor, where the neutron spectrum is similar to the ^{235}U fission spectrum. The fluence of 15-MeV neutrons was 1.8×10^{17} neutrons/cm^2, and the fluence of the fission neutrons was chosen at 5×10^{17} neutrons/cm^2, so that samples from both types of irradiations had approximately the same damage energy.

Figure 3.17 shows electron micrographs of defect clusters observed in the 15-MeV- and fission-neutron-irradiated samples of niobium. The directions of the black-white contrast, which are exhibited by the defect clusters under two-beam dynamical diffraction conditions, indicate that the defect clusters are in the form of dislocation loops and provide information from which the Burgers vectors of the loops can be determined. A recent calculation has shown that the black-white direction is a sensitive function of the directions of the Burgers vector, loop normal, and diffraction vector.[3] By applying the results of this calculation, it was found that in niobium irradiated with 15-MeV and fission neutrons, approximately two-thirds of the observed loops were of perfect $a/2\langle 111\rangle$ type, while the rest of the loops were of faulted $a/2\langle 110\rangle$ type. The foil orientations were such that it was not possible to rule out completely the possible presence of the loops of $a\langle 100\rangle$ type.

The vacancy-interstitial nature of the dislocation loops was determined from the direction of the black-white contrast and the measured depth of the loops in the foils. In niobium, approximately two-thirds of the loops were of interstitial type and one-third were of vacancy type in both the 15-MeV- and fission-neutron-irradiated samples.

It has been reported[4] that 15-MeV neutrons produce many multiple clusters in which two or more vacancy loops are separated by less than 100 Å. The incidence of multiple clusters was studied by observing the spatial distribution of vacancy loops by weak-beam and high-order bright-field stereomicroscopy techniques. The results for the 15-MeV-irradiated specimens showed

---

[1] Summary of paper *Radiation Effects and Tritium Technology for Fusion Reactors*, ed. by F. W. Wiffen and J. S. Watson, ERDA report CONF-750989, Oak Ridge, Tenn. (in press).

[2] Physics Division, ORNL.

[3] J. B. Roberto and M. T. Robinson, "The Energy Dependence of Neutron Damage in Copper and Niobium," this report.

[4] B. C. Larson, *J. Appl. Crystallogr.* 8, 150 (1975).

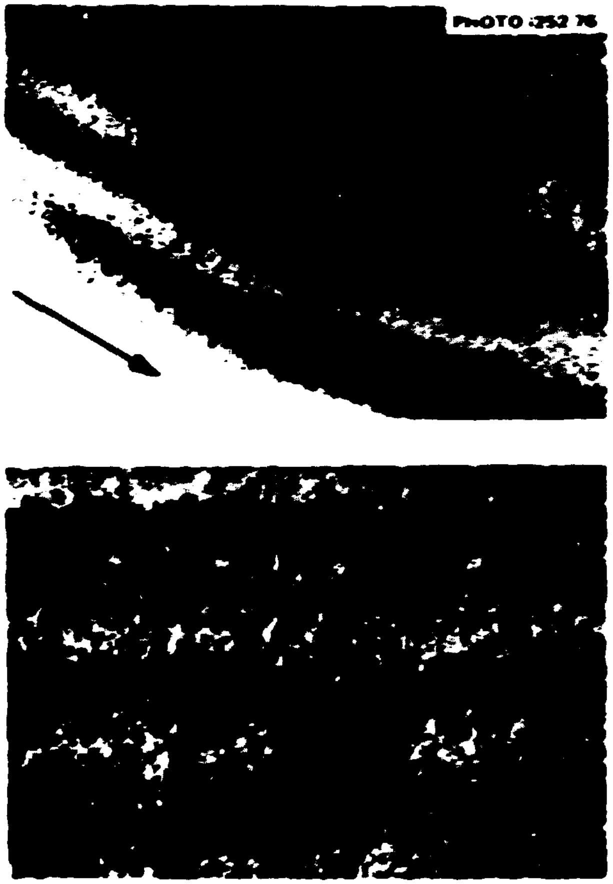

Fig. 3.17. 15-MeV (upper) and fission (lower) neutron damage, imaged under two-beam dynamical diffraction conditions. The direction of the arrow in each micrograph indicates the [1$\bar{1}$0] diffraction vector, and the length of each arrow is 0.2 μm.

that about 2% of the loops were in multiple clusters, and about 0.2% of such incidences were observed in fission-neutron-irradiated samples. The fission-neutron result is consistent with coincidences in a random distribution, and the 15-MeV-neutron result, while apparently larger, is much less than that previously reported.[4] It is believed that this result does not indicate a significant difference between 15-MeV- and fission-neutron damage.

The main conclusion which can be drawn from the present study is that the nature of the 15-MeV-neutron damage is similar to that of the fission-neutron damage. One can, therefore, infer from this observation that the clustering behavior of point defects is nearly independent of the energy of incident neutrons.

[2] J. B. Roberto, J. Narayan, and M. J. Saltmarsh, *Radiation Effects and Tritium Technology for Fusion Reactors*, ed. by F. W. Wiffen and J. S. Watson, ERDA report CONF-750989, Oak Ridge, Tenn. (in press).

[3] S. M. Ohr, to be published.

[4] J. B. Mitchell, R. A. Van Konynenburg, M. W. Guinan, and C. J. Echer, *Philos. Mag.* 31, 919 (1975).

X-RAY AND ELECTRON MICROSCOPE STUDY OF DEFECT CLUSTERS IN SELF-ION-IRRADIATED NICKEL

J. Narayan   Bennett C. Larson

Defect clusters produced by 4-MeV nickel ions in nickel single crystals at room temperature have been studied as a function of depth by transmission electron microscopy (TEM). Size distributions (loop density vs size) at various depths have been determined and compared with the distribution determined by integral

---

[1] Summary of paper to be published.

x-ray diffuse scattering. In the x-ray study, the inhomogeneous nature of the depth distribution of damage has been treated approximately by computing an effective absorption factor based on the total path length of the x rays as a function of depth.[1]

Figure 3.18 shows initial information on the size distributions from nickel-irradiated crystals that were irradiated to fluences of 2.5×10^{13} ions/cm^2 and 5.0×10^{13} ions/cm^2 as obtained from both x-ray and TEM measurements. In sizes above 30 Å (radius) there is good agreement between the two measuring techniques; however, at the smaller sizes there is rather sharp disagreement, and this point is being investigated further. These measurements indicate that only about 1% of the defects generated survive in the form of dislocation loops, which is about a factor of 5 lower than the survival observed in room-temperature nickel-ion-irradiated copper. A study of annealing of defects is in progress to get information concerning migration energies of defects in the various annealing stages (III through V).

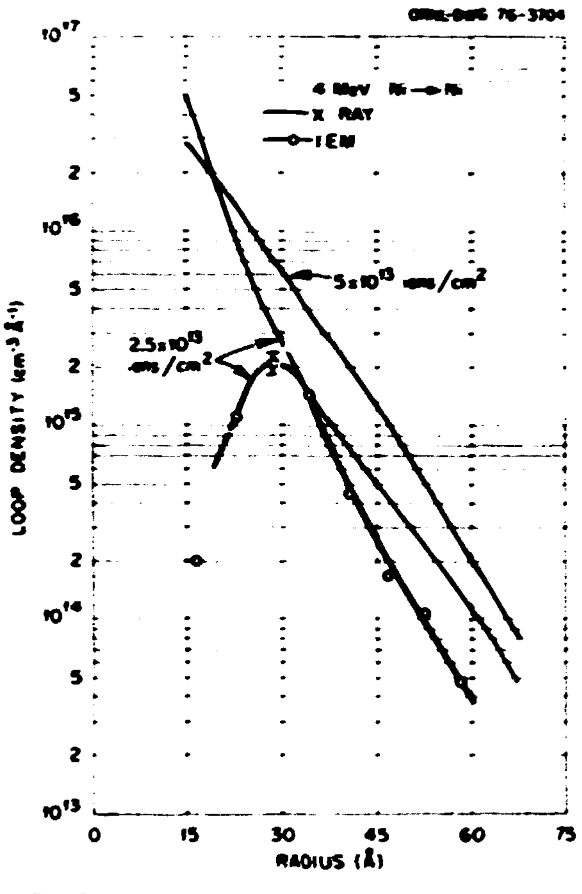

Fig. 3.18. Size distribution of dislocation loops in nickel irradiated with 4-MeV nickel ions for fluences of 2.5 and 5.0 × 10^{13} ions/cm^2, determined by x-ray and electron microscope techniques.

---

[1] J. B. Roberto and J. Narayan, *Fundamental Aspects of Radiation Damage in Metals*, ed. by M. T. Robinson and F. W. Young, Jr., ERDA report CONF-751006, Oak Ridge, Tenn. (in press).

THE DIRECTION OF BLACK-WHITE CONTRAST OF DISLOCATION LOOPS

S. M. Ohr

When small dislocation loops are examined in the electron microscope, the loops lying approximately within one extinction distance from the surface exhibit black-white contrast under two-beam dynamical diffraction conditions. It has been generally accepted in the past that the direction of the black-white contrast was parallel to the direction of the Burgers vector projected onto the image plane, and this direction has accordingly been employed for the determination of Burgers vectors. In recent years, it was found that the direction of black-white contrast was not always parallel to the projected direction of the Burgers vector.[1] In particular, for loops with shear components it was not known how the black-white direction was related to the directions of Burgers vectors and loop plane normals. In the present study, the displacement field of shear, as well as edge, dislocation loops[2] was used to calculate the dependence of the black-white direction on the directions of the Burgers vector, loop normal, and diffraction vector. The calculation consisted of producing simulated electron micrographs by numerically integrating Howie-Whelan equations of the dynamical theory of electron diffraction.

The results show that the direction of black-white contrast is in general not parallel to the projected direction of the Burgers vector. It is found that the angle α measured from the diffraction vector ($\boldsymbol{g}$) to the black-white direction ($\boldsymbol{l}$) is given by a formula

$$\alpha = \frac{\beta + \gamma}{3} .$$

where β and γ are the angles from the diffraction vector ($\boldsymbol{g}$) to the projected directions of the Burgers vector ($\boldsymbol{b}$) and the loop normal ($\boldsymbol{n}$) respectively. This is shown in Fig. 3.19, where α is plotted against $\beta + \gamma$ for various loop orientations found in copper and niobium. The straight line represents the least-squares fit to the points. The only exception to the rule found is in the

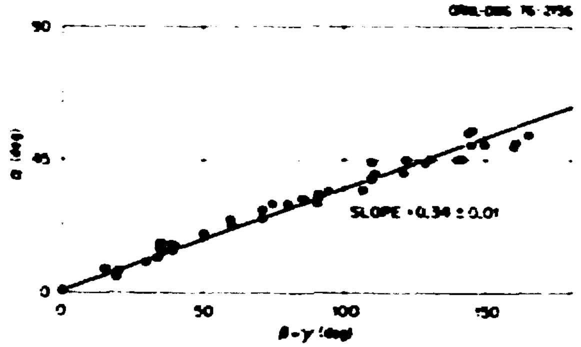

Fig. 3.19. Dependence of the direction of black-white contrast (α) on the directions of the Burgers vector (β) and loop plane normal (γ).

case of $g \cdot b = 0$, that is, when the Burgers vector is parallel to the reflecting plane. In this case, either l is parallel to g or a complex butterfly contrast is expected, depending on the relative orientations of b, n, and g. Preliminary data from neutron-irradiated copper and niobium indicate that the one-third rule is indeed obeyed in many instances and provides experimental support for the theory.

---

1. B. L. Eyre, *Defects in Refractory Metals*, ed. R. DeBatist, J. Nihoul, and L. Stals, S.C.K./C.E.N., Mol, 1972, p. 311.
2. S. M. Ohr, *Philos. Mag.* 26, 1307 (1972).

THE NATURE OF DEFECT CLUSTERS IN ELECTRON-IRRADIATED COPPER[1]

S. M. Ohr[2]

An electron microscope study has been made of the nature of defect clusters observed in electron-irradiated copper annealed in the range of temperatures between stage III and stage V. The sample materials used were (110) single crystals of high-purity copper which were irradiated at 4°K at the 3-MeV Van de Graaff facility of Kernforschungsanlage, Julich. The electron dose was 1.4×10^{19} electrons/cm^2, which resulted in a Frenkel pair density of about 650 ppm. Subsequent to irradiation, samples were annealed for 30 min at a series of temperatures starting just above stage III, namely 23°, 90°, 150°, and 250°C. The latter two temperatures correspond approximately to stages IV and V.

Figure 3.20 shows the electron micrographs taken from samples annealed at each of these annealing temperatures. The damage clusters appearing as black spots were identified as dislocation loops, mostly with Burgers vectors of $a/3\langle 111\rangle$ type. Up to the annealing temperature of 150°C, the size distribution peaks at approximately 35 A in diameter. An increase in the density of the larger loop sizes occurs with increasing annealing temperature, indicating that the smaller loops are coalescing to form larger loops. At 250°C, only about 10% of the loops remain, and their average size has increased by a factor of 2. The density of point defects $C(T_a)$ estimated from the total area of the loops remains essentially constant up to 150°C and decreases by a factor of 2 at 250°C. These results are summarized in Table 3.2.

Table 3.2 also shows the results of the determination of the vacancy-interstitial nature of the loops. Most of the data presented were obtained from the analysis of the black-white contrast under two-beam dynamical diffraction conditions combined with the loop depth measurements by the stereoscopic technique. A small number of large loops, which did not exhibit black-white contrast, were analyzed by the method of inside-outside contrast. The results show that at 23°C (i.e., after stage III annealing), no vacancy loops were found. At the annealing temperatures of 90° and 150°C, approximately 10% of the loops analyzed were of the vacancy type. The fraction of the vacancy-type loops increases to nearly 40% at 250°C, but the concentration of vacancies (C_v) is only slightly higher than that observed at lower temperatures because the total loop density has decreased drastically.

Table 3.2 Density and nature of dislocation loops in electron-irradiated and annealed copper

T_a (°C)	n_{loop} (cm^{-3})	d (A)	$C(T_a)$ (cm^{-3})	n_v/n_{loop} (%)	C_v (cm^{-3})
	$\times 10^{15}$		$\times 10^{18}$		$\times 10^{17}$
23	11.5	41	3.3	<5	<2
90	9.4	46	3.3	12	3.7
150	7.6	48	2.9	11	2.9
250	1.2	95	1.9	37	3.9

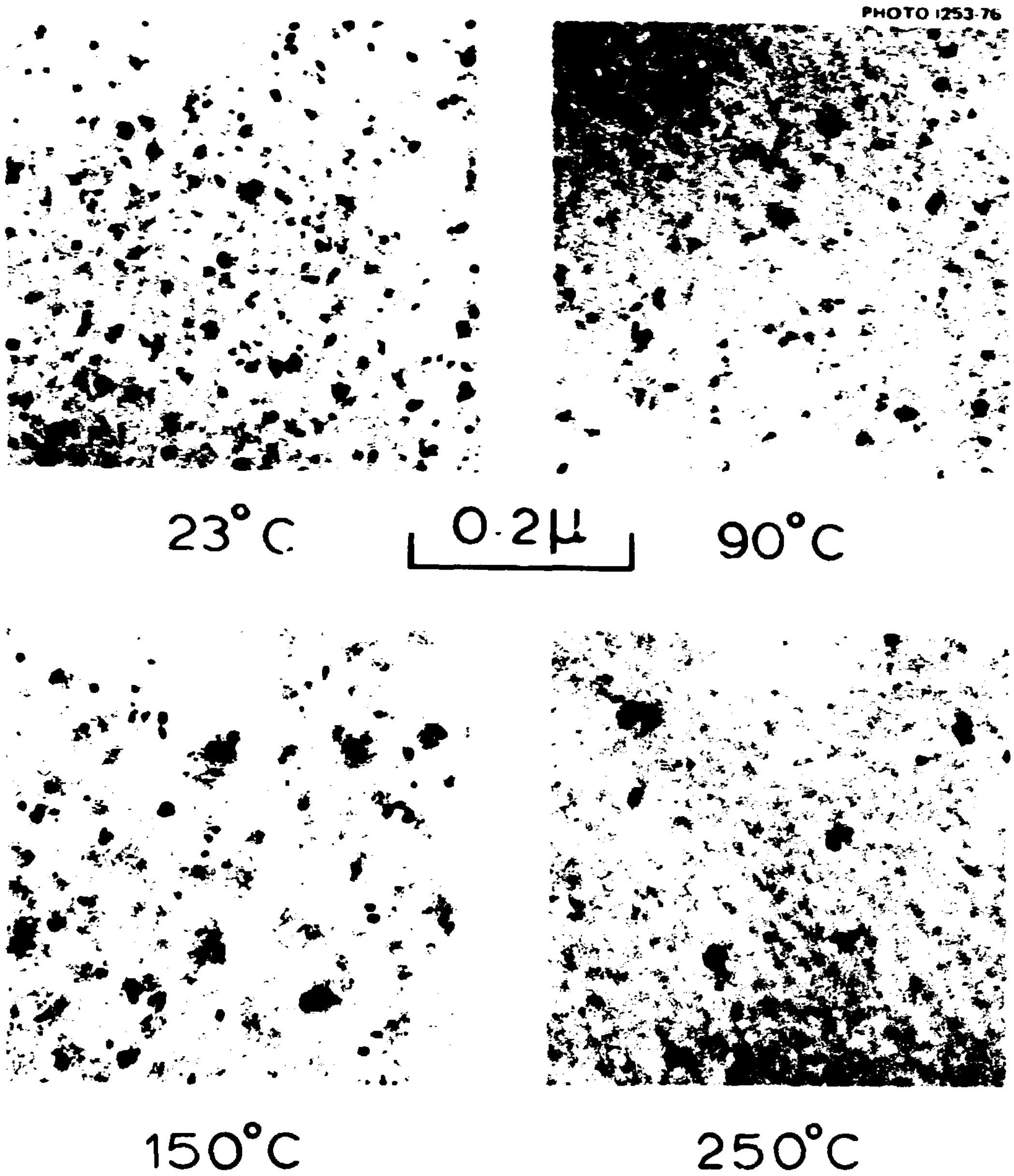

Fig. 3.20. Electron micrographs showing damage clusters observed in copper samples electron-irradiated at 4°K and annealed for 30 min at each of the temperatures indicated.

It is surprising that in samples annealed through stage III, no loops of vacancy type are found. Although this can be interpreted as evidence that vacancies do not migrate in stage III, it is also possible that the vacancies do migrate and cluster during stage III but that the clusters are too small to be visible in the electron microscope. Since the smallest loops analyzed are about 15 Å in diameter, the present work indicates that vacancy clusters containing more than about 35 vacancies in collapsed loops are not present after stage III annealing.

---

1. Summary of paper: *Fundamental Aspects of Radiation Damage in Metals*, ed. by M. T. Robinson and F. W. Young, Jr., ERDA report CONF-751006, Oak Ridge, Tenn. (in press).

2. The author carried out this research while on foreign assignment at Institut für Festkörperforschung, KFA Jülich, Germany, and Institut für Physik, Max-Planck-Institut für Metallforschung, Stuttgart, Germany.

DISLOCATION CHANNELING IN MOLYBDENUM

J. Narayan

In situ deformation studies in the electron microscope have been completed on irradiated and quenched fcc materials and extended to the study of irradiated molybdenum (bcc material).

The development of dislocation channels has been studied from the initiation of a channel due to the passage of a single dislocation to broad channels created by large numbers of dislocations. These observations have shown that dislocations clear the visible radiation damage from a region wider than can be accounted for by "cutting" mechanisms and that the passage of *subsequent* dislocations of the same Burgers vector progressively widens the channel. Evidence for prismatic glide of dislocation loops has been obtained from observations of loop coalescence at the channel margins. Observations of channel branching and changing direction due to cross slip have been made in specimens deformed in the bulk and in the microscope. Many of the observed features of the dislocation channeling cannot be adequately explained by previously proposed mechanisms. Possible channel clearing mechanisms involving dislocation-loop interactions have been developed.

4. Neutron Scattering

The neutron scattering programs of the Solid State Division are concerned with obtaining fundamental microscopic information on condensed matter. Such information is essential not only for increasing our knowledge of the solid state sciences but in helping to solve the long-range energy requirements of our country. Almost every energy technology is materials limited, and a better understanding of the physical properties of materials is necessary for the development and characterization of the new materials that will be required.

These programs exploit the neutron beams at the High Flux Isotope Reactor (HFIR) and at the Oak Ridge Research Reactor (ORR). The beams at the HFIR are the most intense thermal-neutron beams for research in the world, and the experimental facilities associated with them provide powerful and, in some cases, unique tools for materials science research. During the past year, it was necessary to remove all the instrumentation from the beam room at the HFIR to facilitate replacement of the beryllium reflector. This replacement was carried out so smoothly and efficiently that the instruments have been installed again much sooner than anticipated. With the reinstallation of the equipment, an exchange of facilities has been effected with the Chemistry Division, which will add to the strength and versatility of the overall program. The HB-2 instrument has now been converted for use as a triple-axis spectrometer with incident neutrons of variable energy. The spectrum of neutrons available at this beam port is peaked at higher energies and with greater intensity than those of the other beam holes and will permit a number of high-energy-transfer experiments to be performed which would be difficult or impossible to carry out otherwise. For still higher energy transfers, a prototype pulsed-neutron experiment has been set up for test and evaluation at ORELA. The test equipment is built around a triple-axis spectrometer, formerly used at one of the Hanford reactors, which was given to the Solid State Division. On completion of the tests, the spectrometer will be installed as a satellite instrument at HB-1 of the HFIR and will be dedicated to low-energy high-resolution inelastic scattering experiments. The neutron beams at the ORR are provided with experimental facilities of a specialized nature in order to extend the range of problems and materials that can be investigated by neutron scattering methods.

As in past years, because of the properties peculiar to neutrons which are exploited in scattering experiments, the neutron scattering research of the Division falls generally into the areas of lattice dynamics and the magnetic properties of matter. For convenience, the research results that appear in this section have been divided into these two areas and a third area which concerns critical scattering and phase transitions. Other equally good distributions could be made which would reflect the concentration of the research into specific problem areas. It will be noted that a sizable fraction of the research results of the past year concerns the acquisition of fundamental information that is directly related to energy production, storage, and transport, and this fraction will undoubtedly increase with time. A few examples of the recent investigations are cited in the following paragraphs.

For many years, there has been considerable interest in understanding the origin of superconductivity and the properties of superconducting materials. Several types of neutron scattering experiments have been carried out in order to contribute to that understanding. Neutron inelastic scattering has been used to investigate phonon anomalies in hard superconductors and their relations to the electron–phonon interaction which is believed responsible for superconductivity in these materials. Most recently, the alloy systems Mo–Re and Nb–Zr have been investigated. From the technological side, a knowledge of fluxoid motion and pinning in superconductors is of extreme importance. Experiments initiated last year with the small-angle scattering equipment at the ORR on the fluxoid lattice in niobium have been continued. The results are most encouraging and have shown unambiguously the existence of a mixed-intermediate state in pure niobium. The work will be extended to studies of niobium into which pinning centers have been introduced by controlled methods. Original interest in the organic "good-conductor" TTF-TCNQ was high because it was thought that the compound was a high-temperature superconductor. Recent results indicate that this is not the case, but the compound is still highly interesting because the mechanism of its metal-insulator transition near 50° K is unknown. It has been suggested that the transition is associated with a phonon instability (Kohn anomaly). Neutron inelastic scattering experiments are difficult to perform on TTF-TCNQ because of the complexity of its structure, the small single crystals available, and the large background scattering due to the hydrogen in the compound. Nevertheless, a clear demonstration of the phonon instability has been obtained with a sample consisting of many small crystals carefully stacked together.

A very important area of solid state physics to which neutron scattering methods can be applied fruitfully is the study of defects. The term is used here in the broadest sense to include any departure from pure and perfect materials. Perturbations of the phonon spectra of pure metals by very light or very heavy impurities and the dynamics of hydrogen in metals are all under study. During the past year, a significant step was achieved toward the goal of understanding the basic physical mechanisms of radiation damage and annealing. Very precise neutron scattering experiments showed clearly the perturbing effects in the phonon spectrum of copper due to defects produced by neutron irradiation at 4.2° K. The experiment itself was a tour-de-force, having been carried out with a combination of techniques, all of which were pushed to the limit.

The distribution of magnetic moment density in magnetic materials gives information directly about the wave functions of the magnetic electrons. It has been known for a long time that an atomic-like model for the magnetic moment density in the ferromagnetic $3d$ metals iron, cobalt, and nickel is adequate to explain many of their properties. A more rigorous confrontation with theory may be expected from studies of the metals scandium and titanium in which the $3d$ electrons are near the bottom of the band. Measurements made of the induced moments in these paramagnetic materials have shown conclusively that the $3d$ density is much more diffuse than that of the heavier atoms and requires a more complete interpretation.

It should be emphasized that the solution to a given problem is sought by all possible means and with all experimental tools available to the Division members. There is a very close and very important interaction between members of the Neutron Scattering Program, the Solid State Theory Program, and the Superconductivity Program. There is an equally close relationship with members of the Research Materials Program who have provided well-characterized single-crystal specimens for many of the neutron scattering investigations reported here.

MAGNETIC PROPERTIES

MOMENT DISTURBANCES IN NICKEL–COPPER ALLOYS[1]

R. A. Medina[2] J. W. Cable

The moment disturbances in $Ni_{1-c}Cu_c$ alloys were measured with the technique of diffuse magnetic scattering of unpolarized neutrons by Cable, Wollan, and Child[3] (c = 0.2) and by Aldred et al.[4] for a range of concentrations. These experiments seem to imply the existence of a uniform moment and/or a local moment on copper atoms totaling −0.1 μ_B over the range 0–40 at. % copper. This is a surprising result because in the same range the average moment changes from 0.616 μ_B to 0.166 μ_B. On the other hand, the result is inconsistent with the diffraction data of Ito and Akimitsu,[5] which show that the uniform moment decreases monotonically with increasing copper content. This inconsistency suggested a new measurement of the moment disturbances with the diffuse scattering of polarized neutrons, which gives more easily interpretable results.

The experiments were carried out at the polarized neutron facility at the HFIR using polycrystalline ^{62}Ni–Cu samples of concentrations 20, 30, and 53.5 at. % copper. The experiment yields directly both the short-range order-scattering function $S(K)$ and the Fourier transform of the impurity-induced moment disturbance $M(K)$. We have fitted $M(K)/f(K)$ [where $f(K)$ is the nickel form factor] with an expression of the form

$$M(K)/f(K) = \Delta\langle\mu\rangle + \Sigma_\lambda Z_\lambda \gamma_\lambda j_0(KR_\lambda) \, ,$$

where Z_λ is the coordination number and γ_λ is the moment disturbance of the λth shell. The average moment difference $\Delta\langle\mu\rangle = \langle\mu_{Ni}\rangle - \langle\mu_{Cu}\rangle$ was obtained from the fitting. We have also fitted $M(K)/[f(K)S(K)]$ with a similar expression for obtaining the extrapolated value to $K = 0$. The results of those fittings are shown in Table 4.1, and the data are presented in Fig. 4.1. The arrows in Fig. 4.1 stand for the values of $d\langle\mu\rangle/dc$ obtained from the magnetization data. The error quoted for $\langle\mu_{Ni}\rangle - \langle\mu_{Cu}\rangle$ is the statistical error from the fitting. An uncertainty in the multiple-scattering correction of about 0.015 μ_B should be added to this error. Our data are clearly consistent with the assumption that the copper atoms have no moment. The $\Delta\langle\mu\rangle$ values we have obtained are smaller than those obtained with the unpolarized neutron experiment. For example, at 20% copper we obtain $\Delta\langle\mu\rangle$ = 0.478 μ_B compared with the previous result[3,4] of 0.60 μ_B. A large part of this discrepancy comes from an improper spherical average approximation in the earlier analyses. The good agreement between $M(0)/S(0)$ and the derivative of the average moment shows that the moments are determined by their local environment. This implies that the uniform moment is associated with the nickel atoms.

Table 4.1. Comparison of moments and derivatives from neutron and magnetization data

[illegible]	[illegible]	[illegible]	[illegible]	[illegible]	[illegible]
[illegible]	0.478(5)	[illegible]	[illegible]	[illegible]	[illegible]
[illegible]	[illegible]	[illegible]	[illegible]	[illegible]	[illegible]
0.535	[illegible]	[illegible]	[illegible]	[illegible]	[illegible]

---

[1] Summary of paper: *AIP Conf. Proc.* (in press).

[2] ORAU graduate participant from Georgia Institute of Technology, Atlanta, Ga.

[3] J. W. Cable, E. O. Wollan, and H. R. Child, *Phys. Rev. Lett.* **22**, 1256 (1969).

[4] A. T. Aldred, B. D. Rainford, T. J. Hicks, and J. S. Kouvel, *Phys. Rev. B* **7**, 218 (1973).

[5] Y. Ito and J. Akimitsu, *J. Phys. Soc. Japan* **35**, 1000 (1973).

NONLINEAR AND NONLOCAL MOMENT DISTURBANCE EFFECTS IN NICKEL–CHROMIUM ALLOYS[1]

J. W. Cable R. A. Medina[2]

We have made polarized-neutron diffuse-scattering measurements on nickel-rich nickel chromium alloys to determine the magnetic moment distribution on an atomic scale. In contrast to previous unpolarized neutron measurements, these measurements select only those fluctuations at one site correlated with the presence of an impurity at another site. The polarized measurement is therefore intrinsically linear in the impurity site occupation. Comparison of the polarized and unpolarized results shows that nonlinear effects are important for this system and therefore that both measurements are required to describe the spatial moment distribution away from the dilute impurity region. The total moment disturbance per impurity, obtained by fitting the polarized neutron data to the local environment model, decreases rapidly over the concentration region for which $d\bar{\mu}/dc$ from magnetization data remains constant. We conclude that the impurity-induced moment disturbance has two components: a local environment effect, which we detect

ORNL-DWG 75-15845

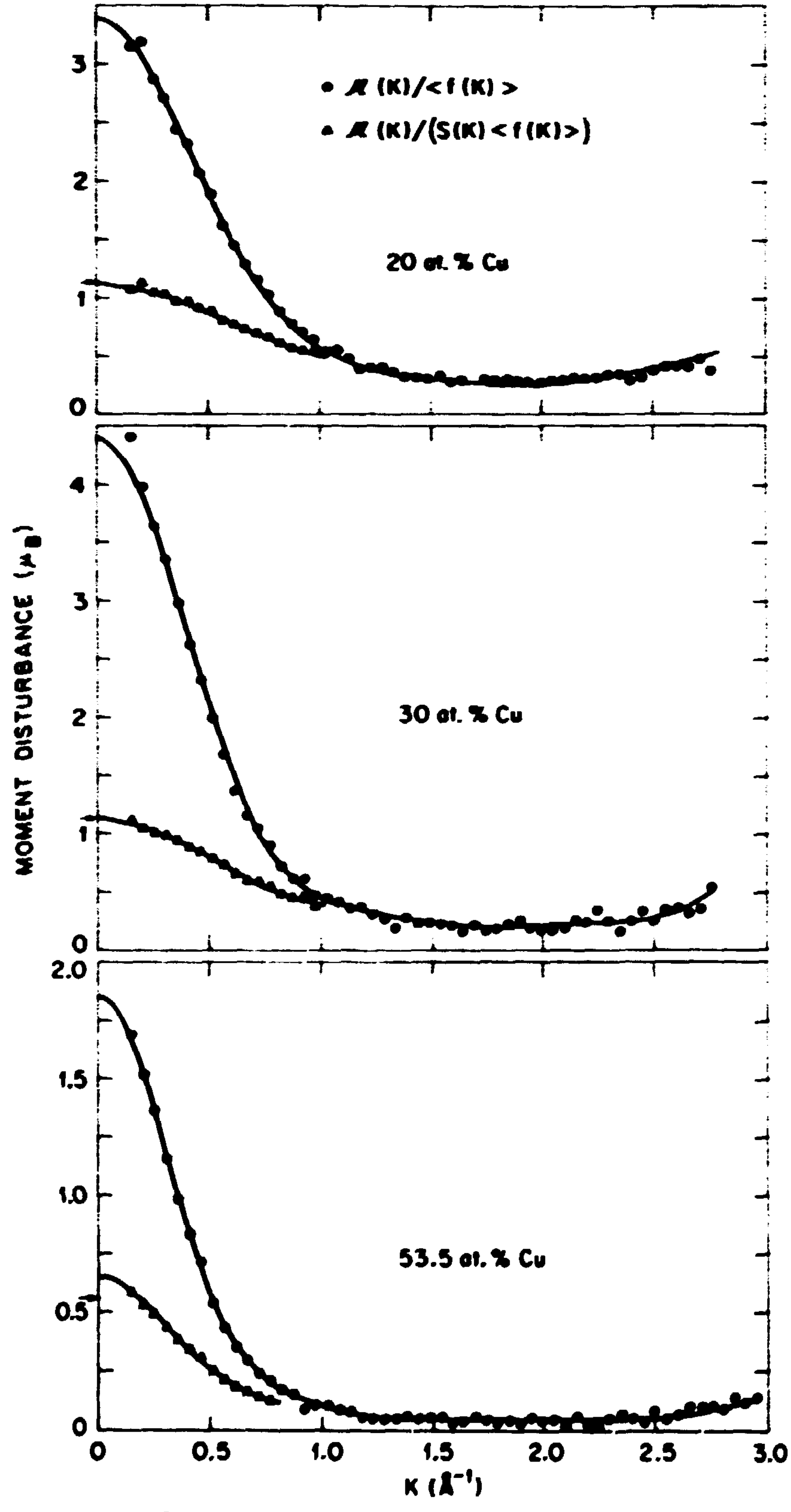

Fig. 4.1. Moment disturbances of nickel–copper alloys.

with neutrons, and a nonlocal effect with range ≥12.5 Å which remains undetected in the neutron experiment. We propose a charge transfer model that contains both the nonlinear and nonlocal effects.

---

1. Abstract of paper to be published.
2. IVIC graduate participant from Georgia Institute of Technology, Atlanta, Ga.

THE ANALYSIS OF MAGNETIC NEUTRON SCATTERING DATA[1]

G. Felcher[2]　J. W. Cable
J. W. Garland[3]　R. Medina[4]

The determination of the proper magnetic form factors for use in the analysis of diffuse-scattering data is discussed, and that information which is immediately available from such data is considered. Apparent discrepancies between the results of diffuse-scattering and diffraction experiments on ferromagnetic nickel copper alloys are resolved. It is shown that the data indicate that the negative spin density usually attributed to conduction electrons instead arises largely from the overlap of localized wave functions, as was first suggested by Moon.

---

1. Abstract of paper to be published.
2. Argonne National Laboratory, Argonne, Ill.
3. Summer research participant from University of Illinois at Chicago Circle, Chicago, Ill.
4. IVIC graduate participant from Georgia Institute of Technology, Atlanta, Ga.

TEMPERATURE DEPENDENCE OF THE MAGNETIC MOMENT DISTRIBUTION AROUND IMPURITIES IN IRON[1]

H. R. Child　J. W. Cable

We have made neutron diffuse-scattering measurements of the magnetic moment distribution around impurities in iron as a function of temperature in an attempt to obtain information regarding the range of the exchange interactions. The measurements were made on iron-based alloys containing 2–3 at. % Si, Ge, Ti, V, Mn, Co, and Ni at temperatures ranging from 300 to 800°K. The FeTi, FeV, FeCo, and FeNi cross sections show very little temperature dependence, while the FeSi, FeGe, and FeMn show pronounced thermal effects. This observation can be explained by a nearest-neighbor molecular-field model by assuming that the impurity-host to host-host exchange ratio is near unity for Ti, V, Co, and Ni impurities and small for Mn impurities, an assumption that is supported by T_C-vs-c data. Furthermore, the observed temperature dependencies for FeSi, FeGe, and FeMn are described reasonably well by this model provided that the low-temperature moment distributions are included in the calculation. We conclude that the magnetic moment of an iron atom depends on its local chemical environment and on its local magnetic environment. We attribute the latter to nearest-neighbor exchange interactions.

---

1. Abstract of paper: *Phys. Rev. B* 13, 227 (1976).

LOCAL ENVIRONMENT EFFECTS IN hcp COBALT-BASED ALLOYS[1]

J. W. Cable　H. R. Child

Polarized-neutron diffuse-scattering measurements were made to determine the magnetic moment distribution in hcp cobalt-based alloys containing 5 at. % V, Cr, Mn, and Ni. The impurity moments determined are 0.18 ± 0.20 μ_B per vanadium, 0.86 ± 0.57 μ_B per chromium, 0.52 ± 0.09 μ_B per manganese, and 0.68 ± 0.10 μ_B per nickel. The cobalt moment in the cobalt nickel alloy is the same as in pure cobalt but varies with local environment for the other alloys. The magnitude and range of the impurity-induced moment reduction at cobalt sites increases with increasing charge contrast. This suggests that charge transfer is an important factor in these local environment effects.

---

1. Abstract of paper to be published.

FIELD-INDUCED PARAMAGNETIC FORM FACTOR OF METALLIC SCANDIUM[1]

W. C. Koehler　R. M. Moon

Our interest in scandium is partly due to an earlier study of the form factor of gadolinium,[2] in which it was found that the total experimental form factor could be separated into a localized component, derived from the 4*f* spin density, and a diffuse component that was attributed to spin polarization of the conduction electrons. In gadolinium it was very difficult to measure the diffuse component with accuracy because of the presence of the much larger 4*f* component. In scandium we have a system with the same crystal structure as gadolinium and a similar outer electron configuration [$nd^1,(n+1)s^2$] for the free atom, but without the large

4f contribution. By applying a large magnetic field, it is possible to induce a small moment in scandium and to observe the spatial distribution of this moment by the polarized neutron technique. It is also of interest to compare the scandium form factor with results obtained for other members of the *3d* transition series. For all the members of this series studied to date (vanadium through nickel), the observed form factors are remarkably like those calculated for the *3d* electrons in the free atoms. We will show that scandium represents a definite departure from this behavior — the observed spin density is much more expanded than that calculated for the *3d* electron in the free atom.

The results reported here were obtained from a specimen cut from a crystal of exceptionally high purity, which was produced at Ames Laboratory.[3] These measurements are a repetition and extension of earlier experiments[4] performed on a sample of lower purity. Our measurements were made in a magnetic field of 57.2 kOe and at a temperature of 100°K. Under these conditions the induced moment is 3.71×10^{-3} Bohr magnetons per atom.

The measurements consist of observing the change in Bragg peak intensities when the direction of the neutron polarization is reversed. Under the experimental conditions, this change in intensity is typically several parts in 10^4, and we have made the measurements with statistical accuracies of about seven parts in 10^5. The ratio of intensities for the two neutron-spin directions is related to the magnetic scattering amplitude $p(\tau)$ by the equation

$$R = 1 + 4p(\tau)/b\,. \tag{1}$$

where τ is a reciprocal lattice vector and b is the nuclear scattering amplitude. The quantity p is proportional to the Fourier coefficient associated with τ in a series expansion of the periodic magnetic moment density.

The crystal was distorted to reduce extinction effects, and measurements on each peak were performed at several wavelengths, selected to minimize the number of simultaneous Bragg reflections. Corrections were applied to the data to account for imperfect beam polarization, for the neutron-spin – neutron-orbit scattering, and for nuclear polarization. These corrections are easily calculated and are quite small. Approximate corrections to account for the induced diamagnetic moment have also been calculated[5] based on a free-atom $3d^2 4s^1$ configuration.

The results are summarized in Fig. 4.2, where the experimental flipping ratios, after correction for the effects mentioned above, have been converted to a form factor by normalization with the appropriately corrected (for diamagnetic and nuclear susceptibilities) experimental susceptibility. This form factor resembles that of the diffuse component obtained for gadolinium in its abrupt drop over the first three reflections; it differs from it in that the form factor at the (102) reflection rises again to a value greater than that at the (101) peak and in that the point at the origin is much larger, relative to the first Bragg peak, in scandium than in gadolinium. The solid line in the figure is a Hartree-Fock free-ion calculation for the spin part of the form factor. Comparison of this curve with the observations shows that, unlike the case of the other *3d* transition metals, the form factor for scandium cannot be interpreted in terms of free-ion form factors. Inclusion of any orbital contribution would make the departure from experiment even greater. A rather good account of the observations has been given, however, by Gupta and Freeman[6] on the basis of APW wave functions determined for metallic scandium. Their results are shown as the solid circles in the figure.

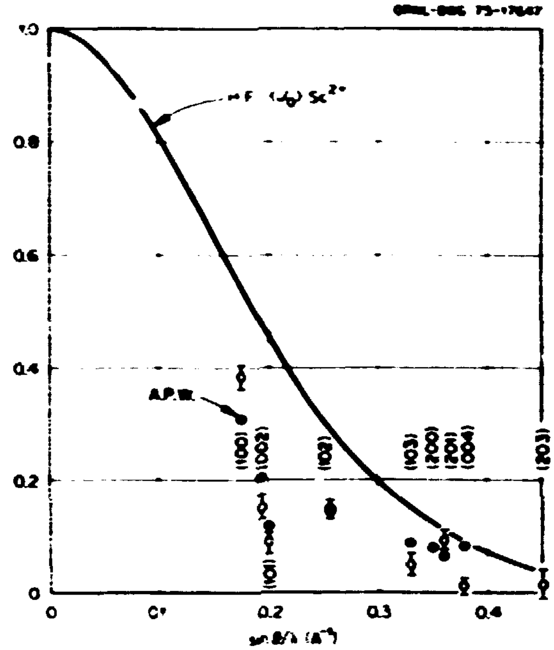

Fig. 4.2. The paramagnetic form factor of metallic scandium. The experimental points, shown as open circles, have been corrected for nuclear polarization, diamagnetism, and neutron-spin – neutron-orbit interaction. The closed circles are from an APW calculation by Gupta and Freeman (ref. 6), and the solid line is a free-ion calculation by Watson and Freeman (ref. 7).

The principal conclusions are that the induced magnetization density in metallic scandium is not like that of a single *3d* electron in atomic scandium and that the

APW calculation of Gupta and Freeman gives reasonably good agreement with our results. Based on the temperature dependence of the susceptibility, Spedding and Croat[8] have suggested that scandium behaves as though there were a single localized $3d$ electron. Our results seem inconsistent with this interpretation.

---

1. W. C. Koehler and R. M. Moon, *Phys. Rev. Lett.* 36, 616 (1976).
2. R. M. Moon, W. C. Koehler, J. W. Cable, and H. R. Child, *Phys. Rev. B* 5, 997 (1972).
3. We are grateful to Professor F. H. Spedding for the loan of this crystal.
4. W. C. Koehler and R. M. Moon, *Solid State Div. Annu. Prog. Rep. Dec. 31, 1973*, ORNL-4952, p. 100.
5. C. Stassis, *Phys. Rev. Lett.* 24, 1415 (1970).
6. G. Gupta and A. J. Freeman, *Phys. Rev. Lett.* 36, 613 (1976).
7. R. E. Watson and A. J. Freeman, *Acta Cryst.* 14, 27 (1961)
8. F. H. Spedding and J. J. Croat, *J. Chem. Phys.* 58, 5514 (1973).

FIELD-INDUCED PARAMAGNETIC FORM FACTOR IN METALLIC TITANIUM[1]

W. C. Koehler J. W. Cable

Polarized neutron diffractometry has been carried out on a specimen of metallic titanium at 100°K in an applied field of 57.2 kOe. Under these conditions a readily observable magnetic moment of 1.36×10^{-3} μ_B per atom is induced in the sample. Polarization ratios of 11 reflections in the $(0kl)$ zone were measured, and a paramagnetic form factor was derived from them. Titanium is the second of the $3d$ transition metals, and its properties are governed by electrons near the bottom of the band. We do not expect, nor do we find, a fit of the data with free-ion Ti^{2+} wave functions even though such divalent ion form factors appear to represent the data from Fe, Co, and Ni, and, surprisingly, from V and Cr. A good fit can be obtained, however, with the neutral atom Ti ($3d^4$) wave functions, which are more extended than those of the divalent ion. This fact is, of course, a fortuitous one. A significant interpretation of the data must await realistic metallic wave functions.

---

1. Abstract of paper to be published.

LIMITATIONS ON THE ACCURACY OF POLARIZED-NEUTRON DIFFRACTOMETRY[1]

R. M. Moon W. C. Koehler
C. G. Shull[2]

The magnetic force on a neutron as it enters a high-field magnet can influence the results of polarized-neutron diffraction experiments. The position of the Bragg peak is slightly different for neutrons in the two spin states, and the peak intensity is slightly different. The magnitudes of these effects are calculated, and experimental evidence confirming the peak shift calculation is presented. Suggestions for experimental procedures to minimize these effects are presented. The discussion is directed toward experiments in which flipping-ratio accuracies approaching 5×10^{-5} are desired.

---

1. Abstract of paper: *Nucl. Instrum. Methods* 129, 515 (1975).
2. Massachusetts Institute of Technology, Cambridge, Mass.

NEUTRON-DIFFRACTION OBSERVATIONS ON THE Cu(Fe) KONDO SYSTEM[1]

M. H. Dickens[2] W. C. Koehler
C. G. Shull[2] R. M. Moon

Polarized-neutron diffraction studies are reported on a series of dilute Cu(Fe) alloys in which the $3d$-electron magnetization induced by an applied magnetic field is sensed in the (111) Bragg reflection. Utilizing the concentration dependence, the isolated-Fe-center magnetization is found to be considerably larger than the total magnetization at temperatures below 10°K. The observations lend support to the development of a Kondo spin-compensated singlet state at low temperature.

---

1. Abstract of paper: *Phys. Rev. Lett.* 35, 595 (1975).
2. Massachusetts Institute of Technology, Cambridge, Mass.

NEUTRON DIFFUSE-SCATTERING STUDY OF CONFIGURATION FLUCTUATIONS IN CERIUM–THORIUM AND $CeAl_3$[1]

A. S. Edelstein[2] H. R. Child

Configuration fluctuation systems in which atoms exist an appreciable fraction of time in more than one electronic configuration have been postulated as the explanation of the collapsed phase of some solids. For example, x-ray photoemission measurements[3] have determined the fractional occupancy of the $4f^5$ and $4f^6$ configurations in anion-substituted SmS under pressure. It has been proposed that αCe, $CeAl_3$, and the α phase of cerium thorium alloys represent examples of such systems, and we have investigated the latter two of these by neutron scattering methods in the past year.

Two double-axis spectrometers, one with $\lambda = 1.005$ Å and the other with $\lambda = 4.4$ Å, at the Oak Ridge

Research Reactor were employed for quasi-elastic measurements in which we detect neutrons of all energies scattered at a fixed scattering angle 2θ. The observed cross section is

$$\frac{d\sigma}{d\Omega} = \int_{-\infty}^{\omega_0} \frac{d^2\sigma}{d\Omega\, d\omega}\, d\omega$$

in which the integral is taken at fixed 2θ. $\hbar\omega_0$ is the incident neutron energy, and $d^2\sigma/d\Omega\, d\omega$ is the diffuse cross section per unit solid angle $d\Omega$ and per unit energy lost by the neutron. The momentum transfer $\hbar Q$ is not precisely determined, but if $|\omega/\omega_0|$ is small, Q is still approximately given by the elastic result $Q = 4\pi(\sin\theta)/\lambda$ for small θ. We interpret our data in this approximation for $d\sigma/d\Omega$ assuming that $\hbar\omega_0 >> |E_\lambda - E_{\lambda'}|$ for all eigenstates E_λ and $E_{\lambda'}$ in the ground state J manifold. For a polycrystalline sample containing uncorrelated spins, one has

$$\frac{d\sigma}{d\Omega} = \frac{2}{3} p_0^2 \int_{-\infty}^{\omega_0} \frac{k'}{k} g^2 \sum_{\lambda,\lambda',\alpha} P_\lambda F^2(Q) \times \langle\lambda|J^\alpha|\lambda'\rangle\langle\lambda'|J^\alpha|\lambda\rangle\,\delta(\hbar\omega + E_\lambda - E_{\lambda'})\,d\omega ,$$

where P_λ is the probability of the eigenstate λ, and the other symbols have their usual meanings. In the approximation mentioned above, the upper limit of integration can be extended to ∞, which, using the δ function and closure, gives

$$\frac{d\sigma}{d\Omega} = \frac{2}{3} p_0^2 g^2 \sum_{\lambda} P_\lambda F^2(Q)\langle\lambda|J^2|\lambda\rangle .$$

Neglecting conduction electron contributions, we write the localized state $|\lambda\rangle$ as

$$\sum_m a_{\lambda m}|m\rangle + b_\lambda|0\rangle ,$$

where $|0\rangle$ is the localized portion of the $4f^0$ and $|m\rangle$ is the portion of the $4f^1$ configuration with $J_z = m$. Substituting into the above equation yields

$$\frac{d\sigma}{d\Omega} = \frac{2}{3} p_0^2 g^2 J(J+1) F^2(Q)\eta ,$$

where

$$\eta = \sum_{\lambda,m} P_\lambda |a_{\lambda m}|^2$$

is the fractional occupancy of the $4f^1$ configuration. Thus η is determined as the ratio of the observed paramagnetic cross section to $(2/3)p_0^2 g^2 J(J+1)$ if F is independent of η.

Values of $d\sigma/d\Omega$ per cerium atom were measured from $CeAl_3$ for $\lambda = 1$ and 4.4 Å as a function of temperature and compared to the elastic result

$$d\sigma/d\Omega_{el} = 387\, T\chi \propto \mu_{eff}^2$$

for χ measured on the same sample. At 1 Å and small Q $d\sigma/d\Omega$ is approximately equal to $(2/3)p_0^2 g^2 J(J+1) =$ 311 mb, predicted for Ce^{3+} with $J = 5/2$, $g = 6/7$, and decreases only about 10% at 11°K, indicating that $\eta =$ 0.9 to 1.0. The 4.4-Å data show a larger decrease at low temperatures, probably due to crystal field effects[4] since $\hbar\omega_0$ is much smaller at this wavelength and since all crystal field levels may not be excited.

Similar data are shown for $Ce_{0.8}Th_{0.2}$ vs T in Fig. 4.3. In this alloy system, Lawrence, Croft, and Parks[5] have detected the α → γ transition of pure cerium and have inferred that there exists a line of first-order transitions ending in a second-order transition critical point at $x = 0.265$ in the phase diagram of $Ce_{1-x}Th_x$. At $x = 0.2$, they observed the first-order transitions at $T = 140$°K in excellent agreement with our data. The 1-Å data shown are extrapolations to $Q = 0$ and show good agreement with the Ce^{3+} form factor as a function of Q when corrected for the thermal diffuse and nuclear

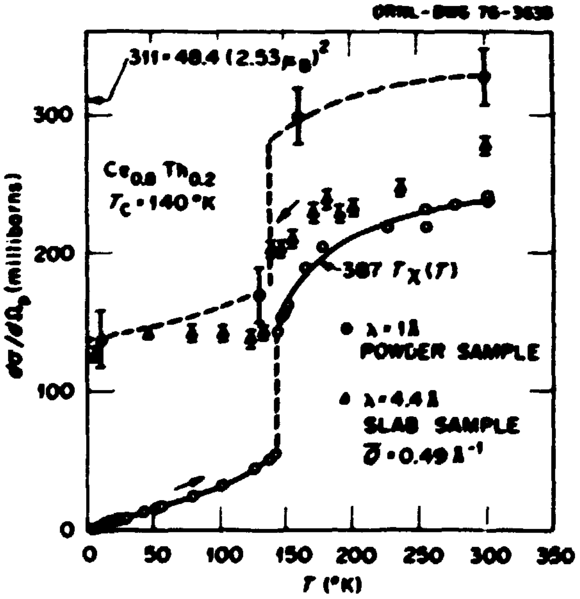

Fig. 4.3. Paramagnetic diffuse cross section (in millibarns per cerium atom per steradian) of $Ce_{0.8}Th_{0.2}$ vs temperature (T).

disorder scattering. As in $CeAl_3$, the 4.4-Å data lie below the 1-Å data, and no evidence for a compensating conduction electron polarization is present. Also shown is the elastic result using χ measured on the same powder sample by Tranchita[6] which, above the transition, can be fit by a Curie Weiss law with $\mu_{eff} = 2.66 \pm 0.2\ \mu_B$ and $\Theta = 132°K$. This Θ value is probably primarily due to a small spin correlation time $\tau \propto \Theta^{-1}$ since it is larger than one would expect from magnetic interactions or from crystal field splitting in this system. Using the fluctuation dissipation theorem and the Kramers Kronig relations, one can show that susceptibility measurements average $\langle J(0)J(t)\rangle$ over a time proportional to T^{-1} so that the susceptibility at low temperatures is determined by both η and τ. In contrast, neutron measurements with energetic neutrons are sensitive only to η provided that τ is large compared to the neutron transit time 10^{-12} to 10^{-13} sec. Therefore, from the 1-Å data, one finds that $\eta \geq 1$ at room temperature and that it decreases 10% above the transition, decreases 40% at the transition, and decreases another 10% at low temperatures. Approximately 0.4 of a localized 4*f* electron remains at 11°K.

---

[1] Summary of paper to be published.

[2] Oak Ridge Associated Universities faculty research participant from University of Illinois at Chicago Circle, Chicago, Ill.

[3] R. A. Pollak, F. Holtzberg, J. L. Freeouf, and D. F. Eastman, *Phys. Rev. Lett.* 33, 820 (1974).

[4] T. Brun, S. Sinha, A. S. Edelstein, R. Majewski, and H. R. Child, *AIP Conf. Proc.* (in press).

[5] J. M. Lawrence, M. C. Croft, and R. D. Parks, *Phys. Rev. Lett.* 35, 289 (1975).

[6] C. Tranchita, private communication.

A STUDY OF THE FREQUENCY-DEPENDENT SUSCEPTIBILITY OF THE COMPOUND $CeAl_3$ BY INELASTIC NEUTRON SCATTERING[1]

T. Brun[2] A. S. Edelstein[3]
S. Sinha[2] R. Majewski[4]
H. R. Child

Using neutron time-of-flight techniques, we measured the Im $\chi(q, \omega)$ for a polycrystalline sample of the compound $CeAl_3$ for $0.5\ Å^{-1} < q < 2.5\ Å^{-1}$. The results are consistent with a crystal field model with the 3/2-level as ground state and the 1/2-level and 5/2-level as first and second excited states. The splitting between the ±3/2- and ±1/2-levels is 5.5 meV. The full widths at half maximum of the quasi-elastic peak at 78, 40, and 7°K are 5, 4, and 2 meV, respectively, and are independent of q. Over the range of q investigated, the amplitude variation is that expected for the form factor of atomic Ce^{3+}. The quasi-elastic peak at 78 and 40°K has contributions from scattering from predominantly the ±3/2- and ±1/2-levels. At 7°K this peak is due only to scattering from the ±3/2-levels. The temperature dependence of the spectra is consistent with a model where the width ΔE of the ±3/2-level is much narrower than that of the ±1/2-level. Susceptibility measurements indicate that χ does not diverge as $T \to 0$. One interpretation is that for $T \to 0$, χ is proportional to the spin correlation time τ. We may have measured this intrinsic spin correlation time ($\tau \approx \hbar/\Delta E$).

---

[1] Abstract of paper: *AIP Conf. Proc.* (in press).

[2] Argonne National Laboratory, Argonne, Ill.

[3] Oak Ridge Associated Universities faculty research participant from University of Illinois at Chicago Circle, Chicago, Ill.

[4] University of Illinois, Chicago, Ill., and Argonne National Laboratory, Argonne, Ill.

POLARIZED NEUTRON STUDY OF CUBIC LAVES PHASE COMPOUNDS RM_2[1]

D. Gignoux[2] F. Givord[3]
D. Givord[3] W. C. Koehler
R. M. Moon

The intermetallic compounds of rare-earth metals R and transition metals M (M = Fe, Co, or Ni) form two groups with widely different magnetic properties, depending upon the concentration of the rare-earth element. In rare-earth-rich alloys the transition metal does not carry a magnetic moment. The magnetic ordering temperatures are low and are determined by oscillatory interactions of the Ruderman Kittel type between rare-earth atoms. In transition-metal-rich alloys, the transition-metal atoms carry an intrinsic magnetic moment that is always antiparallel to the spin of the rare-earth atom. The compounds are thus ferromagnetic with light rare earths and ferrimagnetic with the heavy rare earths. The magnetic interactions are strong and lead to high ordering temperatures. The RM_2 compounds fall between these two groups. As a result of the transfer of conduction electrons from the rare-earth metals to the 3*d* band of the transition metals, the Laves phase compounds exhibit different properties depending upon the particular 3*d* transition metal which is in the compound. For RNi_2 compounds, it appears, from bulk magnetic measurements, that nickel does not carry a moment. In RCo_2 compounds, the moment on cobalt depends on the spin of the rare-earth metal in the compound. The compounds YCo_2 and $LuCo_2$ exhibit a strong Pauli paramagnetism. With magnetically active rare-earth elements, a moment is thought to be created on the cobalt atoms by the magnetic interactions due to the rare-earth atoms (1 μ_B per Co in $GdCo_2$).

The polarized neutron experiments that were started last year on $TmCo_2$ have been extended to higher temperatures and to $LuCo_2$ and $TbNi_2$ in order to measure the distribution of magnetic moment density in these compounds, to determine the degree of localization of the magnetic electrons, and to distinguish between two possible models for the thermal variation of the paramagnetic susceptibility. The crystal structure of the cubic Laves phase is such that three different types of reflections are observed: There are peaks due to the rare-earth atom alone, others due to the transition-metal atom alone, and those due to both types of atoms. Therefore, it is possible, in principle, to measure separately the density due to each type of atom.

Measurements were carried out at temperatures ranging from 4.2 to 250°K in applied fields up to 57.2 kOe at HB-1 of the HFIR. The results obtained are summarized below.

$LuCo_2$

In $LuCo_2$ a magnetization is induced on the cobalt atoms by the applied magnetic field. The form factor of the induced moment is similar to that calculated for localized *3d* electrons. There is additional evidence for an induced magnetization on the lutetium atoms which is, however, an order of magnitude smaller than that on the cobalt. The shape of the form factor associated with this density is unlike that of a moment localized on the lutetium sites. The shape appears to be due to a weak conduction electron polarization.

$TmCo_2$

The crystal of $TmCo_2$ which was studied orders ferromagnetically at 7°K. The localized moments on thulium and cobalt sites have been determined at 4.2 and 100°K from the magnetic densities obtained by Fourier projection. The thulium moment (5.4 μ_B at 4.2°K) is reduced by crystal field effects. A *3d*-type cobalt moment is coupled antiparallel to that of thulium. The magnetic-scattering amplitudes measured for the reflections to which the *4f*-thulium moment does not contribute give direct evidence for the existence of a diffuse magnetic density. This diffuse density is oscillatory with distance and remains similar at all temperatures. The *4f*-thulium and *3d*-cobalt moments have been evaluated at eight temperatures from 4.2 to 250°K. The cobalt susceptibility above 25°K is temperature independent. The cobalt behaves as a Pauli paramagnet under the action of two fields: the molecular field due to thulium atoms and the applied field. A collective electron model is therefore appropriate for the description of the paramagnetic susceptibility. At 4.2°K a large increase of the cobalt susceptibility in the molecular field leads to a value of the cobalt moment of 0.8 μ_B.

$TbNi_2$

Below the Curie temperature, 42°K, a magnetic contribution is observed only on nuclear scattering peaks. Therefore, the terbium atoms form a ferromagnetic structure. Polarized neutron measurements performed in the paramagnetic state in an applied magnetic field of 57.2 kOe reveal a nonuniform polarization of the conduction band. Within the experimental accuracy, no *3d* magnetic moment is observed on nickel atoms. This result is consistent with the assumption of rare-earth magnetic ordering occurring through the polarization of conduction electrons.

---

1. Summary of papers: *Phys. Rev.* and *J. Phys. Chem. Solids* (in press).

2. Laboratoire de Magnetisme, Centre National de la Recherche Scientifique, Grenoble, France.

3. Guest scientists from Laboratoire de Magnetisme, Centre National de la Recherche Scientifique, Grenoble, France.

THE TEMPERATURE DEPENDENCE OF SPIN WAVES IN Ho(Tb)Fe_2

R. M. Nicklow C. M. Williams[1]
N. C. Koon[1] J. B. Milstein[1]

Studies of the spin-wave dispersion relation for the Laves phase compound $Ho_{0.88}Tb_{0.12}Fe_2$ have continued. Neutron scattering experiments carried out at 12°K have indicated that crystal field interactions, which were neglected in our previous analysis of room-temperature data[2] make significant contributions to the spin-wave energies at low temperatures. The measured temperature variation of the acoustic and lower optic branch (see Fig. 4.4) is almost entirely due to the temperature-dependent contributions of the crystal field anisotropy to these branches.

On the other hand, the strong temperature variation of the upper optic branch shown in Fig. 4.4 appears to be satisfactorily explained by the temperature dependence of the ordered moments of the rare-earth and iron sublattices. The temperature dependence of the calculated curve was obtained by setting $S_R^z(T) = S_R^z(0)\sigma_R(T)$ and $S_F^z(T) = S_F^z(0)\sigma_F(T)$, where S_F^z and S_R^z are the appropriate ordered components of the "spins" for the iron and the rare-earth ions, respectively, and $\sigma_F(T)$ and $\sigma_R(T)$ are the corresponding sublattice magnetizations. One is also led to the conclusion that $S_R^z(0) \geq 8$ and that $S_F^z(0) \geq 0.81$. While this result is perhaps not too surprising since it is consistent with the measured magnetic moments, it is interesting that both the static and dynamic magnetic properties of the compound are described by the same effective *nonintegral* spin for iron.

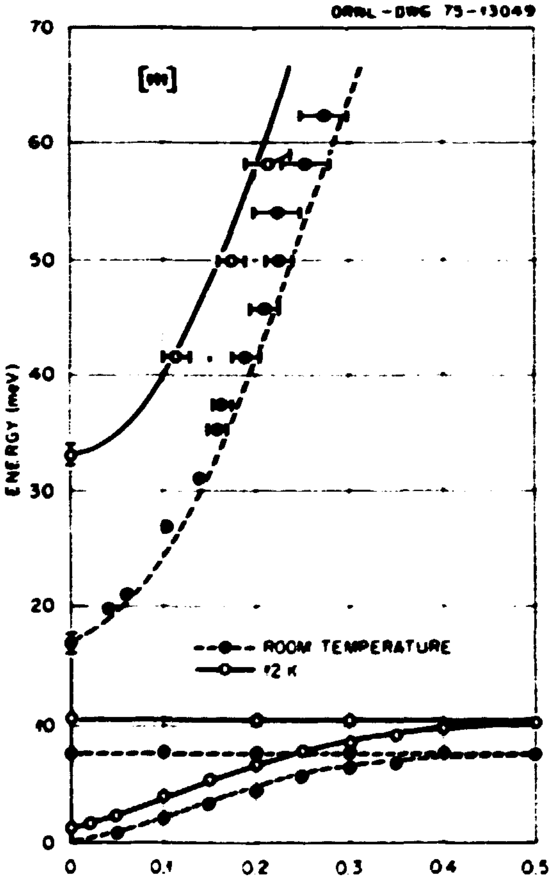

Fig. 4.4. The temperature dependence of the spin-wave dispersion curve in the [111] direction for $Ho_{0.88}Tb_{0.12}Fe_2$. The curves shown are the results of calculations from the model discussed in text.

Table 4.2. Model parameters used for the calculated magnon-dispersion relations shown in Fig. 4.4

Parameter	Value (meV)
J_{FF}	46 ± 3
J_{RF}	0.84 ± 0.06
J_{RR}	0.00 ± 0.01
Δ^-	2.5
Δ^+	2.3
$S_R^z(0)$	8.0
$S_F^z(0)$	0.81

The values for the exchange, J_{RF}, J_{RR}, J_{FF}, and anisotropy parameters, Δ^+, Δ^-, deduced from the data are given in Table 4.2. These exchange parameters are slightly different from the values obtained earlier,[2] because we had previously assumed incorrectly that, at room temperature, $S_F \geq 1.0$. The magnitude of the rare-earth–rare-earth exchange is negligible. The conduction electrons are apparently much more effective in providing an interaction between the rare-earth and iron ions than between the rare-earth ions themselves. Thus the spin-wave energies are described surprisingly well by a very simple near-neighbor exchange model that includes crystal field interactions and temperature renormalization derived from the sublattice magnetization.

---

[1] Naval Research Laboratory, Washington, D.C.

[2] R. M. Nicklow, N. C. Koon, C. M. Williams, and J. B. Milstein, *Solid State Div. Annu. Prog. Rep. Dec. 31, 1974*, ORNL-5028, p. 86.

INELASTIC MAGNETIC SCATTERING FROM AMORPHOUS $TbFe_2$[1]

J. J. Rhyne[2]   D. L. Price[3]   H. A. Mook

Inelastic neutron scattering measurements have been made on sputter-deposited amorphous $Tb_{0.33}Fe_{0.67}$ using time-of-flight spectrometers at Argonne and at Oak Ridge. At 433°K (above T_c) the magnetic-scattering function $S(Q,\omega)$ exhibited an approximate Gaussian dependence on energy transfer characteristic of a paramagnet. Below T_c, at 299°K, a broad distribution of magnetic inelastic scattering is present, centered approximately at $\Delta E = 11$ meV. As expected, this distribution was significantly broadened and was shifted to a lower energy than the equivalent polycrystalline compound $TbFe_2$, which showed a single inelastic peak near 18 meV. Polarized beam time-of-flight data taken at Oak Ridge showed evidence for discrete spin-wave excitations for $Q \lesssim 1.0$ Å^{-1} in the amorphous sample.

---

[1] Abstract of paper: *AIP Conf. Proc.* **24**, 121 (1975).

[2] Naval Ordnance Laboratory, White Oak, Md., and National Bureau of Standards, Washington, D.C.

[3] Argonne National Laboratory, Argonne, Ill.

MAGNETIC EXCITATIONS IN NICKEL

H. A. Mook   D. Tocchetti[1]   F. Mezei[1]

The most advanced calculations of the dynamic susceptibility of ferromagnetic nickel have been performed by J. F. Cooke and H. L. Davis.[2,3] In contrast to previous work, these calculations incorporate momentum-dependent spin-splitting of the electronic energy bands as well as multiband effects. One prediction of these calculations is that for the [100] direction the acoustic spin wave should interact strongly with a polar or optical spin-wave mode at about 130 to 140 meV. This is in contrast to the other principal symmetry directions where the spin waves are expected to disappear as they begin to interact with the Stoner excitations. If the polar mode could be observed, it would serve as an excellent check on the band calculations since the position of the mode is a very sensitive function of the parameters of the calculation including the potential function.

The polar mode should be observable in a neutron scattering experiment, but high-neutron incident energies are required. An experiment to look for this mode was performed on a triple-axis spectrometer located at one of the hot source beam tubes at the Institute Max von Laue - Paul Langevin. A beryllium monochromating crystal that had been brought from Oak Ridge was used, and copper or graphite analyzer crystals were utilized. The sample was a crystal (also brought from Oak Ridge) which had been enriched to about 99% in the isotope ^{60}Ni to cut down on phonon and incoherent scattering. The incident neutron energies utilized ranged from 300 to 750 meV. The most difficult part of the experiment was avoiding higher order scattering resulting from order contamination in the beam. Most of the experiments were performed with fixed E_0 so that an indium filter could be used to adsorb $\lambda/2$ neutrons at an energy of 1.5 eV. Reflections were chosen for the beryllium monochromator so that $\lambda/3$ was absent.

Since part of the polar mode does not have extremely steep dispersion, focusing techniques could be used, and resolution calculations were performed for each scan. An analytical form was chosen for the cross section; this was convoluted with the resolution function for the spectrometer, and the result was compared with the measurement. Very poor energy resolution could be used in the experiment since focusing techniques could be used; otherwise the measurements would be impossible.

Figure 4.5 shows the result of the measurements. The solid lines show the Cooke and Davis calculations, and the dots are the experimental points. Near the zone boundary, good resolution was needed since the lack of focusing made the measurements very difficult. It is planned to check some of the points near the zone boundary using the polarized-beam time-of-flight spectrometer sometime in the near future. It is remarkable that the predictions of the band calculations come so close to the observed measurements. The bands themselves cover several electron volts, and from them are predicted magnetic excitation energies within a few

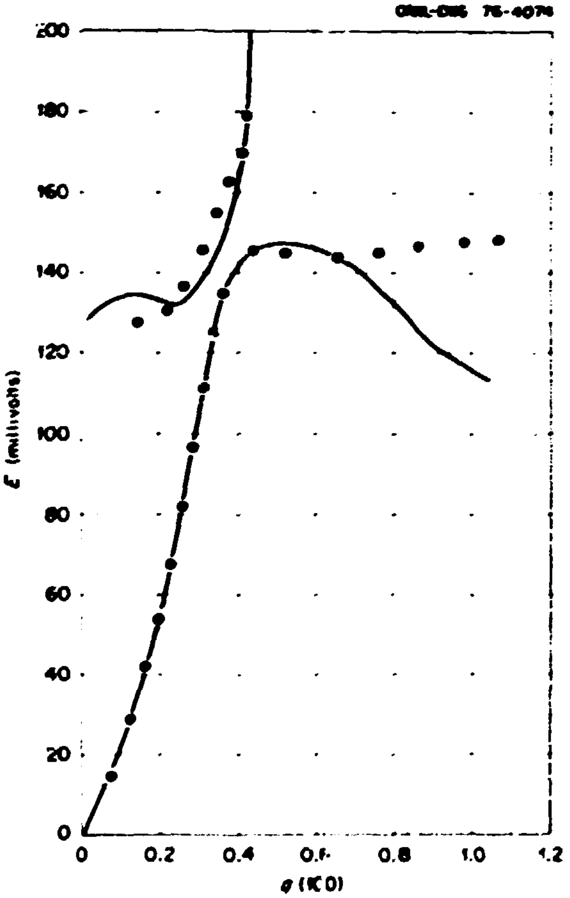

Fig. 4.5. Comparison of calculated and measured magnetic excitations for nickel.

millivolts of those observed. Small changes in the potential are expected to provide an even better fit to the observed points. It is now clear that some existing band calculations in the literature are incorrect, since they suggest a band splitting much too large to account for the neutron scattering measurements. The new measurements provide a sensitive test with which any forthcoming band calculations for ferromagnetic nickel must reckon.

---

[1] Institut Max von Laue Paul Langevin, Grenoble, France.

[2] J. F. Cooke and H. L. Davis, *AIP Conf. Proc.* 10, 1218 (1973).

[3] J. F. Cooke and H. L. Davis, to be published.

MAGNETIC EXCITATIONS IN NEODYMIUM ANTIMONIDE[1]

A. Furrer[2] R. M. Nicklow
W.J.L. Buyers[3] O. Vogt[4]

The magnetic excitation spectrum of the antiferromagnet NdSb (T_N = 13.6°K) has been studied by neutron inelastic scattering. At 4.9°K nearly all the spin-wave strength resides in the transition to the 6th excited state which originates from the exchange split, $\Gamma_8^{(2)}$ quartet ground state and $\Gamma_8^{(1)}$ quartet excited state of the Nd^{3+} ion. A weaker and lower frequency transition between the ground state and the 4th excited state, the lower member of the exchange split Γ_6 doublet, has also been observed. These transitions give rise to spin-wave branches of transverse and longitudinal symmetry, respectively, whose frequencies, measured in this experiment in the (00ζ), (ζζ0), and (ζζζ) directions, are surprisingly independent of wave vector. Measurements at higher temperatures show that there is surprisingly little downward renormalization (≈10%) of the frequency of the main branch of magnetic excitations on passing through the Néel point. The crystal field parameters have been determined from the excitation spectra in the paramagnetic state. From the results at 4.9°K, two bilinear exchange parameters and a large quadrupolar parameter have been obtained with the aid of a pseudoboson spin-wave theory that includes all nine excited states of the Nd^{3+} ion. A good description of the magnetic properties of NdSb is obtained from the model parameters.

---

[1] Abstract of paper to be published.

[2] Eidg. Institüt fur Reaktorforschung, Würenlingen, Switzerland.

[3] Atomic Energy of Canada Ltd., Chalk River, Ontario, Canada.

[4] Laboratorium für Festkörperphysik, ETH, Zürich, Switzerland.

PARAMAGNETIC SCATTERING FROM ALKALI METAL SUPEROXIDES[1]

H. G. Smith J. Schweizer[2]

A polarized-beam polarization-analysis neutron scattering study was made on paramagnetic CsO_2 powder at room temperature under four different configurations flipper on and flipper off with the magnetic field on the sample vertical and then again with the field horizontal. A preliminary study indicated that the usual procedure of determining the paramagnetic scattering in the spin-flip horizontal-field configuration by subtracting the nuclear spin scattering contributions (determined at large scattering angles) from the total spin-flip scattering is probably not valid in CsO_2 because of the large Debye -Waller factor in compounds of this type, since the nuclear spin scattering is not isotropic but angularly dependent. A way to avoid this difficulty is to use the four-configuration technique mentioned above. By changing the magnetic field direction on the sample from horizontal to vertical, only the paramagnetic scattering is affected. For the flipper-off mode, one-half the paramagnetic scattering appears when the field is vertical; for the flipper-on mode, one-half of the total paramagnetic scattering disappears. The sum of these differences gives the total paramagnetic scattering, independent of all other types of scattering. Multiple-scattering corrections are minimized if not eliminated. The data were placed on an absolute scale by comparison with the nuclear Bragg scattering and, within experimental error, agreed with a spin 1/2 system. At low scattering angles [<5°(2θ)] the paramagnetic scattering appeared to be affected by the vertical field. This observation is not understood at this time.

A polarization analysis study was also made on polycrystalline KO_2 and RbO_2 at 1.7°K and above. Both of these compounds have been observed to undergo several structural transitions below room temperature. In the case of KO_2 a structural transition was observed as low as 13°K, and a magnetic ordering transition was observed at 7°K. In the case of RbO_2, extra reflections at low scattering angles had been observed, but it was not determined if they were of magnetic or structural origin. This study confirmed the magnetic ordering in KO_2 and showed conclusively that the lowest angle peak in RbO_2 is magnetic in character and disappears on warming to about 14°K, in the neighborhood of known heat capacity anomalies in this compound. Further studies are necessary to determine the detailed magnetic structure.

LATTICE DYNAMICS

NEUTRON INELASTIC SCATTERING MEASUREMENTS OF PHONON PERTURBATIONS BY DEFECTS IN IRRADIATED COPPER[1]

R. M. Nicklow F. W. Young, Jr.
R. R. Coltman, Jr. R. F. Wood

Theoretical[2] and experimental[3,4] studies have provided strong evidences that the split-interstitial or ⟨100⟩ dumbbell configuration is the stable form for interstitials in copper and aluminum. The theoretical work has also indicated that the dumbbell interstitial possesses a low-frequency librational mode.[2] Wood and Mostoller[5] and Shober et al.[6] have shown that these modes are strongly coupled to the phonons of the host crystal, leading to perturbations of the phonon dispersion relation (i.e., frequency vs q) that possibly could be detected by neutron inelastic scattering. A neutron scattering experiment to search for such perturbations was carried out on a high-purity, low-dislocation-density copper crystal. Because of the large sample size (about 0.5 cm^3) required for the scattering experiment, only thermal-neutron irradiation was capable of creating a homogeneous concentration of defects which were predominantly Frenkel pairs. Therefore the sample crystal was irradiated by thermal neutrons at 4.2°K for 24 days in the low-temperature irradiation facility at the Oak Ridge National Laboratory.[7] The estimated Frenkel pair concentration was about 40 ppm. After irradiation, the sample was transferred at 4.2°K to the neutron spectrometer. Measurements were made at temperatures below 10°K on the sample as irradiated and after several annealing treatments, as well as on an unirradiated crystal.

A portion of the experimental results obtained for the as-irradiated sample for several wave vectors $q = (0,0,\zeta)2\pi/a$ is shown in Fig. 4.6. The vertical dotted line represents for each ζ the position of the peak observed in the neutron intensity distribution measured for the annealed (or unirradiated) sample; that is, the frequency scale is plotted *relative* to the perfect crystal $\nu(q)$. These results show phonon perturbation effects in the form of q-dependent frequency shifts and unusual peak structure. The results obtained for the q dependence of the peak shifts are consistent with a resonance-type behavior. While the present experimental uncertainties are too great to justify a detailed interpretation at this time, an estimate of the resonance frequency corresponding to $\zeta \approx 0.1$ where the shifts tend to zero gives a value of about 0.8 to 0.9

ORNL-DWG 75-6721A

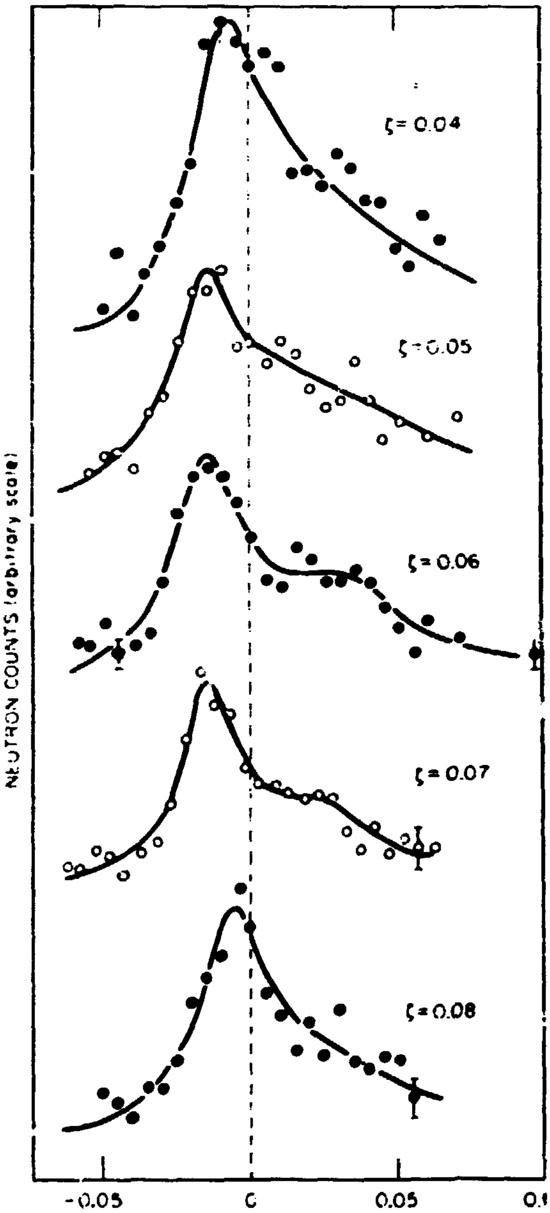

Fig. 4.6. Frequency distributions of neutrons scattered from irradiated copper at 4 K for $q = (0,0,\zeta)2\pi/a$.

---

[1] The author carried out this research while on foreign assignment at Institut Max von Laue–Paul Langevin, Grenoble, France.

[2] Institut Max von Laue–Paul Langevin, Grenoble, France.

THz, which is consistent with theoretical estimates[2] and elastic measurements.[4]

However, serious difficulties are encountered when a detailed explanation of the observed peak shapes is attempted in terms of the simplified theoretical results. Calculations for the ⟨100⟩ split interstitial were carried out to fit the experimental results for q = $(0,0,0.06)2\pi/a$. Although a fairly good fit could be achieved with reasonable parameters, all such calculations also predicted a transferral of intensity from the low-frequency peak to the high-frequency peak with increasing q, in contrast to the experimental results. Furthermore, for all q investigated ($\zeta = 0.04$ to 0.10) an anneal at room temperature eliminated the peak *shifts*. However, for $\zeta = 0.04$ to 0.06 this anneal did not remove all of the excess intensity observed on the high-frequency sides of the main phonon peaks, as is shown in Fig. 4.7 for $\zeta = 0.06$. A further anneal carried out at 800°K did remove the extra intensity while leaving the peak position unchanged. The peak asymmetry that remains after the 800°K anneal is due to the instrumental resolution. This effect is well understood, as is shown by the good agreement between peak shape calculations and the experimental results in Fig. 4.7*c*. The dotted lines in Fig. 4.7*a* and *b*, which provide a visual comparison between those data and the peak shape calculation of Fig. 4.7*c*, indicate that the irradiation also produces a slight broadening of the phonon peaks. The measurements made on the unirradiated sample are indistinguishable from the measurements and calculations shown in Fig. 4.7*c*.

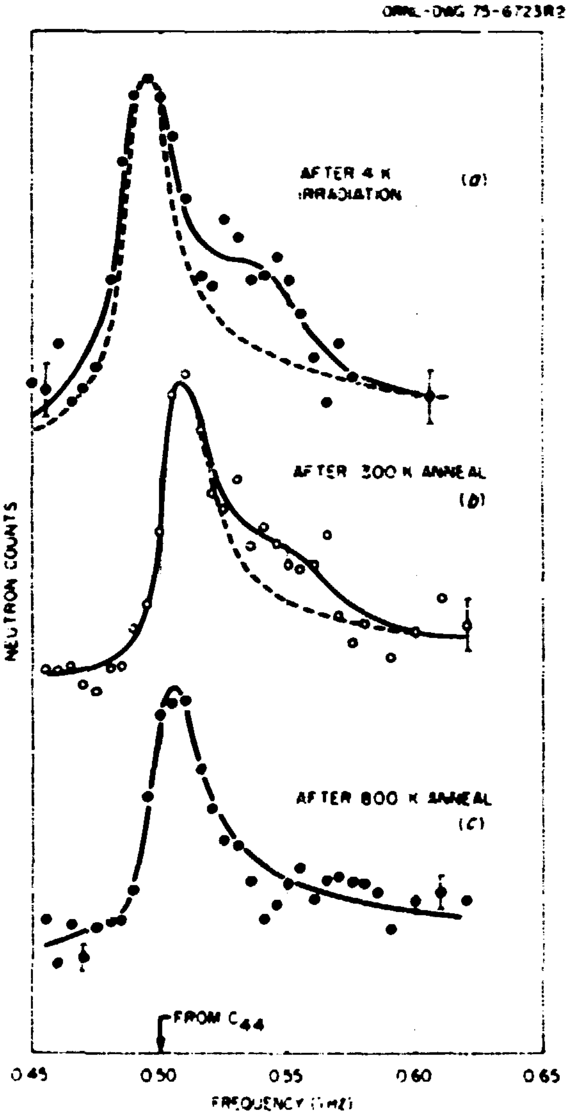
ORNL-DWG 75-6723R2

Fig. 4.7. Frequency distributions of neutrons scattered from as-irradiated and annealed copper for q = $(0,0,0.06)2\pi/a$.

It would appear that the present results cannot be completely explained in terms of the simplified calculations for the ⟨100⟩ split interstitial. The absence of structure in the phonon peaks measured for the unirradiated and the 800°K annealed samples indicates that this structure is produced by the low-temperature irradiation. The fact that nearly 50% of it remains after the 300°K anneal is an unexpected and surprising result, since diffuse x-ray and resistivity studies indicate that 90% of the damage produced by a low-temperature irradiation in copper anneals below 300°K. One possible conclusion is that the split interstitial may be responsible for the frequency shifts and line broadening observed for the irradiated sample as theoretically predicted and that the additional structure observed for $\zeta \leq 0.07$ for the irradiated crystal is due to an as yet unspecified form of radiation damage.

---

1. Summary of paper, *Phys. Rev. Lett.* 35, 1444 (1975).
2. P. H. Dederichs, C. Lehmann, and A. Scholz, *Phys. Rev. Lett.* 31, 1130 (1973).
3. P. Ehrhart, H. G. Haubold, and W. Schilling, *Adv. Solid State Phys.* 14, 87 (1974).
4. J. Holder, A. V. Granato, and L. E. Rehn, *Phys. Rev. Lett.* 32, 1054 (1974); *Phys. Rev. B* 10, 363 (1974).
5. R. F. Wood and Mark Mostoller, *Phys. Rev. Lett.* 35, 45 (1975).
6. H. R. Schober, V. K. Tewary, and P. H. Dederichs, *Z. Phys. B* 21, 255 (1975).
7. R. R. Coltman, Jr., C. E. Klabunde, and J. K. Redman, *Phys. Rev.* 156, 715 (1967).

PHONON DISPERSION CURVES FOR $\mathrm{Ta}_{0.77}\mathrm{W}_{0.23}$

N. Wakabayashi

The relationship between phonon dispersion curves and superconductivity in transition metals and their alloys and compounds is a continuing program in this Laboratory. As part of that study we have measured phonon dispersion curves of $\mathrm{Ta}_{0.77}\mathrm{W}_{0.23}$ for wave vectors along the principal symmetry directions. The results are shown in Fig. 4.8. For comparison the solid and broken lines in the figure represent the experimentally observed dispersion curves for pure tantalum and pure tungsten respectively. The transverse branches along the [110] and [001] directions are almost identical to those for pure tantalum, while the longitudinal branches, which exhibit anomalies in tantalum, show considerable changes. This fact indicates that the anomalies in these longitudinal branches are directly related to the screening effects due to the conduction electrons in these systems. Since the superconducting transition temperature decreases with the concentration of tungsten, the anomalies in the longitudinal branches may, in turn, be related to the superconductivity. The anomalous upward curvature in transverse branch in the [001] direction may also be related to the conducting electrons, though rather indirectly. Therefore, the study of differences in the frequency shifts between the longitudinal and transverse branches should give us some information about the nature of a microscopic link between phonons and superconductivity.

PHONON SPECTRA IN NIOBIUM–ZIRCONIUM ALLOYS

N. Wakabayashi J. G. Traylor[1] S. K. Sinha[2]

The phonon dispersion curves for high-T_c superconductors are known to exhibit strong anomalies, but the basic physical process which links the high T_c and the phonon anomalies is yet to be understood. As a part of the research effort to study phonon anomalies in superconductors, the phonon dispersion curves for the random alloy system $\mathrm{Nb}_{1-x}\mathrm{Zr}_x$ with $x < 0.15$ have been measured by neutron scattering techniques. While T_c decreases for the niobium–molybdenum alloy system as the molybdenum concentration, it increases as zirconium is added to niobium (from T_c = 9°K for x = 0 to 11°K for x = 0.15). Phonon anomalies observed for niobium become less pronounced by adding molybdenum, and one might expect a reverse trend in the niobium–zirconium alloys. Also, for x greater than 0.15, the system seems

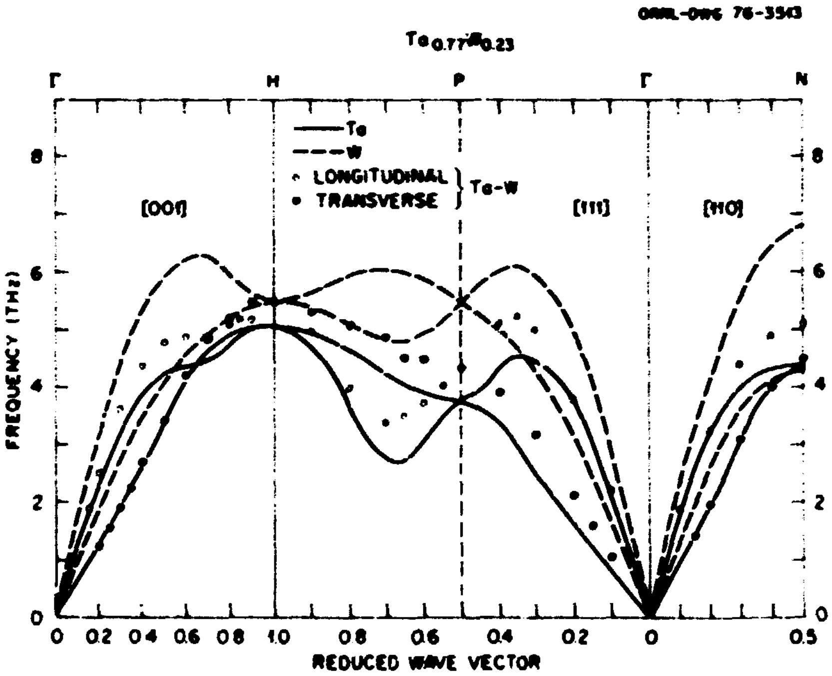

Fig. 4.8. Phonon dispersion curves for $\mathrm{Ta}_{0.77}\mathrm{W}_{0.23}$. Solid (broken) lines represent the data for pure tantalum (tungsten)

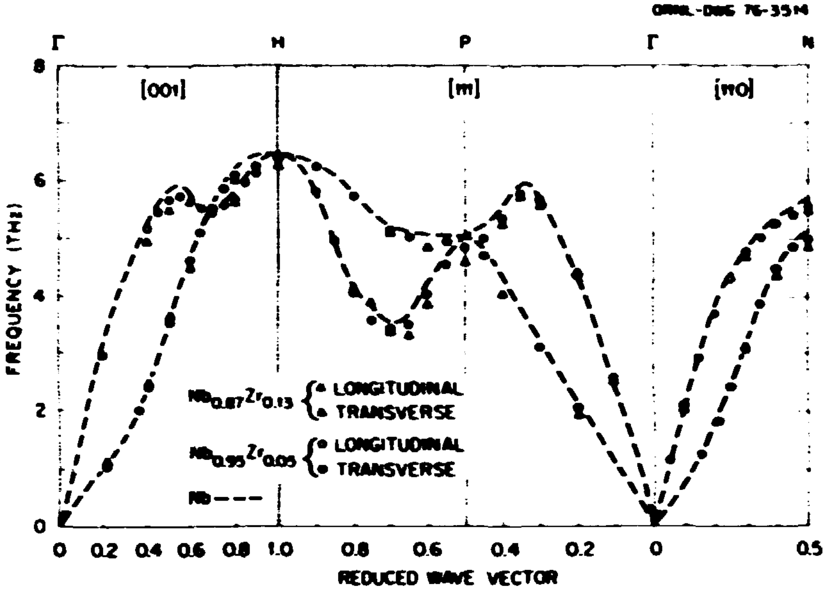

Fig. 4.9. Phonon dispersion curves for $Nb_{0.87}Zr_{0.13}$ and $Nb_{0.95}Zr_{0.05}$. Dotted lines represent those for pure niobium.

to have a mixed bcc diffuse-ω phase at low temperatures. The ω phase has a hexagonal structure giving rise to superlattice reflections at 2/3(111) + τ in cubic indexing, where τ is the reciprocal lattice vector of the bcc structure. This lattice instability might be interpreted as an indication of the softening of the longitudinal phonons at 2/3(111).

Measurements were carried out on $Nb_{0.95}Zr_{0.05}$ and $Nb_{0.87}Zr_{0.13}$ along the principal symmetry directions. Some of the results are summarized in Fig. 4.9, together with the dispersion curves for pure niobium shown by the dotted lines.[3] Larger changes were observed for longitudinal modes, frequencies for the alloys being lower than those for niobium. The most pronounced anomaly for niobium in the (00ζ) longitudinal branch near ζ = 0.7 does not seem to be enhanced noticeably by alloying. The longitudinal phonons around 2/3(111) are well defined, and the softening is rather small. However, rather strong diffuse scattering was observed near this wave vector, which is reported elsewhere.[4] Sinha and Harmon[5] have proposed a model for the lattice dynamics of transition metals which gives large decreases in the longitudinal phonon frequencies near (0.0.0.6) and (0.8.0.8.0.8) due to the intra-*d*-band contribution to the dielectric function. The decrease was found to be very sensitive to the *d*-electron density at the Fermi surface, in accordance with the phonon frequency changes in niobium molybdenum alloys. However, although slight decreases exist near these wave vectors, the largest change in the niobium zirconium alloys is actually near (0.5.0.5.0.5). This indicates that changes other than that in the *d*-electron density are responsible.

The data were fitted to Born von Karman models, and the models were used to calculate the phonon density of states, $g(\nu)$, and various moments of $g(\nu)$. However, changes in the average properties expressed by the moments do not seem to be significant enough to explain the changes in T_c, suggesting the existence of a mode-dependent electron-phonon coupling.

---

1. Iowa State University, Ames, Iowa.

2. Argonne National Laboratory, Argonne, Ill.

3. Y. Nakagawa and A.D.B. Woods, p. 39 in *Lattice Dynamics*, ed. by R. F. Wallis, Pergamon Press, Ltd., Oxford, England, 1965.

4. N. Wakabayashi and J. G. Taylor, "Diffuse Scattering in Niobium Zirconium Alloys," this report.

5. S. K. Sinha and B. N. Harmon, *Phys. Rev. Lett.* 35, 1515 (1975).

PHONON ANOMALIES IN THE $Mo_{1-x}Re_x$ SYSTEM

H. G. Smith N. Wakabayashi

It has become apparent that the complex phonon spectra observed in most superconducting materials are, indeed, related to their superconducting properties, presumably through the electron-phonon interaction. The anomalous features (pronounced dips in the phonon dispersion curves in various regions of the Brillouin zone) are most noticeable when compared with phonon spectra of related materials that either are nonsuperconducting or have low values of T_c. Two well-known examples are the niobium molybdenum system (bcc) and the NbC, ZrC compounds (fcc). The former system had been the most widely studied, and it has been observed that as molybdenum (T_c about 0.9°) is added to niobium (T_c about 9.2°), T_c decreases, and so do the anomalous features. The effects are related to the electron/atom ratios observed for the transition metals where maxima in T_c are obtained for e/a values of approximately 4.7 and 6.5 with a minimum in T_c at 5.8, in approximate agreement with the above example.

Similarly, it has been observed that the addition of hcp rhenium (T_c about 1.7°K) to bcc molybdenum rapidly increases T_c to approximately 10°K at a concentration of 25% rhenium (near the bcc single-phase boundary). At even greater concentration, higher T_c's are attainable, but the crystal structures are more complex, and single crystals are not readily available. It was expected that anomalous dips in the dispersion curves would occur, but it was not known exactly where and to what extent the softening would be, although the [001] zone boundary was suspect.

An inelastic neutron scattering study on several bcc $Mo_{1-x}Re_x$ alloys ($x \leq 0.25$) was initiated. Preliminary results on an $Mo_{0.75}Re_{0.25}$ single crystal revealed a pronounced decrease at the [001] zone boundary where the longitudinal acoustic (LA) and transverse acoustic (TA) modes are degenerate. The anomalous region occurs near the zone boundary in the [001] direction but appears to cover much of the region between zone boundary points *P* and *H* in the [111] direction. The crystal was of very good quality, but the phonon line widths were broad and sometimes showed structure. There are several sources of broadening: (1) mass defects due to the heavy rhenium atoms, (2) force constant disorder, (3) clustering effects due to short-range order, and (4) strong electron-phonon interactions. A combination of all effects is expected but to varying degrees.

A more extensive investigation is under way on the single crystal alloy $Mo_{0.85}Re_{0.15}$, and a preliminary analysis of the dispersion curves and phonon line-shapes reveals that the anomalous features can qualitatively be explained on the basis of CPA mass defect theory. However, it is found that in order to obtain quantitative agreement between experiment and theory, it will be necessary to invoke force-constant changes not only for the heavy mass defect but for the host lattice as well. The phonon frequencies of the modified host lattice have been estimated and are shown by the crosses in Fig. 4.10. For comparison, the dispersion curves for pure molybdenum are shown by dotted lines. The large changes at the zone boundaries in the alloy, which may be attributed to strong electron-phonon interactions, appear to be enhanced by the resonant modes of the rhenium atoms.

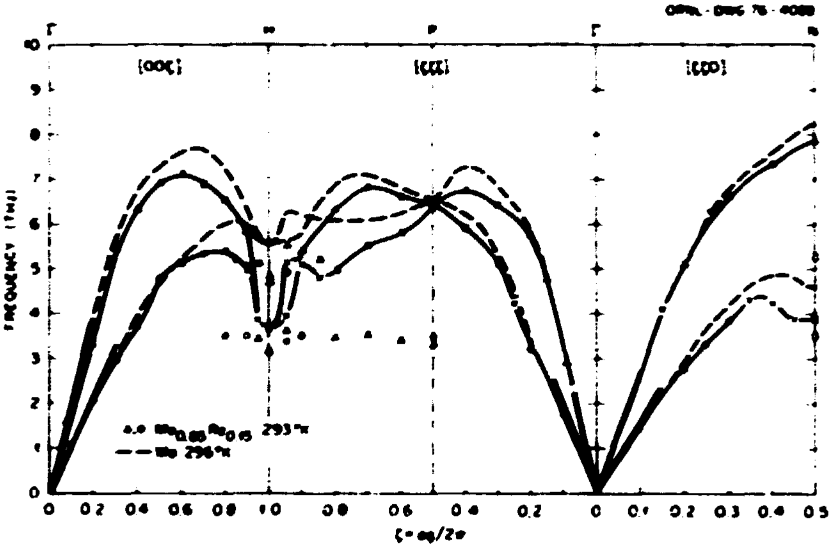

Fig. 4.10. Phonon dispersion curves of $Mo_{0.85}Re_{0.15}$ at room temperature. For comparison the dispersion curves of pure molybdenum are shown by the dotted lines.

PHONONS IN In(10% Tl)

N. Wakabayashi

The indium–thallium alloy system has four distinct crystallographic phases: Indium has a structure that can be described as face-centered tetragonal (fct), and thallium has an hcp structure. When indium is alloyed with 15 to 30% thallium, it undergoes a martensitic transformation from fct to fcc structure, and there is a maximum in the superconducting transition temperature T_c in this range of thallium concentration. The mechanism of the phase transformation is generally regarded as a softening of the transverse phonon in the [110] direction (in the cubic phase) with polarization along the [1$\bar{1}$0] direction. In support of this is the observation that the elastic constant $\frac{1}{2}(C_{11} - C_{12})$ goes to zero at the phase transition. Also, superconducting tunneling experiments have suggested a possible softening of some phonons. Although the tunneling technique can give an indication of soft phonons, one cannot conclude which phonon mode in particular goes soft. This problem is especially serious in alloys, since the phonon lifetime due to randomness may be large and the singularities in the phonon density of states smear out.

In order to investigate the effects of alloying on the individual modes, dispersion curves have been measured for a single-crystal sample of $In_{0.9}Tl_{0.1}$. The results obtained so far are shown in Fig. 4.11. The straight lines near $q = 0$ represent the initial slopes of the dispersion curves estimated from the elastic constants. The alloy has a c/a ratio of 1.06, as compared with the value 1.075 for pure indium. As $c/a \rightarrow 1.00$, the [100] and [001] directions become equivalent and the transverse modes in [100] become degenerate. It has been found that the frequencies of the transverse branch in the [100] direction polarized along [001] (T_{001}) and of the transverse branch in the [001] direction do not show significant shifts from those in pure indium.[1] However, the frequencies of the [100] transverse branch polarized along [010] (T_{010}) show a 5 to 10% decrease, the largest change observed in this alloy. Also, in the [101] direction the initial slope of the branch that may be regarded as nearly transverse, corresponding to $T_{1\bar{1}0}$ in the [110] direction, is rather small, and the branch shows a slightly upward curvature near $q = 0$. This curvature is a precursor of the softening of the mode near the phase transition. The temperature dependence of the initial slope of the $T_{1\bar{1}0}$ branch in the [110] direction has been found to be very similar to that for pure indium. Also shown in Fig. 4.11 is the result of tunneling measurements α^2F on $In_{0.9}Tl_{0.1}$ reported by Dynes.[2] The structure in α^2F seems to be consistent with the shapes of the observed phonon dispersion curves. Broken lines in the figure are the dispersion curves calculated by Gunton and Saunders[3] for In(15% Tl) on the basis of an average pseudopotential form

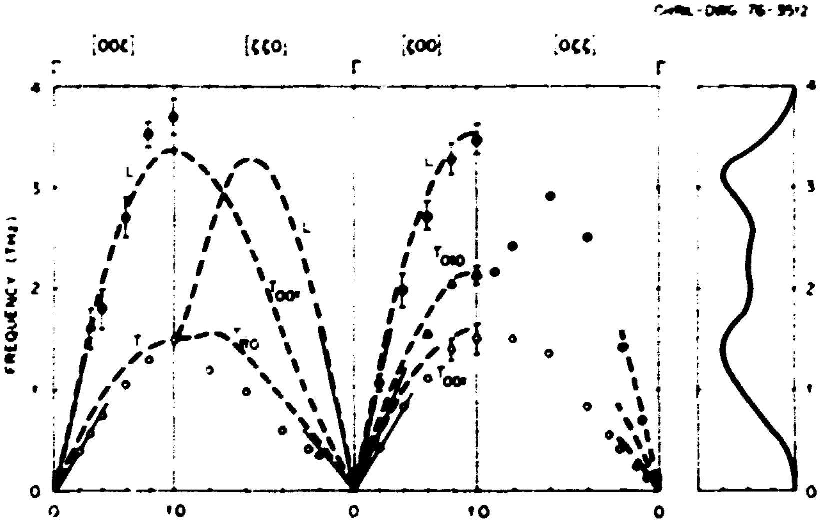

Fig. 4.11. Phonon dispersion in In (10% Tl) compared with predictions of a pseudopotential model (dashed lines), and the results of a tunneling experiment.

factor. However, the apparent agreement with the data may be merely accidental, since their calculation for pure indium shows rather poor agreement.

---

[1] H. G. Smith and W. Reichardt, *Solid State Div. Annu. Prog. Rep. Dec. 31, 1972*, ORNL-4848, p. 3; W. Reichardt and H. G. Smith, *Solid State Div. Annu. Prog. Rep. Dec. 31, 1973*, ORNL-4526, p. 74.

[2] R. C. Dynes, *Phys. Rev. B* 2, 644 (1970).

[3] D. J. Gunton and G. A. Saunders, *Solid State Commun.* 12, 569 (1973).

NEUTRON SPECTROSCOPY OF LOW-FREQUENCY PHONONS IN SOLID MERCURY[1]

W. A. Kamitakahara[2] H. G. Smith N. Wakabayashi

Extensive measurements of the phonon dispersion curves of trigonal mercury have been carried out by neutron inelastic scattering. Some transverse branches of the phonon spectrum have very low frequencies, as small as 0.9 meV at the zone boundary, compared with a maximum lattice frequency of 15 meV. The data have been accurately fitted with an eight-neighbor Born von Karman model, and a reliable phonon density of states $F(\omega)$ has been calculated. Comparison with $\alpha^2(\omega)F(\omega)$ derived from tunneling measurements reveals a substantial increase in $\alpha^2(\omega)$ at low frequencies. Direct calculations of $\alpha^2(\omega)F(\omega)$ from the Born–von Karman model, assuming a simple form for the electron-phonon matrix element, gives $\lambda = 2.0$, as compared with $\lambda = 1.6$ from tunneling. We discuss the origin of the frequency dependence of $\alpha^2(\omega)$.

---

[1] Abstract of paper: *Ferroelectrics*, in press.

[2] Present address: Iowa State University, Ames, Iowa.

LATTICE VIBRATIONS IN $TaD_{0.1}$

N. Wakabayashi T. E. Scott[1]

The behavior of hydrogen in metals is quite interesting from the point of view of both basic and applied research. The microscopic behavior of hydrogen in the bcc transition metals in not understood as well as that of hydrogen in the fcc metal palladium. Previous investigations of the structure, hydrogen diffusion, and vibration of hydrogen have not yet produced a unified model for hydrogen motions in such metals. Interstitial hydrogens are expected to be coupled very strongly with the host lattice, and the study of details of phonon frequency changes and lifetimes due to the presence of hydrogen is essential in making progress toward the goal of obtaining a consistent picture of metal-hydrogen systems.

As part of the effort to understand the microscopic properties of hydrogen dissolved in metals, the phonon spectra of pure tantalum and tantalum containing 10% deuterium have been studied at room temperature. Deuterium is believed to occupy one of the tetrahedral interstitial sites and may add one electron to the *d*-like band of the conduction electrons. Since phonon frequencies are considered quite sensitive to the *d*-electron density, one might expect noticeable changes in the frequencies in $TaD_{0.1}$. However, no significant differences in phonon frequencies could be observed between these two systems, and no lifetime effect was detected. Since $Ta_{0.77}W_{0.23}$, which may be considered to have a slightly higher conduction electron density, did show quite remarkable changes in the phonon spectrum, this result for $TaD_{0.1}$ is somewhat surprising. However, the niobium–deuterium system studied by Rowe et al.[2] also appears to be rather insensitive to the presence of deuterium. Clearly, more experimental information about the electronic as well as vibrational properties of the system is required in order to understand the result.

A study will soon be made to observe the coherent inelastic scattering of neutrons by the deuterium motion in the optic modes, the result of which should be useful in understanding not only vibrational states of hydrogen but also the diffusion mechanism.

---

[1] Iowa State University, Ames, Iowa.

[2] J. M. Rowe, N. Vagelatos, and J. J. Rush, *Phys. Rev. B* 12, 2959 (1975).

LATTICE VIBRATIONS OF MnF_2

C. A. Rotter[1] J. G. Traylor[2] H. G. Smith

The measurements of the phonon spectra of tetragonal MnF_2 were completed on the HB-3 triple-axis spectrometer at the High Flux Isotope Reactor. Data taken in the [100], [110], and [001] directions are displayed in Fig. 4.12. The shell model developed by Traylor et al.[3] for TiO_2 was modified and applied to MnF_2. The modifications included (1) axial symmetry constraints on all short-range interactions, (2) addition of fluorine-fluorine interactions along the *c* axis, (3) application of rotational invariance and elastic constant constraints. The best shell-model fit is also shown in Fig. 4.12. The degree of fit, χ, equals 2.1 as calculated in

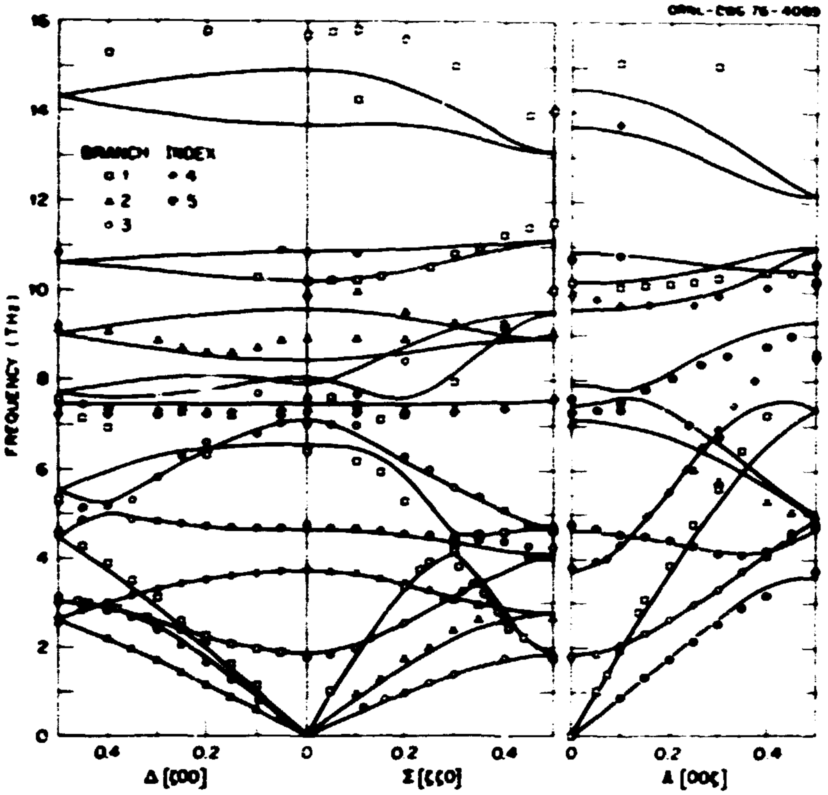

Fig. 4.12. Shell-model fit to MnF_2 data. Thirteen independent parameters were used

the usual fashion. Parameters for this fit are given in Fig. 4.13 along with cell-defining interactions. A and B are bond-stretching ($\partial^2\phi/\partial r^2$) and bond-bending ($(1/r)(\partial\phi/\partial r)$) parameters respectively; K_1, Y_1 and K_3, Y_3 are the core-shell force constants and shell charges for manganese and fluorine atoms respectively. From the shell-model fit of the data, the dielectric constants, density of states, θ (Debye), and specific heat were calculated.

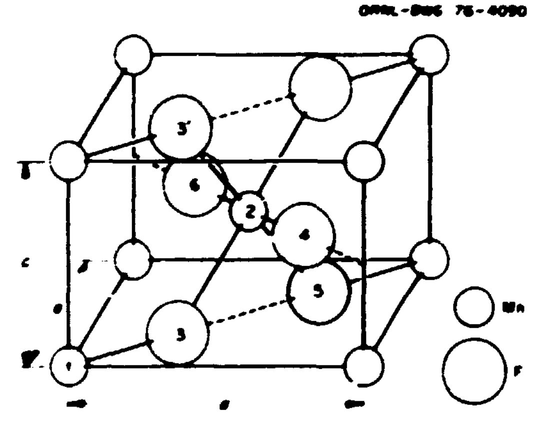

SHORT RANGE INTERACTIONS ($e^2/2V$)	A	B	CHARGE (e)
1-3	97.83	-10.07	$Z_1 = 1.758$
2-3	79.07	-8.62	$Y_1 = -6.64$
3-4	1.92	-0.01	$Y_3 = -4.44$
3-5	2.37	-0.06	
3-3′	1.92	-0.08	
$K_1 = 61150$	$K_3 = 5076$		

Fig. 4.13. MnF_2 unit cell and parameters used in shell-model fit. Labeling of atoms ($Mn_{1,2}$; $F_{3,4,5,6}$) is used to indicate short-range interactions.

PHASE TRANSITIONS AND CRITICAL PHENOMENA

NEUTRON INELASTIC SCATTERING STUDY OF TETRATHIOFULVALINIUM TETRACYANOQUINODIMETHANE (TTF-TCNQ)[1]

H. A. Mook   Charles R. Watson, Jr.[2]

Reports of high conductivities[3,4] found in the charge-transfer salt TTF-TCNQ have stimulated a great

---

[1] GRAU Faculty Research Participant from West Virginia University, Morgantown, W. Va.

[2] Iowa State University, Ames, Iowa.

[3] J. G. Traylor, H. G. Smith, R. M. Nicklow, and M. K. Wilkinson, *Phys. Rev. B* 3, 3457 (1971).

deal of interest in this material. Various measurements of the physical properties[5] of TTF-TCNQ prove that it is not a simple metal, and it has been suggested[6] that the high conductivities are associated with a Peierls instability in which a phonon mode is driven soft by a very strong interaction with the electrons at a wave vector equal to two times the Fermi surface wave vector, $2K_F$. Recent x-ray and neutron scattering measurements have shown that a superstructure exists in TTF-TCNQ at low temperature.[6-8] As the temperature was increased above 55°K, the scattering measurements showed that three-dimensional ordering disappeared. At higher temperatures one expects that any one-dimensional scattering observed by x-ray diffuse measurements would result from a Kohn anomaly in one of the phonon branches. Such one-dimensional x-ray diffuse scattering was observed up to room temperature using counter detection techniques,[8] but no sensitive energy analysis is available with x rays, and neutron inelastic scattering measurements are needed for detailed examination of the Kohn anomaly.

Unfortunately, neutron scattering measurements on TTF-TCNQ can only be performed with considerable difficulty. Only small crystals of this material can be obtained, the largest being about 2 X 0.4 X 0.02 cm. A single crystal is, therefore, not large enough for neutron inelastic scattering measurements, and an assembly of crystals must be constructed. A sample was thus constructed in the following manner. Several batches of crystals were grown from solution using very highly purified starting material in order to obtain the largest possible crystals. A series of slots were then milled in thin aluminum plates about 3 X 4 cm in size, and the largest crystals were positioned in the slots. Around 50 crystals were mounted on a plate, and five of these plates were stacked together to make a complete sample, which had a sample weight of about 300 mg of TTF-TCNQ. Despite the fact that the crystals were slightly irregular, the rocking curve of the whole assembly of about 250 crystals was on the order of 1° in all directions. After cycling the sample through the transition at 55°K a few times, it was found that the alignment had decreased to about 2.5°, but this is still sufficiently good alignment for good phonon measurements, especially in the region of the Kohn anomaly, where the scattering is limited to a one-dimensional sheet.

An additional problem is that the material contains hydrogen and thus has a large incoherent cross section, which causes a high background, especially near zero energy transfer. Some deuterated TTF and TCNQ starting material was provided by Garito, but crystals obtained with this material were quite small, and only limited data were obtained with them.

The experiments were performed on the three-axis spectrometers located at the High Flux Isotope Reactor in Oak Ridge. Graphite monochromating and analyzing crystals were used, and graphite filters were employed to eliminate order contamination. Most of the measurements were made around the (013) lattice point, which is the strongest reflection in the b*, c* plane, although cross checks were made around the (006), (008), (012), (021), and (027) reflections. Measurements of the Kohn anomaly were checked in both energy gain and energy loss and around equivalent points in reciprocal space. In some cases in energy loss, the analyzer was misoriented by 2° and the scans were repeated to prove that the scattering was indeed inelastic and to obtain background information. Figure 4.14 shows some of the dispersion curves measured at room temperature along the b direction. Other modes were observed, but only the strongest ones that were measured in some detail are shown in Fig. 4.14. Most of the modes are nearly flat and probably correspond to intramolecular excitations. These can be closely linked to measurements made with infrared techniques.[9] Modes that at $q = 0$ are mostly transverse and mostly longitudinal were also observed. These are labeled TA and LA in Fig. 4.14.

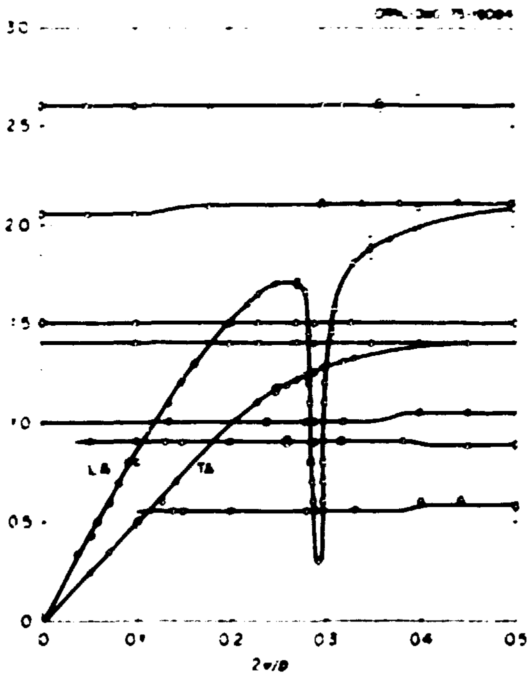

Fig. 4.14. Phonon dispersion curves along the chain direction for TTF-TCNQ.

The most striking feature is the large Kohn anomaly that seems to stem from the LA branch. It is possible that the Kohn anomaly is connected to some other branch, but constant-momentum-transfer scans at 0.295(2π/b), the midpoint of the Kohn anomaly, show peaks in all branches except the LA, which confirms the interpretation shown in Fig. 4.14.

The Kohn anomaly is sufficiently steep that it can only be observed in constant-energy-transfer scans. Fig. 4.15 shows three of these scans plus one scan through the LA phonon. The scans of the Kohn anomaly show two peaks, which have been interpreted as the descending and ascending phonon branches that compose the Kohn anomaly. All the phonon measurements not in the Kohn anomaly and all the elastic Bragg scans show no double structure, which supports the interpretation that the double peaks observed in the Kohn anomaly scans are not the result of misorientations in the sample stacking or some other sample-dependent effect.

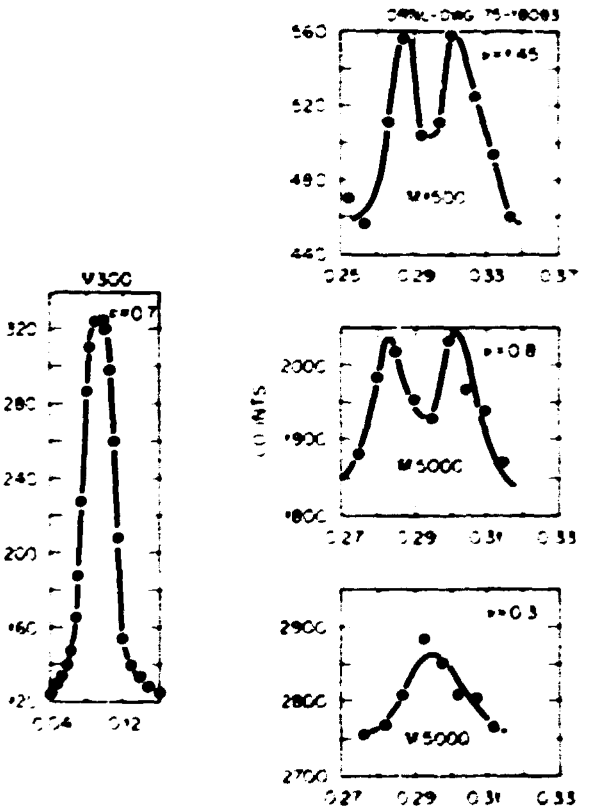

Fig. 4.15. Constant-energy-transfer scans plotted vs 2π/b for TTF-TCNQ. A scan through the LA branch is shown for ν = 0.7 THz. Scans through the Kohn anomaly are shown for 1.45, 0.8, and 0.3 THz. The designation M300 means that the points are counted for 300 monitor counts (about 6 min).

As the scans in Fig. 4.15 show, the Kohn anomaly is rather easy to observe at energies around 1.45 THz but becomes weaker at lower energies, finally becoming almost unobservable at about 0.3 THz. Preliminary measurements show that at lower temperatures the Kohn anomaly sharpens considerably and can be observed at lower energies. The position of the Kohn anomaly agrees precisely with the position along b* of the satellite peak observed in the neutron elastic scattering experiments,[7] confirming the $2k_F$ value of 0.295b*.

---

1. H. A. Mook and Charles R. Watson, Jr., *Phys. Rev. Lett.* 36, 801 (1976).

2. Chemistry Division, ORNL.

3. J. Ferraris, D. O. Cowan, V. Walatka, Jr., and J. H. Perlstein, *J. Am. Chem. Soc.* 95, 948 (1973).

4. L. B. Coleman, M. J. Cohen, D. J. Sandman, F. G. Yamagishi, A. F. Garito, and A. J. Heeger, *Solid State Commun.* 12, 1125 (1973).

5. For background information on TTF-TCNQ, see the chapter by A. J. Heeger and A. F. Garito in *Low Dimensional Cooperative Phenomena*, ed. by H. J. Keller, Plenum, New York, 1975.

6. F. Denoyer, R. Comès, A. F. Garito, and A. J. Heeger, *Phys. Rev. Lett.* 35, 445 (1975).

7. R. Comès, S. M. Shapiro, G. Shirane, A. F. Garito, and A. J. Heeger, *Phys. Rev. Lett.* 35, 1518 (1975).

8. S. Kagoshima, H. Anzai, K. Kajimura, and T. Ishiguro, *J. Phys. Soc. Jpn.* 39, 1143 (1975).

9. The uncorrected data are included in a thesis by L. B. Coleman and were communicated to us by A. F. Garito and A. J. Heeger.

PHASE TRANSITIONS IN RbCaF$_3$. II. NEUTRON SCATTERING[1]

W. A. Kamitakahara[2] C. A. Rotter[3]

The 196°K phase transition of RbCaF$_3$ has been identified as a phonon condensation at the *R* point (cubic [111] zone boundary). Above the transition temperature, a ridge of scattering extending from the [110] zone boundary (*M* point) to the *R* point was observed, corresponding to a line of soft phonons from M_3 to R_{25}. Below the transition the scattering at *M* decreases rapidly with temperature, indicating a lattice stabilization which causes the ridge of scattering to disappear.

---

1. Abstract of paper: *Solid State Commun.* 17, 1347 (1975).

2. Present address: Iowa State University, Ames, Iowa.

3. Oak Ridge Associated Universities faculty research participant from West Virginia University, Morgantown, W. Va.

NEUTRON SCATTERING MEASUREMENTS OF THE α-γ TRANSFORMATION IN CERIUM THORIUM ALLOYS[1]

A. S. Edelstein[2]   H. R. Child

Quasi-elastic neutron scattering measurements using 1.0- and 4.4-A neutrons have been made on polycrystalline fcc alloys of $Ce_{1-x}Th_x$ (x = 0.20, 0.266, 0.29). The first alloy undergoes a first-order transformation at approximately 140°K in which the lattice parameter decreases from 5.13 to 4.98A. The second alloy undergoes a second-order transition and critical fluctuations, while the Bragg peaks of the third broaden and shift in position between 140 and 170°K. For $x = 0.2$ at 296°K the q dependence for $0.4 < q < 6$ A^{-1} of the diffuse scattering is in approximate agreement with that of the square of the atomic 4f form factor of cerium. The extrapolation of the diffuse cross section to $q = 0$ gives a value of 260 mb, which is consistent with a value of $\mu = 2.56\mu_B$. With decreasing temperature the magnitude of the diffuse scattering $d\sigma/d\Omega$ for $x = 0.2$ decreases about 30 mb below the transition and is approximately temperature-independent for $5 \le T \le 130$°K. It is surprising that $d\sigma/d\Omega$ is so large at low temperatures in the α state, which has been described as the nonmagnetic state.

---

[1] Abstract of paper: *AIP Conf. Proc.*, in press.

[2] Oak Ridge Associated Universities faculty research participant from the University of Illinois at Chicago Circle, Chicago, Ill.

DIFFUSE SCATTERING IN NIOBIUM-ZIRCONIUM ALLOYS

N. Wakabayashi   J. G. Traylor[1]

For zirconium concentrations greater than 15%, niobium-zirconium alloys seem to have a mixed bcc diffuse-ω phase at low temperatures. Although this lattice instability might be interpreted as an indication of the soft phonons at 2/3 (111), the phonons observed for $Nb_{0.95}Zr_{0.05}$ and $Nb_{0.87}Zr_{0.13}$ are well defined,[2] and the dispersion curves do not exhibit a significant decrease in the frequencies of the longitudinal mode near 2/3 (111), where the frequency is a minimum in this direction. However, we have observed pronounced diffuse scattering near this wave vector for both of these alloys. Figure 4.16 shows the elastic scans in the [111] direction from (111) to (1.8,1.8,1.8) (in units of $2\pi/a$, where a is the lattice constant) for niobium, $Nb_{0.95}Zr_{0.05}$, and $Nb_{0.87}Zr_{0.13}$. In order to take into account the difference in the sample size, the counts are normalized to the relative intensity of the longitudinal phonon at (0.2,0,0), which seems to be unaffected by alloying. The rise in the count near (111) is due to the high background for the low scattering angles. The scan for $Nb_{0.95}Zr_{0.05}$ does not show the background effect because of its large sample size and, hence, good signal-to-noise ratio. Similar scans from several reciprocal lattice points were carried out, and some of the results for $Nb_{0.87}Zr_{0.13}$ are shown in Fig. 4.17*a*, which includes the scan of Fig. 4.16. Figure 4.17*b* shows the lines in the reciprocal space corresponding to the scans in Fig. 4.17*a*.

Information about the nature of the atomic displacements giving rise to the diffuse scattering may be obtained from the position and width of the peak and

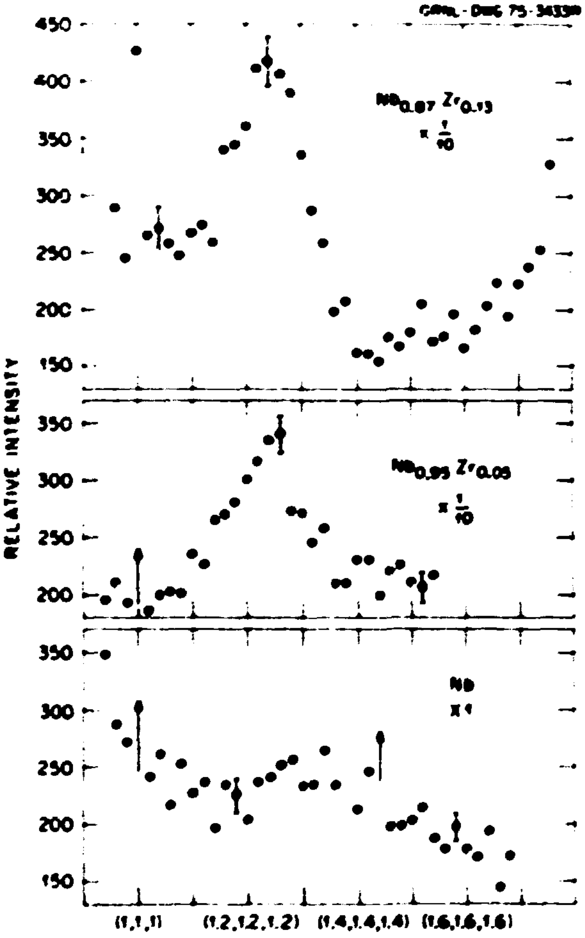

Fig. 4.16. Diffuse scattering peaks observed in niobium and niobium-zirconium alloys.

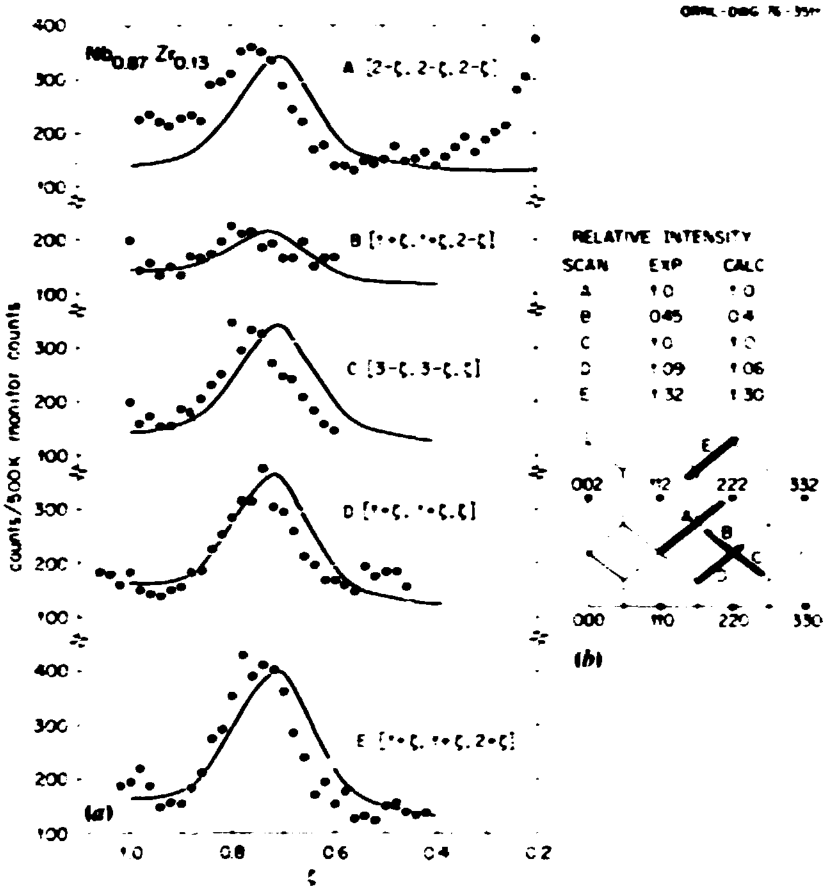

RELATIVE INTENSITY

SCAN	EXP	CALC
A	1.0	1.0
B	0.45	0.4
C	1.0	1.0
D	1.09	1.06
E	1.32	1.30

Fig. 4.17. Diffuse scattering in $Nb_{0.87}Zr_{0.13}$. (*a*) Peaks observed along various ⟨111⟩ directions. Solid lines are calculated intensities. Same background counts and scaling factor are used for all the scans. (*b*) Paths in the reciprocal space corresponding to the scans in *a*.

from the Q dependence of the scattering intensity. The peak position, $q_0 = \frac{3}{4}(111)$, indicates that the periodicity of the atomic displacement is given by $2\pi\, dq_0$, where d is the distance between the planes of atoms perpendicular to the (111) direction, or $d = a/(2\sqrt{3})$. Thus, for $q_0 = (3/4)\sqrt{3}(2\pi/a)$, the number of planes in the repeating unit is 8. However, the observed peak width, $\Delta q = \sqrt{3}(2\pi/a)0.14$, suggests that the size of the region in which the displacements are coherent is represented approximately by 14 planes. Since the periodicity of the microcrystal is comparable with its size, a picture in which the microcrystalline regions are assumed to be randomly embedded in the bcc host crystal may not be a suitable description. Instead, the diffuse scattering may be interpreted as scattering due to a lattice distortion caused by the presence of impurity zirconium atoms, as in the case of Huang scattering. Under certain assumptions, it can be shown that the scattering intensity for q in the (111) direction is proportional to

$$c\,|\mathbf{Q}\cdot\mathbf{e}_L(q)|^2\, e^{\alpha^2|\mathbf{Q}\cdot\mathbf{e}_L(q)|^2}\, W(q)\ . \qquad (1)$$

where c is the impurity concentration, $\mathbf{Q} = \mathbf{q} + \boldsymbol{\tau}$, $\boldsymbol{\tau}$ is the reciprocal lattice vector, $W(q) \propto q^2/\omega_L(q)^4$, $\omega_L(q)$ is the frequency of the longitudinal phonon for wave vector q, and $\mathbf{e}_L(q)$ is the eigenvector of the longitudinal phonon in the (111) direction, namely, $1/\sqrt{3}(111)$ or its equivalent. In principle, α^2 is determined by the amplitude of the atomic displacement. The Q dependence of the peak intensity at $q = q_0$ is determined by the first two factors in Eq. (1). The relative intensities calculated with $\alpha^2 = 0.086(a/2\pi)^2$ are in good agreement, as shown in the table in Fig. 4.17*b*. The q dependence of the intensity, on the other hand, is mainly determined by $W(q)$. The lines in Fig. 4.17*a* represent the intensities calculated from Eq. (1). The same background counts and scaling factor were used for all the scans. The sharp rise in the intensity near $q = 0$ observed experimentally may be explained by the *Umklapp* terms, which are neglected in the approximation and diverge more strongly near $q = 0$ than the normal term given by $q^2/\omega_L^4(q)$. Thus, although the present analysis does not reproduce the details of the experimental observations, it seems that the lattice instability in the niobium-zirconium alloy system could be attributed to a lattice distortion due to the presence of impurity atoms or defects. More work, especially on niobium-molybdenum alloys and tantalum-tungsten alloys, would be quite important in order to understand the nature of the diffuse scattering observed in the present experiment.

---

[1] Iowa State University, Ames, Iowa.

[2] N. Wakabayashi, J. G. Traylor, and S. K. Sinha, "Phonon Spectra in Niobium-Zirconium Alloys," this report.

QUASI-ELASTIC NEUTRON SCATTERING FROM GADOLINIUM

H. R. Child

The study of critical scattering of neutrons from gadolinium metal[1] has been extended to the measurement of quasi-electric scattering of high-energy (about 81-meV) neutrons over a temperature range from 80 to 425°K in an effort to understand this ferromagnetic metal. In gadolinium, the angle ϕ between the ordered magnetic moment and the *c* axis of the hcp crystal[2] is zero at T_C = 291°K, departs from 0 abruptly at T_0 = 232°K, then goes through a broad maximum reaching ϕ = 65° at 183°K, and then decreases to about 32° at 10°K. Low-field magnetization[3] and specific heat[4] data show anomalies at T_0 which led early authors to believe that gadolinium had a spiral structure for $T_0 < T < T_C$ and became ferromagnetic at T_0. Although this interpretation was shown to be incorrect,[2] an explanation of this anomalous behavior is still lacking.

Our previous inelastic scattering results[1] also presented some uncertainties, so the present experiments were undertaken to investigate the isotopic ^{160}Gd crystal under conditions where intensities could be compared over a wide temperature range and where the inelasticity of the scattering could be neglected by using high-energy neutrons. Marshall and Lovesey[5] describe the magnetic scattering cross section near the transition temperature by

$$\frac{d^2\sigma}{d\Omega d\omega} = \text{const}\, f^2(Q)\, k_B T\, \frac{\hbar\omega/k_B T}{e^{\hbar\omega/k_B T} - 1}\, \frac{k_F}{k_I} \times \sum_{\alpha\beta} (\delta_{\alpha\beta} - \hat{Q}_\alpha \hat{Q}_\beta) S^{\alpha\beta}(\mathbf{q}, \omega) \, ,$$

where $\hbar\omega/k_B T\,(e^{\hbar\omega/k_B T} - 1)^{-1}$ is the detailed balance factor, k_I and k_F are the initial and final wave vectors of the neutron, $S^{\alpha\beta}(\mathbf{q}, \omega) = \chi^{\alpha\beta}(\mathbf{q})\, F^{\alpha\beta}(\mathbf{q}, \omega)$ is the Fourier transform of the correlation function $\langle S_0^{\alpha}(0)\, S_R^{\beta}(t)\rangle$ over time and space, and α, β represent *x*, *y*, or *z* coordinates, with $\hat{Q}_\alpha$ the αth component of a unit vector along $\mathbf{Q} = \mathbf{k}_F - \mathbf{k}_I$. If the energy changes $\hbar\omega$ of the neutrons scattered by the sample are small compared with the initial energy of the neutron, the quasi-electric approximation is a valid approximation to the generalized *q*-dependent susceptibility $\chi(q)$ of the sample, since at constant scattering angle, a count will effectively integrate the true energy-dependent scattering over energy at constant q. Since $F(\mathbf{q}, \omega)$, the energy-dependent factor in $S(\mathbf{q}, \omega)$, is defined to be normalized so that the integral over ω of F is unity at constant **q**, the counter performs this integration automatically. In this approximation, then, the intensity is proportional to

$$\sum_{\alpha\beta} (\delta_{\alpha\beta} - \hat{Q}_\alpha \hat{Q}_\beta)\, \chi_{\alpha\beta}(q) = (1 + \hat{Q}_\parallel^2)\, \chi_\perp(\mathbf{q}) + (1 - \hat{Q}_\parallel^2)\, \chi_\parallel(\mathbf{q}) \, ,$$

the parallel sign meaning parallel to the ordered moment. It is necessary to distinguish *x*, *y*, and *z* from ∥ and ⊥ since the ordered-moment direction changes with temperature. When the moment is parallel to the *c* axis, measuring at $\mathbf{Q} = (0, 0, 2 + \zeta)$, $(1 - \hat{Q}_\parallel^2) = 0$, and so only $2\chi_\perp$ will be observed, while for $\mathbf{Q} = (1 + \zeta, 0, 0)$, $\hat{Q}_\parallel^2 = 0$, $\chi_\parallel + \chi_\perp$ will be determined.

Figure 4.18 illustrates the temperature dependence of the peak intensity at points in reciprocal space located at approximately the same magnitude of *q* away from a Bragg peak. The data from which these points were obtained were scans from −0.5 to 0.5 in ζ units perpendicular to the 00ℓ and *h*00 directions with the midpoint of the scan at the **Q** shown. The scans across the 00ℓ line were Lorentzian in shape with peak intensities decreasing with increasing q_z away from (002), while those perpendicular to (*h*00) showed no visible peak at all. Thus the intensity is concentrated in

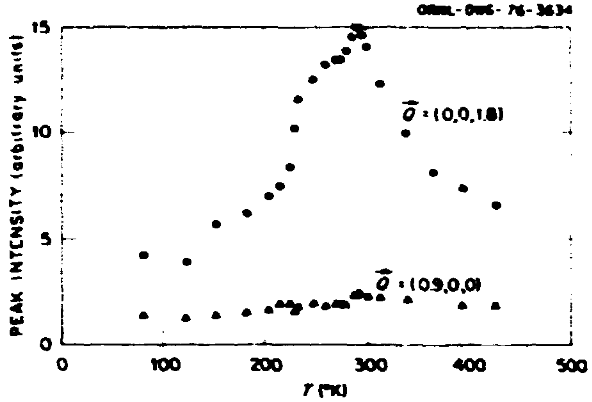

Fig. 4.18. Peak intensity vs temperature from gadolinium at Q near (002) and (100) Bragg reflections.

ridges parallel to $\mathbf{b}_3$ in reciprocal space with peaks around each allowed (00ℓ) Bragg reflection. This indicates that ferromagnetic short-range order exists in the basal planes over distances much larger than between planes even though long-range order exists below T_C = 291°K. The scans near (002) were fitted to Lorentzian by least squares to obtain the width W of these scans which increased with q_z. Interpreting this width as an inverse correlation range ζ, one obtains $\zeta \approx$ 80Å at 80°K, decreasing to around 25 Å at 425°K, and with no dramatic change in ζ at T_C.

The presence of this large amount of short-range order in gadolinium causes problems in the analysis of previous inelastic scattering measurements,[1] since this scattering must be present as a peak, very broad in energy, centered at $\hbar\omega = 0$. The previous measurements were concerned with the dynamic critical behavior and were concentrated too near $\hbar\omega = 0$ to observe this broad peak and therefore failed to reveal it. As a consequence, the previous results must be reevaluated and perhaps extended to include this short-range order in the analysis.

---

1. H. R. Child and R. M. Nicklow, *Solid State Div. Annu. Prog. Rep. Dec. 31, 1974*, ORNL-5028, p. 115.
2. J. W. Cable and E. O. Wollan, *Phys. Rev.* **165**, 733 (1968).
3. H. E. Nigh, S. Legvold, and F. H. Spedding, *Phys. Rev.* **132**, 1092 (1963).
4. M. Griffel, R. E. Skochdopole, and F. H. Spedding, *Phys. Rev.* **93**, 657 (1954).
5. W. Marshall and S. W. Lovesey, chap. 13 in *Theory of Thermal Neutron Scattering*, Oxford University Press, London, 1971.

5. Research Materials

The primary purpose of the Research Materials Program is to develop the necessary techniques required for the growth of ultrahigh-purity and controlled-impurity research specimens of immediate and long-range interest to ORNL and other ERDA installations. The actual choice of materials for examination is based primarily on the potential gain to a fundamental understanding of solids. Progress in understanding the fundamental properties and the ultimate range of properties in many materials has been severely limited in the past by the lack of research quality specimens of high purity and perfection: single crystals are required in many experiments for the unambiguous characterization of various physical phenomena. Certain research materials that have not been investigated previously are now being produced, and new techniques are required for the purification and crystal growth of these new materials.

Information concerning the preparation, availability, and physical properties of high-quality research materials has always been difficult to obtain. Therefore, the Research Materials Information Center was established as a part of the Research Materials Program to provide information to both producers and users on the initial purification, crystal growth, characterization, and availability of research-quality materials. The ready availability of an accurate and up-to-date listing of research materials has served to eliminate much duplication of effort by individual research groups in attempting to produce materials that were already available elsewhere. The simultaneous listing of those research materials that are desired, but are not available, has served to focus the attention of crystal growers on new areas of investigation.

A secondary purpose of the Research Materials Program has been to supply research-quality specimens that are not commercially available to research groups within ORNL and ERDA. During the past few years, due to the redirection of many research programs at ERDA laboratories, much effort has been spent in supplying specimens, which were prepared by techniques that resulted from research conducted in pursuit of the primary purpose of the program. It is appropriate to point out that this procedure cannot be allowed to continue indefinitely as a large effort because the lack of research on new techniques and or new materials will be detrimental to the program.

During the past year a large number of Fe–Cr–Ni alloys were prepared in rod and foil form for irradiation experiments by members of the ORNL Metals and Ceramics Division for a program to develop low swelling stainless steel alloys, and many additional iron- and nickel-based refractory metal alloys were prepared for radiation, tensile test, and phase transformation studies. Samples of lead and lead–0.05 at. % gold alloy were prepared for ground-base and space-flight experiments on surface-tension-induced convection in encapsulated liquid metals in a microgravity environment in the Apollo-Soyuz flight. Extended hot-pressing, zone-melting, and thermal-equilibration experiments were carried out to promote large grain growth in Nb_3Sn. Additional large single crystals of spinel ferrites were grown for use in the ORNL magnetically pulsed neutron time-of-flight spectrometer, and hybrid flux pulling techniques have been initiated in an attempt to produce strontium-substituted Z-ferrite crystals for that facility. Specially doped single crystals of germanium were grown for defect-impurity studies, but the primary emphasis in the semiconducting materials program has been shifted to an investigation of silicon as a candidate for solar photovoltaic conversion; this work is described in the section of this report on Physical Properties of Solids. Equipment has been purchased, constructed, or modified to permit Czochralski and float-zone silicon crystal growth, high-temperature vacuum annealing, high-vacuum evaporation for deposition of metallic films, and a detailed characterization of the electrical properties of silicon ingots, slices, and fabricated devices. Experiments to determine the best techniques for preparing neutron-transmutation-doped (NTD) single-crystal and polycrystalline silicon have been a major part of this investigation.

RESEARCH MATERIALS PROGRAM

J. W. Cleland

The purpose of this program is to develop techniques as required for the initial purification, crystal growth, and characterization or analysis of research specimens of a size and quality as required in programs on materials research of interest to ERDA. The Research Materials Information Center (RMIC) assists in identifying those materials for which a need exists and in supplying information on materials already available. Selected samples are loaned to cooperating research groups for comparative measurements that aid in characterizing these materials. Examples are listed in Table 5.1.

Table 5.1. Loan of single crystals for research outside the Research Materials Program for 1975

Material	Type of study	To whom sent	Organization
Nb	Superconductivity	D. Christen	ORNL
Nb	Scattering experiments	B. Appleton	ORNL
Nb	Vacuum annealing	A. Pasto	ORNL
Nb	X-ray diffraction	H. Yakel	ORNL
Nb	Superconductivity	A. DasGupta	ORNL
Nb	Radiation damage	W. Schilling	Julich, Germany
Nb	Surface superconductivity	A. DasGupta	Karlsruhe, Germany
Nb	Hydride formation	S. Reidinger	Brookhaven
Nb	Plastic deformation	R. Arsenault	Univ. of Maryland
Nb–Zr	Neutron diffraction	N. Wakabayashi	ORNL
Nb–Zr	Radiation damage	J. Narayan	ORNL
Ni	Radiation damage	R. Carpenter	ORNL
Ni	Radiation damage	K. Farrell	ORNL
Ni	Oxygen content studies	G. Peterson	ORNL
Ni	X-ray fluorescence	L. Hulett	ORNL
V	Low-temperature radiation damage	R. Coltman	ORNL
V	Hydride formation	S. Reidinger	Brookhaven
Ta	Scattering experiments	B. Appleton	ORNL
Ta	Hydride formation	S. Reidinger	Brookhaven
Mo	Scattering experiments	B. Appleton	ORNL
Mo–Re	Inelastic neutron scattering	S. Sekula	ORNL
Ti	Radiation damage studies	K. Farrell	ORNL
Re	Radiation damage studies	K. Farrell	ORNL
Nb–V	X-ray scattering and tensile test experiments	C. Sparks	ORNL
Fe–Cr–Ni	Neutron irradiation and ion bombardment	L. Mansur	ORNL

Table 5.1 (continued)

Material	Type of study	To whom sent	Organization
Ni–Al	Radiation damage and phase-transformation studies	R. Carpenter	ORNL
Fe–Ni	Radiation damage and tensile test specimens	C. White and R. Clausing	ORNL
Fe–Cr	Radiation damage and tensile test specimens	C. White and R. Clausing	ORNL
Fe–V	Radiation damage and tensile test specimens	C. White and R. Clausing	ORNL
Fe–Nb	Radiation damage and tensile test specimens	C. White and R. Clausing	ORNL
Fe–Ti	Radiation damage and tensile test specimens	C. White and R. Clausing	ORNL
Fe–Mo	Radiation damage and tensile test specimens	C. White and R. Clausing	ORNL
Fe–Mn	Radiation damage and tensile test specimens	C. White and R. Clausing	ORNL
Fe–W	Radiation damage and tensile test specimens	C. White and R. Clausing	ORNL
Ni–Cr	Radiation damage and tensile test specimens	C. White and R. Clausing	ORNL
Ni–V	Radiation damage and tensile test specimens	C. White and R. Clausing	ORNL
Mo–Ti	Radiation damage and tensile test specimens	C. White and R. Clausing	ORNL
Mo–W	Radiation damage and tensile test specimens	C. White and R. Clausing	ORNL
V–Ti	Radiation damage and tensile test specimens	C. White and R. Clausing	ORNL
V–Mo	Radiation damage and tensile test specimens	C. White and R. Clausing	ORNL
V–Ni	Radiation damage and tensile test specimens	C. White and R. Clausing	ORNL
V–Cr	Radiation damage and tensile test specimens	C. White and R. Clausing	ORNL
Fe–Cr–Ti	Radiation damage and tensile test specimens	C. White and R. Clausing	ORNL
Ge crystal	Far infrared laser window	J. Waldman	ORNL
Si wafers	Neutron scattering	D. Braski	ORNL
Si wafers	Diffusion experiments	J. Roberto	ORNL
Si wafers	Diffusion experiments	R. Perkins	ORNL
Si wafers	Materials studies	S. Spooner	ORNL
Si wafers	Materials studies	D. Zehner	ORNL
Si crystals	Internal zone growth	G. Clark	ORNL
Si crystals	Negative-ion source	G. Alton	ORNL
Neutron-transmutation-doped Si ingots and/or wafers	Electron spin resonance	M. Abraham	ORNL
Neutron-transmutation-doped Si ingots and/or wafers	Scanning electron microscope	L. Hulett	ORNL
Neutron-transmutation-doped Si ingots and/or wafers	Radiation damage annealing	R. Hall	General Electric Co.
Neutron-transmutation-doped Si ingots and/or wafers	Power device fabrication	R. Hysell	General Electric Co.
Neutron-transmutation-doped Si ingots and/or wafers	Avalanche detector fabrication	R. Hysell	General Electric Co.
Neutron-transmutation-doped Si ingots and/or wafers	Avalanche detector studies	G. Huth	UCLA Nuclear Medicine Laboratory
Neutron-transmutation-doped Si ingots and/or wafers	Avalanche detector studies	W. Seibt	UCLA Nuclear Medicine Laboratory

Table 5.1 (continued)

Material	Type of study	To whom sent	Organization
Neutron-transmutation-doped Si ingots and/or wafers	Avalanche detector studies	P. Tove	Uppsala University, Sweden
Neutron-transmutation-doped Si ingots and/or wafers	Photovoltaic device fabrication	P. Iles	Optical Coating Laboratories, Inc.
Neutron-transmutation-doped Si ingots and/or wafers	Resistivity measurements	P. Raccah	Yeshiva Univ.
Neutron-transmutation-doped Si ingots and/or wafers	Photoelectroreflectance measurements	F. Pollack	Yeshiva Univ.
Neutron-transmutation-doped Si ingots and/or wafers	Materials studies	K. Benson	Western Electric, Allentown
Neutron-transmutation-doped Si ingots and/or wafers	Materials studies	J. Stone	Northrop Corp.
Neutron-transmutation-doped Si ingots and/or wafers	*p-n* junction studies	T. Yep	Varian Associates
MgO	Neutron diffraction	H. G. Smith	ORNL
MgO	Diffusion	D. Kingery	MIT
MgO	Lattice parameter	V. Guerary	Univ. Munich
MgO	Deformation	T. J. Turner	Wake Forest Univ.
MgO	Fracture properties	P. S. Nicholson	McMaster Univ.
MgO	Radiation damage	J. Bunch	Los Alamos Scientific Laboratory
MgO	EPR	A. Chatelain	Ecole Polytechnique, Lausanne, Switzerland
MgO	Positron annihilation	W. Mallard	Georgia State Univ.
MgO	Sulfur diffusion	T. Chase	ANL
MgO	Neutron monochromator	A. Freund	Grenoble (I.L.L.)
CaO	Crystal growth experiment	C. B. Finch	ORNL
CaO	Magnetic resonance	G. Ries	Grenoble (I.L.L.)
CaO	Luminescence	L. Vance	Australian National Univ.
CaO	Photoconductivity	G. Summer	Oklahoma State Univ.
CaO	Positron annihilation	W. Mallard	Georgia State Univ.
CaO	Light scattering	D. M. Hwang	Tsing-hua Univ., Taiwan
CaO	EPR	H. Bill	Univ. of Geneva, Geneva, Switzerland
SrO	EPR	W. P. Unruh	Univ. of Kansas
UO_2	Raman	P. J. Colwell	Michigan State Univ.
$ThO_2:Yb^{3+}$	Thermal luminescence	P. J. Harvey	Chalk River Nuclear Laboratory

RESEARCH MATERIALS INFORMATION CENTER

T. F. Connolly   G. C. Battle, Jr.

In 1975 the RMIC answered about 650 questions, two-thirds of them concerning the preparation and properties of materials and one-third seeking information on their availability. The publication, in July, of the RMIC International Directory of Solid State Materials Production and Research (updating a similar 1972 compilation) would be expected to cut down the number of inquiries on the availability of materials, since it describes and indexes by materials about 600 materials science projects in 41 countries.

Work is continuing on the computerizing of special bibliographies on refractive indices and on laser window, filter, and mirror materials.

PREPARATION OF HIGH-PURITY METAL AND METAL-ALLOY SPECIMENS FOR RADIATION DAMAGE INVESTIGATIONS

R. E. Reed[1]   H. E. Harmon

One of the primary objectives of the metals and metal-alloys group during the past year has been to supply programs within ORNL and ERDA with research-quality specimens that are not commercially available. Twelve high-purity alloys of the Fe-Cr-Ni system were prepared by the same techniques reported previously[2] for neutron irradiation and ion bombardment studies undertaken by members of the Metals and Ceramics Division in a program to develop a stainless steel alloy that would not show appreciable swelling after irradiation. Twenty alloys of Fe-Ni, Fe-Cr, Fe-V, Fe-Nb, Fe-Ti, Fe-Mo, Fe-Mn, Fe-W, Fe-Cr-Ti, Ni-Cr, Ni-V, Mo-Ti, V-Ti, V-Mo, V-Ni, V-Cr, Mo-Ti, and Mo-W were prepared as 30-g melts and rolled into 0.30-in. sheets prior to fabrication of tensile test specimens for other radiation damage studies by members of the Metals and Ceramics Division. Twelve additional nickel-based alloys, including Ni-Al, Ni-Ti, Ni-V, and Ni-Mo, were prepared for the Metals and Ceramics Division as 50-g melts from International Nickel Corporation grade 270 nickel, Alcoa reactor-grade aluminum, Bureau of Mines vanadium, Thermo Electron Corporation molybdenum, and titanium as supplied in crystal bar form. These alloys were swaged to provide 0.125-in.-diam rods and will be used in radiation damage and phase-transformation studies. Table 5.1 also lists many metal or refractory-metal single crystals as supplied on request from stock or produced on request for the type of study indicated.

APOLLO-SOYUZ TEST PROJECT MATERIALS EXPERIMENT "SURFACE TENSION INDUCED CONVECTION IN ENCAPSULATED LIQUID METALS IN MICROGRAVITY"

R. E. Reed[1] H. L. Adair H. E. Harmon

Skylab experimental results have indicated that gravity-induced convection is essentially eliminated in space processing; however, convection effects caused by surface tension variations may become an important factor. Surface tension gradients could be caused by thermal or concentration differences in the molten metal, which are not gravity-dependent factors. Experiments performed on Apollo 14 and 17 revealed convection effects due to thermally induced surface tension gradients. The objective of the present experiment is to determine if similar surface-tension-induced convection effects can result from concentration gradients formed by diffusion of one metal species into another.

A diffusion couple of lead and lead 0.05 at. % gold alloy was prepared and encapsulated in wetting and nonwetting capsule materials. During the Apollo-Soyuz flight, these samples were fused in a microgravity environment. A schematic diagram of the arrangement of the specimens in the multipurpose electric furnace aboard the Apollo laboratory is shown in Fig. 5.1.

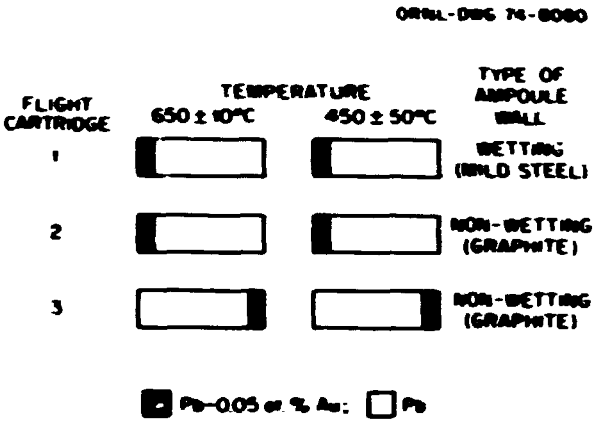

Fig. 5.1. Schematic arrangement of specimens in ASTP MA-041.

Because of the longitudinal heat flow in the furnace upon heating and cooling, the specimens probably melted from left to right, as viewed in the schematic drawing, and solidified in the reverse direction. Our observations thus far have been on space-flight samples and ground base samples contained in nonwetted graphite capsules; the samples were oriented as indicated for flight cartridge 2 in Fig. 5.1. Both space-flight and ground base specimens underwent similar temperature-time histories.

After removal from the graphite-lined capsule, each specimen was potted in epoxy and sectioned longitudinally. The epoxy was then dissolved from the samples, and a sample half from each specimen together with four lead-gold calibration disks was mounted in a 5-cm-diam epoxy mount. Each mount was then metallographically polished and irradiated in the Bulk Shielding Reactor to produce some ^{198}Au throughout the sample. The distribution of gold in the samples can be determined by exposing the polished surfaces of the specimens to a nuclear emission plate that is sensitive to the beta disintegrations of the radioactive ^{198}Au isotope. If no convective stirring effects were present while the samples were molten, then a concentration-distance profile as predicted by normal diffusion of the gold in the lead would be found; however, if convective stirring effects resulted from surface tension variations

---

[1] Deceased.

[2] R. E. Reed, E. D. Bolling, and H. E. Harmon, *Solid State Div. Annu. Prog. Rep. Dec. 31, 1974*, ORNL-5028, p. 122.

caused by gold concentration gradients, these would also be discerned by the autoradiograph technique.

Preliminary examination of the flight samples indicated that a normal diffusion-predicted concentration distance profile of gold was obtained in the sample. The gold concentration distance data have yet to be quantified, but autoradiographs compare favorably with diffusion distance predictions based on the zinc self-diffusion data obtained in Skylab experiment M-558; this comparability would suggest that the diffusion of gold in lead was typical of liquid diffusion. Additional evaluation of all flight samples will be needed to explain the observed curved gold diffusion interface and evidence of diffusion along the cylindrical surface of the melt. Quantitative gold distribution data will be obtained from densitometer measurements of the autoradiographs and will be used to explore these phenomena as well as to determine if surface-tension-induced convection effects were present.

---

[1] Deceased.

Fig. 5.2. Cross section of a thermally equilibrated niobium plus tin sample. Etched, 50X.

GRAIN GROWTH AND THERMAL STABILITY OF Nb_3Sn

U. Roy   W. E. Brundage

Single crystals of Nb_3Sn are needed in order to investigate the lattice dynamics and intrinsic superconductivity. Whereas the feasibility of crystal growth is suggested by the existence of only one stable phase at high temperatures, the compound melts incongruently, and the tin constituent is highly volatile at the peritectic temperature (2130°C). Initial efforts were therefore directed to finding a suitable container. A cold-pressed finger of Nb_3Sn was placed in a snug-fitting graphite tube, and a short inductively heated zone was passed along the length of the tube. Metallographic examination showed decomposition and extensive carbide formation. The critical temperature T_c was 15.5 K. The extent of chemical interaction and thermal stability was further studied by hot-pressing Nb_3Sn powders (60 mesh) at 8000 psi for 10 min at 100°C intervals between 1500 and 1900°C. The T_c remained fairly constant at 17.9°K. The etched and anodized samples show a network of grain formations. Although the inside grain consists of Nb_3Sn, the boundaries contain many phases (NbO, excess tin, free niobium). Regularity in grain shape indicates secondary grain growth.

Additional experiments were performed on thermal equilibration and grain growth using a mixture of niobium and tin in an electron-beam-welded niobium cavity. The samples were vacuum-annealed at 1900°C for 22 hr. Figure 5.2 shows a typical cross section. The excess tin attacks the niobium jacket, resulting in porosity due to the Kerkendall effect as well as a volume change due to compound formation. The inner core consists of large grains up to 1 mm in size. Extended hot-pressing near the melting point, internal zone melting, and thermal equilibration will be continued to effect larger grain growth.

FLUX GROWTH OF STRONTIUM-SUBSTITUTED Z FERRITES

U. Roy   W. E. Brundage

The hexagonal Z ferrites of the chemical formula $Sr_{3-x}Ba_xZn_2Fe_{24}O_{41}$ exhibit a helicoidal spin ordering which is magnetic-field-dependent. Large crystals of the compound corresponding to $x = 0.6$ are needed for the ORNL time-of-flight neutron monochromator and chopper. Growth attempts have been made in accordance with the prescription of Savage and Tauber.[1] Mixtures of oxides and carbonates were slowly heated to 1450°C and then cooled at 2 to 5°C/hr down to 1100°C. Single crystals with linear dimensions up to 10 mm were obtained. They exhibit characteristic hexagonal growth morphology and lattice parameters. Chemical analysis, on the other hand, shows that strontium and barium comprise only 50% of the intended charge. It is anticipated that the stoichiometry will improve if the compound is synthesized before growth. Crystal growth is also being attempted by solidification in a platinum-lined tantalum bomb and hybrid flux pulling.

---

[1] R. O. Savage and A. Tauber, *J. Am. Ceram. Soc.* 47, 13 (1964).

Table 5.2. Chemical synthesis, elemental substitution, and T_c of spinel titanates

Compound	T_c (onset) (K)	T_c (onset), postanneal (K)	ΔT_c (K)	ΔT_c, postanneal (K)	Remarks
$LiTi_2O_4$	11.4		2.6		Arc-melted in Ar plus H_2
$LiTi_2O_4$	11.35		2.95		Same sample measured after ~6 weeks
$CaTi_2O_4$	<1.4				
$(Ca_{0.05}Li_{0.9})Ti_2O_4$	11.4	10.85	7.0	9	
$(K_{0.03}Li_{0.97})Ti_2O_4$	11.55	10.7	~7.2	4.5	
$(K_{0.1}Li_{0.9})Ti_2O_4$	11.25	10.5	7.0	3	
$LiTiZrO_{4.5}$	<1.4				
$Li(Ti_{1.5}Zr_{0.25})O_4$	10.9	8.5	~7.0	4.5	
$LiTi_2O_4 + Sn\ (\sim 1\%)$	11.65	11.1	~7.5	3	
$(Na_{0.1}Li_{0.9})Ti_2O_4$	11.8	10.8	7.6	4.0	
$(Rb_{0.1}Li_{0.9})Ti_2O_4$	11.3	11.3	~7.1	1.5	
$Li(Ti_{1.9}Al_{0.1})O_4$	12.7	11.4	~8.2	2.0	
$LiTi_2O_4$	11.3	11.35	~7	2	

ISOMORPHOUS SUBSTITUTION AND SUPERCONDUCTIVITY IN SPINEL TITANATES

U. Roy   W. E. Brundage
D. K. Christen   S. T. Sekula

A number of spinel titanates based on the chemical formula $LiTi_2O_4$ have been synthesized, in which partial isomorphous substitutions were made for lithium and titanium sites. Powders of reagent-grade Li_2CO_3, $Li_2Ti_2O_5$, Ti_2O_3, TiO_2, Al_2O_3, Na_2CO_3, K_2CO_3, and LiOH were mixed to the desired stoichiometry, cold-pressed, and arc-melted in argon containing 4% dry hydrogen. An ac susceptibility technique, described previously,[1] was used to measure the transition temperature T_c. Most samples exhibited a rather broad transition width (ΔT_c), which indicated an inhomogeneity due to the preparation technique. Samples were wrapped individually in copper foils and encapsulated in quartz ampoules, which were filled with argon and hydrogen. A homogenization anneal at 900°C, followed by slow cooling, improved the material quality. Table 5.2 presents the results of T_c measurements on these cast and postannealed samples. The results are in general agreement with previous investigations.[2] Several partial substitutions have resulted in sharp transitions to the superconducting state without degradation of the transition temperature. Confirmation of these preliminary results is presently under way by means of chemical analysis, x-ray studies, and metallography. We plan to continue a systematic investigation of the fundamental superconducting properties of these materials as a function of crystal chemistry and preparation technique.

---

[1] D. K. Christen, U. Roy, W. E. Brundage, and S. T. Sekula, *Solid State Div. Annu. Prog. Rep. Dec. 31, 1974*, ORNL-5028, p. 48.

[2] D. C. Johnston, H. Prakash, W. H. Zachariasen, and R. Viswanathan, *Mater. Res. Bull.* 8, 777 (1973).

SUPERCONDUCTIVITY IN FILAMENTARY $LiTi_2O_4$

U. Roy   A. DasGupta[1]   C. C. Koch[1]

One- and four-core composite wires of filamentary $LiTi_2O_4$ were prepared from an equimolar mixture of $Li_2Ti_2O_5$ (K & K Laboratories, Inc.) and Ti_2O_3 (Ventron Alfa Products) powders, swaged down in copper tubes, by reaction sintering at 900°C for 24 hr. The critical temperature T_c was about 11.4 K, as determined by an ac susceptibility technique. Preliminary resistive measurements were made at 4.2 K in a transverse applied magnetic field up to about 50 kOe. The apparent critical current density J_c was 2 to 10 A/cm² at $H = 2$ kOe in these porous specimens, and H_{c2} was about 4.0 kOe. Calculations based upon the Goodman–Gor'kov relationship[2] and the available normal-state resistivity data[3] suggest that a semiconductor-to-metal transition precedes the metal-to-superconductor transition at T_c. Work is in progress to prepare $LiTi_2O_4$ by alternative techniques such as hot-pressing, solidification from the melt, and flux growth in order to study the superconducting properties of this oxide compound.

---

[1] Metals and Ceramics Division, ORNL.

[2] B. B. Goodman, *IBM J. Res. Dev.* 6, 63 (1962).

[3] D. Johnston, Ph.D. thesis, University of California, San Diego, 1975.

SILICON–LITHIUM INTERACTIONS IN GERMANIUM

J. W. Cleland

Last year[1] it was reported that certain impurity interactions occur in germanium during crystal growth and sample preparation and that the nature and extent of these interactions must be determined before one can hope to understand any defect-impurity interactions in irradiated germanium. Experimental results were presented to indicate that dissociated oxygen is the only well-established precipitation site for lithium diffused into germanium and that the role of dislocations, hydrogen, or copper as a lithium precipitation site appears to be negligible.

Westbrook,[2] during an examination of the role of silicon or silicon oxide clusters on the rate of trapping in radiation-detector-quality germanium, produced some single-crystal ingots of high-purity germanium that contained a known concentration of silicon. In the present experiments, germanium samples were obtained which contained about 10^{17}, 10^{16}, or essentially no silicon atoms per cubic centimeter, and lithium was diffused in the same manner as previously reported.[1] Figure 5.3 is a graph of the donor concentration as determined at 77 K vs the time of lithium precipitation at 300 K. These data indicate a rapid decrease in the donor concentration due to the diffused lithium if silicon is present in the germanium, but they do not indicate the formation of any type of precipitation site that remains electrically active. It is still evident that

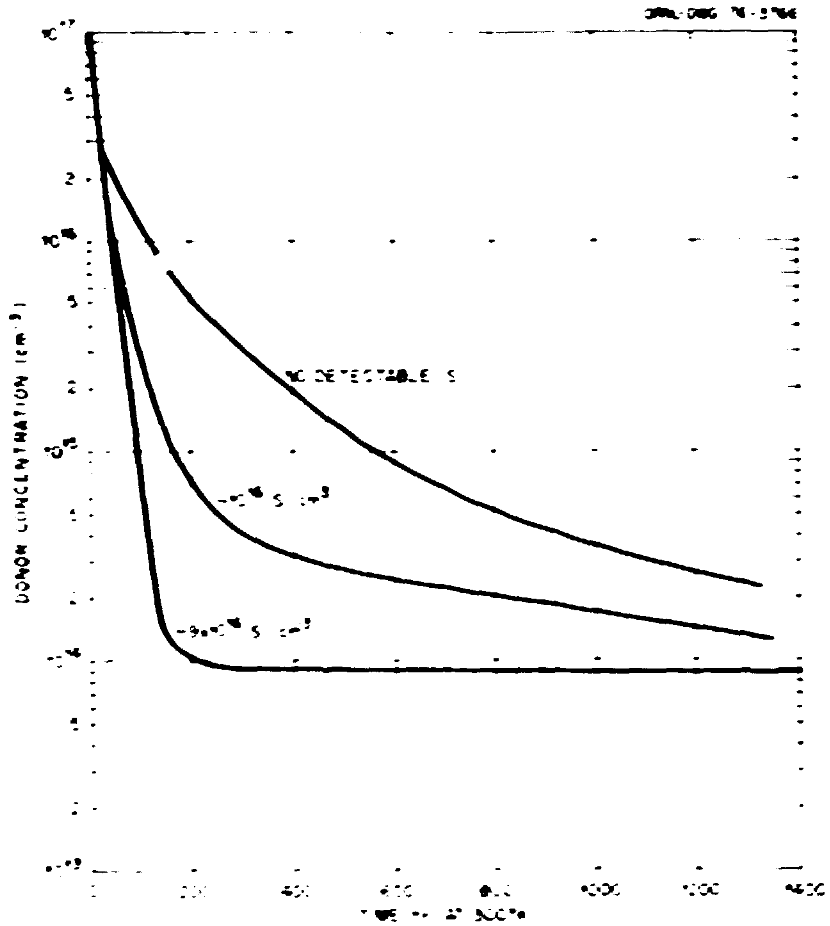

Fig. 5.3. Excess donor concentration at 300 K vs time at 300 K after lithium saturation at 670 K of germanium with about 9 × 10^{18}, 1 × 10^{18}, or no detectable silicon atoms per cubic centimeter.

dissociated oxygen is the only well-established electrically active precipitation site for lithium in germanium but that ≳10^{17} lithium atoms per cubic centimeter can be present in germanium, electrically inactive under certain conditions but electrically active under certain other conditions.

---

1. J. W. Cleland, *Solid State Div. Annu. Prog. Rep. Dec. 31, 1974*, ORNL-5028, p. 126.
2. R. D. Westbrook, *Nucl. Instrum. Methods* **108**, 335 (1973).

LITHIUM DIFFUSION AND PRECIPITATION IN SILICON

R. T. Young   J. W. Cleland

Pell[1] and Ferman,[2] in studies of the precipitation of lithium diffused into silicon of high oxygen concentration, found that the diffusion-limited precipitation model proposed by Ham[3] was not obeyed. They observed two decay constants for silicon containing >10^{17} atoms of oxygen per cubic centimeter and found that the free-carrier concentration at the discontinuity in the decay curves was equivalent to the oxygen content. A systematic study of the oxygen concentration in silicon has been carried out using this technique[4] to a lower limit of sensitivity of about 10^{15} cm^{-3}, and Ham's theory was found to be valid for silicon of low oxygen content.[4]

Previous investigators[1-4] assumed that the carrier mobility would not be affected by the precipitation process, so they used resistivity measurements only to infer the free-carrier concentration. In the present experiments, we diffused lithium at 450 to 620°C into samples of high-purity dislocation-free float-zone silicon with an oxygen concentration less than 5 × 10^{15} cm^{-3} as determined by infrared absorption measurements. The van der Pauw technique was used to determine the carrier concentration and mobility at room temperature as a function of time after lithium diffusion at an elevated temperature T_D and long-term annealing at 130 C.

Figure 5.4, which is a graph of the carrier concentration vs time, indicates that the initial diffused lithium concentration is a strong function of T_D and that the precipitation relaxation time is highly dependent on T_D, but there is no correlation between the breakpoint or discontinuity in the decay curves that can be attributed to the oxygen concentration in these experiments.

Figure 5.5, which is a graph of the carrier mobility vs carrier concentration, indicates that the mobility is well behaved for a sample with lithium diffused at 620 C but that the lithium precipitation behavior is markedly different for a lower T_D in that there is a pronounced mobility minimum during the precipitation process.

These data would suggest that there is a difference in the lithium precipitation mechanism or site which depends on T_D. Seto, in a study of the electrical properties of ion-implanted boron in polycrystalline silicon films (polysilicon), observed a minimum in the mobility which he attributed to carrier trapping at grain boundaries. He concluded that carrier trapping would produce a potential barrier that would exhibit a maximum value as a function of increasing dopant concentration, with a corresponding reduction in the mobility, until the grain boundaries were saturated at very high total dopant concentrations.

Fig. 5.4. Excess donor concentration at room temperature vs time of annealing at 130 C after lithium-saturation of silicon by diffusion at 450, 550, and 620 C.

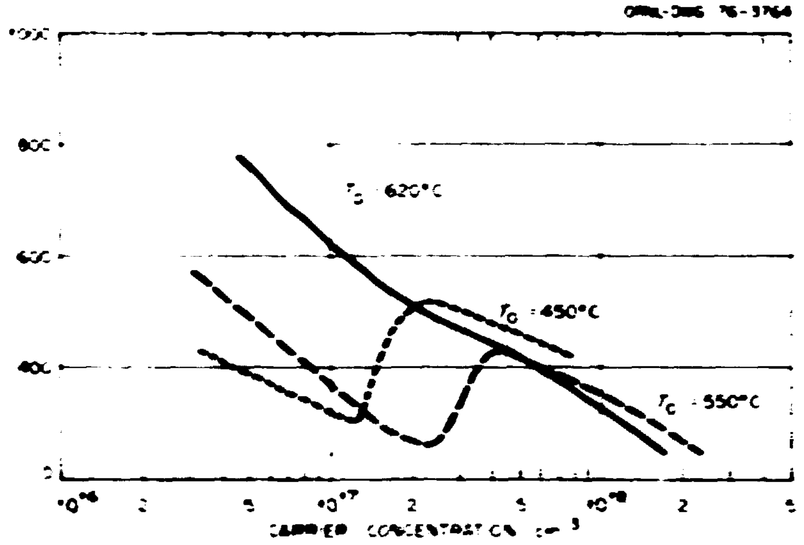

Fig. 5.5. Carrier mobility vs carrier concentration after lithium diffusion of silicon at 450, 550, and 620°C.

Our experiments are in progress, but the results to date suggest that lithium precipitation at vacancy clusters may produce an electron trap with a space charge that serves to decrease the carrier mobility, whereas lithium precipitation on oxygen or on vacancy-oxygen pairs does not produce an electron trap or space-charge region. This type of result is also postulated for Ge(Li) radiation detectors. It is anticipated that lithium diffusion and precipitation experiments on polysilicon may be of value in a determination of the role of the electrical property effect of grain boundaries and in studying the mechanism of any enhanced diffusion of impurities along dislocations or grain boundaries.

---

1. E. M. Pell, p. 261 in *Solid State Physics in Electronics and Telecommunications*, vol. 3, Academic Press, New York, 1960.
2. J. W. Lerman, *J. Appl. Phys.* **39**, 3771 (1968).
3. F. Ham, *J. Phys. Chem. Solids* **6**, 335 (1958).
4. M. I. Iglitsyn, G. P. Pekhtere, and G. A. Lazareva, *Sov. Phys. - Solid State* **6**, 2598 (1965).
5. A. J. R. de Kock and P. J. [illegible], *J. Appl. Phys.* **44**, 2816 (1973).
6. J. Y. W. Seto, *J. Appl. Phys.* **46**, 5247 (1975).

RECOMBINATION RATE IN SEMICONDUCTORS

R. D. Westbrook T. H. Polgreen[1]

When measuring minority-carrier diffusion length or lifetime in a thin slice or near the surface of a sample, it is necessary to eliminate or minimize surface recombination effects. The surface photovoltage (SPV) method[5,6] is under investigation at ORNL[6] because it is a nondestructive test and therefore is an attractive method for characterizing germanium or silicon that is undergoing various material studies such as radiation and annealing experiments. In principle, the SPV method is independent of interferences from surface states as long as they are stable and do not drift during measurement. As it often is necessary to enhance the SPV signal to bring it above the noise level, the surface of an *n*-type sample is driven as far toward the *p*-type condition as possible, and similarly a *p*-type sample is given an *n*-type surface. These surface treatments are done by wet chemistry and are oxidizing and reducing, respectively. We have found that for purposes of this experiment *p*-type surfaces of silicon are more stable with time than *n*-type surfaces, and therefore we achieve more reproducible results with *n*-type samples. Even so, some samples require hours or perhaps a day or two before becoming stable enough for reliable measurement.

There appears to be no effect of crystal orientation on the measured value of lifetime. Both *n*-type and *p*-type crystals of silicon were measured on all three primary faces, (100), (110), (111), with no assignable variations.

The real difficulty in interpretation of the data occurs in some high-resistivity samples. One of the boundary conditions is that the concentration of injected carriers must be small (≤ 0.01) compared with the thermal equilibrium concentration. Violation of this condition results in a nonlinear plot of the data and an erroneously large value of diffusion length, or lifetime. Therefore in high-resistivity samples it is mandatory to run the experiment at several decreasing intensities until constant results are obtained. While most samples yield to this procedure, a significant number do not. We find both *n*- and *p*-type silicon samples that will not reach a stable value of lifetime by this technique, and as yet we have not discovered an explanation. It is always tempting to blame problems in lifetime interpretation on some arcane property of trapping centers, but so far we have found no substantiating evidence of similar problems when examining these samples with the more conventional photoconductive decay method.

---

1. ORAU undergraduate research trainee from Carleton College, Northfield, Minn.
2. E. O. Johnson, *J. Appl. Phys.* 28, 1349 (1957).
3. A. M. Goodman, *J. Appl. Phys.* 32, 2550 (1961).
4. S. C. Choo and S. C. Sanderson, *Solid State Electron.* 13, 609 (1970).
5. W. E. Phillips, *Solid State Electron.* 15, 1097 (1972).
6. R. D. Westbrook, *Solid State Div. Annu. Prog. Rep. Dec. 31, 1974*, ORNL-5028, p. 125.

SEMICONDUCTOR CRYSTAL FURNACES

R. D. Westbrook   C. C. Robinson

Entering the field of research in semiconductor silicon has necessitated construction and rebuilding of a number of furnaces and heat-treating facilities to accommodate anticipated crystal growth and annealing requirements. We now have equipment for both Czochralski and float-zone crystal growth and for high-temperature vacuum annealing up to 1550°C. A high-vacuum evaporation system is ready for application of various metallic films, and a start has been made on attaining instrumentation for detailed characterization of the electrical properties of silicon samples.

6. Isotope Research Materials

For 16 years the preparation of special chemical and physical forms of separated, high-purity isotopes has been the province of the Isotope Research Materials Laboratory (IRML). Research samples using nearly all stable isotopes and many radioisotopes (especially the actinide elements) have been made to customer specifications in support of ERDA research programs throughout the United States and in foreign countries. In addition to satisfying isotope research materials requirements for ERDA programs, IRML provides an international service of sample preparation supplying over 100 universities and commercial firms in more than 30 countries with samples unavailable from commercial sources. During the past year nearly 3000 samples were prepared for the international scientific community. Distribution of prepared samples and allocation of services is required by ERDA to be on a full-cost recovery basis, and therefore IRML has an integral sales function with associated inventory and revenue accounting operations. The research and development activities are funded programmatically through the ERDA Division of Physical Research, whereas the remainder of operating support accrues directly from sales of materials and services.

The technical functions of IRML can be categorized generally into materials research and development, inorganic chemical conversions, preparation of special physical forms, radioisotope source preparations, purifications, single-crystal and epitaxial growth studies, and development of analytical techniques (usually nondestructive methods) compatible with characterization of thin film samples. From inception, IRML has prepared subatomic particle accelerator targets and targets for study of neutron interactions. Technologies of physical vapor deposition, chemical vapor deposition, mechanical rolling of metals, distillation of metals, metal reductions, arc melting, levitation melting, sintering, and myriad other metallurgical and chemical processes are employed to produce unique isotope-containing samples. In all operations, specific efforts to improve and/or maintain conservation of valuable isotopes is of vital importance since the monetary value of isotopes consumed during a preparation may be many times the cost of assigned manpower and ancillary expense.

The unique technical capabilities developed for isotope sample preparations have been frequently applied to the performance of activities not directly related to materials, but rather to the development of technology in support of programs such as waste management, NASA space research, a variety of classified ERDA programs, reactor dosimetry, and preparation of reaction rate standards. For example, during this past year a program was completed in which measurements of the separation factor for hydrogen and deuterium (with calculations for tritium) were made in a diffusive system for the purpose of developing a process to remove tritium from reactor or fuel reprocessing plant effluents. Further work in this category will be initiated in the near future using an aqueous rather than a gaseous process. Technologies developed for thin film preparations in IRML are directly applicable to development programs in solar cell technology, preparation of laser reflection surfaces, optics, and microcircuitry.

Use of stable isotopes in research and development activities related to the physical sciences is well documented, especially in areas of nuclear structure studies, diagnostics of neutron spectra in reactor regimes, chemistry, metallurgy, and solid state physics. Because of present-day interest in high-energy physics research, new technologies have been required to transform large (multigram) quantities of separated isotopes into thick, large-area target samples, whereas developmental efforts in earlier years were concentrated on preparing ultrathin self-supported films suitable for Van de Graaff accelerator experimentation.

Procedures developed for handling stable isotope materials are usually equally applicable to radioisotope sample and source preparation. Adaptation of preparative methods to radioisotopes generally implies modifications for remote operations (hot-cell enclosure of processing equipment) or at least glove-box operations required for personnel protection. Almost all of the above noted operations have been adapted for radioisotope processing. Recently, preparation of ^{252}Cf targets and sources has been reinstated as a standard IRML function after more than three years' discontinuance of such activity. An existing hot-cell facility has been adapted in which evaporation-condensation and self-transfer depositions of californium can be performed without difficulty for quantities of ^{252}Cf up to 10 mg.

REACTOR DOSIMETERS

E. C. Quinby   E. H. Kobisk

Dosimetry is used routinely in EBR-II and other reactors to map and unfold the neutron spectrum by determining neutron energy and flux at specific points throughout the core and reflector regions. Nuclides suitable for transmutation or fission into gamma-emitting isotopes are used to determine the neutron energy frequency distribution; this is a powerful control tool in conjunction with in-core experiments. Subsequent counting of gamma emissions from specific transmuted nuclides or fission products is used to compute the neutronics. The initial nuclidic samples used for dosimetry must be of high purity to avoid extraneous radiations and must be capable of definition to within one error less than 1% in isotope content if sufficiently accurate neutron spectral characteristics are to be determined. Furthermore, in-core materials must survive a temperature condition of nominally 1100°C without significant material loss. Over the past four years, encapsulated powdered oxide samples of designated isotopes and/or mononuclidic elements have been prepared for this purpose. Because of difficulty in quantitative loading of 0.1- to 1-mg quantities into minute capsules, the cost of each dosimeter averaged about $125, which is a relatively large cost since it is estimated that 2000 dosimeters will be consumed per year. In addition, the nominal error for isotope powder loading for each capsule was about 1.5%, as compared with a desired error level of less than 0.5%. Fabrication time per capsule was about 1 hr for each nonradioactive sample and 2 hr for each radioisotope-containing capsule.

During the past year an effort to reduce errors in capsule loading by converting isotope oxide powders into structurally strong and easily handled solid forms that are suitable for direct weighing before encapsulation has resulted in much-improved samples. Ceramic wires of pure actinide oxides, scandium oxide, and a wide variety of dilutions of the desired nuclide oxides in aluminum oxide, for example, 0.1% UO_2 in Al_2O_3, have been prepared; the success of this program is illustrated by the reduction in the average cost of dosimeters by about 50%.

Small-particle-size (about 300 mesh) isotope oxide, either pure or diluted with aluminum oxide, is mixed with a hydrocarbon binder (paraffin, cornstarch, etc.) and is subsequently extruded into uniform-diameter wires. The process of homogenization of starting material is carefully controlled, because the end product must remain constant in isotope content over 1-cm lengths of wire to within 0.5% of the average value. For pure materials, simple homogenization of powdered oxide is adequate; for dilutions in aluminum oxide, coprecipitation from molten urea followed by a calcine at 800°C must be performed to assure uniformity. Depending upon the oxide, various binding agents (or lubricants) are used which, subsequent to extrusion, are volatilized or oxidized to remove gaseous effluents by low-temperature firing in air or argon. After removal of the binding agent, firing at 1200 to 1650°C (depending upon the oxide) sinters the wire (0.5 mm in diameter) into a nondusting ceramic suitable for routine cutting and encapsulation. Error in the weight measurement of segments of ceramic wire is within 0.5% with nearly zero rejections of loaded capsules after welding, because direct weight of the ceramic wire is reproducible on a microbalance and the material neither dusts nor tends to leave the capsule during welding. Ceramic wires have densities between 65% and 85% of the theoretical values, depending upon the oxide material, processing history, and sintering temperature

TRITIUM TARGETS FOR HIGH-YIELD NEUTRON GENERATORS

H. L. Adair J. M. Dailey

Intense monoenergetic (14.5-MeV) neutron fields are being generated for purposes of neutron activation, damage studies, and a variety of biological experiments. Although tritium-containing targets have been made for neutron production purposes for more than 25 years, insignificant quantitative evaluations have been made of neutron yields and target lifetimes as functions of incident deuteron beam energy, target preparation parameters, and the choice of metal used to sorb gaseous tritium in the target.

In support of studies at Lawrence Livermore Laboratory, the Isotope Research Materials Laboratory has been producing large-area tritium targets (an annular ring of 390 cm^2 on a disk 23 cm in diameter) containing approximately 900 Ci of tritium sorbed into a titanium metal matrix. Over the past year, 24 targets of the type described have been prepared; these targets have routinely produced 2×10^{12} neutrons/sec for a 700-mA-hr target half-life (the time required for the neutron yield to drop by a factor of 2). Because of improved preparative procedures, variation of performance among targets is but ±20% as compared with ±200% only two years ago. Quantitative study of neutron yield performance at Lawrence Livermore Laboratory as a function of target fabrication parameters is now being initiated with the intent of increasing neutron yields to more than 10^{13} neutrons/sec.

PREPARATION OF FISSION CHAMBER PLATES FOR CROSS-SECTION MEASUREMENTS

H. L. Adair J. M. Dailey

In support of programs of the ORNL Neutron Physics Division, about 50 well-defined deposits of a variety of fissile isotope oxides were prepared during the past year. Deposited isotope oxides include ^{235}U, ^{238}U, ^{239}Pu, 50% ^{235}U–50% ^{238}U, and ^{240}Pu, and efforts are being made to produce similar deposits of ^{233}U and ^{231}Pa. Numerous plates composed of a 10-cm-diam aluminum substrate and a 5-cm-diam deposit of the desired oxide have been produced for specific actinide isotopes. Electron-beam-heated vaporization sources (about 2300°C) have been used with a variety of crucible configurations to vapor-deposit oxide layers; in some cases, radio-frequency heating of the material in tungsten or tantalum tubular crucibles has been employed because of severe limitations in the amounts of isotopes available. In every case, direct microbalance weight measurements were employed to determine the total amount of oxide deposited to within an error of 1%. Verification of isotope content and uniformity of isotope distribution over the substrate surface was performed by low-geometry counting of alpha or gamma emissions; agreement within 1.5% between weight and counting methods has been routinely achieved.

THICK TRANSURANIUM OXIDE COATINGS

H. L. Adair J. M. Dailey

Vapor deposition techniques have been developed for forming thick transuranium oxide coatings on titanium metal substrates. Examples are the 12- to 14-mg $^{237}NpO_2$ targets that have been prepared for Argonne National Laboratory for use in fission-track recorders and the 3- to 12-mg/cm^2 $^{244}CmO_2$ targets that have been prepared for ORNL and Westinghouse-Hanford for use as alpha sources for helium injection into metals. The latter are used to study the effects of interstitial helium gas atoms in the nucleation and growth of voids and dislocation loops that might occur in materials used in fission or fusion reactors. Methods for vacuum evaporation of the various oxides by radio-frequency induction heating have been developed which are conservative of materials and efficient in terms of uniform deposition. The substrates, normally titanium, were heated to approximately 300°C to obtain excellent bonding of the deposited material.

ACTINIDE METAL PREPARATION

H. L. Adair C. A. Culpepper W. B. Grisham

The Isotope Research Materials Laboratory has continued development efforts in the preparation of high-purity metals of ^{241}Am, ^{243}Am, ^{239}Pu, and ^{244}Cm. The technique usually used for preparing these metals has been a "bomb" calcium reduction of the fluoride, which normally results in metals containing large amounts of impurities. In order to purify the bomb-reduced metal, vacuum distillation can be used wherein high-vapor-pressure impurities are distilled away from the desired metal and, if necessary, the metals can be further purified by subsequent distillation away from lower-vapor-pressure impurities. The major problem with purification by the described vacuum distillation process is that actinide metals react with most crucible materials. By vacuum reduction and distillation of the actinides from their oxides in which thorium is used as the reductant metal, very high purity actinide metals have been produced and then rolled into thin foils for various research purposes. This process has been used to obtain approximately 8 g of ^{239}Pu, 20 g of ^{241}Am, 12 g of ^{243}Am, and 10 g of ^{244}Cm, all of which contained less than 450 ppm total impurities, including oxygen and nitrogen.

LAVES PHASES OF URANIUM AND 3*d* TRANSITION METALS

E. C. Beahm[1] C. A. Culpepper O. B. Cavin[2]

In support of an ORNL Chemical Technology Division program to investigate Laves phases of uranium with 3*d* transition metals (chromium, iron, and nickel), intermetallic compounds of the type AB_2 were prepared. These compounds were produced by accurately weighing component elements (±0.0017%), combining them by arc melting, and homogenizing the specimens through multiple melting and stirring operations. Subsequent annealing of the compound formulations at 800°C for 66 hr in flowing argon was performed before crystal structure parameters were determined. The parameters shown in Table 6.1 were determined by x-ray diffraction.

Table 6.1. Uranium–chromium–iron–nickel Laves phases

Alloy composition (at. %), 33.3 at. % U plus			Lattice constant(s) (Å)	Comments
Cr	Ni	Fe		
			Hexagonal C14	
5.0	61.7		$a = 4.9741 \pm 0.0007$, $c = 8.2511 \pm 0.0007$	
10.0	56.7		$a = 4.9856 \pm 0.0013$, $c = 8.2569 \pm 0.0011$	
15.0	51.7		$a = 4.9902 \pm 0.0007$, $c = 8.2670 \pm 0.0008$	
			Cubic C15	
15.0	51.7		7.1047 ± 0.0018	
23.0	43.7		7.1153 ± 0.0002	
33.3	33.3		7.1425 ± 0.0002	
36.0	30.7		7.1441 ± 0.0004	Very faint Ni lines also present
44.7	22.0		7.1531 ± 0.0006	Cr, Ni lines also present
55.7	11.0		7.1519 ± 0.0025	Cr, Ni lines also present
28.0	31.7	7.0	7.1157 ± 0.0007	
36.0	21.7	9.0	7.1450 ± 0.0006	Faint Fe, Ni lines also present
44.0	11.7	11.0	7.1476 ± 0.0010	Fe, Ni, Cr lines also present

PREPARATION OF SELF-SUPPORTING METALLIC FOILS OF ISOTOPIC CHROMIUM

P. R. Kuehn

Excessive consumption of valuable isotopic material makes production of self-supporting chromium foils by vacuum evaporation and condensation impractical. Electrodeposition has been developed into a dependable and reproducible technique which results in minimal material losses so that chromium isotope target foils can be prepared economically. When used as an accelerator target, the physical properties of a chromium film must necessarily be different from those of decorative chromium, namely, the film must be ductile and free of chemical impurities.

Chemical purity of 99.8% has been obtained using a plating bath temperature of 90°C, as compared with 40 to 55°C used for commercial plating; throwing power and plating efficiency are substantially reduced at this higher bath temperature. Plating cell design and electrode preparation have been developed so that structurally strong foils with thickness variations to within 5% of the average value are reproducibly obtained. Excessive loss of isotopic material is avoided by using inert electrodes, with the result that the Cr III/Cr IV ratio in the bath increases during deposition. optimum current density increases as the valence concentration ratio or the temperature increases. Chemically impure chromium was found to deposit at low current densities, and the resultant foil was stressed at current densities in excess of the optimum value, so that the usable range of current density is only about 0.1 A/cm^2. The bath composition found to be most reproducible for this purpose contains the equivalent of 125 g of CrO_3 per liter of a 1:100 H_2SO_4/H_2O solution. Since only about 1 g of CrO_3 is used, the solution volume is quite small.

Using this formulation, more than 25 self-supported chromium isotope foils were produced during the year with thicknesses of 0.25 mg/cm^2 to 35 mg/cm^2 and areas of 1 cm^2 to 25 cm^2. To provide the films in self-supported form, electrodeposition is performed onto carefully masked, polished brass shim stock, which is later dissolved away from the chromium in dilute nitric acid. Films are usually pinhole-free and can be readily mounted on suitable support frames. Electrodeposition has proven to be ideally suited for foil preparation using separated chromium isotopes. Unused chromium can be salvaged with minor losses through simple chemical processing. Targets prepared by this technique are structurally strong, uniform in thickness, and sufficiently pure for most nuclear applications.

^{10}B TARGETS FOR THE CONTINUOUS PREPARATION OF ^{11}C

E. H. Kobisk T. C. Quinby

Cyclotron bombardment of ^{10}B with protons produces ^{11}C, an important isotope for medical research purposes. In cooperation with personnel at Oak Ridge Associated Universities, a special target was prepared for continuous production and subsequent removal of ^{11}C (as CO_2) during proton bombardment. A 12.5-cm length of molybdenum rod with a diameter of 6 mm was machined to have a triangular cross section with the edges notched parallel to the length of the rod. In this serrated section of the rod, $^{10}B_2O_3$ was deposited by mist-spraying a solution of the oxide in alcohol onto the surface, a process that produced uniform coating of the fin surfaces with oxide at an efficiency of 97% with respect to material utilization. Vacuum degassing and fusion of the coating resulted in a uniform, transparent coating with sufficient adherence to withstand extended proton bombardment (up to 20 hr) in the ORNL 86-Inch Cyclotron. Using a carrier gas (helium) flowing over the target surfaces during bombardment, the large-surface-area target generated 75 to 80% of the maximum quantity of $^{11}CO_2$ and maintained an even distribution of B_2O_3 on the irradiated surfaces even though heat from the proton beam impingement was sufficient to melt the isotopic film. Target development is still in progress.

HYDROGEN ISOTOPE SEPARATIONS SYSTEMS

D. W. Ramey T. C. Quinby

The purpose of this program was to investigate possible separation of tritium from reactor or fuel reprocessing plant effluents using the well-known phenomenon of hydrogen diffusion through palladium or palladium alloys as the separative mechanism. This process provides high throughput capability (tons per year) compatible with volumes encountered in waste effluents. The capability of the Isotope Research Materials Laboratory to roll thin membranes having zero porosity and maximum physical strength permitted measurements of separation factors to be made at temperatures up to 600°C and pressures up to 633 kg/cm^2 (9000 psi).

---

1. Chemical Technology Division, ORNL.
2. Metals and Ceramics Division, ORNL.

Although a number of different alloys of palladium were formulated and rolled into thin membranes, the palladium–25 wt % silver alloy offered better structural stability and the highest gas permeation rates. Membrane thicknesses between 0.0125 mm and 0.0375 mm were employed to obtain high flow rates, and each membrane was supported by a tungsten frit of pore size sufficiently small to permit the self-supported area of membrane to withstand the applied gas pressure at a temperature of 600°C. Indeed, the entire flow system for these experiments was specifically designed to provide maximum strength under these hostile conditions, and choice of structural materials was carefully made to preclude hydrogen embrittlement effects.

In the work reported here, only the flow of pure gases and separation factors associated with hydrogen-deuterium mixtures were measured. The general form of the flow-rate equation, as an extension of Fick's law, is

$$R_i = (D_0K_0)_i(\Delta\sqrt{P})^a \Delta\sqrt{P}A/t \times \exp[(\Sigma E_0/R)_i(\Delta\sqrt{P})^b/T] \quad . \qquad (1)$$

where

R_i = permeation rate for component i (cm³/min).

$(D_0K_0)_i(\Delta\sqrt{P})^a$ = pressure variance equation of the diffusion-solubility frequency factor for component i.

$\Delta\sqrt{P}$ = driving force derived from classical theory: $\Delta\sqrt{P} = \sqrt{P_f} - \sqrt{P_b}$, where P_f is the fore pressure (psia) and P_b is the back pressure, which was constant at 15 psia for this work.

A = membrane area (in.²).

t = membrane thickness (mils).

$(\Sigma E_0/R)_i(\Delta\sqrt{P})^b$ = pressure variance equation of the permeation activation energy for component i.

T = membrane temperature (°K).

The values for the constants in Eq. (1) are given in Table 6.2.

Data for mixed gases were obtained by measuring the flow rates as a function of temperature, pressure, and foil thickness while simultaneously analyzing the separation-stage bleed and product streams for the total hydrogen and deuterium content. Feed composition was varied from 0.65 to 0.45 H_2 mole fraction, and membrane thickness was varied from 1.40 to 0.4 mil. Fore pressures as high as 8000 psia total pressure were used for mixed gas studies, while the back pressure remained constant at 15 psia. The separation-stage schematic diagram in Fig. 6.1 represents the two-component system of this work (H_2–D_2), where X and Y represent mole fractions of components in the respective flow streams.

It has been assumed in this work that the permeation process has a rate which is controlled by diffusion and solubility in the metal lattice. Also, it is generally agreed that the gas diffuses through the metal lattice as atoms rather than as molecules. Therefore, one must conclude that the separation of the isotopes must also take place within the metal lattice rather than on the metal surface. The magnitude of separation of the isotopes must, in turn, be governed by the relative differences in those processes which control the permeation process, namely, diffusion and solubility in the metal lattice.

The definition of the separation factor is

$$S = Y_1(1 - X_1)/X_1(1 - Y_1) \quad . \qquad (2)$$

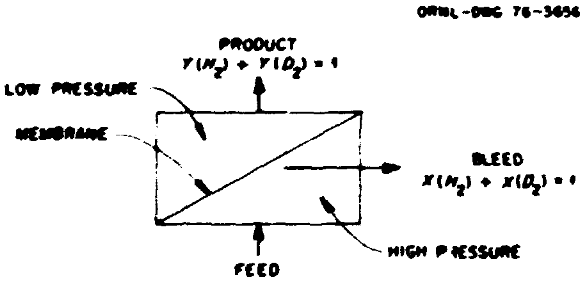

Fig. 6.1. Separation stage schematic.

Table 6.2. Permeation equation constants derived from pure gas flow rate data

Component	D_0K_0	a	$\Delta E_0/R$	b	Temperature range (°C)
H_2	1944.0	1.085	1866	0.0887	200–325
D_2	35.23	1.931	685	0.316	200–325
H_2	37.99	1.612	292	0.412	325–600
D_2	11.75	1.712	153	0.521	325–600

where Y_1 is the mole fraction of hydrogen in the product stream and X_1 is the mole fraction of hydrogen in the bleed stream.

Analysis of the product stream and bleed stream with a mass spectrometer gave the relative concentrations of H_2, D_2, and the intersotopic molecule HD. To determine the total amount of H_2 in each stream, the hydrogen contribution from the HD molecule was calculated as half the HD concentration. It should be emphasized that the HD molecule will always be present in the separation system because of the catalytic action of the metal membrane; however, the presence of HD in the system has little or no effect on the isotopic separation (a bulk metal process), because the HD molecule exists only in the gas phase.

The separation factor temperature dependence was calculated from the data obtained from mixed gas measurements, and the functional relationship between separation factor (S) and temperature can be represented by

$$S = 1.091 \exp(150/T) \quad . \tag{3}$$

where T is in degrees Kelvin. No dependence of separation factor on the system pressure or membrane thickness was noted.

Publications and Papers

JOURNAL ARTICLES

M. M. Abraham, Y. Chen, L. A. Boatner, and R. W. Reynolds, "F^- and F^+ Centers in CaO Single Crystals," *Solid State Commun.* 16, 1209 (1975).

M. M. Abraham, Y. Chen, and W. P. Unruh, "ENDOR Investigations of $F_{(H)}$ Centers in CaO," *Phys. Rev. B* 12, 4766 (1975).

B. R. Appleton, "Ion Implantation: A New Technique in Materials Research," *Oak Ridge National Laboratory Review*, 8(1), 28 (1975).

B. R. Appleton, "Review of *Ion Beams with Applications to Ion Implantation*" (ed. by R. G. Wilson and G. R. Brewer, Wiley-Interscience, New York, 1973) *Science* 188, 1295 (1975). [book review]

J. B. Bates, R. W. Major, and F. A. Modine, "Phase Transitions in $RbCaF_3$. I. Optical Studies," *Solid State Commun.* 17, 1347 (1975).

J. B. Bates and J. C. Pigg, "Resonance Raman and Electronic Absorption Spectra of O_2^- Ions in γ-Irradiated $KClO_4$ and $NaClO_4$," *J. Chem. Phys.* 62, 4227 (1975).

J. B. Bates and A. S. Quist, "Vibrational Spectra of Solid and Molten Phases of the Alkali-Metal Tetrafluoroborates," *Spectrochim. Acta* 31A, 1317 (1975).

J. B. Bates and H. D. Stidham, "^{79}Br and ^{81}Br Isotope Effects in Raman Spectra of Crystalline $NaBrO_3$," *Solid State Commun.* 16, 1223 (1975).

J. B. Bates and R. F. Wood, "High Temperature Luminescence Spectra from *F*-Centers in CaO," *Solid State Commun.* 17, 201 (1975).

J. W. Cable, E. O. Wollan, G. P. Felcher, T. O. Brun, and S. P. Hornfeldt, "Neutron Measurement of Magnetization Density in Palladium," *Phys. Rev. Lett.* 34, 278 (1975).

Y. Chen and M. M. Abraham, "V^- and Other Trapped-Hole Centers in MgO," *New Physics (Korean Physical Society)* 15, 47 (1975).

Y. Chen, M. M. Abraham, L. C. Templeton, and W. P. Unruh, "Role of Hydrogen and Deuterium on the V^--Center Formation in MgO," *Phys. Rev. B* 11, 881 (1975).

Y. Chen, M. M. Abraham, T. J. Turner, and C. M. Nelson, "Luminescence in Deformed MgO, CaO, and SrO," *Phil. Mag.* 32, 99 (1975).

J. W. Cleland, F. W. James, and R. D. Westbrook, "Defect-Impurity Interactions in Irradiated Germanium," *IEEE Trans. Nucl. Sci.* NS-22(6), 2289 (1975).

R. R. Coltman, Jr., C. E. Klabunde, J. K. Redman, and J. M. Williams, "Damage Recovery in Vanadium Between 3.8–6.0° K," *Radiat. Eff.* 24, 69 (1975).

J. F. Cooke, H. L. Davis, and Mark Mostoller, "Interpolated Band Structure Models and Integration Schemes," *Phys. Rev. B* 11, 706 (1975).

M. H. Dickens, C. G. Shull, W. C. Koehler, and R. M. Moon, "Neutron-Diffraction Observations on the Cu(Fe) Kondo System," *Phys. Rev. Lett.* **35**, 595 (1975).

C. B. Duke, L. Pietronero, J. O. Porteus, and J. F. Wendelken, "Surface-Plasmon Dispersion on the (100) Face of Aluminum," *Phys. Rev. B* **12**, 4059 (1975).

E. W. Gray, D. V. McCaughan, J. R. Pharney, and C. W. White, "Arc Duration Reduction in an Organic Atmosphere by Electrode Implantation of Low Ionization Potential Materials," *J. Appl. Phys.* **46**, 678 (1975).

G. H. Jenks, E. Sonder, C. D. Bopp, J. R. Walton, and S. Lindenbaum, "Reaction Products and Stored Energy Released from Irradiated Sodium Chloride by Dissolution and by Heating," *J. Phys. Chem.* **79**, 871 (1975).

L. H. Jenkins, T. S. Noggle, R. E. Reed, M. J. Saltmarsh, and G. J. Smith, "High-Energy Neutron Sputtering Yields from Gold and Niobium," *Appl. Phys. Lett.* **26**, 426 (1975).

W. A. Kamitakahara and C. A. Rotter, "Phase Transitions in $RbCaF_3$. II. Neutron Scattering," *Solid State Commun.* **17**, 1350 (1975).

Quiesup Kim, R. C. Powell, and T. M. Wilson, "Temperature Dependence of the Local Mode in the Vibronic Spectrum of $SrTiO_3:Cr^{3+}$," *J. Phys. Chem. Solids* **36**, 61 (1975).

Quiesup Kim, R. C. Powell, M. Mostoller, and T. M. Wilson, "Analysis of the Vibronic Spectrum of Chromium Doped Strontium Titanate," *Phys. Rev. B* **12**, 5627 (1975).

Bennett C. Larson, "X-ray Studies of Defect Clusters in Copper," *J. Appl. Cryst.* **8**, 150 (1975).

J. W. Lynn, "Temperature Dependence of the Magnetic Excitations in Iron," *Phys. Rev. B* **11**, 2624 (1975).

J. W. Lynn, H. A. Mook, and W.J.L. Buyers, "Exchange-Split Crystal-Field Levels of Fe^{2+} in $FeCO_3$," *Phys. Rev. B* **12**, 238 (1975).

F. A. Modine and R. W. Major, "High Frequency Polarization Modulation Method for Measuring Optical Rotation," *Appl. Opt.* **14**, 761 (1975).

F. A. Modine, R. W. Major, and E. Sonder, "High Frequency Polarization Modulation Method for Measuring Birefringence," *Appl. Opt.* **14**, 757 (1975).

H. A. Mook, N. Wakabayashi, and D. Pan, "Magnetic Excitations in the Amorphous Ferromagnet Co_4P," *Phys. Rev. Lett.* **34**, 1029 (1975).

R. M. Moon and W. C. Koehler, "Magnetic Properties of Gd_2O_3," *Phys. Rev. B* **11**, 1609 (1975).

R. M. Moon, W. C. Koehler, and C. G. Shull, "Limitations on the Accuracy of Polarized-Neutron Diffractometry," *Nucl. Instrum. Methods* **129**, 515 (1975).

R. M. Nicklow, R. R. Coltman, Jr., F. W. Young, Jr., and R. F. Wood, "Neutron Inelastic Scattering Measurements of Phonon Perturbations by Defects in Irradiated Copper," *Phys. Rev. Lett.* **35**, 1444 (1975).

M. J. Norgett, M. T. Robinson, and I. M. Torrens, "A Proposed Method of Calculating Displacement Dose Rates," *Nucl. Eng. Des.* **33**, 50 (1975).

O. S. Oen and M. T. Robinson, "Slowing Down Time of Energetic Ions in Solids," *J. Appl. Phys.* **46**, 5069 (1975).

V. K. Paré, "Resonant Transmission-Line Configurations for Optimum FM Detection of Vibration Using Capacitance Transducers," *J. Acoust. Soc. Am.* **58**, 490 (1975).

J. B. Roberto, B. W. Batterman, V. O. Kastroun, and B. R. Appleton, "Positive-Ion Induced Kossel Lines in Copper," *J. Appl. Phys.* **46**, 936 (1975).

H. G. Smith, M. Nielsen, and C. B. Clark, "Lattice and Molecular Vibrations in Single Crystal I_2 at 77°K by Inelastic Neutron Scattering," *Chem. Phys. Lett.* **33**, 75 (1975).

E. Sonder, "Temperature Dependence of Frenkel Pair Production from Aggregate Center Destruction," *Phys. Rev. B* **12**, 1516 (1975).

N. H. Tolk, J. C. Tully, C. W. White, J. Kraus, and S. H. Neff, "Quasi-molecular States Responsible for Quantum-Mechanical Phase Interference in Low-Energy Na^+-Ne Collisions," *Phys. Rev. Lett.* **35**, 1175 (1975).

C. G. Venkatesh, S. A. Rice, and J. B. Bates, "A Raman Spectral Study of Amorphous Solid Water," *J. Chem. Phys.* **63**, 1065 (1975).

F. L. Vook, H. K. Birnbaum, T. H. Blewitt, W. L. Brown, J. W. Corbett, J. H. Crawford, Jr., A. N. Goland, G. L. Kulcinski, M. T. Robinson, D. N. Seidman, and F. W. Young, Jr., "Report of the APS Summer Study on 'Physics Problems Relating to Energy Technologies: Radiation Effects on Materials,'" *Rev. Mod. Phys.* **47**, Supplement 3 (1975).

N. Wakabayashi, H. G. Smith, and R. M. Nicklow, "Lattice Dynamics of Hexagonal MoS_2 Studied by Neutron Scattering," *Phys Rev. B* **12**, 659 (1975).

C. W. White, D. L. Sims, N. H. Tolk, and D. V. McCaughan, "Effects of Nonradiative De-excitation of Excited Sputtered Atoms Near Silicon and Silicon Dioxide Surfaces," *Surface Sci.* **49**, 657 (1975).

R. F. Wood and Mark Mostoller, "Possibility of Observing Self-Interstitials in Cu and Al by Neutron Scattering," *Phys. Rev. Lett.* **35**, 45 (1975).

R. F. Wood and T. M. Wilson, "Electronic Structure of the F-Center in CaO and MgO," *Solid State Commun.* **16**, 545 (1975).

D. M. Zehner, B. R. Appleton, T. S. Noggle, J. W. Miller, J. H. Barrett, L. H. Jenkins, and O. E. Schow III, "Characterization of Reordered (001) Au Surfaces by Positive-Ion-Channeling Spectroscopy, LEED, and AES," *J. Vac. Sci. and Technol.* **12**, 454 (1975).

BOOKS AND PROCEEDINGS

B. R. Appleton, T. S. Noggle, S. Datz, C. D. Moak, J. A. Biggerstaff, M. D. Brown, and H. F. Krause, "Radiative Electron Capture by Channeled Oxygen Ions," p. 499 in *Atomic Collisions in Solids*, vol. 2, ed. by S. Datz, B. R. Appleton, and C. D. Moak, Plenum Press, New York, 1975.

B. R. Appleton, T. S. Noggle, J. W. Miller, O. E. Schow III, D. M. Zehner, L. H. Jenkins, and J. H. Barrett, "Investigation of Reordered (001) Au Surfaces by Positive Channeling Spectroscopy, LEED and AES," p. 86 in *Proceedings of the Third Conference on Applications of Small Accelerators*, ed by J. L. Duggan and I. L. Morgan, ERDA CONF-74-1040-PK, 1974.

J. H. Barrett, "Validity of the Statistical Equilibrium Hypothesis for Channeling," p. 841 in *Atomic Collisions in Solids*, vol. 2, ed. by S. Datz, B. R. Appleton, and C. D. Moak, Plenum Press, New York, 1975.

J. H. Barrett, B. R. Appleton, T. S. Noggle, C. D. Moak, J. A. Biggerstaff, and S. Datz, "Hyperchanneling," p. 645 in *Atomic Collisions in Solids*, vol. 2, ed. by S. Datz, B. R. Appleton, and C. D. Moak, Plenum Press, New York, 1975.

H. R. Child and J. W. Cable, "Temperature Dependence of Neutron Ferromagnetic Disorder Scattering from Si and Mn Impurities in Fe," p. 118 in *Magnetism and Magnetic Materials-1974*, ed. by C. D. Graham, Jr., G. H. Lander, and J. J. Rhyne, AIP Conference Proceedings No. 24, New York, 1975.

J. W. Cleland, R. D. Westbrook, H. L. Davis, and R. F. Wood, "Photovoltaic Conversion of Solar Energy," p. 62 in *Proceedings of the First ERDA Semiannual Solar Photovoltaic Conversion Program Conference*, JPL-5040-13, 1975.

J. F. Cooke, J. W. Lynn, and H. L. Davis, "Dynamic Susceptibility Calculations in Ferromagnetic Iron," p. 329 in *Magnetism and Magnetic Materials 1974*, ed. by C. D. Graham, Jr., G. H. Lander, and J. J. Rhyne, AIP Conference Proceedings No. 24, 1975.

S. Datz, B. R. Appleton, J. A. Biggerstaff, M. D. Brown, H. F. Krause, C. D. Moak, and T. S. Noggle, "Charge State Dependence of Stopping Power for Oxygen Ions Channeled in Silver," p. 63 in *Atomic Collisions in Solids*, vol. 1, ed. by S. Datz, B. R. Appleton, and C. D. Moak, Plenum Press, New York, 1975.

H. L. Davis, "Exploratory Band Structure Calculations for Actinide Compounds," chapter in *Magnetism in Metals and Metallic Compounds*, ed. by J. T. Lopuszanski, A. Pekalski, and J. Przytawa, Plenum Press, New York, 1975.

H. L. Davis and H. A. Mook, "Neutron Scattering Determination of the Crystal Field Splittings in TmN," p. 229 in *Magnetism and Magnetic Materials 1974*, ed. by C. D. Graham, Jr., G. H. Lander, and J. J. Rhyne, AIP Conference Proceedings No. 24, New York, 1975.

Y. Hashimoto, J. H. Barrett, and W. M. Gibson, "Analysis of Blocking Lifetime Experiments," p. 735 in *Atomic Collisions in Solids*, vol. 2, ed. by S. Datz, B. R. Appleton, and C. D. Moak, Plenum Press, New York, 1975.

D. K. Holmes and M. T. Robinson, "Computer Studies of Replacement Sequences in Solids Associated with Atomic Displacement Cascades," p. 225 in *Atomic Collisions in Solids*, vol. 1, ed. by S. Datz, B. R. Appleton, and C. D. Moak, Plenum Press, New York, 1975.

R. M. Housley, E. H. Cirlin, I. B. Goldberg, H. Crowe, R. A. Weeks, and R. Perhac, "Ferromagnetic Resonance as a Method of Studying the Micrometeorite Bombardment History of the Lunar Surface," p. 3173 in *Proceedings 6th Lunar Science Conference*, vol. 3, Pergamon Press, 1975.

C. D. Moak, B. R. Appleton, J. A. Biggerstaff, S. Datz, and T. S. Noggle, "Velocity Dependence of the Stopping Power of Channeled Iodine Ions," p. 57 in *Atomic Collisions in Solids*, vol. 1, ed. by S. Datz, B. R. Appleton, and C. D. Moak, Plenum Press, New York, 1975.

H. A. Mook, D. Pan, J. D. Axe, and L. Passell, "Magnetic Excitations in Amorphous Co_4P," p. 112 in *Magnetism and Magnetic Materials – 1974*, ed. by C. D. Graham, Jr., G. H. Lander, and J. J. Rhyne, AIP Conference Proceedings No. 24, New York, 1975.

R. M. Moon, "Magnetic Form Factor of Electrons in *3d* Bands," p. 425 in *Magnetism and Magnetic Materials 1974*, ed. by C. D. Graham, Jr., G. H. Lander, and J. J. Rhyne, AIP Conference Proceedings No. 24, New York, 1975.

J. R. Mowat, B. R. Appleton, J. A. Biggerstaff, S. Datz, C. D. Moak, and I. A. Sellin, "Charge State Dependence of Si K X-ray Production in Solid Gaseous Targets by 40 MeV Oxygen Ion Impact," p. 461 in *Atomic Collisions in Solids*, vol. 1, ed. by S. Datz, B. R. Appleton, and C. D. Moak, Plenum Press, New York, 1975.

R. M. Nicklow, N. C. Koon, C. M. Williams, and J. B. Milstein, "Spin-Waves in the Laves Compound $Ho_{0.88}Tb_{0.12}Fe_2$," p. 165 in *Magnetism and Magnetic Materials 1974*, ed. by C. D. Graham, Jr., G. H. Lander, and J. J. Rhyne, AIP Conference Proceedings No. 24, New York, 1975.

J. J. Rhyne, D. L. Price, and H. A. Mook, "Inelastic Magnetic Scattering from Amorphous $TbFe_2$," p. 121 in *Magnetism and Magnetic Materials 1974*, ed. by C. D. Graham, Jr., G. H. Lander, and J. J. Rhyne, AIP Conference Proceedings No. 24, New York, 1975.

K. Rossler and M. T. Robinson, "Radiation Damage in Transition Metal Hexahalo Complexes: The Application of Atomic Collision Dynamics in Hot Atom Chemistry," p. 237 in *Atomic Collisions in Solids*, vol. 1, ed. by S. Datz, B. R. Appleton, and C. D. Moak, Plenum Press, New York, 1975.

M. T. Robinson, "The Production of Displaced Atoms in Solids," p. 18 in *Consultant Symposium on "The Physics of Irradiation Produced Voids,"* ed. by R. S. Nelson, UKAEA Report AERE-R7934, 1975.

S. T. Sekula and R. R. Coltman, Jr., "Thermal Neutron Irradiation at 5 K of Superconducting Vanadium," p. 206 in *Proceedings of the International Discussion Meeting on Flux Pinning in Superconductors*, ed. by P. Haasen and H. C. Freyhardt, Akademie der Wissenschaften, Gottingen, 1975.

REPORTS ISSUED

O. E. Schow, *Safety Analysis of the 2.5 MV Accelerator in the Solid State Division's Positive Heavy Ion Scattering Implantation, Channeling and Sputtering (PHISICS) Facility*, ORNL-TM-5087, September 1975.

J. F. Guess, R. W. Boom, R. R. Coltman, Jr., and S. T. Sekula, *A Survey of Radiation Damage Effects in Superconducting Magnet Components and Systems*, ORNL-TM-5187, December 1975.

George C. Battle, T. F. Connolly, and Anne M. Keesee, *International Directory of Solid State Materials Production and Research*, ORNL-RMIC-13, June 1975.

R. E. Reed, *Progress Report of Apollo-Soyuz Test Project Experiment No. MA-041 for the Period, September 1–December 31, 1974*, ORNL-TM-4842, April 1975.

THESES

J. F. Wendelken, "High Resolution Low Energy Electron Diffraction from the Aluminum (100) Surface," thesis submitted to the Graduate College of the University of Illinois in partial fulfillment of the requirements for the Ph.D. degree, January 1975.

SEED MONEY PROPOSALS GRANTED

J. B. Roberto, R. R. Coltman, Jr., and J. Narayan, "Evaluation of a Deuteron Breakup Neutron Source for Simulation of CTR Radiation Damage"

B. R. Appleton and G. J. Clark, "Ion Implantation"

J. W. Cleland and R. F. Wood, "Nuclear Doping of Silicon for Solar Cells"

PAPERS PRESENTED AT TECHNICAL MEETINGS

6th Lunar Science Conference, Houston, Texas, March 17–21, 1975:

E. H. Cirlin, I. B. Goldberg, R. M. Housley, R. A. Weeks, and R. Perhac, "Ferromagnetic Resonance as a Method of Studying the Micrometeorite Bombardment History of Lunar Fines"

Fruhjahrstagung der Deutschen Physikalischen Gesellschaft, Münster, Germany, March 17–22, 1975:

G. Maderlechner, R. Behrisch, B.M.U. Scherzer, and M. T. Robinson, "Computer Simulation von Eindringtiefen- und Schadenverteilungen fur 0.5–10 keV He-Ionen in kristallinem und amorphem Niob"

American Physical Society Meeting, Denver, Colorado, March 31–April 3, 1975:

M. M. Abraham, Y. Chen, and W. P. Unruh, "ENDOR of V_{OH} Centers in CaO" [*Bull. Am. Phys. Soc.* **20**, 328 (1975)]

Y. Chen, M. M. Abraham, L. A. Boatner, and R. W. Reynolds, "Cation Vacancies in CaO" [*Bull. Am. Phys. Soc.* **20**, 328 (1975)]

W. A. Kamitakahara and H. G. Smith, "Lattice Dynamics and Electron-Phonon Interaction in Solid Mercury" [*Bull. Am. Phys. Soc.* **20**, 299 (1975)]

H. R. Kerchner, S. T. Sekula, and J. R. Clem, "AC Permeability of Defect-Free Type-II Superconductors" [*Bull. Am. Phys. Soc.* **20**, 293 (1975)]

C. E. Klabunde, J. M. Williams, and R. R. Coltman, Jr., "Unusual Aspects of Low-Temperature Recovery in Thermal Neutron-Irradiated Vanadium," [*Bull. Am. Phys. Soc.* **20**, 296 (1975)]

F. A. Modine and R. W. Major, "Birefringence Produced by the Cubic-to-Tetragonal Structural Phase Transition in $RbCaF_3$" [*Bull. Am. Phys. Soc.* **20**, 285 (1975)]

J. Narayan, T. S. Noggle, and O. S. Oen, "Radiation Damage in Copper Using MeV He and Ni Ions" [*Bull. Am. Phys. Soc.* **20**, 351 (1975)]

O. S. Oen and M. T. Robinson, "Computer Simulation of the Reflection of Light Ions from Solid Surfaces" [*Bull. Am. Phys. Soc.* **20**, 352 (1975)]

J. B. Roberto and J. Narayan, "Characteristics of Heavy Ion Damage in Ni Irradiated Cu and Nb" [*Bull. Am. Phys. Soc.* **20**, 351 (1975)]

Mark T. Robinson, "Theory of Damage Production" [*Bull. Am. Phys. Soc.* **20**, 397 (1975)] (invited paper)

C. A. Rotter, J. G. Traylor, and H. G. Smith, "Phonon Spectrum of MnF_2" [*Bull. Am. Phys. Soc.* **20**, 300 (1975)]

L. C. Templeton, E. Sonder, Y. Chen, and M. M. Abraham, "Effect of Plastic Deformation on Trapped-Hole Centers in MgO" [*Bull. Am. Phys. Soc.* **20**, 432 (1975)]

J. G. Traylor, N. Wakabayashi, and S. K. Sinha, "Phonon Dispersion Relations in $Nb_{[illegible]}Zr_{[illegible]}$" [*Bull. Am. Phys. Soc.* **20**, 300 (1975)]

T. M. Wilson and F. A. Modine, "Spin-Orbit Splitting in the Excited State of the F^+ Center in CaO" [*Bull. Am. Phys. Soc.* **20**, 432 (1975)]

R. F. Wood and Mark Mostoller, "Neutron Scattering from Copper Self-Interstitials" [*Bull. Am. Phys. Soc.* **20**, 351 (1975)]

D. M. Zehner, J. R. Noonan, L. H. Jenkins, and T. Kaplan, "Angular Distribution of Auger Electron Emission from a Clean Cu (110) Surface" [*Bull. Am. Phys. Soc.* **20**, 357 (1975)]

ARPA/NBS Conference on Silicon Surface Analysis, Gaithersburg, Maryland, April 23–24, 1975:

C. W. White, "Surface Composition by Analysis of Impact Radiation" (invited paper)

American Ceramic Society Meeting, Washington, D.C., May 3–8, 1975:

M. M. Abraham and Y. Chen, "Cation Vacancies in Crystalline CaO" [*Am. Ceram. Soc. Bull.* **54**, 404 (1975)]

J. C. Pigg and R. A. Weeks, "Potential Problems with MgO as an Electrical Insulator in High-Temperature Applications" [*Am. Ceram. Soc. Bull.* **54**, 402 (1975)]

Workshop on Defects in Magnesium Oxide and Related Materials, Canton, North Carolina, May 26–28, 1975:

Y. Chen, "Radiation Effects in Crystalline MgO" (invited paper)

Y. Chen, M. M. Abraham, T. J. Turner, and C. M. Nelson, "Luminescence in Deformed Alkaline-Earth Oxides"

J. B. Hartmann, H. Weinstock, and Y. Chen, "Thermal Conductivity of Radiation-Damaged and Deformed MgO"

F. A. Modine, R. W. Major, and T. M. Wilson, "Magnetic Circular Dichroism of Defects"

R. A. Weeks, J. C. Pigg, and L. D. Hulett, "Reduction of Fe^{3+} in MgO Single Crystals by Application of Electric Fields"

T. M. Wilson and R. F. Wood, "Electronic Structure of the *F* Center in CaO and MgO"

R. F. Wood, "Electronic Structure of Point Defects in Alkaline-Earth Oxides" (invited paper)

35th Annual Conference on Physical Electronics, Pennsylvania State University, University Park, Pennsylvania, June 2-4, 1975:

J. F. Wendelken, "An Apparent Temperature Dependence of the Surface Plasmon Dispersion Relation for Al (100)"

D. M. Zehner, J. R. Noonan, L. H. Jenkins, T. Kaplan, and H. L. Davis, "Diffraction Effects in the Angular Emission of Auger Electrons from a Clean Cu (110) Surface"

56th Annual Meeting, American Geophysical Union, Washington, D.C., June 16-18, 1975:

S. Arafa, A. Bishay, R. Giegengack, and R. A. Weeks, "Libyan Desert Glass Electron Magnetic Resonance Spectra of Fe^{3+} and Its Relation to Total Iron Content"

Thirtieth Symposium on Molecular Structure and Spectroscopy, The Ohio State University, Columbus, Ohio, June 16-20, 1975:

J. B. Bates and H. D. Stidham, "Resonance Raman and Electronic Absorption Spectroscopy of Electron- and γ-Ray-Irradiated Single Crystals of Alkali-Metal Chlorates"

H. D. Stidham and J. B. Bates, "Isotope Effects in Raman Spectra of Ionic Crystals"

1975 IEEE Annual Conference on Nuclear and Space Radiation Effects, Arcata, California, July 14-17, 1975:

J. W. Cleland, F. J. James, and R. D. Westbrook, "Defect-Impurity Interactions in Irradiated Germanium"

Gordon Research Conference on Electronic Materials, Plymouth, New Hampshire, July 21-25, 1975:

C. W. White, "Surface Analysis by Photon Emission Produced in Partial-Solid Collisions" (invited paper)

First ERDA/NSF/JPL Semiannual Solar Photovoltaic Conversion Program Conference, Jet Propulsion Laboratory, Los Angeles, California, July 22-25, 1975:

J. W. Cleland, R. D. Westbrook, H. L. Davis, and R. F. Wood, "Photovoltaic Conversion of Solar Energy"

Ninth International Conference on the Physics of Electronic and Atomic Collisions, Seattle, Washington, July 25, 1975:

S. Datz, B. R. Appleton, J. A. Biggerstaff, H. F. Krause, C. D. Moak, T. S. Noggle, and R. H. Ritchie, "Radiative Electron Capture by 17-40 MeV Oxygen Ions"

International Union of Crystallography, Amsterdam, The Netherlands, August 8-12, 1975:

B. C. Larson and F. W. Young, Jr., "The Effect of Irradiation Temperature on Dislocation Loops in Neutron-Irradiated Copper"

XIV Low Temperature Conference, Helsinki, Finland, August 14-20, 1975:

H. A. Mook, "Neutron Scattering Studies of TTF-TCNQ" (invited paper)

Second International Conference on Phonon Scattering in Solids, Nottingham, England, August 27-30, 1975:

J. B. Hartmann, H. Weinstock, and Y. Chen, "Thermal Conductivity of Radiation-Damage, Additively Colored and Deformed MgO"

NATO International Advanced Study Institute on Defects and Their Structure in Non-Metallic Solids, University of Exeter, Devonshire, England, August 24-September 6, 1975:

F. A. Modine, "Experimental Aspects of Magnetic Circular Dichroism"

International Conference on the Applications of Ion Beams to Materials, University of Warwick, Coventry, England, September 8–12, 1975:

Ordean S. Oen and Mark T. Robinson, "Computer Studies of the Penetration Depth of Low-Energy Light Ions in Solids"

II International Conference on Ion Beam Surface Layer Analysis, Kernforschungszentrum, Karlsruhe, Germany, September 15–19, 1975:

B. R. Appleton, D. M. Zehner, T. S. Noggle, J. W. Miller, O. E. Schow III, L. H. Jenkins, and J. H. Barrett, "Characterization of Reordered (001) Au Surfaces by the Combined Techniques of Positive Ion Channeling Spectroscopy (PICS), LEED–AES, and Computer Simulation"

J. W. Miller, B. R. Appleton, and J. R. Gavaler, "Characterization of High Transition Temperature Nb–Ge Thin Films by Ion Scattering, Ion-Induced X-rays, and Ion Resonance Techniques"

First ASTM–EURATOM Symposium on Reactor Dosimetry: Developments and Standardization, Petten, The Netherlands, September 22–26, 1975:

H. T. Kerr, H. L. Adair, and E. J. Allen, "Dosimeter Materials for High-Temperature Applications"

VI International Conference on Atomic Collisions in Solids, Amsterdam, The Netherlands, September 22–26, 1975:

B. R. Appleton, J. A. Biggerstaff, T. S. Noggle, R. M. Ritchie, S. Datz, C. D. Moak, and H. Verbeek, "Radiative Electron Capture by Highly Stripped Ions in Single Crystal Channels"

S. Datz, B. R. Appleton, J. A. Biggerstaff, T. S. Noggle, and H. Verbeek, "Electron Emission from Fast Oxygen and Copper Ions Emerging from Thin Gold Crystals in Channeled and Random Directions"

S. Datz, C. D. Moak, B. R. Appleton, J. A. Biggerstaff, and T. S. Noggle, "Hyperchanneling and Planar Channeling of Charge State Selected 27.5-MeV Oxygen Ions in Ag"

W. Heiland, E. Taglauer, and M. T. Robinson, "Multiple Scattering of Low-Energy Rare Gas Ions: A Comparison of Experiment and Computer Simulation"

Marc Hou and Mark T. Robinson, "Computer Studies of Low-Energy Scattering in Crystalline and Amorphous Targets"

U. Littmark, G. Maderlechner, R. Behrisch, B.M.U. Scherzer, and M. T. Robinson, "Calculations of the Moments of the Range and Damage Distributions for Low-keV Light-Ion Bombardment of Amorphous Solids"

C. D. Moak, B. R. Appleton, J. A. Biggerstaff, M. D. Brown, S. Datz, T. S. Noggle, and H. Verbeek, "The Velocity Dependence of the Stopping Power of Channeled Iodine Ions from 0.6 to 60 MeV"

O. S. Oen and M. T. Robinson, "Computer Studies of the Reflection of Light Ions from Solids"

N. H. Tolk, L. C. Feldman, J. Kraus, G. H. Wheatley, and C. W. White, "Quantum Mechanical Phase Interference in Low-Energy Ion-Surface Scattering"

W. F. Van der Weg, N. H. Tolk, and C. W. White, "Optical Excitation During Ion Bombardment of Copper Under Channeling Conditions"

C. W. White, N. H. Tolk, and W. F. Van der Weg, "Continuum Optical Radiation Produced by Low-Energy Heavy-Particle Bombardment of Metal Targets"

United States–Japan Seminar on Radiation-Produced Defects and Defect Clusters and Their Effects in Metals, Ames, Iowa, September 28–30, 1975:

R. R. Coltman, Jr., "Electrical Resistivity Measurements on Low-Temperature Neutron-Irradiated fcc and bcc Metals"

Fourth International Conference of the Nuclear Target Development Society, Argonne National Laboratory, Argonne, Illinois, September 29–October 1, 1975:

H. L. Adair and E. H. Kobisk, "Target Preparations and Thickness Measurements"

International Conference on Radiation Effects and Tritium Technology for Fusion Reactors, Gatlinburg, Tennessee, October 1–3, 1975:

Y. Chen, M. M. Abraham, M. T. Robinson, J. B. Mitchell, and R. A. Van Konynenburg, "Production of Point Defects in 14.8-MeV Neutron-Irradiated MgO"

J. B. Roberto, J. Narayan, and M. J. Saltmarsh, "15-MeV Neutron Damage in Cu and Nb"

International Conference on Fundamental Aspects of Radiation Damage in Metals, Gatlinburg, Tennessee, October 6–10, 1975:

G. Antesberger, K. Sonnenberg, P. Wienhold, R. R. Coltman, Jr., C. E. Klabunde, J. M. Williams, and R. L. Chaplin, "Influence of Divacancies on Stage III Recovery in Cu"

Y. K. Chang, A. J. Arko, G. W. Crabtree, J. B. Ketterson, L. R. Windmiller, R. J. Higgins, and F. W. Young, Jr., "Measurements of Conduction Electron Scattering in Neutron-Irradiated Copper by the deHaas-von-Alphen Effect"

R. R. Coltman, Jr., C. E. Klabunde, and J. K. Redman, "Recovery in Stages I and II of Thermal and Fission Neutron-Irradiated Molybdenum"

C. E. Klabunde, R. R. Coltman, Jr., and J. M. Williams, "Low-Temperature Recovery of Radiation Damage in Vanadium"

B. C. Larson, "X-ray Studies of Irradiation-Induced Dislocation Loops in Metals" (invited paper)

J. Narayan, T. S. Noggle, and O. S. Oen, "Depth Distribution of Damage in Copper Irradiated with MeV Ni and He Ions"

R. M. Nicklow, R. R. Coltman, Jr., F. W. Young, Jr., and R. F. Wood, "Dynamics of the [100] Dumbbell Interstitial in Copper"

S. M. Ohr, "The Nature of Defect Clusters in Electron-Irradiated Copper"

J. B. Roberto and J. Narayan, "Ni Ion Damage in Cu and Nb"

Mark T. Robinson, "The Theory of Radiation-Induced Defect Production" (invited paper)

H. Schroeder, K. Sonnenberg, P. Wienhold, R. R. Coltman, Jr., C. E. Klabunde, and J. M. Williams, "Indirect Evidence for Vacancy Clustering During Stage II Annealing in Cu"

Integrated Contractors Meeting, Bendix Corporation, Kansas City, Missouri, October 22–23, 1975:

H. L. Adair, "Preparation of Well Defined Actinide Targets by Vacuum Evaporation"

22nd National Symposium of the American Vacuum Society, October 28–31, 1975:

D. M. Zehner, J. R. Noonan, and L. H. Jenkins, "Angular-Resolved Auger Emission Spectra from a Clean Cu (100) Surface"

Conference on Preliminary Assessment Review of Multipurpose Furnace Experiments Performed on Apollo-Soyuz Test Project, NASA, George C. Marshall Space Flight Center, Huntsville, Alabama, October 29, 1975:

R. E. Reed, "A 'Quick Look' Assessment of ASTP Experiment MA-041 Subsequent to the Apollo-Soyuz Test Project Mission for the Period August 4, 1975, to October 10, 1975"

ASM Materials Science Seminar on Radiation Damage in Metals, Cincinnati, Ohio, November 9–10, 1975:

Mark T. Robinson, "The Theory of Radiation-Induced Defect Production" (invited paper)

F. W. Young, Jr., "Annealing Processes in Metals" (invited paper)

Review on Fundamental Research in Catalysis, ERDA, Washington, D.C., November 11–12, 1975:

L. H. Jenkins, "Solid State Aspects of Heterogeneous Catalysis"

1975 Southeastern Section Meeting, American Physical Society, Auburn, Alabama, November 13–15, 1975:

R. R. Coltman, Jr., D. K. Christen, S. T. Sekula, and J. M. Williams, "Search for an Effect of Fluxoid Motion on Irradiation Defects in Vanadium"

H. A. Mook, "Neutron Scattering Study of TTF-TCNQ" (invited paper)

R. M. Nicklow, "Observations of Self-Interstitials in Copper by Inelastic Neutron Scattering" (invited paper)

International Conference on Low-Lying Vibrational Modes and Their Relationship to Superconductivity and Ferroelectricity, San Juan, Puerto Rico, December 1–3, 1975:

W. A. Kamitakahara, H. G. Smith, and N. Wakabayashi, "Neutron Spectroscopy of Low-Frequency Phonons in Solid Hg"

H. A. Mook, "Neutron Scattering Investigation of Peierls' Transition in TTF-TCNQ"

21st Annual Conference on Magnetism and Magnetic Materials, Philadelphia, Pennsylvania, December 9–12, 1975:

T. Brun, S. Sinha, A. S. Edelstein, R. Majewski, and H. R. Child, "A Study of the Frequency Dependent Susceptibility of the Compound, CeAl$_3$, by Inelastic Neutron Scattering"

A. S. Edelstein and H. R. Child, "Neutron Scattering Measurements of the α-γ Transformation in CeTh Alloys"

G. Felcher, J. W. Garland, J. W. Cable, and R. Medina, "The Analysis of Magnetic Neutron Scattering Data"

R. A. Medina and J. W. Cable, "Moment Disturbances in Ni–Cu Alloys"

Seminars

SOLID STATE DIVISION SEMINARS AT ORNL

M. M. Abraham succeeded J. W. Cable as Seminar Chairman during the year 1975. The following seminars were held during the period covered by this report:

"Neutron Scattering and Sightseeing in India and Pakistan," W. C. Koehler, Solid State Division, ORNL.

"Evidence of Phase Mixing During the Ferroelectric Phase Transition of KD_2PO_4," H. Meister, Euratom, Ispra, Italy

"Point Defect Production by Irradiation of Solids,"[2] M. T. Robinson, Solid State Division, ORNL

"Linear Accelerator Source for Neutron Scattering," O. K. Harling, Battelle-Northwest, Richland, Washington

"Spatial Distribution of Damage Energy in Solids by Fast-Ion Irradiation,"[2] O. S. Oen, Solid State Division, ORNL

"Magnetic Resonance"[2] (Parts 1 and 2), M. M. Abraham, Solid State Division, ORNL

"Characteristics of Thermal and Fission Neutron Damage in Metals,"[1] R. R. Coltman, Jr., Solid State Division, ORNL

"Electronic Properties of Ultra-Thin Films and Coatings of Transition and Noble Metals," B. R. Cooper, University of West Virginia, Morgantown, West Virginia

"Segregation of Vacancies and Interstitials in High-Temperature Irradiations,"[1] W. G. Wolfer, Metals and Ceramics Division, ORNL

"Materials Problems of MHD Electric Generator Systems," Neil Loeffler, University of Tennessee Space Institute, Tullahoma, Tennessee

"Recovery Spectrum After Electron Irradiation,"[1] K. Sonnenberg, Solid State Division, ORNL

"Investigation of Jahn-Teller Effects by Electron Paramagnetic Resonance," L. A. Boatner, Texas Christian University, Forth Worth, Texas

"Amorphous Solid Water," A. H. Narten, Chemistry Division, ORNL

"Swelling in Nickel Due to Carbon and Nickel Ion Bombardment,"[1] A. Taylor, Argonne National Laboratory, Argonne, Illinois

"Recovery Studies in Cu and Pb," K. Sonnenberg, Kernforschungsanlage, Julich, Germany

"Elastic Interaction and Diffusion Reaction of Point Defects,"[1] M. H. Yoo, Metals and Ceramics Division, ORNL

"Near-Surface Studies of Single Crystals by Positive-Ion Channeling Spectroscopy," B. R. Appleton, Solid State Division, ORNL

"Void Growth Kinetics in Irradiated Metals,"[1] L. K. Mansur, Metals and Ceramics Division, ORNL

"Electronically Driven Lattice Instabilities," S. K. Sinha, Argonne National Laboratory, Argonne, Illinois

"Radiation-Induced Creep,"[1] W. G. Wolfer, Metals and Ceramics Division, ORNL

"Optical Radiation Produced in Low-Energy Particle Solid Collisions," C. W. White, Bell Laboratories, Murray Hill, New Jersey

"Elementary Survey of Electron Spin Lattice Relaxation," H. J. Stapleton, University of Illinois, Urbana, Illinois

"A Metallurgical Approach to High Critical Temperature in Superconducting A-15 Compounds," David Dew-Hughes, Brookhaven National Laboratory, Upton, New York

"Influence of Chemical Bonds on Collision Cascades in Nonmetals," K. Rossler, Kernforschungsanlage, Julich, Germany

"Critical Currents in Sintered Niobium Nitride Compounds," Ronald Powell, Harvard University, Cambridge, Massachusetts

"CH_4: Rotational Excitations and Phase Transition in a Quantum Molecular Crystal," Werner Press, Kernforschungsanlage, Julich, Germany

"Radiation Damage in Fe_3Al," H. P. Leighly, University of Missouri, Rolla, Missouri

"A Study of Radiation-Induced Effects in Silicon Using Infrared Spectroscopy and Photoconductivity Measurements," Rosa T. Young, Eastern Kentucky State College, Richmond, Kentucky

"Induced Neutron Magnetic Form Factor of Chromium," Kye H. Oh, Ames Laboratory, Iowa State University, Ames, Iowa

"Electronic Structure and Cohesive Energies of Transition Metals and Their Hydrides," C. D. Gelatt, Jr., Harvard University, Cambridge, Massachusetts

"Magneto Optical Studies in Lead Tin Telluride," Jeremiah Ralph Lowney, Massachusetts Institute of Technology, Cambridge, Massachusetts

"Pulsed Neutron Sources for Utilization in Condensed Matter Research," M. Kimura, Tohoku University, Sendai, Japan

"Luminescence of Defects and Ions in CaO and MgO," A. E. Hughes, Atomic Energy Research Establishment, Harwell, England

"Structure and Dynamics of Gases Adsorbed on Graphite Studied by Neutron Scattering," Kim Carneiro, Brookhaven National Laboratory, Upton, New York

"Energy Loss Spectra of A-15 Superconductors," Lawrence Y. L. Shen, Bell Laboratories, Murray Hill, New Jersey

"Channeling in the Superionic Conductor β Alumina," L. C. Feldman, Bell Laboratories, Murray Hill, New Jersey

"Electron States of Silver in Glasses," Salah Arafa, American University in Cairo, Cairo, Egypt

"Neutron Damage Simulation by 5-Mev $^{20}Ne^{+}$ Bombardment in MgO," Bruce Evans, Naval Research Laboratory, Washington, D.C.

"Densities of States and Spectral Weight Functions in Disordered Alloys," A. Gonis, University of Illinois at Chicago Circle, Chicago, Illinois

"Fundamental Aspects of Flux Pinning in Type II Superconductors," E. J. Kramer, Argonne National Laboratory, Argonne, Illinois

"Recovery of Irradiated Metals: Old and New Questions," W. Schilling, Kernforschungsanlage, Julich, Germany

"Charge Density Waves in Chromium and Its Alloys," N. Kunitomi, Osaka University, Osaka, Japan

"Spinodal for Hydrogen in Niobium," Georg Alefeld, Technical University in Munich, Munich, Germany

"Diffraction Effects in Photoemission from Localized Adsorbate Levels," A. Liebsch, University of Pennsylvania, Philadelphia, Pennsylvania

"Trace Element Analysis in Blood Using Proton-Induced X-Ray Fluorescence," Robert C. Bearse, University of Kansas, Lawrence, Kansas

"Survey of Ionic Transport Processes in Silver Halide Crystals," Robert J. Friauf, University of Kansas, Lawrence, Kansas

"Sputtering As a Tool for the Investigation of Atomic Collision Cascades in Solids,"[3] H. H. Andersen, Aarhus University, Aarhus, Denmark

"Electronic Structure and Physical Properties of Metals," Allan Mackintosh, Atomic Energy Commission Risø, Roskilde, Denmark

"Neutron Scattering Studies of Liquid and Amorphous Materials Using a Pulsed Source,"[4] K. Suzuki, Research Institute for Iron, Steel, and Other Metals, Tohoku University, Sendai, Japan

"Theory of Excitations and Phase Diagrams for Rare-Earth Metals and Alloys," P. A. Lindgard, Atomic Energy Commission Riso, Roskilde, Denmark

"Neutron Inelastic Scattering in the Antiferromagnets NiS and $KNiF_3$:Mn," Georges Parisot, Institute Max von Laue–Paul Langevin, Grenoble, France

"Radiation Effects in Insulators or Printing Without Ink," W. A. Sibley, Oklahoma State University, Stillwater, Oklahoma

---

1. Joint Metals and Ceramics and Solid State Divisions Radiation Damage Symposium.
2. Tutorial Lectures.
3. Sponsored jointly by Physics Division and Solid State Division.
4. Sponsored jointly by Chemistry Division and Solid State Division.

LECTURES AND SEMINARS

Lectures and seminars presented by Division members during the year included the following:

M. M. Abraham—University of Kansas, Lawrence, Kansas, "Dynamic Nuclear Polarization in Solids"; University of Geneva, Geneva, Switzerland, and Ecole Polytechnique Federale, Lausanne, Switzerland, "Magnetic Resonance" (six lectures)

Y. Chen—Texas Christian University, Fort Worth, Texas, "Radiation Damage in MgO"; Georgia State University, Atlanta, Georgia, "Radiation Induced Defects in MgO and CaO"

J. F. Cooke—Danish Atomic Energy Commission Research Establishment Risø, Roskilde, Denmark, "Theoretical Investigation of Spin Waves in Nickel and Iron" and "First-Principles Calculation of Phonon Spectra in High T_c Transition Metal Superconductors"; Kernforschungsanlage, Jülich, Germany, "Theoretical Description of Spin Waves in $3d$ Transition Metal Ferromagnets"; Institute Max von Laue–Paul Langevin, Grenoble, France, "Inelastic Neutron Scattering Calculations in Ferromagnetic Nickel"

H. L. Davis—The Ohio State University, Columbus, Ohio, "Crystal-Field Spectroscopy via Inelastic Neutron Scattering"

W. C. Koehler—Iowa State University, Ames, Iowa, "Neutron Scattering and the Rare-Earths—Fifteen Years of Study"

B. C. Larson—University of Oslo, Oslo, Norway, "Dynamical and Kinematical X-ray Studies of Defect Clusters in Copper"; University of Munich, Munich, Germany, and Max-Planck-Institut fur Metallforschung, Stuttgart, Germany, "The Effect of Irradiation Temperature on Dislocation Loops in Neutron-Irradiated Copper"

F. A. Modine—Laboratoire d'Optique Physique at Ecole Superieure de Physique et de Chimie Industrielles de La Ville de Paris, Paris, France, and Centre d'Etudes Nucléaires de Grenoble, Grenoble, France, "Polarization Modulation Spectroscopy at ORNL"

H. A. Mook—Institute Max von Laue–Paul Langevin, Grenoble, France, "Magnetic Excitations in Crystalline and Amorphous Transition Metal Ferromagnets" and "A Magnetically Pulsed Time-of-Flight Spectrometer for Neutron Inelastic Scattering Research"

J. Narayan—Radiation Effects and Microstructural Analysis Group, Metals and Ceramics Division, ORNL, "Characteristics of 15-MeV Neutron Damage in Metals"

J. B. Roberto—Radiation Effects and Microstructural Analysis Group, Metals and Ceramics Division, ORNL, "High-Energy Neutron Damage Calculations in Metals"

S. T. Sekula—Naval Research Laboratory, Washington, D.C., "Radiation Damage in Type II Superconductors"

H. G. Smith—Max-Planck-Institut für Metallforschung, Stuttgart, Germany, "Lattice Dynamics of Layered Compounds"; Kernforschungsanlage, Julich, Germany, "Phonon Anomalies in Superconductors"; ETH, Zurich, Switzerland, "Neutron Scattering Work at ORNL"

N. Wakabayashi—Ohio University, Athens, Ohio, "Slow Neutron Spectrometry"

R. A. Weeks—University of Missouri, Rolla, Missouri, and Vanderbilt University, Nashville, Tennessee, "Charge Trapping in and Polarization of Glass Insulators"; St. Louis University, St. Louis, Missouri, "Magnetic Anisotropies of Small-Particle Ferrites: Ferromagnetic Resonance Experiments"; Vanderbilt University, Nashville, Tennessee, "Diffusion of Mn in MgO Single Crystals: Application of Paramagnetic Resonance Spectroscopy"; Knoxville Gem and Mineral Society, Knoxville, Tennessee, "Colors of Crystals and Minerals"

R. F. Wood—Oklahoma State University, Stillwater, Oklahoma, "Electronic Structure of Color Centers in Alkaline Earth Oxides"; University of North Carolina, Chapel Hill, North Carolina, "Color Centers in Alkaline Earth Oxides"

D. M. Zehner—Florida Technical Institute, Orlando, Florida, University of South Florida, Tampa, Florida, and University of Puerto Rico, Mayaguez, Puerto Rico, "Anomalous Surface Structure Examined by Low-Energy Electron Diffraction, Auger Electron Spectroscopy and Rutherford Ion Backscattering"; and University of Puerto Rico, Rio Piedras, Puerto Rico, "Studies of Surface Structure with Low-Energy Electron Diffraction and Auger Electron Spectroscopy"

Scientific Professional Activities

M. M. Abraham	Recipient. Industrial Research 100 Award for 1975 Visiting Professor. Troisieme Cycle Romand de Chimie – Convention Intercantonale pour L'Enseignement de la Chimie et Physique (CICP). University of Geneva. Geneva. Switzerland Session Chairman. Workshop on Defects in Magnesium Oxide and Related Materials. Canton. North Carolina Participant. MIT/AEC Meeting on Critical Needs and Opportunities in Fundamental Ceramic Research. January 1975
B. R. Appleton	Editor. *Atomic Collisions in Solids*. vols. 1 and 2. Plenum Press. New York. 1975 Member. Graduate School Doctoral Committee. Department of Physics and Astronomy. University of South Carolina. Columbia. South Carolina Adjunct Professor. Department of Physics. North Texas State University. Denton. Texas Member. Organizational and Advisory Committee. Fourth Conference on the Use of Small Accelerators (to be held in 1976)
J. B. Bates	General Chairman. 6th Meeting of the Fourier Transform Spectroscopy Group. The Pittsburgh Conference on Analytical Chemistry and Applied Spectroscopy. Cleveland. Ohio. March 1975 Member. Steering Committee. Fourier Transform Spectroscopy Technical Group Lecturer. ORAU Traveling Lecture Program. 1975–1976
J. W. Cable	Chairman. Program Committee. Conference on Neutron Scattering (to be held in 1976) Lecturer. ORAU Traveling Lecture Program. 1974–1975 Member. Ph.D. Thesis Committee. Department of Physics. Georgia Institute of Technology. Atlanta. Georgia
Y. Chen	Recipient. Industrial Research 100 Award for 1975 Session Chairman and participant. MIT/AEC Meeting on Critical Needs and Opportunities in Fundamental Ceramic Research. January 1975 Lecturer. ORAU Traveling Lecture Program. 1974–1975 Member. Organizing Committee. Workshop on Defects in Magnesium Oxide and Related Materials. Canton. North Carolina Member. Advisory Panel on Publishing. American Institute of Physics
J. W. Cleland	Lecturer. ORAU Traveling Lecture Program. 1974–1975
R. R. Coltman. Jr.	Member. Reactor Experimental Review Committee. ORNL Member. Radiation Damage Working Group of the Clinton P. Anderson Meson Physics Facility. LASL Lecturer. ORAU Traveling Lecture Program. 1975–1976
T. F. Connolly	Editor. *Solid State Physics Literature Guides*. vol. 7. Plenum Press. New York. 1975
J. F. Cooke	Guest scientist. Danish Atomic Energy Commission Research Establishment Risø. Roskilde. Denmark. 1975–1976
H. L. Davis	Member. Thesis Committee. Department of Physics. The University of Tennessee. Knoxville. Tennessee
D. K. Holmes	Member. Editorial Advisory Board. *Radiation Effects*

L. H. Jenkins	Member, Ph.D. Recruiting Program, ORNL Member, ORNL Eugene P. Wigner Fellows Selection Panel Member, ORNL Graduate Selection Panel
W. C. Koehler	Member, Neutron Diffraction Commission, International Union of Crystallography Member, Editorial Advisory Board, *International Journal of Magnetism* General Chairman, Conference on Neutron Scattering (to be held in 1976) Participant, Workshop on Uses of Advanced Pulsed Neutron Sources, Argonne, Illinois, 1975 Member, Editorial Advisory Board, *Magnetism Letters* Member, ORNL Neutron Beam Users' Organizing Committee Editor, *Magnetic Form Factor Data Sheets*, International Union of Crystallography Member, Ph.D. Thesis Committee, Department of Physics, Georgia Institute of Technology, Atlanta, Georgia
B. C. Larson	Guest scientist, Institut fur Festkorperforschung, Kernforschungsanlage, Julich, Germany, 1974 - 1975 Participant, Workshop on Uses of Advanced Pulsed Neutron Sources, Argonne, Illinois, 1975
F. A. Modine	Member, Organizing Committee, Workshop on Defects in Magnesium Oxide and Related Materials, Canton, North Carolina
H. A. Mook	Member, ORNL Neutron Source Committee Member, Seed Money Proposal Review Committee, ORNL Guest scientist, Institute Max von Laue - Paul Langevin, Grenoble, France, Summer 1975 Member, Ph.D. Recruiting Program, ORNL Participant, Workshop on Uses of Advanced Pulsed Neutron Sources, Argonne, Illinois, 1975
R. M. Moon	Chairman, ORNL Neutron Source Committee Chairman, ORNL Neutron Beam Users' Organizing Committee Member, Commission on Electron Charge, Spin, and Momentum Densities of the International Union of Crystallography Editor, *Magnetic Form Factor Data Sheets*, International Union of Crystallography Member, ORNL Program Planning and Analysis Office Staff Coordinator, ORNL Long-Range Program Planning Participant, Workshop on Uses of Advanced Pulsed Neutron Sources, Argonne, Illinois, 1975
M. Mostoller	Lecturer, ORAU Traveling Lecture Program, 1975 - 1976
R. M. Nicklow	Lecturer, ORAU Traveling Lecture Program, 1975 - 1976 Member, Program Committee, Conference on Neutron Scattering (to be held in 1976) Member, ORNL Neutron Beam Users' Organizing Committee
T. S. Noggle	Member, American Society for Testing Materials E-10 Task Group on Description of Radiation Damage in Metals Using Electron Microscopy Member, Graduate School Doctoral Committee, Department of Physics and Astronomy, University of South Carolina, Columbia, South Carolina
S. M. Ohr	Member, American Society for Testing Materials E-10 Task Group on Description of Radiation Damage in Metals Using Electron Microscopy Guest scientist, Institut fur Physik, Max-Planck-Institut fur Metallforschung, Stuttgart, Germany, 1975 Member, Local Arrangements Committee, International Conference on Fundamental Aspects of Radiation Damage in Metals, Gatlinburg, Tennessee, 1975
R. F. Reed	Secretary, Vacuum Metallurgy Division, American Vacuum Society, 1974 - 1975 Special Proceedings Editor, *Second Conference on Structure-Property Relationships in Thick Films and Bulk Coatings*, 1975
J. B. Roberto	Member, Synchrotron X-ray and Photon Source Task Force, ORNL Contributor, ORNL Intense Neutron Generator for Radiation Induced Damage (INGRID) Proposal
M. T. Robinson	Editor, *Proceedings International Conference on Fundamental Aspects of Radiation Damage in Metals*

	Member, Steering Committee, Workshop on Uses of Advanced Pulsed Neutron Sources, Argonne, Illinois, 1975
	Participant, Workshop on Uses of Advanced Pulsed Neutron Sources, Argonne, Illinois, 1975
	Member, Radiation Damage Subgroup of the IAEA Working Group on Reactor Radiation Measurements
	Lecturer, ORAU Traveling Lecture Program, 1974 - 1975
	Member, ORNL Neutron Source Committee
O. E. Schow	Member, Laboratory Director's Safety Review Committee for Accelerators and Radiation Sources
S. T. Sekula	Lecturer, ORAU Traveling Lecture Program, 1975 - 1976
H. G. Smith	Guest scientist, Institute Max von Laue - Paul Langevin, Grenoble, France, 1974 - 1975
	Co-Sponsor, The International Conference on Low-Lying Vibrational Modes and Their Relationship to Superconductivity and Ferroelectricity, San Juan, Puerto Rico, December 1975
E. Sonder	Visiting Professor, Department of Physics, Oklahoma State University, Stillwater, Oklahoma, 1974 - 1975
N. Wakabayashi	Research collaborator, Brookhaven National Laboratory Summer Program on Neutron Scattering
R. A. Weeks	Member, Editorial Committee, *Journal of the American Ceramic Society*
	Member, Editorial Board, *Journal of Nonmetals and Semiconducting Solids*
	External Examiner, Ph.D. Thesis, Vanderbilt University, Nashville, Tennessee
	Consultant, Promotion of Member of Staff, Faculty of Philosophy II, University of Zurich, Zurich, Switzerland
	Lecturer, ORAU Traveling Lecture Program, 1975
	External Examiner, Ph.D. Thesis, Faculty of Science, Cairo University, Cairo, Egypt
R. D. Westbrook	Member, ASTM Committee F1, Chairman of Subcommittee on Germanium
M. K. Wilkinson	Professor (Adjunct), Department of Physics, Georgia Institute of Technology, Atlanta, Georgia
	Member, Advisory Panel of the Solid State Sciences Committee of the National Research Council
	Secretary, Advisory Committee of Conference on Magnetism and Magnetic Materials
	Member, Ph.D. Thesis Committee, Department of Physics, Georgia Institute of Technology, Atlanta, Georgia
	Chairman, Evaluation Panel for Reactor Radiation Division, National Bureau of Standards
	Member, Evaluation Panel for Institute for Materials Research, National Bureau of Standards
	Member, Executive Committee, Southeastern Section of American Physical Society
	Member, ORNL Committee on Research Reactors
R. F. Wood	Chairman, Organizing Committee, International Conference on Color Centers (to be held in 1977)
	Editor, Solid State Physics, *Computer Physics Communications*, North Holland Publishing Company
	Session Chairman, American Physical Society Meeting, Denver, Colorado, 1975
	Session Chairman, Workshop on Defects in Magnesium Oxide and Related Materials, Canton, North Carolina
F. W. Young, Jr.	Member, Editorial Advisory Board, *Crystal Synthesis*, Springer-Verlag, New York, Inc.
	Member, Executive Committee, American Association of Crystal Growth
	Participant, MIT/AEC Meeting on Critical Needs and Opportunities in Fundamental Ceramic Research, January 1975
	General Chairman, International Conference on Fundamental Aspects of Radiation Damage in Metals, Gatlinburg, Tennessee, 1975
	Editor, *Proceedings International Conference on Fundamental Aspects of Radiation Damage in Metals*
	Teller, DSSP Section, American Physical Society Election
D. M. Zehner	Lecturer, ORAU Traveling Lecture Program, 1974 - 1975

Personnel Changes

New Staff Members

- a. Scientific Staff
  - E. H. Kobisk (transferred from Isotopes Division)
  - H. L. Adair (transferred from Isotopes Division)
  - D. W. Ramey (transferred from Isotopes Division)
  - P. R. Kuehn (transferred from Isotopes Division)
  - B. F. Early (transferred from Isotopes Division)
  - R. T. Young, Assistant Professor, Eastern Kentucky University, Richmond, Kentucky
  - C. W. White, Technical Staff Member, Bell Laboratories, Murray Hill, New Jersey
- b. Administrative and Technical Staff
  - B. A. Caylor, Secretary (transferred from Isotopes Division)
  - K. B. Campbell, Senior Laboratory Technician (transferred from Isotopes Division)
  - C. A. Culpepper, Senior Laboratory Technician (transferred from Isotopes Division)
  - J. M. Dailey, Senior Laboratory Technician (transferred from Isotopes Division)
  - W. B. Grisham, Science Technologist (transferred from Isotopes Division)
  - T. C. Quinby, Science Technologist (transferred from Isotopes Division)
  - J. L. Sellers, Engineering Technologist (transferred from Instrumentation and Controls Division)
  - J. L. Moore, Senior Engineering Assistant (transferred from Instrumentation and Controls Division)
  - L. W. Hinton, Secretary

Staff Transfers and Terminations

- E. D. Bolling, Science Technologist (voluntary resignation)
- J. R. Savage, Senior Laboratory Technician (deceased)
- J. W. Miller, Research Staff Member (completion of temporary appointment)
- K. W. Lagerfelt, Secretary (voluntary resignation)
- W. A. Kamitakahara, Research Staff Member (completion of temporary appointment)
- L. C. Templeton, Research Staff Member (retirement)
- R. E. Reed, Research Staff Member (deceased)

Guest Assignments

- a. Scientific Staff
  - G. Leibfried, Kernforschungsanlage, Julich, Germany

F. J. F. Tasset. Institut Max von Laue Paul Langevin (I.L.L.). Grenoble. France

J. R. Seretlo. University of Fort Hare. South Africa

W. Uelhoff. Kernforschungsanlage. Julich. Germany

D. W. Kammer. Albion College. Albion. Michigan

H. P. Leighly. University of Missouri Rolla. Rolla. Missouri

C. A. Rotter. West Virginia University. Morgantown. West Virginia

K. Sonnenberg. Kernforschungsanlage. Julich. Germany

H. D. Stidham. University of Massachusetts. Amherst. Massachusetts

H. Verbeek. Max-Planck-Institut fur Plasmaphysik. Garching bei Munchen. Germany

T. M. Wilson. Oklahoma State University. Stillwater. Oklahoma

b. Graduate Students

O. J. Rubio. National University of Mexico. Mexico

O. W. Holland. North Texas State University. Denton. Texas

W. P. Crummett. West Virginia University. Morgantown. West Virginia

R. A. Medina. Georgia Institute of Technology. Atlanta. Georgia

Q. C. Murphree. University of South Carolina. Columbia. South Carolina

Summer Assignments

a. Scientific Staff

J. W. Garland. University of Illinois at Chicago Circle. Chicago. Illinois

A. Chatelain. Ecole Polytechnique Institute. Lausanne. Switzerland

A. Goins. University of Illinois at Chicago Circle. Chicago. Illinois

C. L. Hosley. Morehouse College. Atlanta. Georgia

F. J. James. University of North Carolina. Chapel Hill. North Carolina

C. C. Watson. Yale University. New Haven. Connecticut

F. B. Tubbs III. Earlham College. Richmond. Indiana (Great Lakes College Association. ORNL Science Semester Program)

S. Spooner. Georgia Institute of Technology. Atlanta. Georgia

b. Clerical Staff

R. A. Johnson. Secretary. Tennessee Technological University. Cookeville. Tennessee

D. L. Smalley. Secretary. The University of Tennessee. Knoxville. Tennessee

c. ORAU University Faculty

A. S. Edelstein. University of Illinois at Chicago Circle. Chicago. Illinois

G. E. Shankle. San Angelo State University. San Angelo. Texas

J. F. Guess. Trevecca Nazarene College. Nashville. Tennessee

d. ORAU – Undergraduate Research Trainees

D. W. Harmony. Oklahoma State University. Stillwater. Oklahoma

J. E. Breitling. Bethany Nazarene College. Bethany. Oklahoma

T. L. Polgreen. Carleton College. Northfield. Minnesota

K. F. Kelton. Arkansas Polytechnic College. Russellville. Arkansas